Secondary Metabolites of Fungi from Diverse Ecological Sources: Chemistry and Bioactivity

Der Fakultät für Lebenswissenschaften

der Technischen Universität Carolo-Wilhelmina zu Braunschweig

zur Erlangung des Grades einer

Doktorin der Naturwissenschaften

(Dr. rer. nat.)

eingereichte

D i s s e r t a t i o n

Kumulative Arbeit

von Natalia Andrea Llanos-López
aus Cali, Kolumbien

1. Referent: Prof. Dr. Marc Stadler
2. Referent: Prof. Dr. André Fleißner

eingereicht am:
mündliche Prüfung (Disputation) am:
Druckjahr 2025

Vorveröffentlichungen der Dissertation

Teilergebnisse aus dieser Arbeit wurden mit Genehmigung der Fakultät für Lebenswissenschaften, vertreten durch den Mentor der Arbeit, in folgenden Beiträgen vorab veröffentlicht:

Publikationen

Roman numerals within the text correspond to the following publications.

I. **Llanos-López NA**, Ebada SS, Vasco-Palacios AM, Sánchez-Giraldo LM, López L, Rojas LF, Mándi A, Kurtán T, Marin-Felix Y (**2023**). Panapophenanthrin, a rare oligocyclic diterpene from *Panus strigellus*. *Metabolites* 13(7):848. https://doi.org/10.3390/metabo13070848.

II. Phutthacharoen K†, **Llanos-López NA**†, Toshe R, Noisripoom W, Khonsanit A, Luangsa-Ard JJ, Hyde KD, Ebada SS, Stadler M (**2024**). Bioactive bioxanthracene and cyclodepsipeptides from the entomopathogenic fungus *Blackwellomyces roseostromatus* BCC56290. *Antibiotics* 13(7):585. https://doi.org/10.3390/antibiotics13070585.

III. **Llanos-López NA**†, Wennrich J-P†, Miled J, Ashrafi S, Maier W, Surup S, Stadler M (**2025**). Polydosetins & pullularins – Bioactive tetramic acids & cyclodepsipeptides from the endophytic and nematophagous fungus *Polydomus karssenii*. *Natural Products and Bioprospecting* (accepted).

IV. Wennrich J-P, Sepanian E, Ebada SS, **Llanos-López NA**, Ashrafi S, Maier W, Kurtán T, Stadler M (**2023**). Bioactive naphtho-α-pyranones from two endophytic fungi of the genus *Polyphilus*. *Antibiotics* 12(8):1273. https://doi.org/10.3390/antibiotics12081273.

V. Phutthacharoen K, Toshe R, Khalid SJ, **Llanos-López NA**, Wennrich J-P, Schrey H, Ebada SS, Hyde KD, Stadler M (**2024**). Lachnuoic acids A–F: Ambuic acid congeners from a saprotrophic *Lachnum* species. *Chemistry & Biodiversity* 21(4):e2024003. https://doi.org/10.1002/cbdv.202400385.

VI. Wennrich J-P, Schmidt K, Ashrafi S, **Llanos-López NA**, Kaspara F, Hermann J, Stradal T, Held J, de Carvalho LP, Maier W, Surup F, Stadler M (**2025**). Pochoniatoxin, a cytotoxic pentacyclic metabolite from the nematode-associated fungus *Pochonia chlamydosporia*. *ACS Omega* (submitted).

† these authors contributed equally to this work

Weitere Publikationen, die nicht Gegenstand der vorliegenden Arbeit sind.

VII. Hassan K, Chepkirui C, **Llanos-López NA**, Matasyoh JC, Decock C, Marin-Felix Y, Stadler M (**2022**). Meroterpenoids possibly produced by a bacterial endosymbiont of the tropical basidiomycete *Echinochaete brachypora*. *Biomolecules* 12(6):755. https://doi.org/10.3390/biom12060755.

VIII. España-Puccini P, Muñoz-Acevedo A, **Llanos-López NA**, Stadler M, Ganoza-Yupanqui ML, Martínez-Habibe MC (**2025**). Chemical diversity of three lichens of genus *Graphis* (*Graphidaceae*) of the tropical dry forest from the northern region of Colombia. *Mycological Progress* 24(1):68. https://doi.org/10.1007/s11557-025-02080-5.

Tagungsbeiträge

Llanos-López NA. Isolation and characterization of nematicidal and antimicrobial agents from three fungal Phaeosphaeriaceous species. Oral presenter at Pure and Applied Chemical International Conference 2023 (PACCON2023), Chiang Rai, Thailand (January 20–21, 2023).

Llanos-López NA. Isolation and characterization of nematicidal and antimicrobial agents from three *Polydomus karssenii* strains. Oral presenter at the Deutsche Gesellschaft für Mykologie (DGfM) Scientific Conference 2023, Lehesten, Germany (September 15–21, 2023).

Llanos-López NA. Exploring natural products from nematode-associated fungi. Invited speaker at Julius Kühn-Institut (JKI) Kolloquium, Braunschweig, Germany (April 1, 2025).

Llanos-López NA. Exploring natural products from nematode-associated fungi of the order Pleosporales. Oral presenter at the Deutsche Gesellschaft für Mykologie (DGfM) Scientific Conference 2025, Springe, Germany (September 29–October 2, 2025).

Posterbeiträge

Llanos-López NA. Isolation and characterization of nematicidal and antimicrobial agents from three fungal Phaeosphaeriaceous species. PhD Assembly for HZI and UdS Doctoral Researchers 2023, Saarbrücken, Germany (May 4–5, 2023).

Llanos-López NA. Isolation and characterization of nematicidal and antimicrobial agents from three *Polydomus karssenii* strains. 3rd International Conference of Faculty of Pharmacy, Cairo, Egypt (November 19–20, 2023).

Llanos-López NA. Isolation and characterization of nematicidal and antimicrobial agents from three fungal *Polydomus karssenii* strains. 12th International Mycological Congress (IMC12), Maastricht, Netherlands (August 11–15, 2024).

Llanos-López NA. Exploring natural products from nematode-associated fungi of the order Pleosporales. Root-benefit symposium, Münchenberg, Germany (May 21–22, 2025).

Declaration of Contribution to the Publications

The contributions of Natalia A. Llanos-López (NAL-L) and the co-authors of the listed publications are described below.

I. Conceptualization: NAL-L and YM-F; methodology: NAL-L, SSE, AMV-P, LMS-G, and LL; formal analysis: NAL-L, SSE, and YM-F; TDDFT-ECD: AM and TK; software: SSE; resources: AMV-P; writing—original draft preparation: NAL-L, SSE, and AMV-P; writing—review and editing: NAL-L, SSE, and YM-F; project administration: YM-F and LFR; funding acquisition: LFR. All authors have read and agreed to the published version of the manuscript.

II. Conceptualization: KP, SSE, and MS; fungal isolation and identification: AK, WN, and JJL-A; methodology: KP, NAL-L, RT, and SSE; formal analysis: KP, NAL-L, RT, and SSE; data curation and structure elucidation: SSE; nematicidal activity: NAL-L; writing—original draft preparation: KP, AK, NAL-L, and SSE; writing—review and editing: KDH, SSE, and MS; project administration: MS; funding acquisition: MS. All authors have read and agreed to the published version of the manuscript.

III. Conceptualization: NAL-L, J-PW, and MS; fungal isolation and identification: SA and WM; methodology: NAL-L, J-PW, and JM; data curation and interpretation: NAL-L, FS, and J-PW; visualization: NAL-L and FS; writing—original draft preparation: NAL-L and FS; writing—review and editing: NAL-L and MS; project administration: MS; funding acquisition: MS. All authors have read and agreed on the published version of the manuscript.

IV. Conceptualization: J-PW, SSE, and MS; culture characterization: SA and WM; methodology and investigation: J-PW, ES, and NAL-L; data curation and interpretation: J-PW, SSE, and TK; visualization: J-PW and SSE; writing—original draft preparation: J-PW and SSE; writing—review and editing: all authors. All authors have read and agreed to the published version of the manuscript.

V. Conceptualization: KP, SSE and MS; fungal isolation and identification: KP, MS; methodology: KP, RT, and SSE; formal analysis: KP, RT, and SSE; data curation and structure elucidation: SSE; antibiofilm assay: HS and SJK; nematicidal activity: NAL-L and J-PW; writing—original draft preparation: KP, RT, and SSE; writing—review

and editing: SSE and MS; project administration: MS; funding acquisition: MS. All authors have read and agreed on the published version of the manuscript.

VI. Conceptualization: J-PW, FS, MS, and TEBS; strain isolation and characterization: SA, WM; methodology and investigation: J-PW, LPC, KS, JH, and NAL-L; data curation and interpretation: J-PW, FS, SA, WM, and JH; visualization: J-PW, FS, and KS; writing—original draft preparation: J-PW, FS, and KS; writing—review and editing: All authors read and approved the final manuscript.

VII. Conceptualization: KH, CC, and MS; methodology: KH, CD, NAL-L, and YM-F; software: YM-F; resources: MS; writing—original draft preparation: KH, CC, and NAL-L; writing—review and editing: YM-F, CC, JCM, and MS; funding acquisition: MS. All authors have read and agreed to the published version of the manuscript.

VIII. Sample collection and preparation: PE; isolation, chemical analysis, and review: PE, AM, and NAL-L; data analysis: PE and AM; writing—original draft preparation: PE and AM; LC–MS/MS (QqQ) analysis and review: MLG; review and editing: MS and MCM. All authors contributed to the study conception and design. All authors read and approved the final manuscript.

Acknowledgements

I would like to begin by expressing my deepest and sincerest gratitude to my supervisor, Marc Stadler. His continuous guidance, support, and trust throughout this journey have been invaluable. From the moment he welcomed me during my internship, he believed in my potential and supported my application for the DAAD (German Academic Exchange Service) scholarship. His mentorship and encouragement throughout my PhD have shaped my personal and professional growth.

I extend my thanks to Prof. Dr. André Fleißner for kindly agreeing to serve as the second reviewer of this thesis, and to Prof. Dr. Ingo Ott for chairing my defense. My sincere appreciation goes to Dr. Kirsten Harmrolfs and Dr. Wolfgang Maier for their guidance and support as members of my thesis committee.

I gratefully acknowledge the DAAD for supporting my PhD through a scholarship, as well as the "Mycobiomics" project, funded by the European Union's Horizon 2020 research and innovation program (RISE) under the Marie Skłodowska-Curie grant, for supporting my three-month research stay at BIOTEC in Thailand.

I am also profoundly grateful to Dr. Njogu M. Kimani, Prof. Dr. Sherif S. Ebada, and PD Dr. Frank Surup, whose work in structure elucidation was essential to the success of this thesis. My gratitude extends to Dr. Samad Ashrafi for his valuable contributions to the isolation and description of the fungal strains.

My heartfelt thanks extend to Khadija and JP, who supervised me during my internship and the early stages of my PhD, respectively. Their patience, knowledge, and kindness helped me build confidence in the laboratory and set the foundation for the work that followed.

A very special thank you goes to Dr. Jennifer Luangsa-ard, Tony, Aey, Peem, View, and Wawa for the unforgettable months I spent at BIOTEC in Thailand. Your warm hospitality made me feel at home from the very first day. I am deeply grateful for your guidance, the joyful atmosphere in the lab, our road trips, and for introducing me to Thai culture.

I am also grateful to my master's student, Janette; working with you was a great pleasure and a privilege to get to know the wonderful person you are. I also appreciate the opportunity to

collaborate with Aida, Lina, Diego, Pierine, and Yoyo during their research stays at MWIS. I learned something valuable from each of you.

Special thanks to my dear friends from the "big office"—Özge, Rita, and Blondelle. You turned long working hours into something meaningful, filled with shared stories, laughter, support, and invaluable companionship. I feel lucky to have crossed paths with you. And Rita and Özge, our "3-country trips" and all the amazing journeys we shared will remain cherished memories.

A warm thank you goes to Ruth, my partner in crime, for our spontaneous and crazy plans. You have become a truly special friend, and I am deeply grateful for welcoming me to Spain and for visiting Colombia to let me share my country with you. I look forward to our future adventures. My heartfelt appreciation also goes to Laura for being such a wonderful friend, bringing joy into my life, and offering warmth and sincerity. Although our time together in Germany was brief, it was more than sufficient to establish a lifelong friendship, and I am immensely proud of you.

I also wish to thank my "brothers-in-law"—Esteban, Sebastian, and Bank—for the many shared moments, laughter, support, and the warmth of family you brought into my life.

My appreciation extends to Alexandra, Lilly, Yang-Peng, Peggy, Rahel, Marjorie, Carolina, Karen, Java, and Nina for their kindness, encouragement, and the positive energy they each contribute. Thank you as well for the many delightful moments we have shared.

I would like to express my gratitude to the current and former members of MWIS—including PhD students, lab mates, technicians, and everyone I met along this journey—Silke, Tanja, Esther, Manuela, Lisha, Renato, Ew, Changlin, Aileen, Christiane, Christopher, Winnie, Birthe, Hedda, Anke, Shabari, Caren, Ellen, Miriam, Christin, Wera, Adela, Tian, Gicky, Gift, Hao, Dana, Max, and Axel. My apologies if I have forgotten anyone.

Of course, I am deeply thankful to my best friends in Colombia—Sara, Luisa, Isabella, Camilo, Mauricio, Alejandra, Juan Manuel, and Jhan. Your unconditional support over the years and the countless plans we have shared have brought me immense joy. I truly value the effort you all make to spend time together, almost every day, during my visits to Colombia in December. Your friendship is a constant source of joy and comfort, and I feel incredibly fortunate to have such amazing people by my side.

I must also express my heartfelt gratitude to my Colombian adoptive family in Germany—Rosa, Howard, Victoria, and Sofía—for opening your home to me, caring for me, and making me feel like part of the family. I also wish to thank Michael for his generosity and for welcoming me into his home.

My heartfelt and loving thanks go to mi monito, Nathan. Je weet dat ik van je hou met heel mijn hart, en elke dag ben ik dankbaar dat ik jou aan mijn zijde heb. Dank je om bijzondere en mooie momenten met mij te delen die alleen wij begrijpen. Dank je om voor mij te zorgen, mij te steunen en mij kracht te geven in moeilijke tijden. Het is een geschenk om te weten dat ik altijd op jou kan rekenen, dat je er zult zijn om mij te beschermen en mijn leven mooier te maken met je liefde.

Finalmente, estoy profundamente agradecida con mis papás, quienes han sido mi mayor pilar durante todos estos años. Gracias por su apoyo incondicional, por estar siempre pendientes aunque estemos a la distancia, y por acompañarme en cada paso de mis estudios. Gracias por enseñarme, con su ejemplo, la importancia del esfuerzo, la perseverancia y la honestidad, y por darme siempre el ánimo y la confianza para seguir adelante. No habría llegado hasta aquí sin ustedes, y en gran parte todo lo que soy se lo debo a su amor y guía constantes.

Table of Contents

Zusammenfassung

Pilze stellen eine der vielfältigsten und ökologisch wichtigsten Organismengruppen dar. Sie sind dafür bekannt, dass sie eine breite Palette von Sekundärmetaboliten produzieren, die ökologische Interaktionen vermitteln und bemerkenswerte biologische Aktivitäten aufweisen. Diese Metaboliten, darunter Polyketide, nichtribosomale Peptide, Terpenoide und Alkaloide, dienen seit jeher als wertvolle Quellen für antitumorale, entzündungshemmende, immunsuppressive und cholesterinsenkende Wirkstoffe sowie für Antibiotika, Antimykotika und Anthelmintika. Trotz ihrer etablierten Bedeutung bleibt das Potenzial des Pilzsekundärstoffwechsels weitgehend ungenutzt, insbesondere bei ökologisch spezialisierten Gruppen wie Nematoden-assoziierten, entomopathogenen und Weißfäulepilzen.

Die zunehmende Bedrohung durch antimikrobielle Resistenzen unterstreicht den dringenden Bedarf an der Entdeckung und Entwicklung neuer Wirkstoffe mit neuartigen Wirkmechanismen, wobei Pilze als unschätzbare, aber noch wenig erforschte Reservoirs chemischer Vielfalt und bioaktiver Sekundärmetaboliten gelten. In dieser Arbeit wird die Vielfalt der Sekundärmetaboliten von Pilzen unterschiedlicher ökologischer Herkunft untersucht, darunter neun Nematoden-assoziierte Stämme der Ordnung Pleosporales, der entomopathogene Pilz *Blackwellomyces roseostromatus* und der Weißfäulepilz *Panus strigellus*. Darüber hinaus wurden im Rahmen von Kooperationsprojekten die Sekundärmetaboliten der nematodenfeindlichen Pilze *Pochonia chlamydosporia, Polyphilus frankenii*, *P. sieberi*, und *Lachnum* sp. sowie vierzehn entomopathogene Stämme aus der Ordnung Hypocreales untersucht. Alle untersuchten Stämme wurden sowohl unter flüssigen als auch unter festen Fermentationsbedingungen kultiviert, und ihre Extrakte wurden mittels HPLC-DAD/MS analysiert, gefolgt von einer Fraktionierung durch chromatographische Techniken. Die Strukturaufklärung der isolierten Verbindungen erfolgte durch fortschrittliche spektroskopische Methoden, einschließlich 1D- und 2D-NMR, ECD, UV, OR und HR-ESI-MS, sowie bei Bedarf durch Derivatisierungsmethoden wie die Analyse nach Marfey oder Mosher. Die isolierten Metaboliten wurden auf ihre biologische Aktivität gegenüber einer Reihe von grampositiven und gramnegativen Bakterien, Pilzen, Säugetierzelllinien und dem Fadenwurm Caenorhabditis elegans untersucht.

Diese Forschung führte zur Isolierung und Charakterisierung von mehr als 60 Verbindungen, darunter noch nie dagewesene Sekundärmetaboliten mit weitreichenden biologischen

Eigenschaften. Zu den bemerkenswerten Entdeckungen aus Nematoden-assoziierten Pilzen gehören neuartige Cyclodepsipeptide und Tetraminsäuren aus *Polydomus karssenii*, die selektive antimikrobielle und nematizide Aktivitäten zeigten. Verbindungen aus *Murispora* sp. zeigten ebenfalls eine starke antimikrobielle und nematizide Wirkung, was ihr Potenzial für die biologische Bekämpfung von Nematoden unterstreicht. Darüber hinaus produzierten vier Pleosporales-Stämme, die bisher unbeschriebene Taxa darstellen, Preussomerine und Makrolide mit starken zytotoxischen und antimikrobiellen Aktivitäten. Bemerkenswerterweise wurde ein Mykotoxin aus dem biologischen Nematodenbekämpfungsmittel *Pochonia chlamydosporia* entdeckt, das eine unerwartete Facette seines Sekundärstoffwechsels offenbart. Außerdem wurden aus *Pyrenochaeta* sp. neue Xanthon- und Anthrachinon-Derivate gewonnen. Der entomopathogene Pilz *B. roseostromatus* produzierte bioaktive Metaboliten mit selektiver zytotoxischer und nematizider Wirkung, während Metaboliten aus dem Weißfäulepilz *Panus strigellus* antimikrobielle und zytotoxische Eigenschaften zeigten.

Insgesamt unterstreicht diese Forschung die bemerkenswerte chemische Vielfalt und das biologische Potenzial von Pilzsekundärmetaboliten und erweitert das chemische und biologische Wissen über Nematoden-assoziierte, entomopathogene und Weißfäulepilze erheblich. Die Ergebnisse zeigen das ungenutzte Potenzial dieser Pilze als Quelle neuartiger Naturstoffe mit vielversprechenden Anwendungen in der biologischen Schädlingsbekämpfung und in der Pharmazie.

Summary

Fungi represent one of the most diverse and ecologically important groups of organisms, renowned for producing a vast array of secondary metabolites that mediate ecological interactions and exhibit remarkable biological activities. These metabolites, including polyketides, nonribosomal peptides, terpenoids, and alkaloids, have historically served as valuable sources of antitumor, anti-inflammatory, immunosuppressive, and cholesterol-lowering agents, as well as antibiotics, antifungals, and anthelmintics. Despite their established importance, the potential of fungal secondary metabolism remains largely untapped, particularly among ecologically specialized groups such as nematode-associated, entomopathogenic, and white-rot fungi.

The escalating threat of antimicrobial resistance underscores an urgent need for the discovery and development of new compounds with novel mechanisms of action, positioning fungi as invaluable yet underexplored reservoirs of chemical diversity and bioactive secondary metabolites. This thesis investigates the diversity of secondary metabolites from fungi of different ecological origins, including nine nematode-associated strains of the order Pleosporales, the entomopathogenic fungus *Blackwellomyces roseostromatus*, and the white-rot fungus *Panus strigellus*. Additionally, as part of collaborative projects, this thesis also studied the secondary metabolites of the nematode-antagonistic fungi *Pochonia chlamydosporia*, *Polyphilus frankenii*, *P. sieberi*, and *Lachnum* sp., along with fourteen entomopathogenic strains from the order Hypocreales. All studied strains were cultivated under both liquid and solid-state fermentation conditions, and their extracts were analyzed using HPLC-DAD/MS, followed by fractionation through chromatographic techniques. Structural elucidation of the isolated compounds was achieved through advanced spectroscopic methodologies, including 1D and 2D NMR, ECD, UV, OR, and HR-ESI-MS, along with derivatization methods such as Marfey's and Mosher's analyses when required. The isolated metabolites were evaluated for biological activity against a panel of Gram-positive and Gram-negative bacteria, fungi, mammalian cell lines, and the nematode *Caenorhabditis elegans*.

This research led to the isolation and characterization of over 60 compounds, including unprecedented secondary metabolites with wide-ranging biological properties. Notable discoveries from nematode-associated fungi include novel cyclodepsipeptides and tetramic acids from *Polydomus karssenii*, which demonstrated selective antimicrobial and nematicidal

activities. Compounds from *Murispora* sp. also exhibited strong antimicrobial and nematicidal activity, highlighting their potential for nematode biocontrol. Furthermore, four Pleosporales strains representing yet undescribed taxa produced preussomerins and macrolides with potent cytotoxic and antimicrobial activities. Remarkably, a mycotoxin was discovered from the nematode biocontrol agent *Pochonia chlamydosporia*, revealing an unexpected facet of its secondary metabolism. In addition, *Pyrenochaeta* sp. yielded novel xanthone and anthraquinone derivatives. The entomopathogenic fungus *B. roseostromatus* produced bioactive metabolites with selective cytotoxic and nematicidal effects, while metabolites from the white-rot fungus *Panus strigellus* showed antimicrobial and cytotoxic properties.

Collectively, this research underscores the remarkable chemical diversity and biological potential of fungal secondary metabolites and significantly expands the chemical and biological knowledge of nematode-associated, entomopathogenic, and white-rot fungi. The findings reveal the untapped potential of these fungi as sources of novel natural products with promising applications in biological control and pharmaceuticals.

Abbreviations

3-DTAs	3-decalinoyltetramic acids
BCC	BIOTEC Culture Collection
BGCs	biosynthetic gene clusters
BRFT	brown rice solid medium
CD	circular dichroism
$CDCl_3$	chloroform-*d* (deuterated chloroform)
COSY	correlation spectroscopy
DAD	diode array detection
DCM	dichloromethane
DKPs	diketopiperazines
DMSO	dimethyl sulfoxide
DNA	Deoxyribonucleic acid
DSM	German Collection of Microorganisms and Cell Cultures (DSMZ)
ECD	electronic circular dichroism
EF1	elongation factor 1 alpha
ESI	electrospray ionization
EtOAc	ethyl acetate
FA	formic acid
GC-MS	gas chromatography–mass spectrometry
HMBC	heteronuclear multiple-bond correlation spectroscopy
HPLC	high performance liquid chromatography
HRMS	high resolution mass spectrometry
HSQC	heteronuclear single-quantum coherence spectroscopy
HR	high resolution
HZI	Helmholtz Centre for Infection Research GmbH
IC_{50}	half-maximal inhibitory concentration
ITS	internal transcribed spacer region (rDNA)
JKI	Julius Kühn-Institut
LC	liquid chromatography
LSU	large subunit (25-28S) ribosomal RNA
MeCN	acetonitrile

MeOH	methanol
MHB	Mueller-Hinton broth
MIC	minimum inhibitory concentration
MRSA	methicillin-resistant *Staphylococcus aureus*
MS	mass spectrometry
NMR	nuclear magnetic resonance
NOESY	nuclear Overhauser effect spectroscopy
NP	normal phase
PCR	polymerase chain reaction
PPNs	plant-parasitic nematodes
Q6 ½	cottonseed-flour-medium
QS	quorum sensing
RNA	ribonucleic acid
ROESY	rotating-frame Overhauser effect spectroscopy
RP	reversed phase
RPB2	RNA polymerase II largest subunit
SAR	structure-activity relationship
TDDFT	time-dependent density functional theory
UV-VIS	ultraviolet–visible spectroscopy
VLC	vacuum liquid chromatography
TOCSY	total correlation spectroscopy
WHO	World Health Organization
WRF	white-rot fungi
YM 6.3	yeast-malt extract medium
ZM ½	sugar-malt-medium

1 Introduction

Fungi are one of the most diverse and ecologically vital kingdoms of life, playing essential roles in natural ecosystems. They are key agents in nutrient cycling, particularly through the degradation of complex biopolymers such as cellulose, lignin, and chitin, thereby releasing nutrients essential for ecosystem balance and productivity (Pointing, 2001; Treseder and Lennon, 2015; Hyde et al., 2019). In addition to their ecological roles, fungi engage in a wide range of symbiotic and pathogenic interactions with other organisms, thereby contributing to the maintenance of ecological balance (Fisher et al., 2012; Bahram and Netherway, 2022; Case et al., 2025). Since the Neolithic era, fungi have also been an integral part of human society, serving as valuable resources in food production and medicine (Castañeda-Ruiz and LaMondia, 2016). The domestication of *Saccharomyces cerevisiae* for brewing and baking represents one of the earliest documented examples of applied mycology, marking the beginning of humanity's deliberate use of fungi for practical purposes such as food production (Replansky et al., 2008). Apart from the multitude of positive aspects of fungi, many fungal species are pathogenic to humans, animals, and plants, causing significant economic losses and global health challenges (Hyde et al., 2018; Fisher et al., 2020). Despite their ecological and economic importance, fungi remain relatively understudied compared to other major kingdoms, such as animals and plants (Hyde et al., 2018). Nevertheless, fungi constitute a highly diverse and biotechnologically valuable group of organisms, with great potential for industrial and pharmaceutical exploitation (Willis, 2018; Hyde et al., 2019; Roth et al., 2023).

Secondary metabolites, often referred to as natural products, are small organic molecules produced by diverse organisms, including plants, bacteria, and fungi, and are derived from intermediates of primary metabolic pathways (Larsen et al., 2005; Keller, 2019). They play vital roles in various ecological processes, including communication, competition, and defense, thereby enhancing the survival of organisms in complex environments. Unlike primary metabolites, which are essential for growth, development, and reproduction and are directly involved in fundamental metabolic processes, secondary metabolites provide adaptive advantages that help organisms to thrive within specific ecological niches (Larsen et al., 2005; Krauss and Nies, 2015; Schrey et al., 2025). To date, over 500,000 secondary metabolites have been described (Bills and Gloer, 2016), with more than 30,000 characterized from fungi (Riedling and Rokas, 2025), highlighting their remarkable chemical diversity. This diversity is often attributed to the immobile nature of fungi and intense ecological competition for space

and resources against other organisms (Spiteller, 2008; Bills and Gloer, 2016; Schrey et al., 2025).

The discovery rate of new fungal metabolites has increased significantly in recent decades, particularly among filamentous Ascomycota and Basidiomycota (Bills and Gloer, 2016). These two fungal phyla are characterized by their complex and diverse secondary metabolisms, driven by extensive biosynthetic gene clusters (BGCs) in their genomes (Rokas et al., 2020). BGCs encode multidomain enzymes, including polyketide synthases, nonribosomal peptide synthetases, terpene synthases, and hybrid systems, that catalyze the synthesis of the backbone of the metabolite (Keller, 2019; Rokas et al., 2020). The intricate biochemical pathways in fungi give rise to an impressive array of secondary metabolites, such as polyketides, nonribosomal peptides, terpenoids, and alkaloids, as well as mixed-origin compounds like meroterpenoids, all exhibiting a broad range of biological activities, enabling fungi to succeed in a wide variety of ecological habitats (Bills and Gloer, 2016; Keller, 2019; Schrey et al., 2025).

1.1 History and Applications of Fungal Secondary Metabolites

Fungal secondary metabolites have long attracted scientific interest as valuable sources of bioactive natural products. They display a broad spectrum of biological activities, including antimicrobial, cytotoxic, immunosuppressive, and nematicidal effects (Bills and Gloer, 2016; Hyde et al., 2019; Schrey et al., 2025), and have found diverse applications in medicine, agriculture, and industry (Bills and Gloer, 2016). Fungi have played a key role in the development of numerous important pharmaceuticals, such as β-lactam antibiotics, statins, and cyclosporin, among other therapeutically relevant compounds (Schrey et al., 2025). Conversely, some fungal metabolites are highly toxic; mycotoxins such as aflatoxins, trichothecenes, fumonisins, and ochratoxin pose serious threats to human and animal health (Bräse et al., 2009; Bills and Gloer, 2016).

Prior to the emergence of modern pharmaceuticals, natural products were the foundation of traditional medicine systems worldwide. Ancient civilizations and indigenous cultures relied on plants, fungi, and other natural sources to prevent and treat diseases, as well as to maintain overall health and well-being (Dias et al., 2012). The modern medical importance of fungi started with the discovery of mycophenolic acid in 1893, the first antibiotic isolated from *Penicillium brevicompactum*. However, its toxic side effects prevented it from being marketed

as an effective antibacterial treatment (Florey et al., 1946; Bentley, 2000). A pivotal milestone occurred in 1928 when Alexander Fleming discovered penicillin G from *P. rubens*, marking the beginning of the "golden age of antibiotic discovery." This period revolutionized global healthcare through the development of numerous antimicrobial agents (Figure 1) (Fleming, 1929; Hutchings et al., 2019). In 1953, Edward Abraham made significant advancements in this field by isolating cephalosporin C from *Acremonium chrysogenum,* a fungus originally isolated and studied by Giuseppe Brotzu in 1945. Cephalosporin C demonstrated antibacterial activity and served as a precursor to the well-known semi-synthetic cephalosporins (Abraham, 1979, 1987; Prescott et al., 2023). By 1964, the first cephalosporin antibiotic, cephalotin, was introduced to the market, and since then, several generations of cephalosporin derivatives have been developed, forming a broad class of clinically important drugs (Newman and Cragg, 2020; Lin and Kück, 2022). In the subsequent years, the discovery of many additional fungal metabolites marked the pharmaceutical industry. For instance, the immunosuppressant cyclosporin A, isolated from *Tolypocladium inflatum* in 1976, revolutionized organ transplantation by preventing the rejection of transplanted organs (Borel et al., 1976; Rüegger et al., 1976; Survase et al., 2011). Similarly, the discovery of lovastatin from *Aspergillus terreus* in 1978 led to the development of the first cholesterol-lowering statin, which was introduced to the market in 1987 and has significantly benefited patients with hypercholesterolemia (Alberts et al., 1980; Tobert, 2003).

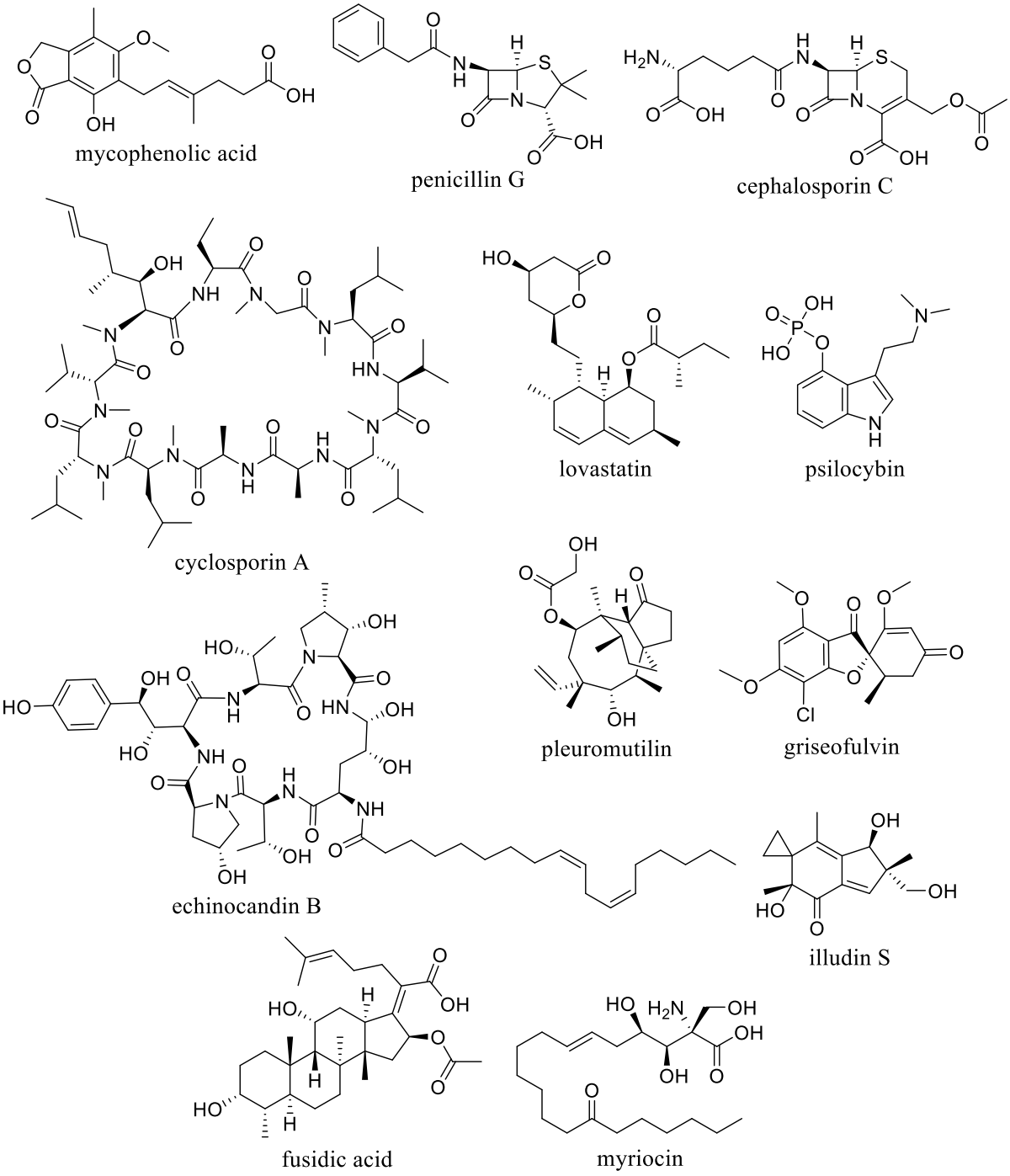

Figure 1. Chemical structures of representative fungal secondary metabolites with major pharmaceutical applications.

The isolation of psilocybin from the fungus *Psilocybe mexicana* in 1958 marked another remarkable milestone. Psilocybin was shown to induce a psychoactive state characterized by physical relaxation and mental alterations (Hofmann et al., 1958). In recent years, psilocybin has gained renewed scientific attention, with growing evidence supporting its potential therapeutic use in treating depression and anxiety disorders (Ross et al., 2016; Kargbo, 2020). Another landmark discovery was the isolation of the first echinocandin, echinocandin B, from

A. delacroxii in 1974, which exhibited potent antifungal activity (Benz et al., 1974). Subsequently, additional echinocandins were discovered, including pneumocandins A_0 and B_0 from *Glarea lozoyensis* and FR901379 from *Coleophoma empetri* (Schwartz et al., 1992; Iwamoto et al., 1994). These natural products served as precursors for the semi-synthetic antifungal drugs anidulafungin, rezafungin, micafungin, and caspofungin (Schrey et al., 2025). Notably, caspofungin was the first semi-synthetic echinocandin approved for medical use in the early 2000s and remains a first-line treatment for invasive mycoses (Johnson and Perfect, 2003; Hüttel, 2021). The most recent class of antibiotics of fungal origin to be introduced for human use is the pleuromutilins. Although pleuromutilin was discovered in 1951 from *Clitopilus passeckerianus* (Kavanagh et al., 1951), its semisynthetic derivative, retapamulin, only entered the market in 2007, marking the first new antibiotic class in decades and the first Basidiomycota-derived antibiotic for human use (Novak, 2011; Paukner and Riedl, 2017). More recently, lefamulin, another semisynthetic pleuromutilin antibiotic, was approved in 2020 for the systemic treatment of bacterial infections (Veve and Wagner, 2018; Newman and Cragg, 2020; Mapook et al., 2022). Beyond the aforementioned classes, several other fungal metabolites, such as illudins, griseofulvin, cytochalasins, fusidic acid, and myriocins, have demonstrated remarkable biological and pharmacological importance. These compounds exhibit diverse properties, ranging from anticancer and antifungal activities to antibacterial and immunosuppressive effects, underscoring the immense potential of fungi as prolific sources of therapeutically valuable natural products (Bills and Gloer, 2016; Schrey et al., 2025).

In agriculture, fungal-derived strobilurins revolutionized crop protection due to their potent fungicidal properties. In 1977, Anke et al. (1977) isolated strobilurin A from *Strobilurus tenacellus*, which later served as the lead structure for the development of several synthetic derivatives, including azoxystrobin and kresoxim-methyl. These compounds significantly improved the control of fungal plant diseases; however, their site-specific mode of action makes them susceptible to rapid resistance development. To mitigate this issue, strobilurin-based fungicides are often applied in combination with other antifungal agents (Bartlett et al., 2002; Debbab and Proksch, 2011; Prado et al., 2025). Another noteworthy example of fungal-derived metabolites with agricultural potential is the class of omphalotins, first discovered from *Omphalotus olearius* in the late 1990s (Sterner et al., 1997). These cyclopeptides, particularly omphalotin A, exhibit highly selective nematicidal activity against root-knot nematodes like *Meloidogyne incognita*. To date, omphalotins have been identified only in *Omphalotus* species (Mayer et al., 1999; Liermann et al., 2009). Their potency and specificity highlight their

promise for environmentally friendly nematode control agents. In the field of veterinary medicine, the contribution of fungal metabolites is also noteworthy. The cyclodepsipeptide PF1022A, isolated from *Rosellinia* sp. in 1992, served as the precursor of emodepside, a semi-synthetic derivative introduced in 2005 as a broad-spectrum anthelmintic for veterinary use. Emodepside is marketed in combination with praziquantel for the treatment of gastrointestinal nematode and cestode infections in cats and dogs (Sasaki et al., 1992; Böhm et al., 2015; Wittstein et al., 2020).

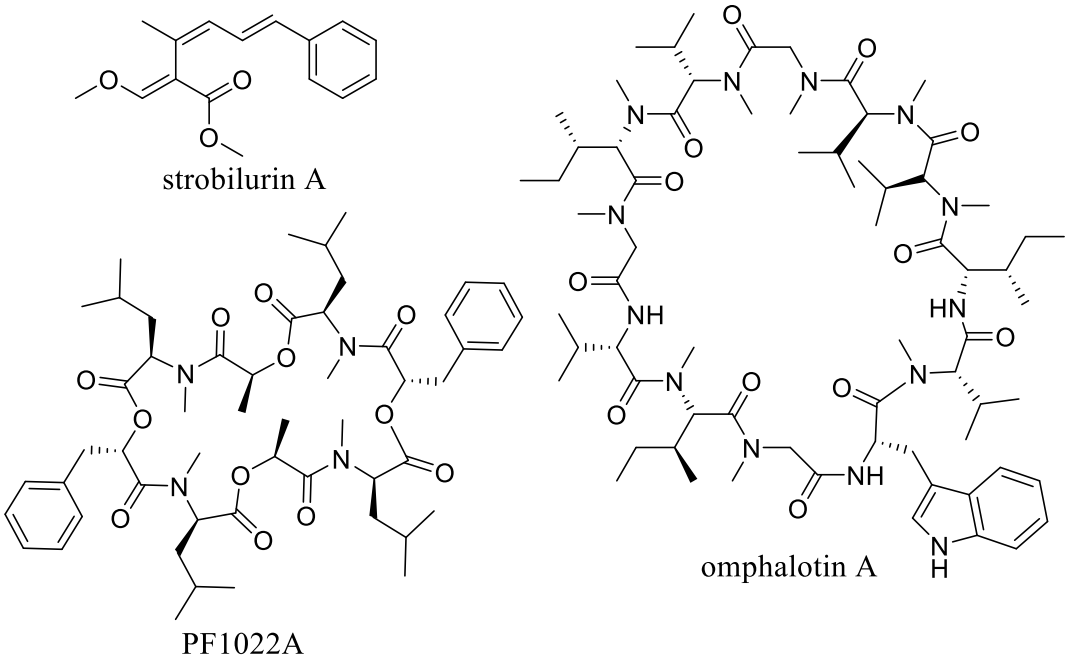

Figure 2. Representative fungal secondary metabolites with agricultural and veterinary applications.

Despite significant advances in modern medicine, antimicrobial-resistant infections currently cause over one million deaths annually worldwide, and it is projected to rise to nearly 10 million deaths per year by 2050 (Naghavi et al., 2024; World Health Organization, 2025). The rapid global spread of antibiotic resistance poses an increasing threat to public health and will continue unless effective interventions are implemented. These interventions include the discovery and development of new drugs with novel modes of action, an urgent need given that most antibiotics currently in use were discovered between the 1950s and 1970s (Fair and Tor, 2014; Naghavi et al., 2024).

1.2 Natural Products from Ecologically Diverse Fungi

1.2.1 Nematode-Associated Fungi

Nematodes (Nematoda) represent one of the most diverse animal phyla, with over 28,000 species described worldwide, many of which pose significant threats to agriculture and human well-being. Nematodes exhibit diverse lifestyles, ranging from free-living species, such as *Caenorhabditis elegans*, to parasitic forms that infect animals, humans, and plants. (Decraemer and Hunt, 2013; Hodda, 2022). Among these, plant-parasitic nematodes (PPNs) are particularly detrimental to global agriculture. Notable examples include root-lesion nematodes (*Pratylenchus* spp.), root-knot nematodes (*Meloidogyne* spp.), and cyst nematodes (*Heterodera* spp. and *Globodera* spp.). PPNs damage plant roots by inducing root-knot galls or infecting the cortical parenchyma, thereby impeding the uptake of water and nutrients by the plant host (Esteves et al., 2015; Mejias et al., 2019; Seong et al., 2021). These infestations result in substantial crop losses, estimated to exceed 150 billion USD annually worldwide. The damage caused by PPNs not only reduces crop productivity but can also lead to plant death, representing a critical challenge for food security and agricultural sustainability (Singh et al., 2015; Degenkolb and Vilcinskas, 2016; Mendoza-De Gives, 2022).

Historically, nematicidal chemicals such as methyl bromide, a genotoxic soil fumigant, have been widely employed to control PPNs (Noling and Becker, 1994). However, their use is associated with serious adverse effects, including indiscriminate destruction of beneficial soil organisms, significant contribution to ozone layer depletion, and increased risk of stomach cancer and other health issues in humans (Noling and Becker, 1994; Barry et al., 2012). Consequently, the use of methyl bromide and similar nematicides has been drastically restricted or banned (Barry et al., 2012; Hyde et al., 2019). There is increasing interest in finding safer and more sustainable alternatives, with natural products emerging as an up-and-coming option. In this context, biological control strategies that use secondary metabolites from nematophagous fungi are gaining attention as a practical and environmentally friendly approach for managing PPNs (Hyde et al., 2019; Seong et al., 2021).

Nematophagous fungi, a diverse group predominantly within the phylum Ascomycota, are fungi associated with nematodes that serve as natural predators and parasites of nematodes. They utilize specialized morphological adaptations, such as hyphal traps, adhesive spores, and egg-penetrating structures, to capture, kill, and digest nematodes (Nordbring-Hertz et al.,

2011). Based on their infection strategies, these fungi are typically classified into three main groups: nematode-trapping, endoparasitic, and egg- or cyst-parasitic fungi. The latter group develops specialized infection structures at the hyphal tips called appressoria to penetrate and colonize the nematode eggshell (White and Rodriguez-Kabana, 1984; Lopez-Llorca et al., 2002; Nordbring-Hertz et al., 2011). During early infection stages, fungal hyphae enclose or tightly adhere to the eggshell before penetrating it through a combination of mechanical, biochemical, and enzymatic processes (Lopez-Llorca et al., 2008; Rahman et al., 2023). Many nematophagous fungal species are also associated with plants as endophytes or function as wood decomposers (Luo et al., 2004; Larriba et al., 2014; de Mattos-Shipley et al., 2016). The endophytic lifestyle is notably common among nematophagous and entomopathogenic fungi within the order Hypocreales. This lifestyle may have evolved as part of a symbiotic relationship, where the fungus protects the plant against parasites while benefiting from the association (Naranjo-Ortiz and Gabaldón, 2019). Notably, nematophagous fungi produce a broad array of secondary metabolites with nematicidal, antimicrobial, and cytotoxic properties that enhance host infection and ecological competitiveness. This remarkable biosynthetic capacity underscores their potential as valuable sources of novel, environmentally safe nematicidal agents (Degenkolb and Vilcinskas, 2016; Seong et al., 2021; Al-Ani et al., 2022).

Several nematophagous fungal species have been identified as valuable sources of potent natural products (Figure 3) with diverse biological activities. For example, the egg-parasitic fungus *Pochonia chlamydosporia*, which infects the PPNs *Heterodera* spp. and *Meloidogyne* spp., produces several bioactive metabolites, including the polyketides pochonin A, monorden, and aurovertin D. These compounds exhibit antiviral, antifungal, and nematicidal activities, respectively (Hellwig et al., 2003; Stadler et al., 2003; Wang et al., 2015). Another noteworthy fungus, *Paecilomyces variotii*, parasitizes eggs of the soybean cyst nematode *H. glycines* and produces sphingofungins E and F, and viriditoxin, which display antifungal and cytotoxic properties, respectively (Horn et al., 1992; Samson et al., 2009). Additionally, *Ijuhya vitelline*, isolated from eggs of the cereal cyst nematode *H. filipjevi*, produces the cytotoxic compounds chaetoglobosins A and B, along with the nematicidal leucinostatins Q, P, and U (Ashrafi et al., 2017; Moussa et al., 2020). Recent studies have further discovered bioactive compounds from various fungi associated with *H. filipjevi* eggs: *Polydomus karssenii* produces ophiotine, which is effective against its nematode host (Helaly et al., 2018); *Laburnicola nematophila* yields dactylfungin derivatives with potent antifungal activity against azole-resistant *Aspergillus fumigatus* (Wennrich et al., 2024); and *Polyphilus sieberi* produces talaroderxine D, which

inhibits biofilm formation by *Staphylococcus aureus* (Wennrich et al., 2024). Collectively, the rich diversity of fungal natural products from nematophagous fungi holds significant promise as environmentally friendly biocontrol agents for managing PPNs and antimicrobial agents (Degenkolb and Vilcinskas, 2016; Seong et al., 2021; Al-Ani et al., 2022; Rahman et al., 2023).

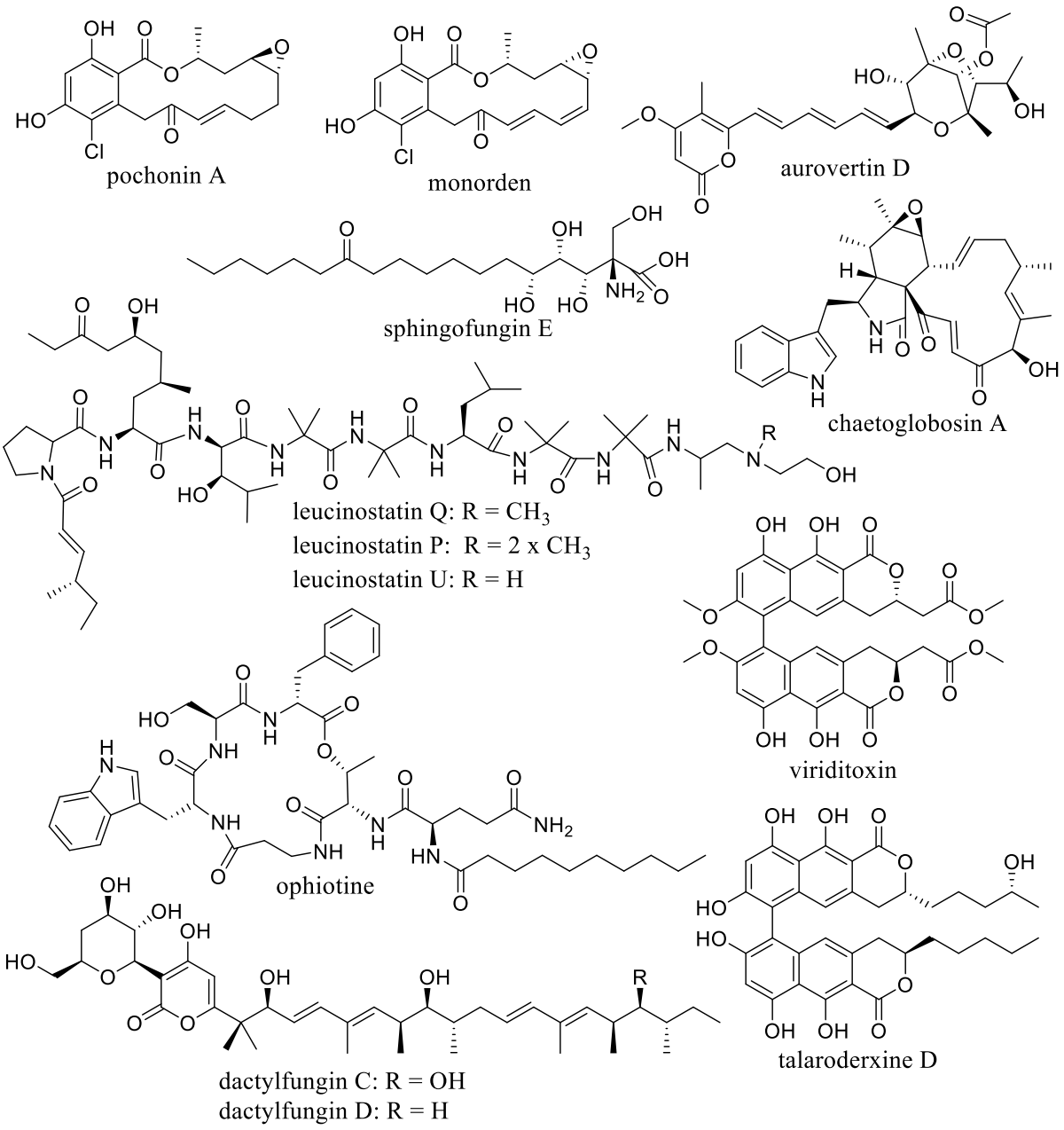

Figure 3. Chemical structures of representative secondary metabolites from nematophagous fungi.

1.2.2 Entomopathogenic Fungi

Insects are the most taxonomically diverse group of organisms on Earth, with over 1 million described species, representing more than half of all known species (Tihelka et al., 2021; Schowalter, 2022). Many insect species pose serious challenges in agriculture and forestry as major crop pests, causing considerable economic losses worldwide, particularly in tropical and subtropical regions. These pests threaten global food security by substantially reducing crop yields and impairing tree growth and productivity in forests (Oerke, 2006; Kenis et al., 2017). As a result, there is increasing scientific interest in developing safer and more sustainable insect pest management strategies. Among these approaches, biological control has emerged as a promising and environmentally friendly method, utilizing natural enemies such as predators, parasitoids, and entomopathogenic organisms to effectively regulate insect populations (Van Lenteren and Bigler, 2008; Kenis et al., 2017; Bout et al., 2022).

Entomopathogenic fungi, particularly those belonging to the order Hypocreales (class Sordariomycetes), stand out as notable biological control agents due to their unique mode of action against insects (Meyling and Eilenberg, 2007; Lovett and St. Leger, 2017). Fungal conidia adhere to and germinate on the insect cuticle, followed by the enzymatic degradation of the cuticle by proteases, chitinases, and lipases, allowing these fungi to penetrate their host. Once inside, these fungi induce insect death through several mechanisms, including nutrient depletion, fungal proliferation, and the secretion of insecticidal secondary metabolites (Ortiz-Urquiza and Keyhani, 2013). Prominent fungal entomopathogenic genera include *Beauveria*, *Metarhizium*, *Isaria*, and *Cordyceps*, with *Beauveria* and *Metarhizium* being the most extensively studied and widely used as biological control agents (L. Zhang et al., 2020; Sharma et al., 2023). *Beauveria* species, especially *B. bassiana*, are well-known for producing a variety of bioactive metabolites, including beauvericin, bassianolide, bassianin, tenellin, and oosporein (Figure 4), which exhibit potent insecticidal, cytotoxic, and antimicrobial properties (Gibson et al., 2014). On the other hand, *Metarhizium* species, particularly *M. anisopliae*, are prolific producers of structurally and functionally diverse secondary metabolites, with destruxins being among the most well-characterized (Figure 4). Destruxins exhibit a broad spectrum of beneficial properties, including antibiotic, antitumoral, antifungal, anti-inflammatory, and immunosuppressant effects (Wang et al., 2012; Barelli et al., 2022). In addition to their roles as entomopathogens, these bioactive compounds hold significant promise for biotechnological and pharmaceutical applications, driving growing interest in their potential use as novel

therapeutics and biopesticides. Recent advances in fungal genomics and metabolomics have revealed that entomopathogenic fungi possess remarkably rich BGCs, many of which remain unexplored. This indicates a vast reservoir of untapped chemical diversity, waiting to be discovered and utilized (Gibson et al., 2014; L. Zhang et al., 2020; Bamisile et al., 2021).

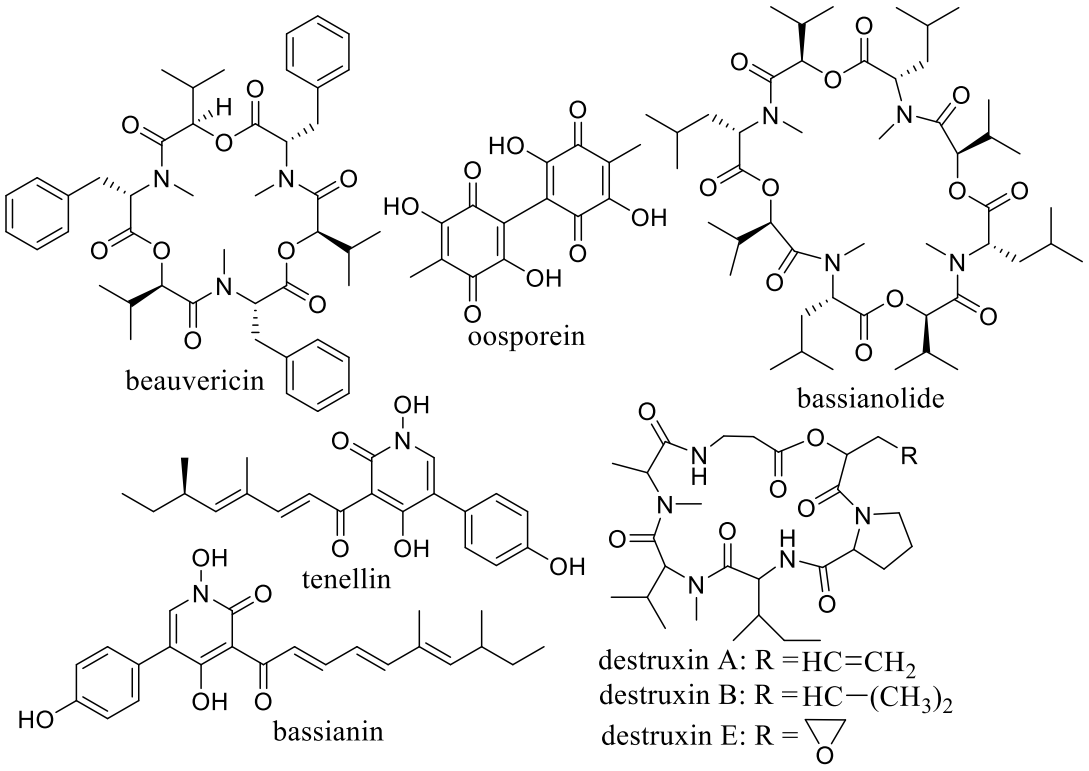

Figure 4. Chemical structures of representative secondary metabolites from entomopathogenic fungi.

1.2.3 White-Rot Fungi

Basidiomycota are renowned for their ability to produce a wide range of secondary metabolites that exhibit various beneficial properties, including antioxidant, antimicrobial, anti-inflammatory, antifungal, and antiviral effects. Notably, some species also produce cytotoxic compounds with potential anticancer applications (Sum et al., 2023; Pinar and Rodríguez-Couto, 2024). Among the basidiomycetes, white-rot fungi (WRF) stand out for their remarkable capacity to decompose all major components of wood, playing an essential role in carbon and nitrogen cycling by breaking down non-living organic matter (Pointing, 2001; Pinar and Rodríguez-Couto, 2024). Although most WRF are basidiomycetes, a few ascomycete genera within the Xylariales are also involved in lignin and wood decay processes, with white-

rot-like activity in wood decomposition (Eaton and Hale, 1993; Pointing, 2001; Rajtar et al., 2023; Janusz et al., 2024).

WRF predominantly inhabit hardwood forest ecosystems and are prolific producers of structurally diverse secondary metabolites (Figure 5) that exhibit a wide range of biological activities (Zheng et al., 2010; Shankar and Sharma, 2022; Pinar and Rodríguez-Couto, 2024). Among the notable compounds produced by WRF with pharmaceutical applications is sizofiran, isolated from *Schizophyllum commune*. Sizofiran functions as an immunoadjuvant and has been used in the treatment of various neoplasms, particularly gastric and cervical cancers (Miyazaki et al., 1995; Chaichian et al., 2020). Schizostatin, also derived from *S. commune*, exhibits antifungal activity against plant pathogens such as *Colletotrichum gloeosporioides* and *Botrytis cinerea* (Park et al., 2020; Shankar and Sharma, 2022). Another noteworthy compound is irofulven, produced by *Omphalotus olearius*, which has demonstrated antitumor efficacy in patients with advanced pancreatic cancer (Eckhardt et al., 2000). *Inonotus obliquus* yields lanostane-type triterpenoids (e.g., inotodiol) that exhibited anti-neuroinflammatory effects and cytotoxicity against human lung adenocarcinoma cells (Taji et al., 2008; F. Zhao et al., 2015; Kou et al., 2021). Furthermore, *Hericium erinaceus* produces erinacines and hericenones, known for their neuroprotective properties, including inhibition of inflammatory cytokine expression (Lee et al., 2014; Thongbai et al., 2015). Notably, erinacine A has been shown to improve Alzheimer's disease-related pathologies in transgenic mouse models (Tsai-Teng et al., 2016). The ongoing discovery and characterization of secondary metabolites from WRF highlight the importance of continued research to harness the therapeutic and industrial benefits of these fungi (Kijpornyongpan et al., 2022; Pinar and Rodríguez-Couto, 2024).

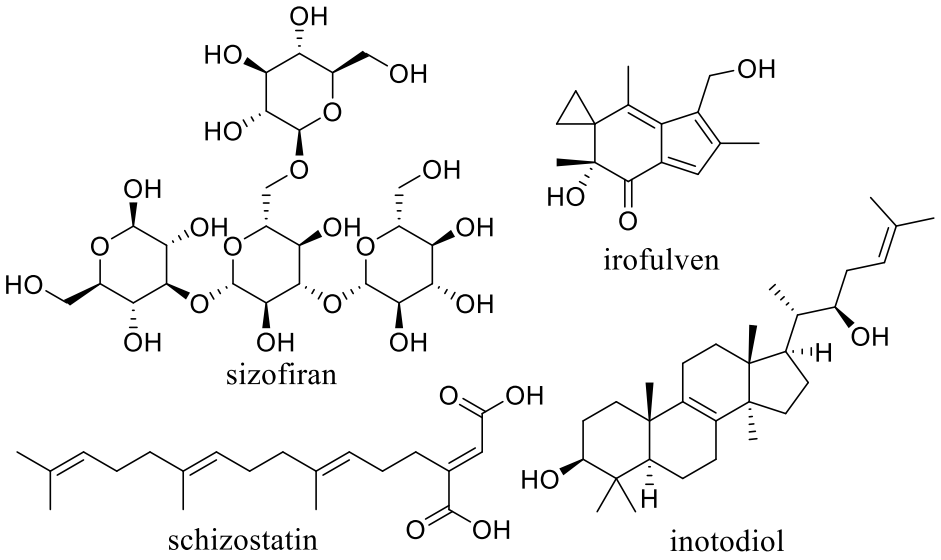

Figure 5. Chemical structures of representative secondary metabolites from white-rot fungi.

1.3 Aim and Outline of the Thesis

This thesis aims to explore the chemical diversity and biological potential of secondary metabolites produced by fungi from various ecological sources, highlighting their promise as novel biocontrol agents and therapeutic leads. The thesis focuses primarily on the secondary metabolites of nematode-associated fungi belonging to the order Pleosporales (Dothideomycetes, Ascomycota), most of which are still undescribed species. In addition, the secondary metabolites of the entomopathogenic fungus *Blackwellomyces roseostromatus* (Hypocreales, Sordariomycetes) and the white-rot fungus *Panus strigellus* (Polyporales, Agaricomycetes) were studied. Although these fungi are recognized for their ecological significance and potential biotechnological applications, their secondary metabolism remains largely unexplored.

Therefore, the main objectives of this research were to isolate and structurally characterize fungal secondary metabolites from different ecological sources, and to evaluate their biological activities, with particular focus on antimicrobial, cytotoxic, and nematicidal properties. To achieve these goals, fungal strains were cultivated under different culture conditions to induce metabolite biosynthesis. The resulting crude extracts were then fractionated using advanced chromatographic techniques, and the pure compounds were structurally elucidated. Both previously undescribed and known metabolites were subsequently assessed for their biological activities using standardized bioassays.

This thesis begins with an introduction that provides the scientific background of the topic, emphasizing the historical importance and untapped potential of fungi as prolific sources of natural products for pharmaceutical, agricultural, and environmental applications. Following this, the general methodology employed throughout the thesis is outlined. The core findings are then presented, focusing on the chemical diversity and biological evaluation of secondary metabolites from the studied fungal strains representing nematode-associated, entomopathogenic, and white-rot fungi. Subsequently, the key contributions of the research are summarized, along with a discussion on the future research directions to further explore natural product discovery. Finally, the discoveries from collaborative projects conducted during the course of this work are presented.

2 Materials and Methods

2.1 Fungal Material

The nematode-associated fungal strains studied in this thesis were provided by Dr. Samad Ashrafi from the Julius Kühn Institute (JKI – Federal Research Centre for Cultivated Plants, Braunschweig, Germany) and by the Leibniz Institute DSMZ, also in Braunschweig, Germany. Special emphasis was placed on fungi isolated from the eggs of the cereal cyst nematode *Heterodera filipjevi*, collected from agricultural fields in Turkey. Additional comparative analyses included related strains isolated as endophytes from the roots of *Microthlaspi perfoliatum*, *Asclepias syriaca*, and *Pinus sylvestris* to evaluate their similarities and potential differences from those parasitizing nematode eggs. *Lachnum* sp. DSM 116717, originally isolated from the dead stalk of the reed grass *Phragmites communis*, was also included in this study for evaluation as a potential nematode antagonist. The entomopathogenic fungal strain *Blackwellomyces roseostromatus* BCC56290 was isolated from a lepidopteran larva in Thailand and provided by M.Sc. Artit Khonsanit through collaboration with the National Center for Genetic Engineering and Biotechnology (BIOTEC, Bangkok, Thailand). Additionally, the white-rot fungal strain *Panus strigellus* CM-UDEA-H9 was isolated from decayed hardwood in Colombia and provided by Dr. Aida M. Vasco-Palacios through collaboration with the University of Antioquia in Medellin, Colombia. An overview of the fungal strains used in this study, including their systematic placement, isolation source, host or substrate, and lifestyle, is summarized in Table 1. All strains were maintained on YM 6.3 agar (10 g/L malt extract, 4 g/L D-glucose, 4 g/L yeast extract, 20 g/L agar; pH adjusted to 6.3 before autoclaving) at 23 °C in the dark.

Table 1. Fungal strains investigated during the course of this study

Order	Genus	Species	Strain ID	Isolation source	Host / Substrate	Lifestyle / Role	Publication
Pleosporales	*Polydomus*	*karssenii*	JKI 73120	roots	*Microthlaspi perfoliatum*	Endophyte	III
			DSM 11209	cyst/egg	*Heterodera filipjevi*	Nematode-associated	
			DSM 1106825	cyst/egg	*H. filipjevi*	Nematode-associated	Unpublished
	Murispora	unknown*	JKI 72806	cyst/egg	*H. filipjevi*	Nematode-associated	Unpublished
	unknown*	unknown*	JKI 73016	cyst/egg	*H. filipjevi*	Nematode-associated	Unpublished
			JKI 72728	cyst/egg	*H. filipjevi*	Nematode-associated	Unpublished
		unknown*	JKI 73278	roots	*M. perfoliatum*	Endophyte	Unpublished
			JKI 73275	roots	*M. perfoliatum*	Endophyte	Unpublished
	Pyrenochaeta	sp.	JKI 72955	cyst/egg	*H. filipjevi*	Nematode-associated	Unpublished
Helotiales	*Polyphilus*	*siebri*	DSM 106515	roots	*Asclepias syriaca*	Endophyte	IV
		frankenii	DSM 106521	roots	*Pinus sylvestris*	Endophyte	
	Lachnum	sp.	DSM 116717	dead stalk	*Phragmites communis*	Saprotroph/nematode antagonist	V
Hypocreales	*Pochonia*	*chlamydosporia*	DSM 119501	cyst/egg	*H. filipjevi*	Nematode-associated	VI
	Blackwellomyces	*roseostromatus*	BCC 56290	larva	Lepidoptera sp.	Entomopathogen	II
Polyporales	*Panus*	*strigellus*	CM-UDEA-H9	decayed hardwood	unknown	White-rot saprotroph	I

*: Previously undescribed.

2.2 HPLC Profiling of Fungal Secondary Metabolites

To investigate the secondary metabolite profiles of the fungal strains studied in this thesis, a variety of liquid and solid media were evaluated to identify optimal growth conditions and maximize metabolite diversity. Liquid-state fermentation was carried out using three different media: YM 6.3 (10 g/L malt extract, 4 g/L D-glucose, 4 g/L yeast extract, pH 6.3 before autoclaving), Q6 ½ (10 g/L glycerol, 5 g/L cotton seed flour, 2.5 g/L D-glucose, pH 7.2 before autoclaving), and ZM ½ (5 g/L molasses, 5 g/L oatmeal, 4 g/L mannitol, 4 g/L sucrose, 1.5 g/L $CaCO_3$, 1.5 g/L D-glucose, 0.5 g/L lactalbumin enzymatic hydrolysate, 0.5 g/L $(NH_4)_2SO_4$, pH 7.2 before autoclaving). For solid-state fermentation, BRFT and WOFT media (1 g/L yeast extract, 0.5 g/L K_2HPO_4, and 0.5 g/L sodium tartrate; 100 mL of this solution was added to 28 g of brown rice or whole oats prior to autoclaving) were used.

2.2.1 Cultivation for Secondary Metabolite Screening

The fungal strains were initially cultivated on YM 6.3 agar (10 g/L malt extract, 4 g/L D-glucose, 4 g/L yeast extract, 20 g/L agar; pH 6.3 before autoclaving) at 23 °C. For liquid-state fermentation, five small agar pieces (0.25 cm^2) from well-grown cultures were used to inoculate 500 mL Erlenmeyer flasks containing 200 mL of the selected liquid medium. The cultures were incubated at 23 °C on a rotary shaker at 140 rpm in the dark, and glucose concentration was monitored daily with Medi-Test glucose strips (Macherey-Nagel®, Düren, Germany). To assess the effect of different cultivation times, fermentations were terminated after 2 and 5 days of glucose consumption. For solid-state fermentation, six 500 mL Erlenmeyer flasks containing the selected solid medium were inoculated with 6 mL of pre-cultured YM 6.3 seed culture and incubated at 23 °C in the dark. Solid cultures were harvested in duplicates after 2, 3, and 4 weeks.

2.2.2 Extraction of Secondary Metabolites from Liquid-State Fermentation

Mycelium and supernatant were separated using vacuum filtration with a Büchner funnel lined with a filter disk. Following pH measurement, the supernatant was extracted three times with an equal volume of ethyl acetate (EtOAc) in a separatory funnel. The combined organic phases were dried over anhydrous sodium sulfate (Na_2SO_4) and concentrated under vacuum using a rotary evaporator at 40 °C. The mycelium was covered with acetone and extracted in an ultrasonic bath at 40 °C for 30 minutes. This extraction was repeated two more times. The combined acetone extracts were evaporated under vacuum, resulting in a residual aqueous

phase that was then extracted with EtOAc, following the same procedure used for the supernatant. After drying, all extracts were dissolved in a 1:1 mixture of methanol (MeOH) and acetone and transferred to 4 mL brown glass vials. The extracts were dried under a nitrogen flow at 37 °C, quantified, and stored at -20 °C for future analysis.

2.2.3 Extraction of Secondary Metabolites from Solid-State Fermentation

The solid cultures were initially treated with acetone. The extraction process followed the same steps used for the mycelium from liquid-state fermentation. To remove high concentrations of fatty acids, the crude extracts were dissolved in 10 mL of MeOH and then extracted twice with 45 mL of *n*-heptane. The MeOH and *n*-heptane fractions were collected separately and dried under vacuum at 40 °C. The dried crude extracts were dissolved in a MeOH and acetone (1:1) solution, transferred to 4 mL brown glass vials, dried under nitrogen flow at 37 °C, quantified, and stored at −20 °C until further analysis.

2.2.4 Identification and Dereplication of Secondary Metabolites by HPLC-DAD/MS and HPLC-HRMS

The crude extracts from the screening cultures were analyzed for secondary metabolite profiling using high-performance liquid chromatography coupled with diode array detection and mass spectrometry (HPLC-DAD/MS). Dried extracts were dissolved in a 1:1 mixture of MeOH and acetone and adjusted to a concentration of 4.5 mg/mL. From this solution, 2 µL was injected into an UltiMate® 3000 Series UHPLC system (Thermo Fisher Scientific, Waltman, MA, USA) equipped with an electrospray ionization (ESI) ion trap mass spectrometer (amaZon speed™, Bruker Daltonics GmbH, Bremen, Germany) operating in both positive and negative ionization modes. Separation was carried out using an Acquity® UPLC BEH column (2.1 x 50 mm, 1.7 µm; Waters, Milford, MA, USA) as the stationary phase with a mobile phase of solvent A (HPLC-grade water + 0.1% formic acid (FA)) and solvent B (acetonitrile (MeCN) + 0.1% FA). The gradient elution started with 5% B for 0.5 min, increased linearly to 100% B over 19.5 min, then held at 100% B for 5 min, with a flow rate of 0.6 mL/min. Detection was performed using DAD in the range of 190–600 nm.

In order to identify the structural formulas of the metabolites from the most promising extracts, high-resolution measurements were performed at 1 mg/mL using HPLC-high resolution MS (HPLC-HRMS). This involved the use of an Agilent 1200 Infinity Series HPLC (Agilent Technologies, Santa Clara, CA, USA) in combination with a maXis® time-of-flight mass

spectrometer (ESI-TOF-MS, Bruker). The same stationary phase, mobile phase, and gradient elution were used as for HPLC-DAD/MS. Parameters included a scan range of 100–2500 m/z, scan rate of 2 Hz, capillary voltage of 4500 V, and dry gas temperature of 200 °C. The acquired spectra were analyzed with Bruker DataAnalysis software (version 6.1), and molecular formulas were deduced from fragmentation patterns. Finally, dereplication of known metabolites was performed by comparison with commercial databases (Dictionary of Natural Products, SciFinder) and publicly available repositories such as the Natural Products Atlas.

2.2.5 Antimicrobial Bioactivity Screening of Crude Extracts

The antimicrobial activity of the crude extracts was assessed using a serial dilution assay against the Gram-positive bacterium *Bacillus subtilis* DSM 10, the Gram-negative bacterium *Escherichia coli* DSM 1116, the yeast *Candida albicans* DSM 1665, and the filamentous fungus *Mucor hiemalis* DSM 2656. Stock cultures were prepared and adjusted to the appropriate optical densities (OD) in the respective media: 0.01 OD at 600 nm in Mueller–Hinton Broth (MHB) for *B. subtilis* and *E. coli*, and 0.1 OD at 600 nm in YM 6.3 medium for *C. albicans* and *M. hiemalis*. Crude extracts were dissolved in MeOH or DMSO:MeOH (1:10) to a concentration of 4.5 mg/mL. For the assay, 150 µL of microbial suspension was added to each well of a 96-well microtiter plate. An additional 130 µL of microbial suspension and 20 µL of the crude extract were added to the first row. Serial dilutions across the plate reached concentrations from 300 to 2.34 µg/mL. MeOH served as the negative control, while nystatin and ciprofloxacin, starting at 66.6 µg/mL, served as positive controls for fungi and bacteria, respectively. Plates were incubated on a microplate shaker at 180 rpm in the dark at 30 °C for fungi and at 37 °C for bacteria. The minimum inhibitory concentration (MIC), defined as the lowest concentration of a substance that inhibits visible microbial growth, was determined after 24 hours for bacteria and yeast, and after 48 hours for *M. hiemalis*.

2.3 Scale-Up Fermentation and Extraction of Secondary Metabolites

Strains selected for scale-up fermentation were chosen based on several criteria, including bioactivity in initial screenings, the presence of potentially novel metabolites, the yield of crude extract per flask, and the complexity of the crude extract. To capture both major and minor metabolites, optimal growth conditions, including medium composition, cultivation time, and inoculation procedures, were determined prior to the scale-up fermentation.

2.3.1 Liquid-State Fermentation

Pre-cultures for each strain were prepared in 100 mL of Q6 ½ medium using 250 mL flasks. Three 0.25 cm² agar pieces from overgrown YM 6.3 plates were added to each flask, and the cultures were incubated in the dark at 23 °C with shaking at 140 rpm for five days. Once the desired biomass was reached without depleting the free glucose, pre-cultures were homogenized using an Ultra-Turrax (T25 easy clean digital, IKA) at 5000 rpm for 30 seconds. Scale-up fermentation was carried out in twelve 1 L Erlenmeyer flasks per strain, each containing 400 mL of the selected medium, resulting in a total volume of 4.8 L. Inoculation was performed with 0.5% (2 mL) of homogenized pre-culture per flask. The cultivation was maintained at 23 °C and 140 rpm in the dark, with daily monitoring of glucose levels. As a control, all media were incubated under the same conditions without fungal inoculation.

After the free glucose was consumed and fermentation was complete, mycelia were separated from the supernatant using vacuum filtration. The mycelial extraction followed the same procedure as in the screening fermentations, with acetone and EtOAc extractions repeated three times to maximize metabolite recovery. The supernatant was treated with 2% (m/v) AmberLite^{TM} XAD16N adsorbent resin, incubated for four hours with shaking, filtered, and eluted with 500 mL of acetone three times. This process was repeated twice. The resulting extracts were evaporated, and the remaining aqueous phase was extracted following the same protocol as the mycelial samples. The extracts were further analyzed by HPLC-DAD/MS.

2.3.2 Solid-State Fermentation

Selected fungal strains were cultivated in twelve 500 mL flasks per strain, each containing either BRFT or WOFT medium. Each flask was inoculated with 6 mL of pre-culture, prepared following the same procedure as described for the liquid scale-up fermentation. The flasks were incubated at room temperature in the dark. For each strain, four flasks were harvested at three different time points, after 2, 4, and 6 weeks of fermentation, to monitor changes in metabolite production over time. Control flasks, which contained medium but no fungal inoculation, were included and incubated under identical conditions. For metabolite recovery, solid cultures were extracted three times with acetone in an ultrasonic bath at 40 °C, filtered, and concentrated to the aqueous phase following the same procedure as used in the screening fermentation. The aqueous phase was then extracted three times with EtOAc, dried over Na_2SO_4, and evaporated. The residue was dissolved in MeOH and extracted three times with *n*-heptane. The fractions

were evaporated under vacuum and analyzed using HPLC-DAD/MS. Further details on the scale-up cultivation methods can be found in publications **I**–**VI**.

2.4 Isolation and Purification of Secondary Metabolites

Extracts from both liquid and solid-state fermentations were initially pre-fractionated and purified to isolate the secondary metabolites of interest. The extracts were analyzed by reversed-phase (RP) chromatography analytical HPLC-DAD/MS to identify any highly hydrophobic compounds (e.g., fatty acids and steroids) that could interfere with the separations. When necessary, extracts were solubilized in dichloromethane (DCM), *n*-heptane, tert-Butyl methyl ether (TBME), or mixtures of these solvents, and then subjected to normal-phase flash chromatography using a Grace Reveleris® X2 Flash system (Büchi Labortechnik GmbH, Flawil, Switzerland) equipped with FlashPure ID Silica cartridges of appropriate size for the sample. Hydrophobic compounds were eluted first, followed by more polar metabolites with increasingly polar eluents. Fractions were collected based on UV absorption at 210 nm and evaporative light scattering detection (ELSD), concentrated under reduced pressure at 40 °C, transferred, and analyzed by HPLC–DAD/MS.

Fractions containing metabolites of interest were further purified by preparative RP-HPLC using different chromatographic systems. Compounds with detectable UV/VIS absorbance were separated using Gilson PLC 2250 or PLC 2050 systems (Gilson Inc., Middleton, WI, USA), whereas compounds with weak UV/VIS signals were purified using a Büchi FlashPrep C-850 system (Büchi Labortechnik AG) equipped with ELSD. C18 columns, including Gemini C18 (250 × 50 mm, 10 µm; Phenomenex, Aschaffenburg, Germany), Nucleodur C18ec (250 × 40 mm, 10 µm; Macherey-Nagel, Düren, Germany), Luna C18 (250 × 21 mm, 7 µm; Phenomenex), Synergi™ Polar RP (250 × 50 mm, 10 µm; Phenomenex), and XBridge BEH C18 (250 × 19 mm, 5 µm; Waters), were employed as stationary phases. The mobile phase consisted of ultrapure water as solvent A and MeCN as solvent B, both supplemented with 0.1% FA, with gradient elutions optimized based on analytical LC-MS data. For fractions smaller than 10 mg, semi-preparative RP-HPLC was performed on an Agilent 1200 Infinity Series system (Agilent Technologies, Santa Clara, CA, USA) equipped with a fraction collector. Fractions were collected either by UV detection at 210 nm or through time-based collection following test runs. These fractions were separated using columns such as Luna C18 (250 × 10 mm, 5 µm; Phenomenex), Gemini C18 (250 × 10 mm, 5 µm; Phenomenex), or XBridge BEH C18 (250 × 10 mm, 5 µm; Waters). All fractions were dried under vacuum, then

dissolved in a MeOH/acetone (1:1) mixture for quantification and analysis using HPLC-DAD/MS. Additional details regarding UV detection, gradient conditions, and purification steps can be found in publications **I**–**VI**.

2.5 Structural Elucidation and Spectroscopic Characterization of Isolated Metabolites

Isolated compounds were assessed for purity and molecular formula determination using ultra-high-resolution HPLC (timsTOF Pro 2, Bruker Daltonics GmbH & Co. KG, Bremen, Germany). Samples were dissolved in a 1:1 mixture of MeOH and acetone at a concentration of 0.5 mg/mL. Compounds with sufficient purity were then dissolved in deuterated solvents, including acetone-*d6*, DMSO-*d6*, $CDCl_3$, MeOH-*d4*, or pyridine-*d5*, based on their solubility and stability, and transferred into NMR tubes. Samples over 1 mg were dissolved in 600 µL of solvent and analyzed in standard 5 mm tubes, while smaller amounts were prepared in 200 µL of solvent and measured in 3 mm tubes. Nuclear magnetic resonance (NMR) spectra were acquired using a Bruker Avance III 500 MHz (^{1}H-NMR: 500 MHz, ^{13}C-NMR: 125 MHz), a Bruker Avance III 600 MHz (^{1}H-NMR: 600 MHz, ^{13}C-NMR: 150 MHz), and a Bruker Avance III 700 MHz (^{1}H-NMR: 700 MHz, ^{13}C-NMR: 175 MHz) spectrometers (Bruker Daltonics GmbH & Co KG). One-dimensional ^{1}H and ^{13}C spectra were recorded for initial assignments, along with two-dimensional experiments including COSY (^{1}H-^{1}H correlation spectroscopy), HSQC (heteronuclear single quantum coherence), HMBC (heteronuclear multiple bond correlation), TOCSY (total correlation spectroscopy), and ROESY (rotational nuclear Overhauser effect spectroscopy) to elucidate structural and relative stereochemistry. Two-dimensional experiments were used to determine structural connectivity: COSY identified proton-proton couplings; HSQC correlated ^{1}H and directly attached ^{13}C nuclei; HMBC provided long-range ^{1}H-^{13}C correlations to connect subunits; TOCSY detected entire spin systems in overlapping signals; and ROESY experiments were used to establish relative stereochemistry.

Absolute stereochemistry was determined using chiral derivatization methods, including Mosher's method for secondary alcohols (Dale et al., 1969; Hoye et al, 2007) and the advanced Marfey's method for amino acid residues (Viehrig et al., 2013). If necessary, methylation of carboxylic acids was performed using a diazomethane reaction, generated from Diazald® (Sigma-Aldrich, Deisenhofen, Germany), following the manufacturer's instructions, to facilitate structural elucidation. Additional support for stereochemical assignments was obtained through optical rotation measurements using an MCP 150 polarimeter (Anton Paar,

Seelze, Germany) and electronic circular dichroism (ECD) spectroscopy with a J-815 spectropolarimeter (JASCO, Pfungstadt, Germany). Complementary UV/Vis spectra were recorded on a Shimadzu UV-2450 spectrophotometer (Shimadzu, Kyoto, Japan). Comparative analysis with previously reported reference data was used to confirm structural and stereochemical assignments. Comprehensive details on the structure elucidation of the published compounds, carried out with the support of Dr. Njogu M. Kimani, Prof. Dr. Sherif S. Ebada, and PD Dr. Frank Surup, are available in publications **I**–**VI**.

2.6 Biological Activity Assays of Isolated Metabolites

Purified metabolites obtained from the scale-up fermentations and subsequent chromatographic purification were evaluated for biological activity to identify compounds with antibacterial, antifungal, nematicidal, and cytotoxic properties. The selection of compounds for testing was based on their chemical novelty, the availability of sufficient quantities for bioassays, and comparison with previously reported biological activities in the literature.

2.6.1 Antimicrobial Assay

The antimicrobial activity of the isolated metabolites was assessed using serial dilution assays in 96-well microtiter plates to determine the minimum inhibitory concentration (MIC) against a panel of yeasts, filamentous fungi, and Gram-positive and Gram-negative bacteria, following the protocol described by Harms et al. (2021). The tested microorganisms included the yeasts *Schizosaccharomyces pombe* (DSM 70572), *Wickerhamomyces anomalus* (DSM 6766), *Candida albicans* (DSM 1665), and *Rhodosporidium toruloides* (DSM 10134); the filamentous fungus *Mucor hiemalis* (DSM 2656); the Gram-positive bacteria *Bacillus subtilis* (DSM 10), *Mycobacterium smegmatis* (ATCC 700084), and *Staphylococcus aureus* (DSM 346); as well as the Gram-negative bacteria *Acinetobacter baumannii* (DSM 30008), *Chromobacterium violaceum* (DSM 30191), *Escherichia coli* (DSM 1116), and *Pseudomonas aeruginosa* (DSM 19882). Stock solutions of pure compounds were prepared at a concentration of 1 mg/mL in MeOH or acetone, depending on their solubility, and further diluted to achieve final assay concentrations ranging from 66.7 µg/mL to 0.52 µg/mL. Positive controls included oxytetracycline for *B. subtilis* and specific antibiotics such as ciprofloxacin for *A. baumannii*, kanamycin for *M. smegmatis*, and gentamicin for *S. aureus, C. violaceum*, *E. coli,* and *P. aeruginosa*. Nystatin was used as a positive control for yeasts and *M. hiemalis*. The corresponding solvent (20 µL MeOH or acetone) served as a negative control to exclude

solvent-related effects. MIC values were determined as the lowest concentrations at which no visible microbial growth was observed after incubation under the standard culture conditions. The serial dilution assay was performed by Wera Collisi (MWIS, Helmholtz Centre for Infection Research (HZI)).

2.6.2 Cytotoxic Assay

The cytotoxic potential of the isolated metabolites was evaluated in vitro using the MTT (3-(4,5-dimethylthiazol-2-yl)-2,5-diphenyltetrazolium bromide) assay in 96-well microtiter plates, following the protocol established by Harms et al. (2021). Initially, the compounds were tested on two mammalian cell lines: human endocervical adenocarcinoma KB 3.1 and mouse fibroblasts L929. Stock solutions of the metabolites were prepared in the same solvent used for the antimicrobial assay, with epothilone B serving as the positive control and the chosen solvent as the negative control. Cells were cultured in Dulbecco's Modified Eagle's Medium (DMEM) supplemented with 10% fetal bovine serum. The compounds were combined with the cell lines and serially diluted to final concentrations ranging from 37 to 0.6 µg/mL, followed by incubation for five days at 37 °C under 10% CO_2. Cell viability was determined by MTT staining, and the results were quantified with a microplate reader at 595 nm to calculate half-maximal inhibitory concentrations (IC_{50}). Metabolites that exhibited cytotoxicity in the initial assay were further tested against five additional cancer cell lines: breast adenocarcinoma MCF-7, lung carcinoma A549, ovarian adenocarcinoma SKOV3, prostate adenocarcinoma PC-3, and epidermoid carcinoma A431, following the same procedure. The cytotoxic assay was carried out by Wera Collisi (MWIS, HZI).

2.6.3 Nematicidal Assay

The nematicidal activity of the isolated compounds was evaluated against the nematode *Caenorhabditis elegans* (N2 wild-type strain from the Caenorhabditis Genetics Center). To ensure reproducibility, nematodes were synchronized to the same developmental stage. *C. elegans* cultures were maintained monoxenically on nematode growth medium (NGM; per liter: 3 g NaCl, 2.5 g peptone, 20 g agar; supplemented post-autoclaving at 55 °C with 1 mL 1 M $CaCl_2$, 25 mL 1 M KPO_4 [pH 6.0], 1 mL 1 M $MgSO_4$, and 1 mL cholesterol [5 mg/mL in ethanol]) seeded with *E. coli* OP50 and incubated at 19 °C until a high density of eggs was obtained. Synchronization was achieved by rinsing nematodes with 0.9% NaCl, followed by centrifugation and bleaching with sodium hypochlorite and NaOH to digest adult worms while

preserving eggs. Eggs were subsequently washed, resuspended in 0.9% NaCl, and incubated at 23 °C with shaking (80 rpm) for 18 hours to allow hatching. Hatched larvae were transferred to fresh NGM plates and incubated at 19 °C for 48 h to reach the L4/adult stages.

For the nematicidal assay, compounds were dissolved in MeOH at a stock concentration of 0.15 mg/mL and applied to 48-well microtiter plates to obtain final assay concentrations of 10, 50, and 100 µg/mL. MeOH served as the negative control, while ivermectin (1 µg/mL) was used as the positive control. After solvent evaporation under nitrogen flow, 300 µL of the synchronized nematode suspension (1000 nematodes/mL) was added per well. Plates were incubated on a microplate shaker at 150 rpm in the dark at 23 °C for 18 hours. Live (motile) and dead (erect and immobile) nematodes were counted from 30 µL aliquots in triplicate, and mortality rates were corrected using the Schneider-Orelli formula (Schneider-Orelli, 1947). Compounds inducing a corrected mortality rate of ≥50% at 100 µg/mL were classified as active. Detailed descriptions of nematode culture, synchronization, and assay procedure are provided in publications **II**, **III**, **V**, and **VI**.

3 Results and Discussion

3.1 Secondary Metabolites from Nematode-Associated Fungi

Nematophagous fungi are a diverse group of organisms capable of feeding on nematodes, making them important targets for biocontrol research (Y. Zhang et al., 2020; Ahmad et al., 2021; Rahman et al., 2023). These nematode-associated fungi employ diverse strategies to capture nematodes, including the production of a wide array of secondary metabolites with various biological activities, among them nematicidal effects (Ahmad et al., 2021; Rahman et al., 2023). The fungal-derived nematicidal compounds can be employed in biological control strategies, such as the suppression of plant-parasitic nematodes through antagonistic interactions (Fang et al., 2023; Schrey et al., 2025). However, the chemical diversity and ecology of nematophagous fungi are underexplored and still not well understood. Therefore, it is crucial to screen different nematophagous fungal species for their secondary metabolite production and evaluate these metabolites against various nematodes as well as other microorganisms, some of which have significant economic, medical, and societal impacts. This section of the thesis focuses on the secondary metabolism of fungi associated with nematodes, particularly those from the order Pleosporales (Dothideomycetes, Ascomycota).

3.1.1 Unprecedented Cyclodepsipeptides and Tetramic Acids from *Polydomus karssenii*

The nematode-associated genus *Polydomus* was recently introduced by Ashrafi et al. (2023) as a monophyletic lineage within the family Phaeosphaeriaceae (Pleosporales, Dothideomycetes). In the same study, the morphological characteristics and multilocus phylogeny of *P. karssenii* strains JKI 73120 and DSM 111209 were thoroughly described. This species exhibits a bifunctional lifestyle, acting both as a plant-inhabiting dark-septate endophyte and as a nematode parasite. Strain JKI 73120 was isolated as an endophyte from *Microthlaspi perfoliatum* roots, while DSM 111209 was isolated from infected eggs of the plant-parasitic nematode *Heterodera filipjevi* (Ashrafi et al., 2023).

In publication **III**, the secondary metabolites obtained from the liquid (Q6 ½) and solid (BRFT and WOFT) cultures of the two aforementioned *P. karssenii* strains are reported. After fractionation of the crude extracts using normal-phase flash chromatography, followed by multiple rounds of preparative and semipreparative RP-HPLC, a total of seven undescribed compounds were isolated from these strains. The isolated compounds included the tetramic acids polydosetins A–E (**1**–**5**), which belong to the class of 3-decalinoyltetramic acids

(3-DTAs), and the cyclodepsipeptides pullularins G and H (**6** and **7**) (Figure 6). Compounds **2**, **3**, and **5**–**7** were isolated from the endophytic strain JKI 73120, whereas compounds **1**, **2**, and **4** were obtained from the nematode-associated strain DSM 111209. The absolute configuration of the cyclodepsipeptides was determined using a combination of advanced Marfey's derivatization. For polydosetin C (**3**), the absolute configuration was established through Mosher's method and by methylation experiments.

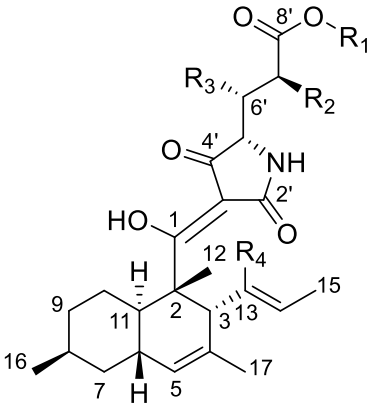

polydosetin A (**1**): R_1 = H, R_2 = OH, R_3 = OH, R_4 = CH_3
polydosetin B (**2**): R_1 = H, R_2 = OH, R_3 = OH, R_4 = H
polydosetin C (**3**): R_1 = CH_3, R_2 = OH, R_3 = OH, R_4 = CH_3
polydosetin D (**4**): R_1 = H, R_2 = H, R_3 = OH, R_4 = CH_3
polydosetin E (**5**): R_1 = H, R_2 = H, R_3 = H, R_4 = CH_3

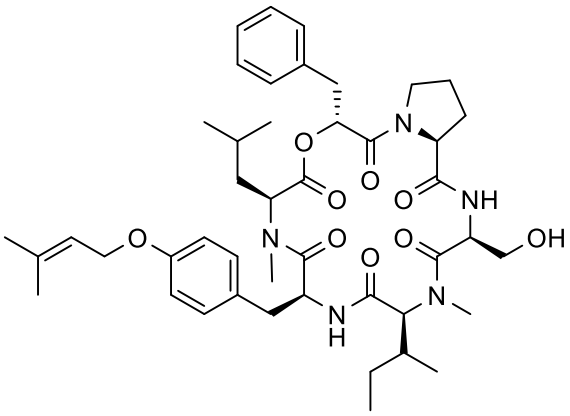

pullularin G **(6)**

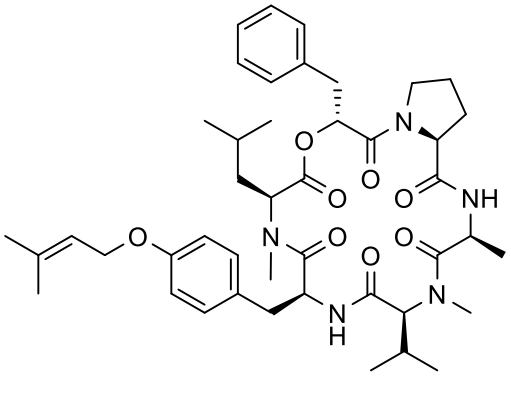

pullularin H **(7)**

Figure 6. Chemical structures of polydosetins A–E (**1**–**5**) and pullularins G and H (**6** and **7**) produced by *Polydomus karssenii* strains JKI 73120 and DSM 111209.

In our efforts to discover new bioactive natural products, compounds **1**–**7** were evaluated for their antimicrobial, cytotoxic, and nematicidal activities. Compounds **1**, **3**, **5**, and **7** displayed activity against the Gram-positive bacterium *B. subtilis*, with compound **3** being the most potent (MIC = 16.6 µg/mL). Compound **3** also exhibited moderate activity against *S. aureus* (MIC = 33.3 µg/mL), while compound **7** showed weak activity against *S. aureus* and *M. smegmatis*, both at 66.6 µg/mL. Additionally, compound **5** displayed antifungal activity against *C. albicans*, *R. toruloides*, and *M. hiemalis*, with the strongest effect observed against *M. hiemalis* (MIC = 16.6 µg/mL). Compound **3** also inhibited *M. hiemalis* but was less

effective, with an activity of 66.6 µg/mL. The complete MIC data set is available in publication **III**. None of the tested compounds inhibited Gram-negative bacteria at the concentrations tested. The antimicrobial profiles of the tetramic acids **1**–**5** align with previous findings on 3-DTAs, which are generally active against Gram-positive bacteria such as *B. subtilis* and methicillin-resistant *S. aureus* (MRSA). In contrast, activity against Gram-negative bacteria is rare, likely due to their outer membrane that limits compound penetration unless sufficient lipophilic groups are present (Kim et al., 2024). Notably, polydosetin C (**3**), the methyl ester derivative of polydosetin A (**1**), exhibited broader antimicrobial activity. This suggests that chemical modifications such as methylation can significantly enhance biological activity, consistent with previous structure–activity relationship (SAR) studies reported by Yan et al. (2021). In line with existing literature, several fungal cyclodepsipeptides have demonstrated selective activity against Gram-positive bacteria, especially against *B. subtilis* and *Mycobacterium* spp. (Haritakun et al., 2010; Wang et al., 2018; Liang et al., 2021; Liu et al., 2023); however, only pullularins H (**7**) exhibited antimicrobial effects in this study.

All compounds were evaluated for cytotoxic activity against the mammalian cell lines, mouse fibroblasts (L929) and endocervical adenocarcinoma (KB3.1) cells. Among them, only compounds **5** and **7** exhibited cytotoxic effects, showing weak activity against KB3.1 cells, with IC_{50} values of 53.6 µM and 24.1 µM, respectively. These results indicate that overall, the compounds isolated from *P. karssenii* strains are non-cytotoxic under the tested conditions, which is favorable for their potential use in further biological studies and applications.

Regarding the nematicidal activity, tetramic acids **1** and **2** are particularly interesting. In the nematicidal assay against *C. elegans*, **1** and **2** showed significant activity, with corrected mortality rates of 57.6% and 83.1% at 100 µg/mL, respectively. Structural comparison suggests that hydroxylation and methylation patterns play a key role in nematicidal activity. Tetramic acids featuring hydroxyl groups at positions C–6′ and C–7′, combined with a carboxylic acid group at C–8′, exhibited nematicidal activity (Figure 7). Compounds lacking these features demonstrated no significant activity. Furthermore, compound **2** showed the strongest activity and is the only tetramic acid among those tested that lacked methylation at position C–13 (Figure 7), implying that the absence of this methyl group may enhance nematicidal effectiveness. Notably, compounds **1** and **2** were non-cytotoxic, supporting their potential as promising leads for safe nematicidal and biocontrol agents. To the best of our knowledge, this is the first report of 3-DTAs exhibiting nematicidal properties. The full dataset of corrected

nematode mortality rates can be found in publication **III**. Interestingly, compound **2** was isolated from both endophytic and nematode-associated strains of *P. karssenii*, suggesting that this metabolite may play a crucial role in both ecological functions of this species. Additionally, polydosetins A–E (**1**–**5**) are structurally similar to Sch 210972 and Sch 213766, isolated from *Chaetomium globosum*, which demonstrated inhibitory activity in a CCR-5 membrane binding assay, indicating their potential as inhibitors of the chemokine receptor CCR-5, an important antiviral target (SW. Yang et al., 2006, 2007). The 3-DTAs **1**–**5** also share structural similarities with equisetin, trichosetin, and beauversetin, well-studied molecules with a broad range of activities, including phytotoxicity, anti-HIV properties, cytotoxic and antimicrobial activities (Hazuda et al., 1999; Marfori et al., 2002; Neumann et al., 2009; D. Zhao et al., 2019), suggesting that polydosetins A–E (**1**–**5**) may possess additional activities worth exploring. Since the mode of action of 3-DTAs remains unclear, this represents an important avenue for future research.

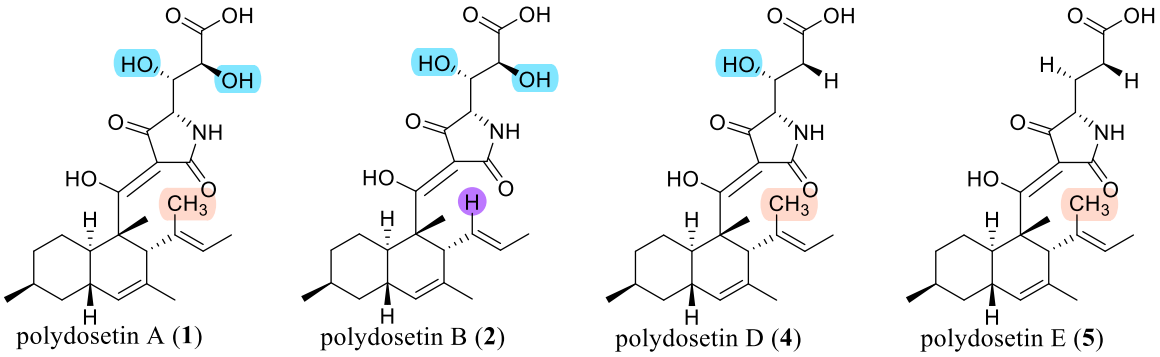

Figure 7. Overview of the tetramic acids **1**, **2**, **4**, and **5** examined for their biological effects, highlighting key structural modifications (blue: hydroxylation; orange: methylation; purple: protonation).

Although neither of the two studied cyclodepsipeptides exhibited nematicidal activity, previous reports on cyclodepsipeptides such as PF1022A have demonstrated their potential for anthelmintic applications. The cyclodepsipeptide PF1022A, first isolated from an endophytic fungus of the genus *Rosellinia*, exhibits nematicidal activity against *Ascaridia galli* in chickens (Sasaki et al., 1992; Wittstein et al., 2020), and its semisynthetic derivative, emodepside, is marketed as a veterinary anthelmintic used to treat both gastrointestinal and extraintestinal nematodes (Wang et al., 2018; Krücken et al., 2021). The biological role of cyclodepsipeptides **6** and **7** in *P. karssenii* is still unknown, and further studies are necessary to clarify their activity and potential uses.

In parallel, *P. karssenii* strain DSM 106825 was also studied for its production of secondary metabolites. This strain was isolated from infected eggs of the plant-parasitic nematode

H. filipjevi. Prior to its formal taxonomic description, Helaly et al. (2018) reported several metabolites produced by this strain, including ophiotine, xanthomide Z, arthrichitin, and arthrichitins B and C (Figure 8). Notably, ophiotine exhibited nematicidal activity, causing 59% mortality in the host nematode *H. filipjevi* at a concentration of 10 µg/mL. The crude extracts obtained from the liquid-state fermentation in Q6 ½ medium of strain DSM 106825 were fractionated by size-exclusion chromatography, followed by multiple rounds of preparative and semipreparative RP-HPLC. Three previously undescribed cyclodepsipeptides, including compound **8** (Figure 8), were isolated. These cyclodepsipeptides are currently in the process of having their absolute configurations determined. Preliminary bioassay results indicate that one of these new compounds exhibits weak cytotoxic activity against KB3.1 cells.

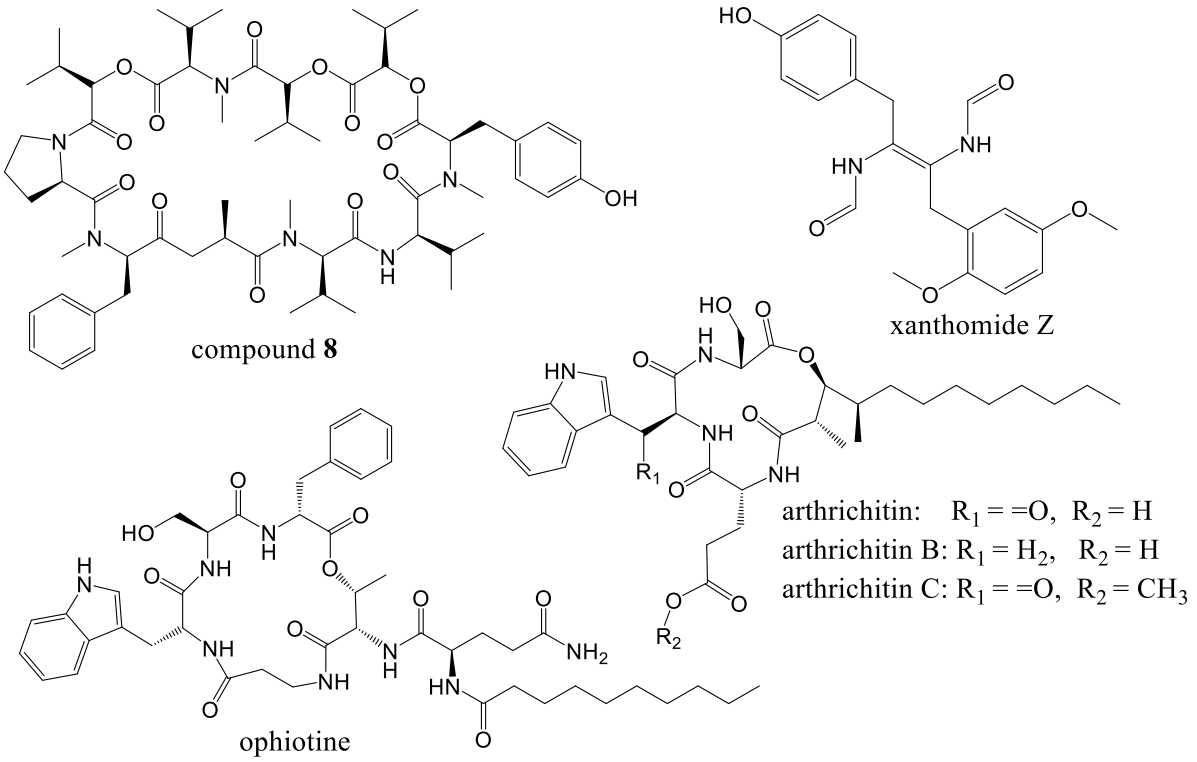

Figure 8. Chemical structures of metabolites from *Polydomus karssenii* (DSM 106825), including ophiotine, xanthomide Z, arthrichitin, and arthrichitins B and C.

3.1.2 Bioactive Secondary Metabolites Produced by *Murispora* sp.

Strain JKI 72806 was isolated from eggs of the cereal cyst nematode *H. filipjevi* collected in Yozgat, Turkey. The taxonomic identification of strain JKI 72806 is still ongoing and has been preliminarily assigned to *Murispora* sp. (Pleosporales, Dothideomycetes), suggesting it may represent a new species (Ashrafi, pers. comm.). *Murispora* sp. (JKI 72806) was cultivated in

ZM ½ liquid medium, and the crude extracts from the supernatant and mycelium were fractionated separately using preparative RP-HPLC. This process led to the isolation of nine compounds, including one novel sesquiterpenoid (**9**); four glycerolipids: MGTA(18:1) (**10**), LDGTS(18:1) (**11**), MGTA(18:2) (**12**), and LDGTS(18:2) (**13**); and four diketopiperazines (DKPs): cyclo-(L-Ile-L-Pro) (**14**), cyclo-(L-Leu-L-Pro) (**15**), cyclo(D-Pro-L-Phe) (**16**), and cyclo-(L-Phe-L-Pro) (**17**) (Figure 9). Structural characterization of the compounds was achieved by 1D and 2D NMR analyses and HR-ESI-MS. The absolute configuration of the new sesquiterpenoid was determined through TDDFT-ECD calculations.

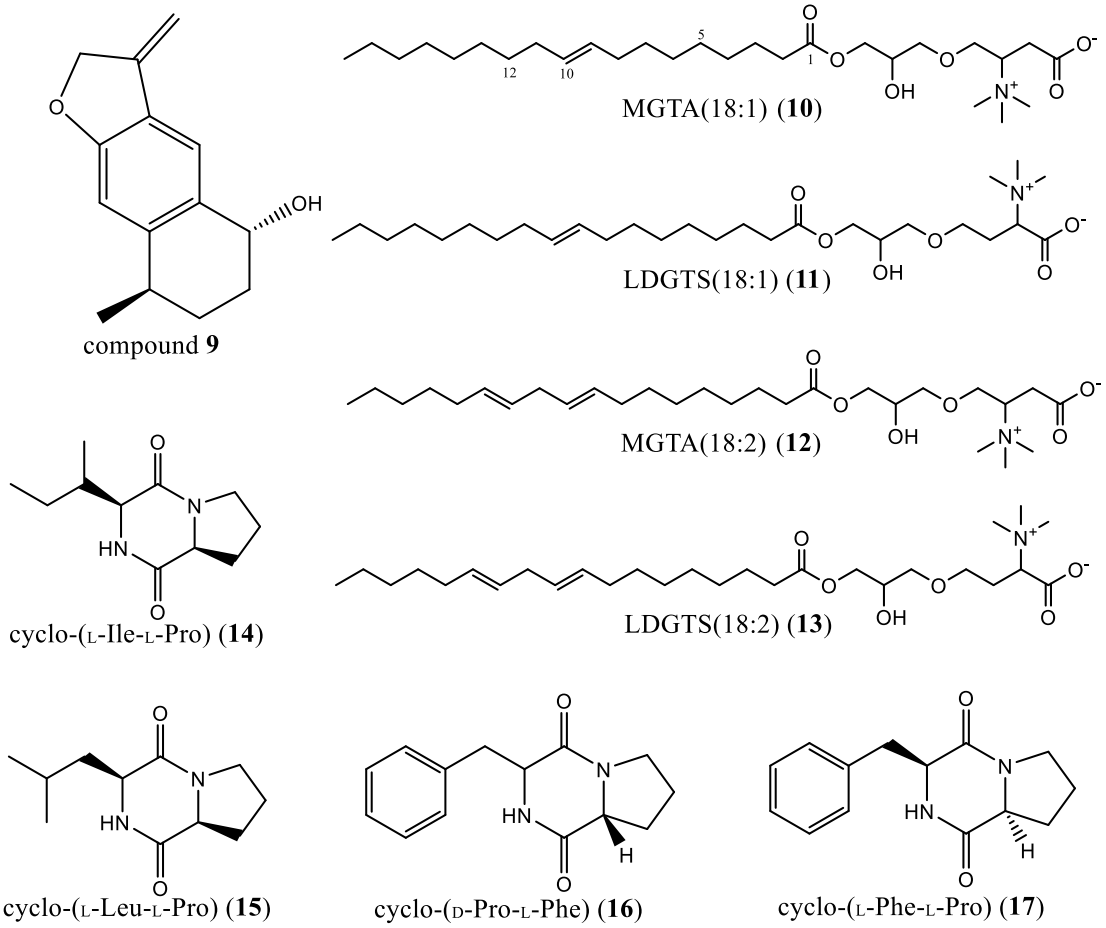

Figure 9. Chemical structures of metabolites (**9**–**17**) produced by *Murispora* sp. (JKI 72806).

Compounds **9**–**17** were evaluated for their antimicrobial, cytotoxic, and nematicidal activity. The glycerolipid MGTA(18:2) (**12**) showed potent inhibition of the yeasts *S. pombe* and *R. toruloides* at 8.3 µg/mL and 16.6 µg/mL, respectively, and weak inhibition of *W. anomalus* at 66.6 µg/mL. Compound **12** also inhibited the Gram-positive bacteria *B. subtilis* and *S. aureus* at 16.6 µg/mL and 66.6 µg/mL, respectively. In the nematode assay, MGTA(18:2) (**12**) exhibited moderate activity against *C. elegans* with a corrected mortality rate of 52.54% at

100 µg/mL. LDGTS(18:2) (**13**), an isomer of **12**, displayed a similar profile, with strong inhibition of *S. pombe* and *R. toruloides* at 8.3 µg/mL and 16.6 µg/mL, respectively, and inhibition of *B. subtilis* and *S. aureus* at 8.3 µg/mL and 33.3 µg/mL, respectively. In the nematode assay, **13** also showed moderate activity, with a corrected mortality rate of 52.42% at 100 µg/mL. In contrast, MGTA(18:1) (**10**) and LDGTS(18:1) (**11**) were inactive in all tested bioassays, despite their close structural similarity to compounds **12** and **13**. These findings suggest that the biological activity of glycerolipids **12** and **13** can be attributed to the double bond at position C–12, which is absent in the inactive analogues **10** and **11** (Figure 9). Furthermore, the lack of cytotoxic activity observed for **10** and **11** underscores their potential as safe candidates for development as biocontrol or antimicrobial agents. The complete data set of MIC, IC_{50}, and corrected nematode mortality rate values is provided in the Appendix.

Compounds **10**–**13** belong to the class of betaine lipids, which are non-phosphorus glycerolipids, and include both DGTS- and MGTA-type betaine lipids (Oppong-Danquah et al., 2023; Salomon et al., 2025). The first DGTS was described in 1969 from the stramenopile *Ochromonas danica* and later also from the fungus *Xylaria hypoxylon* (Nichols and Appleby, 1969; Künzler and Eichenberger, 1997). The highly polar lipid LDGTS(18:2) (**13**) has previously been analyzed through a lipidomic approach using gas chromatography–mass spectrometry (GC-MS) and has been detected in numerous edible basidiomycetous fungi, including *Laccaria laccata*, *Termitomyces eurrhizus*, *Cantharellus cibarius*, *Tricholoma matsutake*, *Boletus speciosus*, *Sarcodon aspratus, Thelephora ganbajun*, and *Boletus bainiugan* (F. Yang et al., 2021). LDGTS(18:1) (**11**), in contrast, was analyzed via LC-MS/MS and found in the fungus *Pestalotiopsis kenyana* and the white truffle *Tuber magnatum* (Liu et al., 2022; Tejedor-Calvo et al., 2024). The MGTA-type lipids, including MGTA(18:1) (**10**) and MGTA(18:2) (**12**), have been previously identified through lipidomic signature approaches in the brown algae *Fucus vesiculosus* (Da Costa et al., 2019). DGTS and MGTA lipids are mainly studied in lipidomics and metabolomics for the identification of fungi or plants based on their lipid profiles (Da Costa et al., 2019; F. Yang et al., 2021; Oppong-Danquah et al., 2023; Costa et al., 2024). Consequently, they have not been previously isolated, and the structures of compounds **10**–**13** have so far only been described using MS/MS or GC-MS. To the best of our knowledge, this study constitutes the first report of the isolation and complete structural elucidation of compounds **10**–**13**. Overall, only limited properties of betaine lipids are known, and they remain an under-researched class of glycerolipids, primarily described from algae

(Salomon et al., 2025). Based on the literature, the glycerolipids **10**–**13** are being tested for the first time for cytotoxic, antimicrobial, and nematicidal activities in the context of this thesis.

Regarding the DKPs, only cyclo-(L-Pro-L-Phe) (**17**) showed antimicrobial activity against *M. hiemalis* at 66.6 µg/mL. In contrast, the other DKPs exhibited no significant activity in the assays conducted in this study. However, previous reports suggest that the studied DKPs may interfere with bacterial quorum sensing (QS). Specifically, cyclo-(L-Pro-L-Ile) (**14**) and cyclo-(L-Pro-L-Phe) (**17**) have been reported to inhibit QS signal production in *Chromobacterium violaceum* and *E. coli* pSB401, whereas cyclo-(L-Pro-L-Leu) (**15**) has been shown to reduce QS only in *E. coli* pSB401 (Abed et al., 2013). Inhibition of QS can prevent biofilm formation and may have important implications for controlling bacterial infections (Bian and Wang, 2022).

Motivated by the potential of *Murispora* sp. (JKI 72806) to produce compounds with a broad range of biological activities, including nematicidal effects, and its lack of cytotoxicity, the strain was co-cultured with 1,000 *C. elegans* nematodes per plate to assess its nematicidal activity. Notably, after 48 hours, a corrected mortality rate of 100% was observed, suggesting that this fungus could serve as a potential biocontrol agent against nematodes. Future studies should explore its effects on other nematode species, especially plant-parasitic nematodes. To the best of our knowledge, compounds **9**–**17** represent the first reported secondary metabolites derived from a fungus of the genus *Murispora,* and the results from this study will be included in a manuscript currently in preparation while writing this thesis.

3.1.3 Secondary Metabolites Isolated from an Undescribed Genus of Pleosporales

Four nematode-associated fungal strains (JKI 73016, JKI 72728, JKI 73278, and JKI 73275) belonging to the order Pleosporales were investigated for their secondary metabolite production in the framework of this thesis. Strains JKI 73016 and JKI 72728 were isolated from infected eggs of the plant-parasitic nematode *H. filipjevi*, while JKI 73278 and JKI 73275 were isolated as endophytes from *M. perfoliatum* roots. Ongoing molecular identification and multilocus phylogenetic analyses indicate that these four strains most likely represent two undescribed species, forming a sister relationship within a lineage that may constitute a new genus within Pleosporales (Ashrafi pers. comm.). The nematode-derived strains JKI 73016 and JKI 72728 appear to be conspecific, and the endophytic strains JKI 73278 and JKI 73275 represent the second undescribed species.

Considering that these strains may represent two previously undescribed species within a potentially new genus, their secondary metabolism was investigated to assess possible differences in their chemical profiles. The crude extracts from the scale-up fermentation were initially pre-fractionated using normal-phase flash chromatography and subsequently purified by preparative and semi-preparative RP-HPLC. The structures of the compounds were elucidated using 1D and 2D NMR spectroscopy combined with HR-ESI-MS data. The isolated compounds were evaluated for antimicrobial, cytotoxic, and nematicidal activities.

Fermentation of the nematode-associated strain JKI 73016 in liquid ZM ½ medium led to the isolation of thirteen compounds, two of which are novel to science. Eleven of these metabolites belong to the preussomerin class, including the two previously undescribed derivatives (**18** and **19**) and nine previously reported compounds: preussomerin A (**20**), preussomerin D (**21**), preussomerin J (**22**), 3'-*O*-desmethyl-1-epipreussomerin C (**23**), 3'-*O*-demethylpreussomerin L (**24**), spiropreussomerin A (**25**), palmarumycin C12 (**26**), ymf 1029A (**27**), and ymf 1029B (**28**) (Figure 10). In addition, the macrolides macrosphelide C (**29**) and 14-deoxymacrosphelide C (**30**) were also isolated.

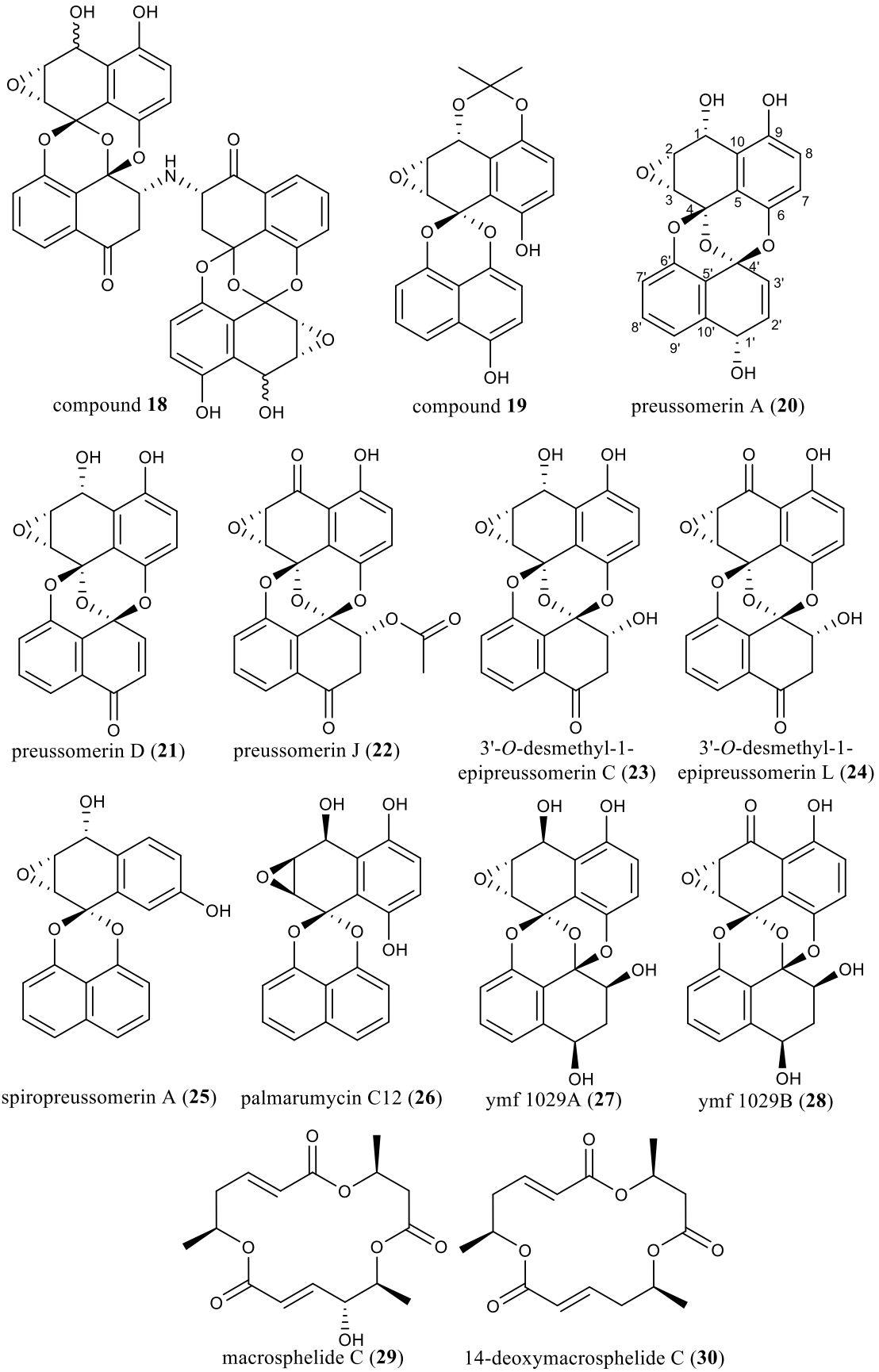

Figure 10. Chemical structures of metabolites (**18**–**30**) produced by the nematode-associated strain JKI 73016, which belongs to a new genus within the order Pleosporales.

In the antimicrobial assay, preussomerin A (**20**), preussomerin D (**21**), 3'-*O*-demethylpreussomerin L (**24**), and ymf 1029B (**28**) showed activity against Gram-positive bacteria. All four compounds inhibited *B. subtilis*, with **20** and **21** being the most active, displaying MIC values of 8.3 µg/mL and 16.6 µg/mL, respectively. Compounds **20**, **21**, and **24** also demonstrated moderate to weak activity against *S. aureus*, with MIC values of 33.3 µg/mL and 66.6 µg/mL, while compound **28** exhibited weak inhibition of *M. smegmatis* at 66.6 µg/mL. Additionally, compounds **21**, **24**, and **25** showed moderate to weak antifungal activity against *M. hiemalis*, with MIC values of 33.3 µg/mL and 66.6 µg/mL. Spiropreussomerin A (**25**) also displayed weak activity against *R. toruloides* (MIC = 66.6 µg/mL). In the cytotoxicity assay, the preussomerins **20**, **21**, **24**, and **28** showed the most potent cytotoxic effects, with IC_{50} values between 0.66 µM and 1.98 µM against L929 cells. Meanwhile, compounds **24** and **28** also demonstrated cytotoxicity against KB3.1 cells, with IC_{50} values of 1.95 µM and 2.30 µM, respectively. Further evaluation of compounds **20**, **21**, **24**, and **28** against human cancer cell lines (A431, MCF-7, A549, and PC-3) revealed notable cytotoxic effects. Ymf 1029B (**28**) exhibited strong pancytotoxic activity, with IC_{50} values ranging from 0.36 µM to 1.71 µM across all tested cell lines. Preussomerin A (**20**) showed activity against A431, MCF-7, and PC-3, with IC_{50} values between 3.00 µM and 4.37 µM, whereas 3'-O-demethylpreussomerin L (**24**) was active only against A549, with an IC_{50} of 1.67 µM. None of the compounds showed noteworthy nematicidal activity against *C. elegans* at the tested concentrations. Furthermore, the biological activity of the new preussomerins **18** and **19** will be evaluated once their absolute configurations have been determined. The complete data set of MIC, IC_{50}, and corrected nematode mortality rate values is provided in the Appendix.

Although ymf 1029A (**27**) and ymf 1029B (**28**) are both preussomerin analogues, only **27** displayed antimicrobial and cytotoxic activity in the bioassays performed. The differing activity profiles suggest that the ketone group at C–1 in compound **28**, rather than the hydroxyl group at C–1 in compound **27** (as shown in Figure 10), is likely a key factor influencing the observed bioactivity. Further SAR studies are needed to confirm this hypothesis. Ymf 1029A (**27**) and ymf 1029B (**28**) were previously isolated from an unidentified freshwater fungus and reported to exhibit weak nematicidal activity against the pine wood nematode *Bursaphelenchus xylophilus* (Dong et al., 2008). In the same study, several related compounds were evaluated for nematicidal effects, with preussomerin D (**21**) displaying the highest activity by achieving a mortality rate of 53.8% at 100 µg/mL (Dong et al., 2008). Interestingly, compounds **21**, **27**,

and **28** showed no activity against *C. elegans* in our assay, indicating a degree of selectivity toward the plan-parasitic nematode *B. xylophilus*. Preussomerins constitute a distinctive class of bis-spirobisnaphthalene natural products, distinguished by their highly oxygenated structures and unique bis-spiroacetal core (Chi and Heathcock, 1999; Ando et al., 2022). Chemically, they are particularly intriguing due to their polycyclic aromatic (naphthalene-derived) structure and the spiro-linked oxygen bridges that form the bis-spiroacetal core (Ando et al., 2022). Preussomerins have been identified in several fungal species, including *Preussia isomera* (Weber and Gloer, 1991) and the endophytes *Hormonema dematioides* (Polishook et al., 1993) and *Lasiodiplodia theobromae* (Chen et al., 2016). They are of significant interest due to their diverse biological activities. These include antifungal effects against phytopathogenic fungi such as *Phytophthora capsici*, *P. parasitica*, and *Fusarium oxysporum* (Macías-Rubalcava et al., 2008); antibacterial activity against *S. aureus* (Chen et al., 2016); and cytotoxic effects against human cancer cell lines (Seephonkai et al., 2002; Chen et al., 2016). The contrasting results observed here further emphasize that subtle structural variations within this compound class can influence their bioactivity profiles.

In parallel, following the fractionation of the supernatant crude extract from the nematode-associated strain JKI 72728 grown in Q6 ½ liquid medium, several metabolites were isolated, including the cyclodepsipeptides SCH 218157 (**31**) and SCH 217048 (**32**), along with the macrolides macrosphelide A (**33**), macrosphelide B (**34**), and 14-deoxymacrosphelide C (**30**) (Figure 11). The latter compound was also obtained from the aforementioned nematode-associated JKI 73016. SCH 218157 (**31**) showed no significant activity in the bioassays performed. However, previous studies have reported that **31** exhibits antimalarial activity against *Plasmodium falciparum* K1 and acts as an antagonist of the neurokinin 2 receptor (NK2R) (Isaka et al., 2014). SCH 217048 (**32**) exhibited only weak inhibition of *M. hiemalis* with an MIC of 66.6 µg/mL, and in previous studies, it was likewise reported to exhibit antimalarial and NK2R antagonist activities (Isaka et al., 2014). Macrosphelide B (**34**) showed cytotoxic effects against the L929, A431, and MCF-7 mammalian cell lines, with IC_{50} values ranging from 6.17 µM to 8.23 µM. Additionally, **34** inhibited all tested Gram-positive bacteria, *B. subtilis* (MIC = 66.6 µg/mL), *M. smegmatis* (MIC = 16.6 µg/mL), and *S. aureus* (MIC = 33.3 µg/mL), and displayed moderate inhibition of *M. hiemalis* (MIC = 33.3 µg/mL). In contrast, macrosphelide A (**33**) showed no significant activity in the conducted bioassays. These two macrolides differ by an oxidation at the C–14 atom (Takamatsu et al., 1996). The ketone group at C–14 in macrosphelide B (**34**) may play a key role in the increased biological

activity that was observed. The complete data set of bioassay results is provided in the Appendix.

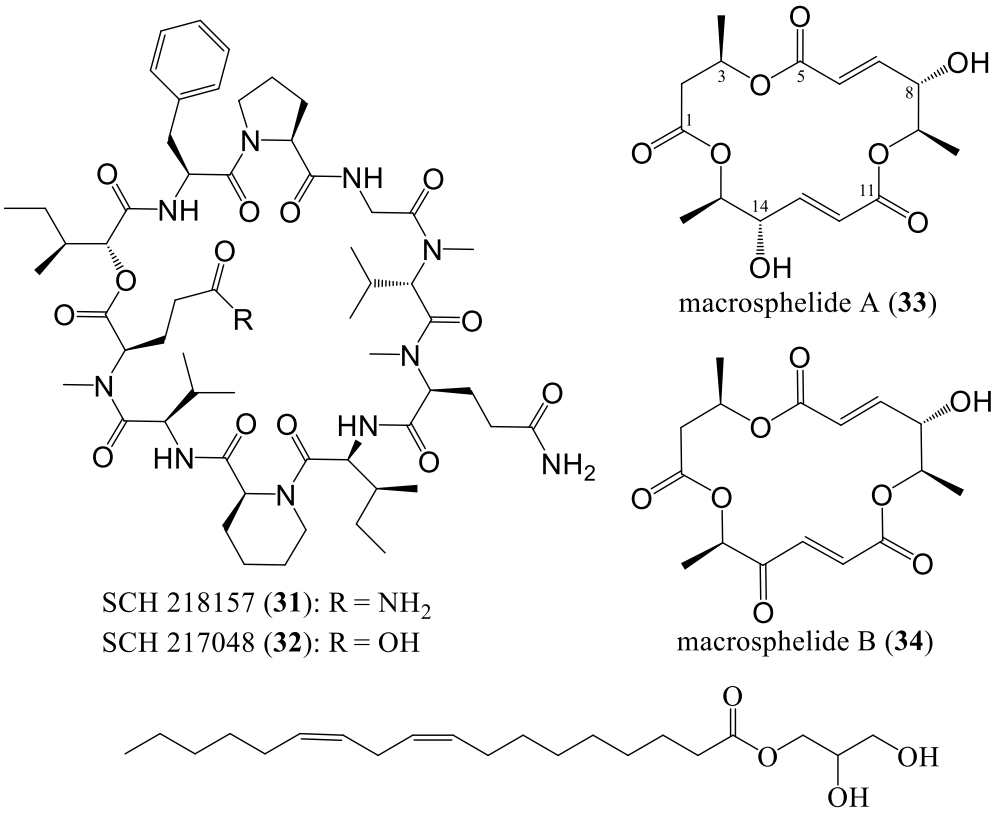

Figure 11. Chemical structures of metabolites (**31**–**35)** produced by nematode-associated and endophytic strains belonging to a new genus within the order Pleosporales.

In addition, fractionation of the supernatant crude extract from the endophytic strain JKI 73278 grown in YM 6.3 liquid medium led to the isolation of ymf 1029A (**27**), also obtained from the nematode-associated JKI 73016, and the DKPs cyclo-(L-Pro-L-Ile) (**23**) and cyclo-(L-Pro-L-Leu) (**24**). Interestingly, the latter two DKPs were also isolated from the aforementioned strain, *Murispora* sp. (JKI 72806). Moreover, the mycelial crude extract of the endophytic strain JKI 73275 cultivated in ZM ½ yielded the compounds 2,3-dihydroxypropyl (9Z,12Z)-octadeca-9,12-dienoate (**35**) (Figure 11) and macrosphelide A (**33**). Compound **35** showed activity against the Gram-positive bacteria *B. subtilis* and *S. aureus*, with MIC values of 8.3 µg/mL and 33.3 µg/mL, respectively. Furthermore, solid-state fermentation of strain JKI 73275 on BRFT resulted in the isolation of compound **35** and the cyclodepsipeptides SCH 218157 (**31**) and SCH 217048 (**32**).

The investigation of the nematode-associated strains JKI 73016 and JKI 72728, and the endophytic strains JKI 73278 and JKI 73275, representing two undescribed sister species in a new genus-level lineage of Pleosporales, revealed remarkable chemical diversity as well as notable similarities in their secondary metabolite profiles. These strains produce a wide range of compound classes, including preussomerins, macrolides, cyclodepsipeptides, DKPs, and glycerolipids. This chemical diversity highlights the metabolic potential of these fungi as sources of unique natural products with various biological activities. Interestingly, several metabolites are shared among the strains, indicating the presence of conserved biosynthetic pathways and common structural features. For instance, the preussomerin ymf 1029B (**28**) was found in both nematode-associated strains (JKI 73016 and JKI 72728). Similarly, 14-deoxymacrosphelide C (**30**) was produced by the two nematode-associated strains, while the cyclodepsipeptides SCH 218157 (**31**) and SCH 217048 (**32**), along with macrosphelide A (**33**), were isolated from both the nematode-associated JKI 72728 and the endophytic JKI 73275 strains. The results of this study will be published after the completion of the taxonomic description of these strains.

3.1.4 Secondary Metabolites Produced by *Pyrenochaeta* sp.

Strain JKI 72955, which was isolated from eggs of the cereal cyst nematode *H. filipjevi*, has been putatively identified as *Pyrenochaeta* sp. (Pleosporales, Dothideomycetes) based on molecular DNA sequence data (Ashrafi, pers. comm.), although a precise molecular identification at species level is still in progress. *Pyrenochaeta* sp. (JKI 72955) was cultivated on BRFT solid-state medium, and the crude extract was purified using chromatographic methods, including normal-phase flash chromatography and preparative RP-HPLC, leading to the isolation of six new compounds (**36**–**41**). The tentative structures are shown in Figure 12. Compounds **36**–**41** are classified as xanthone and anthraquinone derivatives, two classes of compounds known for their diverse biological activities and significance as scaffolds in natural product and medicinal chemistry (Zhao and Zheng, 2023; Oriola and Kar, 2024). Xanthones have been reported to exhibit anticancer, antibacterial, antifungal, antioxidant, anti-inflammatory, antimalarial, antiviral, and enzyme inhibitory activities (Shagufta and Ahmad, 2016; Oriola and Kar, 2024). Anthraquinones are similarly known for their anticancer, antimicrobial, antioxidant, anti-inflammatory, antidiabetic, and enzyme inhibitory properties (Hafez-Ghoran et al., 2022; Zhao and Zheng, 2023). The absolute configurations of compounds

36–**41** are currently being determined to enable subsequent evaluation of their biological activities.

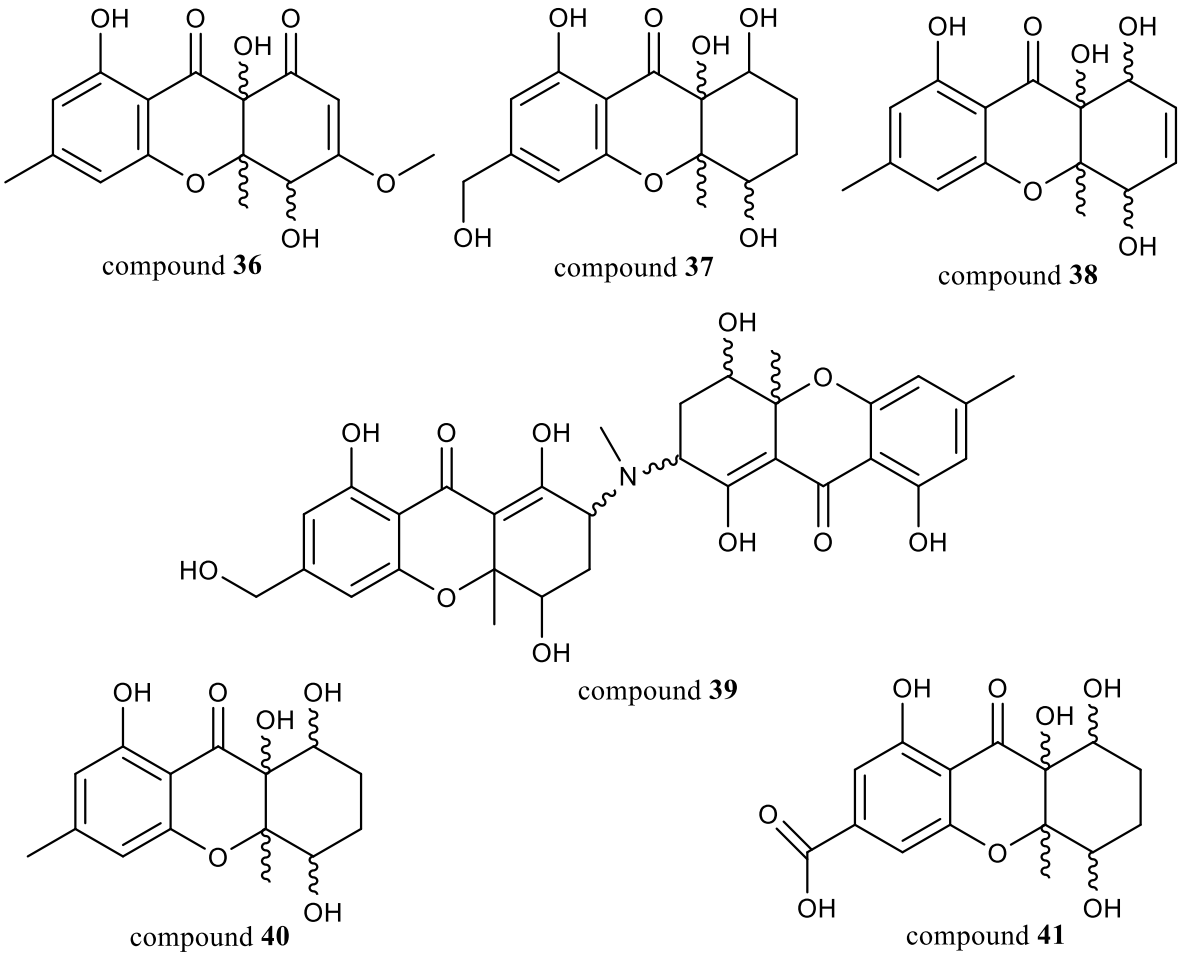

Figure 12. Tentative chemical structures of metabolites (**36**–**41**) produced by *Pyrenochaeta* sp. (JKI 72955).

3.2 Bioactive Secondary Metabolites from the Entomophatogenic Fungus *Blackwellomyces roseostromatus*

Entomopathogenic fungi are predominantly soil-dwelling fungi that infect insects during at least one stage of their life cycle. Most entomopathogenic fungi belong to the order Hypocreales (Sordariomycetes, Ascomycota) (Venkatesh et al., 2022). These fungi are widely recognized as important biocontrol agents, playing a key role in regulating insect populations (Shah and Pell, 2003). Besides this role, they are also known for their ability to produce a wide variety of secondary metabolites with diverse structural and pharmacological properties, some of which are currently used in pharmaceuticals and agrochemicals (Molnár et al., 2010; Gibson et al., 2014; L. Zhang et al., 2020). The family Cordycipitaceae is a speciose lineage of

entomopathogenic fungi, comprising well-known species used in traditional Chinese medicine such as *Cordyceps militaris* and *C. sinensis* (now *Ophiocordyceps sinensis*) (Kepler et al., 2017; Cao et al., 2020). Kepler et al. (2017) conducted a comprehensive taxonomic revision of this group based on a five-loci phylogenetic reconstruction, aiming to establish a stable nomenclature based on the "one fungus = one name" principle and monophyletic groups. Their analysis resolved many *Cordyceps* species, including the type, as a well-supported clade interspersed with genera initially described from asexual morphs, such as *Evlachovaea*, *Isaria*, and *Microhilum*. Furthermore, the study demonstrated that this core *Cordyceps* clade is not monophyletic with *C. cardinalis* and *C. pseudomilitaris*, consistent with findings by Sung et al. (2007). Consequently, these two species were reclassified into the newly erected genus *Blackwellomyces*, named in honor of Meredith Blackwell, a distinguished mycologist recognized for her work on arthropod-associated fungi (Kepler et al., 2017). Later, Mongkolsamrit et al. (2020) expanded the genus by describing four additional species: *B. aurantiacus*, *B. roseostromatus*, *B. calendulinus*, and *B. minutus*. In this thesis, the study of the entomopathogenic fungus *B. roseostromatus* (Hypocreales, Sordariomycetes) led to the identification and characterization of six metabolites, including four unprecedentedly reported natural products, as described in publication **II**.

The fungal strain *B. roseostromatus* BCC56290 was isolated from an infected lepidopteran larva found in Chiang Mai Province, Thailand. The pure culture was deposited in the BIOTEC culture collection (BCC). The identity of the strain was confirmed through molecular multilocus phylogenetic analyses, including the ITS, LSU, EF1, and RPB1 loci, which placed it in a clade together with BCC91358, the ex-type strain of *B. roseostromatus*. The *B. roseostromatus* strain BCC56290 was grown on BRFT solid-state medium, and the crude extract was fractionated using vacuum liquid chromatography (VLC) and preparative RP-HPLC. This process resulted in the isolation of the four previously undescribed metabolites ES-242-9 (**42**), beauveriolides T (**43**) and U (**44**), and cardinalisamide D (**45**), along with two known cyclodepsipeptides, cardinalisamides B (**46**) and C (**47**) (Figure 13).

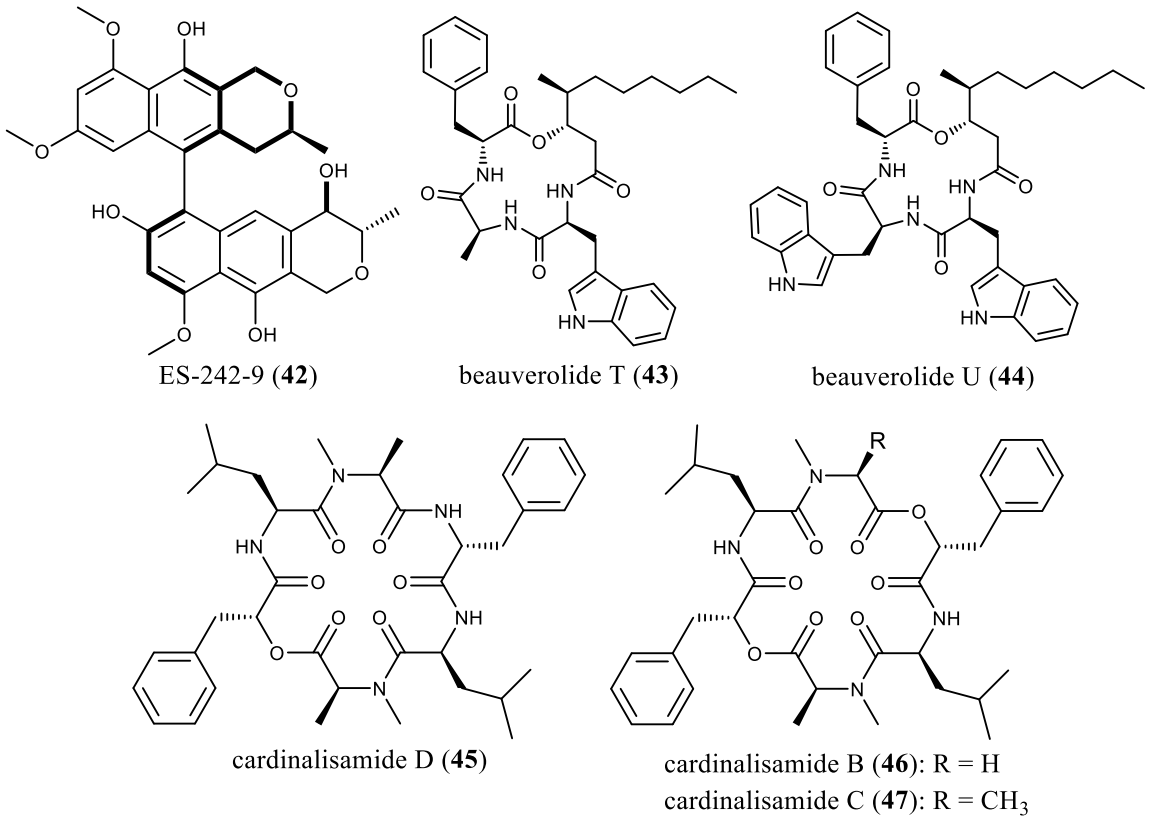

Figure 13. Chemical structures of metabolites (**42**–**47**) produced by *Blackwellomyces roseostromatus* (BCC56290).

Compound ES-242-9 (**42**) was characterized as a dimeric naphthopyran bioxanthracene derivative, and its structure and relative stereochemistry were elucidated using comprehensive ROESY correlations, confirming it as an ES-242 derivative. The absolute configuration of the cyclodepsipeptides beauveriolides T (**43**) and U (**44**) was determined using Marfey's method and supported by biosynthetic comparisons with beauveriolides, cyclic tetradepsipeptides previously reported from entomopathogenic fungi of the genera *Beauveria* (Elsworth and Grove, 1977; Jegorov et al., 1994; Matsuda et al., 2004), *Cordyceps* (Helaly et al., 2019; X. Wang et al., 2020), and *Isaria fumosorosea* (formerly *Paecilomyces fumosoroseus*) (Jegorov et al., 1994, 2004). Cardinalisamide D (**45**) is a previously unknown cyclohexadepsipeptide, structurally related to cardinalisamide C (**47**), and its amino acid sequence was established based on Marfey's analysis. Cardinalisamides B (**46**) and C (**47**) were identified by comparing their NMR and HR-ESI-MS data with previously reported literature.

The antimicrobial, cytotoxic, and nematicidal activities of isolated compounds (**42**–**47**) were evaluated against a range of bacterial and fungal strains, mammalian cell lines, and the nematode *C. elegans*. Cytotoxicity assays revealed that cardinalisamides B (**46**) and C (**47**)

exhibited significant pancytotoxic effects against human cancer cell lines, with IC_{50} values ranging from 2.2 µM to 13.9 µM. These compounds showed minimal toxicity toward mouse fibroblast cells (L929), indicating selective anticancer activity. In contrast, compounds **42**–**45** displayed little to no cytotoxic activity. None of the compounds demonstrated noteworthy antimicrobial effects against the tested bacteria and fungi. In the nematicidal assay, ES-242-9 (**42**) and cardinalisamide C (**47**) showed corrected mortality rates of 51.1% and 53.6%, respectively, at a concentration of 100 µg/mL, while the remaining compounds were inactive. Notably, ES-242-9 (**42**) exhibited selective nematicidal activity without significant cytotoxic or antimicrobial effects, highlighting its potential as a candidate for further development as a nematode-targeting biocontrol agent. ES-242 compounds, including **42**, are bioxanthracene derivatives that have been previously isolated from fungi of the genera *Verticillium* and *Cordyceps* (Toki et al., 1992a; Isaka et al., 2007). These compounds are known for their strong antagonistic effects on N-methyl-D-aspartate receptor, which is a critical component of the nervous system (Toki et al., 1992a, 1992b; Lin and Lane, 2019). The complete data set of MIC, IC_{50}, and corrected nematode mortality rate values can be found in publication **II**.

The genus *Blackwellomyces* is known to infect both coleopteran (beetles) and lepidopteran (moths and butterflies) insects (Kepler et al., 2017; Mongkolsamrit et al., 2020; Li et al., 2023). Only a few secondary metabolites have been reported from this genus, including compounds isolated from *B. cardinalis* NBRC 103832 prior to its formal description, such as the antitrypanosomal cyclohexadepsipeptides cardinalisamides A–C (Umeyama et al., 2014; Nakamura et al., 2024), and oosporein, a bibenzoquinone derivative with potent antimicrobial, antifungal, and insecticidal activities (Feng et al., 2015; Nakamura et al., 2024). Therefore, the compounds isolated from *B. roseostromatus* (BCC56290) might exhibit a wide range of biological activities, which are worth investigating.

3.3 Secondary Metabolites Produced by the Basidiomycete *Panus strigellus*

White rot fungi (WRF), an ecological group of basidiomycetes capable of degrading lignin (Suryadi et al., 2022), have been widely studied for their outstanding ability to decompose and remediate organic contaminants such as pharmaceutically active compounds, polychlorinated biphenyls, polycyclic aromatic hydrocarbons, and specific pesticides (Wu and Yu, 2007; Schlosser and Wick, 2011; Kristanti et al., 2011; Chen et al., 2022). The genus *Panus* belongs to the family Panaceae (Polyporales, Agaricomycetes) (Justo et al., 2017). It is morphologically characterized by an agaricoid growth habit with centrally to eccentrically stipitate basidiomata,

decurrent gills, and a dimitic hyphal system (comprising generative and skeletal hyphae) (Justo et al., 2017; Sousa-Guimarães et al., 2024; Yue et al., 2024). *Panus* species grow on dead wood, and some of them are identified as WRF, playing a vital role in organic matter decomposition (Corner, 1981; Senthilarasu, 2015; Vargas-Isla et al., 2015). The type species of the genus, *P. conchatus*, was initially described from Sweden (Sousa-Guimarães et al., 2024). However, much of the recently discovered species diversity is found in (sub)tropical regions (Sousa-Guimarães et al., 2024; Yue et al., 2024). Although WRF are well-studied for bioremediation, their potential for producing secondary metabolites is less explored. Aiming to explore the potential of WRF from Colombia, in publication **I**, the taxonomic identification of *P. strigellus* (CM-UDEA-H9) was reported, as well as the isolation, structural elucidation, and biological evaluation of its secondary metabolites.

The specimen of *P. strigellus* studied in this thesis (2574a AMV) was collected in Santa Fe de Antioquia, Colombia. This area has an elevation of 571 meters above sea level and an average temperature of 28 °C. The color of the basidiome was described using the Methuen Handbook of Colour (Kornerup and Wanscher, 1978). The specimen was deposited in the University of Antioquia herbarium (HUA), and a pure culture was obtained by isolating small fragments of the pileus. This culture was preserved on potato dextrose agar (PDA) at 4 °C until used in experiments and was subsequently deposited in the Microorganism Collection of the School of Microbiology at CM-EM-UdeA (CM-UDEA-H9). The specimen was initially identified as *P. strigellus* based on morphological traits, which were later confirmed by a molecular identification, involving a BLAST search in GenBank, using LSU and ITS sequences. The ITS sequence showed the highest similarity (99.76% and 99.05%) to *P. strigellus* reference sequences. The LSU sequence exhibited high similarity to *P. conchatus* (99.25%) and to *P. lecomtei* (99.17%). Despite some similarities to other *Panus* species in the LSU region, the morphological analysis of the voucher specimen, 2574a AMV, confirmed its identification as the tropical species *P. strigellus*.

P. strigellus (CM-UDEA-H9) was cultivated in liquid YM 6.3 medium, and from the supernatant crude extract, a new oligocyclic diterpenoid named panapophenanthrin (**48**) was isolated, along with the two known metabolites panepophenanthrin (**49**) and dihydrohypnophilin (**50**) (Figure 14). The isolation was performed using preparative RP-HPLC, and the absolute configuration of panapophenanthrin (**48**) was determined through ROESY correlations and TDDFT-ECD calculations. Panepophenanthrin (**49**), previously

isolated from *P. rudis*, has been extensively studied for its ability to inhibit the ubiquitin-activating enzyme, which is essential in the ubiquitin-proteasome pathway (Sekizawa et al., 2002; Moses et al., 2003; Lohr et al., 2010). Dihydrohypnophilin (**50**) is a hirsutane sesquiterpenoid compound that was previously isolated from fungi of the genus *Lentinus* (Abate and Abraham, 1994; Rukachaisirikul et al., 2005; Cota et al., 2008).

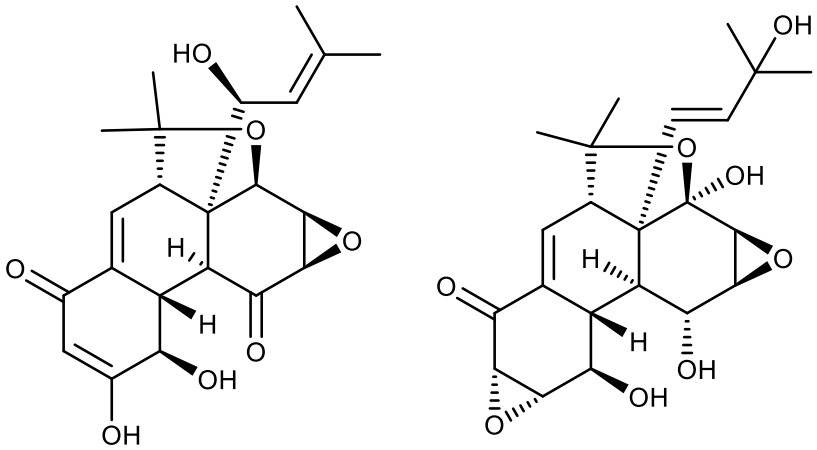

panapophenanthrin (**48**) panepophenanthrin (**49**)

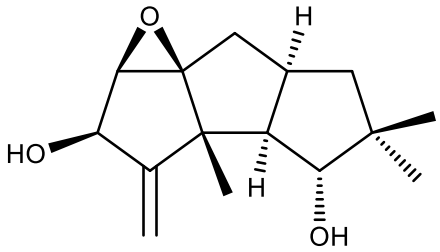

dihydrohypnophilin (**50**)

Figure 14. Chemical structures of metabolites (**48**–**50**) produced by *Panus strigellus* (CM-UDEA-H9).

Compounds **48**–**50** were evaluated for their antimicrobial and cytotoxic activity. Compounds **48** and **50** displayed weak to moderate antimicrobial effects. Specifically, panapophenanthrin (**48**) showed moderate activity against the Gram-positive bacterium *B. subtilis* (MIC = 33.3 µg/mL) and weak activity against *S. aureus* (MIC = 66.6 µg/mL). Dihydrohypnophilin (**50**) exhibited weak activity against *B. subtilis* (MIC = 66.6 µg/mL) and was inactive against the other tested organisms. Panepophenanthrin (**49**) showed no activity in any of the bioassays performed. Regarding the cytotoxic activity, **48** exhibited potent activity against both L929 (IC_{50} = 13.2 µM) and KB3.1 (IC_{50} = 17.9 µM) cells, and **50** showed weak to no cytotoxic activity against the tested cell lines in this study. However, prior studies revealed that the latter compound (**50**) exhibits activity against L929 cells, as well as activity

against the malarial parasite *P. falciparum*, and human small lung cancer (NCI-H187) cell lines (Rukachaisirikul et al., 2005). Interestingly, panapophenanthrin (**48**) demonstrated both antimicrobial and cytotoxic activities, whereas panepophenanthrin (**49**) was inactive in these assays, despite **48** being a derivative of **49**. This contrast underscores substantial differences in their biological properties and suggests that specific structural modifications present in **48** are responsible for its activity, warranting further investigation. The complete data set of MIC and IC_{50} values can be found in publication **I**.

Previous studies have identified various secondary metabolites in *Panus sensu lato* species, including epoxy compound derivatives (Sikder and Acharya, 2019; Song et al., 2021), sesquiterpenes (Ding et al., 2018), and other bioactive substances (S-X. Wang et al., 2020). However, research on their pharmacological properties and potential health benefits remains limited. One notable example is panepoxydone, first isolated from *Lentinus crinitus*, the type species of the genus *Lentinus* (Polyporaceae) (Anke and Sterner, 1996). Panepoxydone has also been identified in *P. conchatus* and *P. rudis* (Panaceae) and is known to disrupt NF-κB signaling, thereby inhibiting tumor growth (Anke and Sterner, 1996; Sikder and Acharya, 2019). Another example is hexacyclinol, isolated from *P. rudis*, which has demonstrated antiproliferative activity against L929 cells (Schlegel et al., 2002).

The taxonomy and systematics of the genus *Panus*, in which more than 100 published names are known, remain largely unresolved. For a long time, the genus *Panus* was interpreted as a subgenus of the morphologically similar genus *Lentinus* (Pegler, 1983). Recent multilocus phylogenetic reconstructions challenged this view and showed that the type species of *Panus* and *Lentinus* belong to two distinct families in the order Polyporales, namely Panaceae and Polyporaceae, respectively (Justo et al., 2017; Yue et al., 2024). However, many *Panus* species are still residing under the genus *Lentinus*, and taxonomic revisions are necessary to resolve the circumscriptions of both genera, their systematic placement, as well as species delineation. Continued research is needed to elucidate the chemical diversity and biological activities of secondary metabolites in these genera and to clarify their evolutionary relationships. Taken together, the genus *Panus* represents a promising source of biologically active secondary metabolites, underscoring the importance of investigating its diverse chemical profile.

4 Conclusion and Outlook

This thesis underscores the remarkable chemical diversity and biological potential of fungal secondary metabolites, positioning fungi as largely untapped sources of biologically active natural products. Through the investigation of fungi with distinct ecological roles and interactions, such as nematode-associated, entomopathogenic, and white-rot fungi, a broad range of new and known compounds from various structural classes was isolated. These include tetramic acids, cyclodepsipeptides, glycerolipids, DKPs, preussomerins, macrolides, xanthones, anthraquinones, sesquiterpenoids, and diterpenoids.

Several of the isolated metabolites exhibited remarkable antimicrobial, nematicidal, and cytotoxic activities. Notably, tetramic acids from *P. karssenii* and glycerolipids from *Murispora* sp. demonstrated potent nematicidal activity devoid of cytotoxic effects, marking them as promising candidates for the development of safe nematode biocontrol agents. Furthermore, comparative metabolite profiling of endophytic and nematode-associated strains from two sister species of a previously undescribed genus within Pleosporales revealed shared biosynthetic pathways, suggesting adaptive chemical strategies that facilitate a dual ecological strategy involving both plant association and nematode parasitism. These strains produced preussomerins and macrolides that demonstrated strong antimicrobial and cytotoxic effects. Additionally, *Pyrenochaeta* sp. yielded novel xanthone and anthraquinone derivatives, compound classes known for their diverse bioactivities. Structurally unique compounds such as panapophenanthrin from *P. strigellus* and ES-242-9 from *B. roseostromatus* were also characterized; the latter exhibited selective nematicidal activity, further emphasizing its potential in nematode-targeted control strategies.

Despite these promising findings, significant challenges remain in unraveling the mechanisms of action and the natural ecological roles of these metabolites. Future research should aim to broaden bioactivity assays against a wider range of pathogens and pest organisms. Therefore, compounds available in sufficient quantities will be submitted for bioactivity screening as part of a collaborative program with the Helmholtz Institute for Pharmaceutical Research in Saarbrücken (HIPS). Additionally, further exploration of nematicidal compounds against a wider array of nematode species, particularly plant-parasitic nematodes, is essential. Moreover, molecular identification and multilocus phylogenetic analyses of the undescribed nematode-associated species are crucial for linking their unique metabolite profiles to their evolutionary relationships.

In summary, this study enhances the current knowledge of fungal secondary metabolism, highlighting the remarkable chemical and biological diversity within ecologically specialized taxa. It also underscores the importance of a thorough understanding of fungal taxonomy and ecological strategies to enable effective targeted screening of fungal secondary metabolites. The insights gained serve as a solid foundation for future natural product discovery and underscore the importance of continued exploration of understudied fungal groups as sources of new bioactive metabolites with potential applications in pharmaceuticals, agriculture, and environmental science.

5 Additional Projects

5.1 Cytotoxic Metabolite from the Nematode-Associated Fungus *Pochonia chlamydosporia*

The nematode-associated fungal strain *Pochonia chlamydosporia* DSM 119501 (Clavicipitaceae, Hypocreales) was studied as part of our ongoing search for novel fungal biocontrol agents targeting PPNs. Isolated from eggs of the cereal cyst nematode *H. filipjevi*, DSM 119501 was identified based on multigene phylogenetic analysis and morphological features. *Pochonia* species are recognized for producing a variety of bioactive secondary metabolites and have been extensively studied for their potential as biocontrol agents, particularly against PPNs (Manzanilla-López et al., 2013; Niu, 2017). From submerged cultures of *P. chlamydosporia* DSM 119501 grown in Q6 ½ medium, a novel tetramic acid derivative named pochoniatoxin (**51**) (Figure 15) was isolated along with characteristic nematicidal resorcylic acid lactones: monocillin II (**52**), monocillin III (**53**), monocillin IV (**54**), and monorden (**55**). The structure of pochoniatoxin (**51**) was elucidated using HR-ESI-MS and comprehensive 1D and 2D NMR analyses. The relative and absolute configurations were determined by coupling constant analysis, ROESY correlations, and Marfey's method.

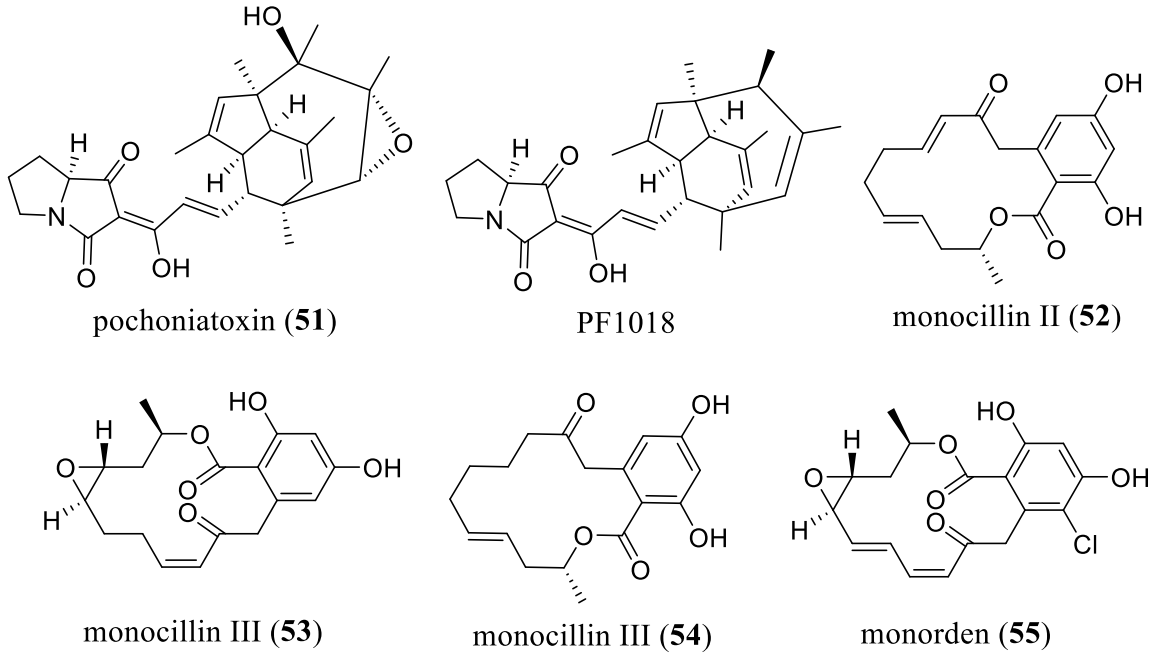

Figure 15. Chemical structures of metabolites (**51**–**55**) produced by *Pochonia chlamydosporia* DSM 119501, along with PF1018.

Biological assays revealed that pochoniatoxin (**51**) exhibits potent nematicidal activity against *C. elegans*, with an 82.1% mortality rate at 2 µg/mL. Additionally, **51** demonstrated moderate

antiplasmodial activity against *P. falciparum* (IC_{50} = 15 µM for the chloroquine-sensitive 3D7 strain and 8.2 µM for the chloroquine-resistant Dd2 strain). However, no antibacterial or antifungal activity was observed against standard test organisms. Cytotoxicity assays revealed strong activity of **51** against the human cancer cell lines PC-3 (IC_{50} = 8 nM), KB3.1 (IC_{50} = 107 nM), A431 (IC_{50} = 112 nM), and SK-OV-3 (IC_{50} = 97 nM), while murine non-malignant L929 cells exhibited lower sensitivity (IC_{50} = 10.5 µM), suggesting selectivity towards malignant cells. The study of the mechanism of action of the cytotoxic effects of pochoniatoxin (**51**) in U-2OS cells indicated that **51** induces apoptosis and necrosis, suppresses proliferation, and impairs lamellipodial dynamics, without affecting microtubule integrity, implying interference with actin-driven motility and potential cell-cycle regulators. Interestingly, these cytotoxic properties differ markedly from those of PF1018 (Figure 15), an insecticidal tetramic acid isolated from a "*Humicola* sp." with a structurally related scaffold, which was reported to exhibit no significant cytotoxicity against certain cancer cell lines (Gomi et al., 1994). The absence of antibacterial activity of compound **51** can be explained by its specific action on eukaryotic targets. However, it remains unclear why fungi, which share a similar cytoskeleton, are not affected by **51**. One possible explanation is that fungi may not effectively take up the compound. The complete data set of bioassay results is provided in publication **VI**.

This study highlights the remarkable biosynthetic capacity of *Pochonia* species, which produce diverse secondary metabolites such as tetrapeptides and monorden derivatives known for their antiparasitic, nematicidal properties, and generally low cytotoxicity. In contrast, the strong cytotoxicity of pochoniatoxin (**51**) indicates its potential as a promising lead for anticancer drug development, showing activity against malignant cells comparable to that of precursors of already marketed anticancer agents. These findings also underscore the need for a careful evaluation of toxin-producing strains prior to their use in biocontrol. Given the widespread interest in *P. chlamydosporia* as a myconematicide, this work reinforces the importance of assessing both efficacy and safety in the development of fungal strains for sustainable biocontrol applications.

5.2 Bioactive Metabolites from Endophytic Fungi of the Genus *Polyphilus*

The endophytic fungal strains *Polyphilus frankenii* DSM 106521 and *P. sieberi* DSM 106515, isolated from the roots of *Pinus sylvestris* and *Asclepias syriaca*, respectively, were investigated for their ability to produce secondary metabolites with potential antimicrobial activity. Notably, *P. sieberi* exhibits a dual lifestyle, as it has also been reported as a nematode-

associated fungus (Ashrafi et al., 2018). Crude extracts from the strains grown in YM 6.3, BRFT, and WOFT media were purified through chromatographic techniques. This study led to the isolation of two previously unreported naphtho-α-pyranone derivatives: a monomeric compound, named semitalaroderxine C (**56**), and its symmetric 6,6′-homodimer, named talaroderxine C (**57**) (Figure 16). Additionally, two known diketopiperazine derivatives, outovirin B (**58**) and (3S,6S)-3,6-dibenzylpiperazine-2,5-dione (**59**), were isolated. The compounds were characterized by 1D and 2D NMR, as well as HR-ESI-MS. The absolute configurations of the newly discovered naphtho-α-pyranones were determined by comparing their experimental ECD spectra with those of structurally related analogues.

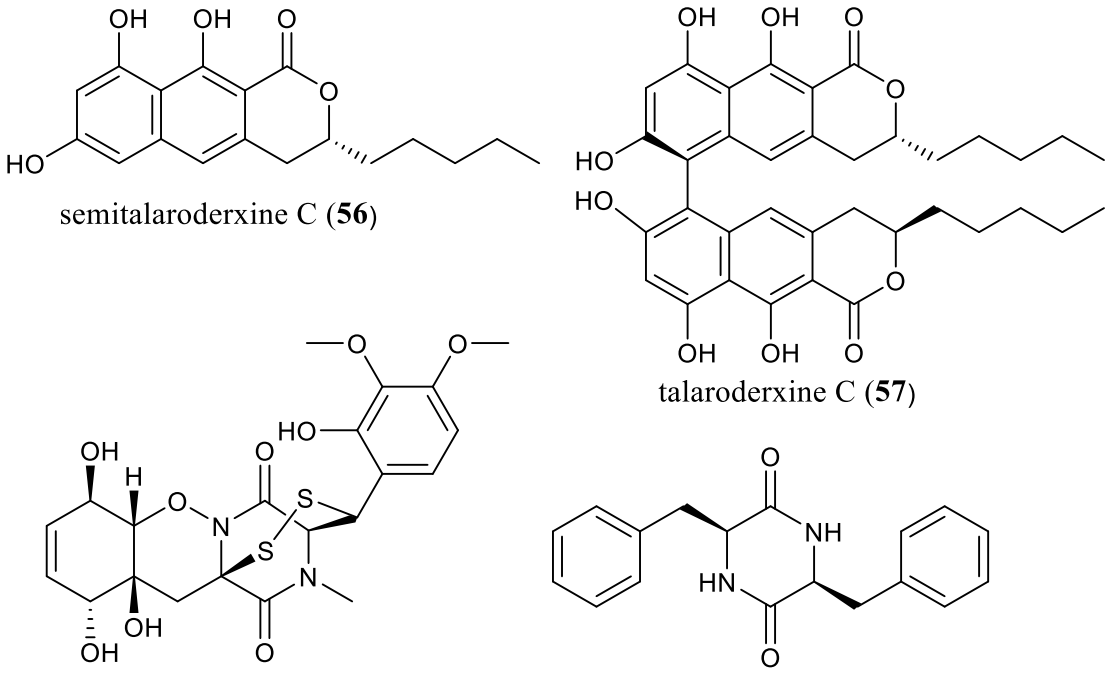

Figure 16. Chemical structures of metabolites (**56**–**59**) produced by *Polyphilus frankenii* (DSM 106521) and *P. sieberi* (DSM 106515).

Due to the limited quantities of compounds **56**, **58**, and **59**, only talaroderxine C (**57**) was evaluated for its antimicrobial and cytotoxicity activity. Biological evaluation revealed that **57** exhibited strong antimicrobial activity against *B. subtilis* (MIC = 0.52 µg/mL) and moderate inhibition of *S. aureus* (MIC = 66.6 µg/mL). Moreover, **57** demonstrated significant cytotoxicity across several mammalian cell lines, with IC_{50} values in the low micromolar to nanomolar range. Notably, **57** showed potent activity against MCF-7 cells, with an IC_{50} value of 68 nM. The complete data set of MIC and IC_{50} values of **57** can be found in publication **IV**.

This study represents the first report on secondary metabolites from the genus *Polyphilus*. The discovery of semitalaroderxine C (**56**) and talaroderxine C (**57**) broadens the understanding of the chemical diversity of this recently established genus and highlights its potential to produce biologically active compounds. The findings of this study indicate that *Polyphilus* strains produce highly cytotoxic secondary metabolites, suggesting that they should be deprioritized for future biocontrol applications in favor of other strains devoid of toxic metabolites.

5.3 Secondary Metabolites Produced by *Lachnum* sp.

The saprotrophic fungal strain *Lachnum* sp. DSM 116717, isolated from *Lachnum* apothecia growing on the dead stalk of *Phragmites communis* (common reed grass), was tentatively identified as *Lachnum* (cf.) *carneolum* based on morphological features and preliminary molecular characterization. This strain was selected for chemical prospecting due to its diverse secondary metabolite profile and the strong biological activity observed in its crude extract. Crude extracts obtained from fermentation in ZM ½ liquid medium were separated by preparative RP-HPLC, yielding six new ambuic acid analogues, named lachnuoic acids A–F (**60**–**65**) (Figure 17). The structures of these compounds were elucidated through comprehensive spectroscopic analyses, including 1D and 2D NMR, HR-ESI-MS, and Mosher's ester method.

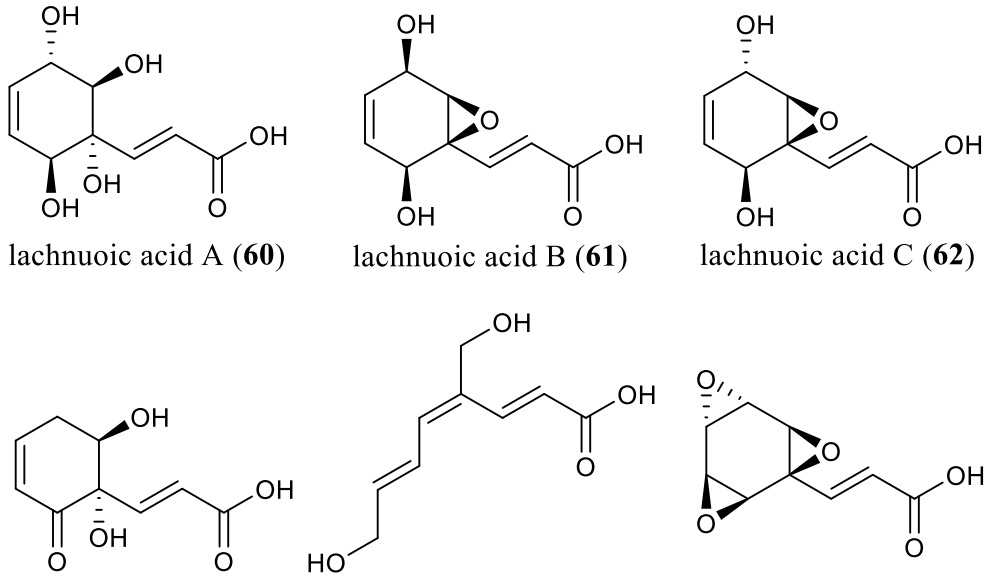

Figure 17. Chemical structures of metabolites (**60**–**65**) produced by *Lachnum* sp. (DSM 116717).

All six compounds were evaluated for cytotoxic, antimicrobial, antibiofilm, and nematicidal activities. Among them, lachnuoic acid A (**60**) exhibited strong antimicrobial activity against

the Gram-positive bacteria *B. subtilis* (MIC = 8.3 µg/mL) and *S. aureus* (MIC = 16.6 µg/mL). The remaining compounds (**61**–**65**) showed no significant activity in the assays performed. The complete data set of MIC, IC_{50}, corrected nematode mortality rate, and biofilm inhibition values is provided in publication **V**.

This study represents the first report of ambuic acid-type metabolites from a member of the Leotiomycetes, as these compounds had previously only been identified from species belonging to the Sordariomycetes. The crude extract of *Lachnum* sp. DSM 116717 exhibited strong biological activity; however, after purification, only lachnuoic acid A (**60**) showed significant antimicrobial properties. This finding suggests that other bioactive but potentially unstable compounds may have been degraded or lost during the purification process.

Although none of the compounds isolated in this study exhibited nematicidal activity, the genus *Lachnum* is well known for its ability to produce nematicidal secondary metabolites. *L. papyraceum*, for example, produces chlorinated metabolites such as lachnumon, lachnumol A, and mycorrhizin derivatives (Stadler et al., 1993a, 1993b, 1995a, 1995b; Shan et al., 1996), which have demonstrated nematicidal effects against *C. elegans*, with mycorrhizin A showing the highest activity (LD_{90} = 1 µg/mL). Furthermore, recent polyphasic taxonomic studies have identified the nematicidal compounds lachnumon, lachnumol A, and dechloromycorrhizin A in other *Lachnum* species (Demir et al., 2024), suggesting that nematicidal potential is not limited to a single species within the genus. The potential of *Lachnum* species to produce diverse nematicidal metabolites underscores their ecological role as nematode antagonists and highlights their promise as sources for nematode biocontrol strategies.

5.4 Secondary Metabolites from Entomopathogenic Fungi from Thailand

During a secondment at BIOTEC-NSTDA in Pathum Thani, Thailand, as part of the RISE project funded by the EU to explore the mycobiota of Asia, Africa, and Europe for beneficial metabolites and potential biocontrol agents using -OMICS techniques, the secondary metabolite profiles of fourteen strains belonging to the genera *Cordyceps*, *Ophiocordyceps*, *Pleurocordyceps*, *Polycephalomyces*, *Samsoniella*, and *Tolypocladium* (Ascomycota) were studied. These strains were collected in Thailand and isolated from insects of the superfamily Cicadoidea (Khonsanit, pers. comm.). An upscaling process was conducted for all strains due to their potential for further investigation, as they represent new species. At BIOTEC (Thailand), fermentation was carried out using two different media, each selected according to

the specific strain. The resulting crude extracts were transported to HZI (Germany), where HPLC-MS dereplication of all crude extracts was performed by analyzing their HR-ESI-MS data in combination with literature searches. Crude extracts from five strains belonging to the genera *Ophiocordyceps*, *Pleurocordyceps*, and *Tolypocladium* were further separated. Since the strains mainly produced fatty acids, few compounds were isolated and their structures elucidated. In total, 13 known compounds were isolated, with only stipitalide (**66**), 4-hydroxy-3,6-dimethyl-2-pyrone (**67**), and 3-methylorsellinic acid (**68**) (Figure 18) from *Pleurocordyceps* sp. (MY06270) considered interesting for science. These compounds were tested for antimicrobial, cytotoxic, and nematicidal activities, and none of the compounds showed noteworthy effects. The results from this work will be published in a taxonomic journal, including descriptions of new species of the genus *Pleurocordyceps* along with their secondary metabolite profiles.

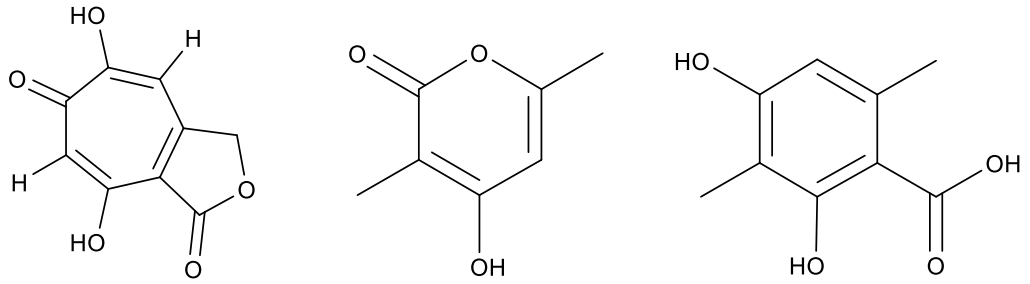

stipitalide (**66**) | 4-hydroxy-3,6-dimethyl-2-pyrone (**67**) | 3-methylorsellinic acid (**68**)

Figure 18. Chemical structures of metabolites (**66**–**68**) produced by *Pleurocordyceps* sp. (MY06270).

6 References

Abate D & Abraham WR (1994). Antimicrobial metabolites from *Lentinus crinitus*. *The Journal of Antibiotics* 47(11): 1348–1350. https://doi.org/10.7164/antibiotics.47.1348.

Abed RMM, Dobretsov S, Al-Fori M, Gunasekera SP, Sudesh K & Paul VJ (2013). Quorum-sensing inhibitory compounds from extremophilic microorganisms isolated from a hypersaline cyanobacterial mat. *Journal of Industrial Microbiology and Biotechnology* 40(7): 759–772. https://doi.org/10.1007/s10295-013-1276-4.

Abraham EP (1979). A glimpse of the early history of the cephalosporins. *Reviews of Infectious Diseases* 1(1): 99–105. https://doi.org/10.1093/clinids/1.1.99.

Abraham EP (1987). Cephalosporins 1945–1986. *Drugs* 34(2): 1–14. https://doi.org/10.2165/00003495-198700342-00003.

Ahmad G, Khan A, Khan AA, Ali A & Mohhamad HI (2021). Biological control: A novel strategy for the control of the plant parasitic nematodes. *Antonie van Leeuwenhoek*. Springer Science and Business Media Deutschland GmbH 885–912. https://doi.org/10.1007/s10482-021-01577-9.

Al-Ani LKT, Soares FE de F, Sharma A, de los Santos-Villalobos S, Valdivia-Padilla AV & Aguilar-Marcelino L (2022). Strategy of nematophagous fungi in determining the activity of plant parasitic nematodes and their prospective role in sustainable agriculture. *Frontiers in Fungal Biology* 3: 863198. https://doi.org/10.3389/ffunb.2022.863198.

Alberts AW, Chen J, Kuron G, Hunt V, Huff J, Hoffman C, Rothrock J, Lopez M, Joshua H, Harris E, *et al.* (1980). Mevinolin: A highly potent competitive inhibitor of hydroxymethylglutaryl-coenzyme A reductase and a cholesterol-lowering agent. *Proceedings of the National Academy of Sciences of the United States of America* 77(7 II): 3957–3961. https://doi.org/10.1073/pnas.77.7.3957.

Aly AH, Debbab A & Proksch P (2011). Fifty years of drug discovery from fungi. *Fungal Diversity* 50(1): 3–19. https://doi.org/10.1007/s13225-011-0116-y.

Ando Y, Ogawa D, Ohmori K & Suzuki K (2022). Enantioselective total syntheses of preussomerins: Control of spiroacetal stereogenicity by photochemical reaction of a naphthoquinone through 1,6-hydrogen atom transfer. *Angewandte Chemie - International Edition* 62(5): e202213682. https://doi.org/10.1002/anie.202213682.

Anke T, Oberwinkler F, Steglich W & Schramm G (1977). The strobilurins - new antifungal antibiotics from the basidiomycete *Strobilurus tenacellus*. *The Journal of Antibiotics* 30(10): 806–810. https://doi.org/10.7164/antibiotics.30.806.

Ashrafi S, Helaly S, Schroers HJ, Stadler M, Richert-Poeggeler KR, Dababat AA & Maier W (2017). *Ijuhya vitellina* sp. nov., a novel source for chaetoglobosin A, is a destructive parasite of the cereal cyst nematode *Heterodera filipjevi*. *PLoS ONE* 12(7): e0180032. https://doi.org/10.1371/journal.pone.0180032.

Ashrafi S, Knapp DG, Blaudez D, Chalot M, Maciá-Vicente JG, Zagyva I, Dababat AA, Maier W, Kovács GM (2018). Inhabiting plant roots, nematodes, and truffles—*Polyphilus*, a new helotialean genus with two globally distributed species. *Mycologia* 110(2): 286–299. https://doi.org/10.1080/00275514.2018.1448167.

Ashrafi S, Wennrich JP, Becker Y, Maciá-Vicente JG, Brißke-Rode A, Daub M, Thünen T, Dababat AA, Finckh MR, Stadler M, *et al.* (2023). *Polydomus karssenii* gen. nov. sp. nov.

is a dark septate endophyte with a bifunctional lifestyle parasitising eggs of plant parasitic cyst nematodes (*Heterodera* spp.). *IMA Fungus* 14(1): 1–20. https://doi.org/10.1186/s43008-023-00113-w.

Bahram M & Netherway T (2022). Fungi as mediators linking organisms and ecosystems. *FEMS Microbiology Reviews* 46(2): 1–16. https://doi.org/10.1093/femsre/fuab058.

Bale JS, Van Lenteren JC & Bigler F (2008). Biological control and sustainable food production. *Philosophical Transactions of the Royal Society B: Biological Sciences* 363(1492): 761–776. https://doi.org/10.1098/rstb.2007.2182.

Bamisile BS, Akutse KS, Siddiqui JA & Xu Y (2021). Model application of entomopathogenic fungi as alternatives to chemical pesticides: Prospects, challenges, and insights for next-generation sustainable agriculture. *Frontiers in Plant Science* 12: 741804. https://doi.org/10.3389/fpls.2021.741804.

Barelli L, Behie SW, Hu S & Bidochka MJ (2022). Profiling destruxin synthesis by specialist and generalist *Metarhizium* insect pathogens during coculture with plants. *Applied and Environmental Microbiology* 88(12). https://doi.org/10.1128/aem.02474-21.

Barry KH, Koutros S, Lubin JH, Coble JB, Barone-Adesi F, Beane Freeman LE, Sandler DP, Hoppin JA, Ma X, Zheng T, *et al.* (2012). Methyl bromide exposure and cancer risk in the Agricultural Health Study. *Cancer Causes and Control* 23(6): 807–818. https://doi.org/10.1007/s10552-012-9949-2.

Bartlett DW, Clough JM, Godwin JR, Hall AA, Hamer M & Parr-Dobrzanski B (2002). The strobilurin fungicides. *Pest Management Science* 58(7): 649–662. https://doi.org/10.1002/ps.520.

Bentley R (2000). Mycophenolic acid: A one hundred year odyssey from antibiotic to immunosuppressant. *Chemical Reviews* 100(10): 3801–3825. https://doi.org/10.1021/cr990097b.

Benz F, Knüsel F, Nüesch J, Treichler H, Voser W, Nyfeler R & Keller-Schierlein W (1974). Stoffwechselprodukte von Mikroorganismen 143. Mitteilung. Echinocandin B, ein neuartiges Polypeptid-Antibioticum aus *Aspergillus nidulans* var. *echinulatus*: Isolierung und Bausteine. *Helvetica Chimica Acta* 57(8): 2459–2477. https://doi.org/10.1002/hlca.19740570818.

Bills GF & Gloer JB (2016). Biologically active secondary metabolites from fungi. *Microbiology Spectrum* 4(6). https://doi.org/10.1128/microbiolspec.funk-0009-2016.

Böhm C, Wolken S, Schnyder M, Basso W, Deplazes P, Di Cesare A, Deuster K & Schaper R (2015). Efficacy of emodepside/praziquantel spot-on (Profender®) against adult *Aelurostrongylus abstrusus* nematodes in experimentally infected cats. *Parasitology Research* 114(1): 155–164. https://doi.org/10.1007/s00436-015-4521-0.

Borel JF, Feurer C, Gubler HU & Stähelin H (1976). Biological effects of cyclosporin A: A new antilymphocytic agent. *Agents and Actions* 6(4): 468–475. https://doi.org/10.1007/BF01973261.

Bout A, Ris N, Multeau C & Mailleret L (2022). Augmentative biological control using entomophagous arthropods. in X. Fauvergue (ed.) *Extended Biocontrol*. Springer, Dordrecht 43–53. https://doi.org/10.1007/978-94-024-2150-7_4.

Bräse S, Encinas A, Keck J & Nising CF (2009). Chemistry and biology of mycotoxins and

related fungal metabolites. *Chemical Reviews* 109(9): 3903–3990. https://doi.org/10.1021/cr050001f.

Case NT, Gurr SJ, Fisher MC, Blehert DS, Boone C, Casadevall A, Chowdhary A, Cuomo CA, Currie CR, Denning DW, *et al.* (2025). Fungal impacts on Earth's ecosystems. *Nature* 638(8049): 49–57. https://doi.org/10.1038/s41586-024-08419-4.

Cao C, Yang S, Zhou Z (2020). The potential application of *Cordyceps* in metabolic-related disorders. *Phytotherapy Research* 34(2): 295–305. https://doi.org/10.1002/ptr.6536.

Chaichian S, Moazzami B, Sadoughi F, Haddad Kashani H, Zaroudi M & Asemi Z (2020). Functional activities of beta-glucans in the prevention or treatment of cervical cancer. *Journal of Ovarian Research* 13(1): 1–12. https://doi.org/10.1186/s13048-020-00626-7.

Chen L, Zhang X, Zhang M, Zhu Y & Zhuo R (2022). Removal of heavy-metal pollutants by white rot fungi: Mechanisms, achievements, and perspectives. *Journal of Cleaner Production* 354: 131681. https://doi.org/10.1016/j.jclepro.2022.131681.

Chen S, Chen D, Cai R, Cui H, Long Y, Lu Y, Li C & She Z (2016). Cytotoxic and antibacterial preussomerins from the mangrove endophytic fungus *Lasiodiplodia theobromae* ZJ-HQ1. *Journal of Natural Products* 79(9): 2397–2402. https://doi.org/10.1021/acs.jnatprod.6b00639.

Chi S & Heathcock CH (1999). Total syntheses of (±)-preussomerins G and I. *Bioorganic & Medicinal Chemistry Letters* 1(1): 3–5. https://doi.org/10.1021/ol990020+.

Corner EJH (1981). The agaric genera *Lentinus*, *Panus*, and *Pleurotus*, with particular reference to Malaysian species. *Nova Hedwigia* 69: 1–169.

Da Costa E, Domingues P, Melo T, Coelho E, Pereira R, Calado R, Abreu MH & Domingues MR (2019). Lipidomic signatures reveal seasonal shifts on the relative abundance of high-valued lipids from the brown algae *Fucus vesiculosus*. *Marine Drugs* 17(6). https://doi.org/10.3390/md17060335.

Costa KA, Maldonado A, Donaldson J, Guingab-Cagmat J, Garrett T & Bowden JA (2024). Examining the sublethal impacts of environmentally relevant concentrations of *Karenia brevis* on three South Florida reef-building coral species using a multi-omics workflow. *Coral Reefs* 43(6): 1703–1716. https://doi.org/10.1007/s00338-024-02567-9.

Cota BB, Rosa LH, Fagundes EMS, Martins-Filho OA, Correa-Oliveira R, Romanha AJ, Rosa CA & Zani CL (2008). A potent trypanocidal component from the fungus *Lentinus strigosus* inhibits trypanothione reductase and modulates PBMC proliferation. *Memórias do Instituto Oswaldo Cruz* 103(3): 263–270. https://doi.org/10.1590/S0074-02762008000300007.

Dale JA, Dull DL & Mosher HS (1969). α-Methoxy-α-trifluoromethylphenylacetic acid, a versatile reagent for the determination of enantiomeric composition of alcohols and amines. *Journal of Organic Chemistry* 34(9): 2543–2549. https://doi.org/10.1021/jo01261a013.

Decraemer W & Hunt DJ (2013). Structure and classification. in *Plant nematology*. 2nd ed. UK: CABI 3–39. https://doi.org/10.1079/9781780641515.0003.

Degenkolb T & Vilcinskas A (2016). Metabolites from nematophagous fungi and nematicidal natural products from fungi as an alternative for biological control. Part I: metabolites from nematophagous ascomycetes. *Applied Microbiology and Biotechnology* 100(9):

3799–3812. https://doi.org/10.1007/s00253-015-7233-6.

Demir Ö, Chen Y, Lambert C, Schüffler A, Surup F & Stadler M (2024). Elucidation of the life cycle of a saprotrophic inoperculate discomycete that is associated with pinesap using a polyphasic taxonomic approach. *Mycological Progress* 23(1): 1–11. https://doi.org/10.1007/s11557-024-01978-w.

Dias DA, Urban S & Roessner U (2012). A historical overview of natural products in drug discovery. *Metabolites* 2(2): 303–336. https://doi.org/10.3390/metabo2020303.

Ding J-H, Li Z-H, Feng T & Liu J-K (2018). A new cadinane sesquiterpenoid from cultures of the basidiomycete *Panus conchatus*. *Natural Product Research* 32(19): 2333–2337. https://doi.org/10.1080/14786419.2017.1413559.

Dong JY, Song HC, Li JH, Tang YS, Sun R, Wang L, Zhou YP, Wang LM, Shen KZ, Wang CR, *et al.* (2008). Ymf 1029A-E, preussomerin analogues from the fresh-water-derived fungus YMF 1.01029. *Journal of Natural Products* 71(6): 952–956. https://doi.org/10.1021/np800034g.

Eaton RA & Hale MDC (1993). *Wood: Decay, pests and protection*. London: Chapman and Hall. Available at: https://www.cabidigitallibrary.org/doi/full/10.5555/19940606334.

Eckhardt SG, Baker SD, Britten CD, Hidalgo M, Siu L, Hammond LA, Villalona-Calero MA, Felton S, Drengler R, Kuhn JG, *et al.* (2000). Phase I and pharmacokinetic study of irofulven, a novel mushroom-derived cytotoxin, administered for five consecutive days every four weeks in patients with advanced solid malignancies. *Journal of Clinical Oncology* 18(24): 4086–4097. https://doi.org/10.1200/JCO.2000.18.24.4086.

Elsworth JF & Grove JF (1977). Cyclodepsipeptides from *Beauveria bassiana* bals. Part 1. Beauverolides H and I. *Journal of the Chemical Society, Perkin Transactions 1* (3): 270–273. https://doi.org/10.1039/p19770000270.

Erkel G, Anke T & Sterner O (1996). Inhibition of NF-κB activation by panepoxydone. *Biochemical and Biophysical Research Communications* 226(1): 214–221. https://doi.org/10.1006/bbrc.1996.1335.

Esteves I, Maleita C & Abrantes I (2015). Root-lesion and root-knot nematodes parasitizing potato. *European Journal of Plant Pathology* 141(2): 397–406. https://doi.org/10.1007/s10658-014-0551-1.

Fair RJ & Tor Y (2014). Antibiotics and bacterial resistance in the 21st century. *Perspectives in Medicinal Chemistry* (6): 25–64. https://doi.org/10.4137/PMC.S14459.

Fang M, Long W, Sun J, Wang A, Chen L, Cui Y, Huang Z, Li J, Ruan W, Rasmann S, *et al.* (2023). Toxicity of fungal-derived volatile organic compounds against root-knot nematodes. *Pest Management Science* 79(12): 5162–5172. https://doi.org/10.1002/ps.7719.

Feng P, Shang Y, Cen K & Wang C (2015). Fungal biosynthesis of the bibenzoquinone oosporein to evade insect immunity. *Proceedings of the National Academy of Sciences of the United States of America* 112(36): 11365–11370. https://doi.org/10.1073/pnas.1503200112.

Fisher MC, Henk DA, Briggs CJ, Brownstein JS, Madoff LC, McCraw SL & Gurr SJ (2012). Emerging fungal threats to animal, plant and ecosystem health. *Nature* 484(7393): 186–194. https://doi.org/10.1038/nature10947.

Fisher MC, Gurr SJ, Cuomo CA, Blehert DS, Jin H, Stukenbrock EH, Stajich JE, Kahmann R, Boone C, Denning DW, *et al.* (2020). Threats posed by the fungal kingdom to humans, wildlife, and agriculture. *mBio* 11(3). https://doi.org/10.1128/mBio.00449-20.

Fleming A (1929). On the antibacterial action of cultures of a *Penicillium*, with special reference to their use in the isolation of *B. influenzae*. *The British Journal of Experimental Pathology* 10(3): 226–236. https://doi.org/10.1093/clinids/2.1.129.

Florey HW, Jennings MA, Gilliver K & Sanders AG (1946). Mycophenolic acid an antibiotic from *Penicillium brevicompactum* Dierckk. *The Lancet* 247(6385): 46–49. https://doi.org/10.1016/S0140-6736(46)90242-5.

Gibson DM, Donzelli BGG, Krasnoff SB & Keyhani NO (2014). Discovering the secondary metabolite potential encoded within entomopathogenic fungi. *Natural Product Reports* 31(10): 1287–1305. https://doi.org/10.1039/c4np00054d.

Gomi S, Imamura KI, Yaguchi T, Kodama Y, Minowa N, Koyama M (1994). PF1018, a novel insecticidal compound produced by *Humicola* sp. *The Journal of Antibiotics*. 47(5): 571–580. https://doi.org/10.7164/antibiotics.47.571.

Hafez-Ghoran S, Taktaz F, Ayatollahi SA & Kijjoa A (2022). Anthraquinones and their analogues from marine-derived fungi: Chemistry and biological activities. *Marine Drugs* 20(8): 474. https://doi.org/10.3390/md20080474.

Haritakun R, Sappan M, Suvannakad R, Tasanathai K & Isaka M (2010). An antimycobacterial cyclodepsipeptide from the entomopathogenic fungus *Ophiocordyceps communis* BCC 16475. *Journal of natural products* 73(1): 75–78. https://doi.org/10.1021/np900520b.

Harms H, Schlosser D & Wick LY (2011). Untapped potential: Exploiting fungi in bioremediation of hazardous chemicals. *Nature Reviews Microbiology* 9(3): 177–192. https://doi.org/10.1038/nrmicro2519.

Harms K, Surup F, Stadler M, Stchigel AM & Marin-felix Y (2021). Morinagadepsin, a depsipeptide from the fungus *Morinagamyces vermicularis* gen. et comb. nov. *Microorganisms* 9(6): 1191. https://doi.org/10.3390/microorganisms9061191.

Hazuda D, Blau CU, Felock P, Hastings J, Pramanik B, Wolfe A, Bushman F, Farnet C, Goetz M, Williams M, *et al.* (1999). Isolation and characterization of novel human immunodeficiency virus integrase inhibitors from fungal metabolites. *Antiviral Chemistry and Chemotherapy* 10(2): 63–70. https://doi.org/10.1177/095632029901000202.

Helaly SE, Ashrafi S, Teponno RB, Bernecker S, Dababat AA, Maier W & Stadler M (2018). Nematicidal cyclic lipodepsipeptides and a xanthocillin derivative from a phaeosphariaceous fungus parasitizing eggs of the plant-parasitic nematode *Heterodera filipjevi*. *Journal of Natural Products* 81(10): 2228–2234. https://doi.org/10.1021/acs.jnatprod.8b00486.

Helaly SE, Kuephadungphan W, Phainuphong P, Ibrahim MAA, Tasanathai K, Mongkolsamrit S, Luangsa-Ard JJ, Phongpaichit S, Rukachaisirikul V & Stadler M (2019). Pigmentosins from *Gibellula* sp. as antibiofilm agents and a new glycosylated asperfuran from *Cordyceps javanica*. *Beilstein Journal of Organic Chemistry* 15(1): 2968–2981. https://doi.org/10.3762/bjoc.15.293.

Hellwig V, Mayer-Bartschmid A, Müller H, Greif G, Kleymann G, Zitzmann W, Tichy HV & Stadler M (2003). Pochonins A-F, new antiviral and antiparasitic resorcylic acid lactones from *Pochonia chlamydosporia* var. *catenulata*. *Journal of Natural Products* 66(6): 829–

837. https://doi.org/10.1021/np020556v.

Hodda M (2022). Phylum Nematoda: A classification, catalogue and index of valid genera, with a census of valid species. *Zootaxa* 5114(1): 1–289. https://doi.org/10.11646/zootaxa.5114.1.1.

Hofmann A, Heim R, Brack A & Kobel H (1958). Psilocybin, a psychotropic substance from the Mexican mushroom *Psilocybe mexicana* Heim. *Experientia* 14(3): 107–109. https://doi.org/10.1007/BF02159243.

Horn WS, Smith JL, Bills GF, Raghoobar SL, Helms GL, Kurtz MB, Marrinan JA, Frommer BR, Thornton RA & Mandala SM (1992). Sphingofungins E and F: Novel serinepalmitoyl trans-ferase inhibitors from *Paecilomyces variotii*. *The Journal of Antibiotics* 45(10): 1692–1696. https://doi.org/10.7164/antibiotics.45.1692.

Hoye TR, Jeffrey CS & Shao F (2007). Mosher ester analysis for the determination of absolute configuration of stereogenic (chiral) carbinol carbons. *Nature Protocols* 2(10): 2451–2458. https://doi.org/10.1038/nprot.2007.354.

Hutchings M, Truman A & Wilkinson B (2019). Antibiotics: Past, present and future. *Current Opinion in Microbiology* 51: 72–80. https://doi.org/10.1016/j.mib.2019.10.008.

Hüttel W (2021). Echinocandins: structural diversity, biosynthesis, and development of antimycotics. *Applied Microbiology and Biotechnology* 105(1): 55–66. https://doi.org/10.1007/s00253-020-11022-y.

Hyde KD, Al-Hatmi AMS, Andersen B, Boekhout T, Buzina W, Dawson TL, Eastwood DC, Jones EBG, de Hoog S, Kang Y, *et al.* (2018). The world's ten most feared fungi. *Fungal Diversity* 93(1): 161–194. https://doi.org/10.1007/s13225-018-0413-9.

Hyde KD, Xu J, Rapior S, Jeewon R, Lumyong S, Niego AGT, Abeywickrama PD, Aluthmuhandiram JVS, Brahamanage RS, Brooks S, *et al.* (2019). The amazing potential of fungi: 50 ways we can exploit fungi industrially. *Fungal Diversity* 97(1): 1–136. https://doi.org/10.1007/s13225-019-00430-9.

Isaka M, Srisanoh U, Lartpornmatulee N & Boonruangprapa T (2007). ES-242 derivatives and cycloheptapeptides from *Cordyceps* sp. strains BCC 16173 and BCC 16176. *Journal of Natural Products* 70(10): 1601–1604. https://doi.org/10.1021/np070357h.

Isaka M, Palasarn S, Komwijit S, Somrithipol S & Sommai S (2014). Pleosporin A, an antimalarial cyclodepsipeptide from an elephant dung fungus (BCC 7069). *Tetrahedron Letters* 55(2): 469–471. https://doi.org/10.1016/j.tetlet.2013.11.063.

Iwamoto T, Fujie A, Sakamoto K, Tsurumi Y, Shigematsu N, Yamashita M, Hashimoto S, Okuhara M & Kohsaka M (1994). WF11899A, B and C, novel antifungal lipopeptides. I. Taxonomy, fermentation, isolation and physico-chemical properties. *The Journal of Antibiotics* 47(10): 1084–1091. https://doi.org/10.7164/antibiotics.47.1084.

Janusz G, Pawlik A, Sulej J, Świderska-Burek U, Jarosz-Wilkołazka A, Paszczyński A (2017). Lignin degradation: Microorganisms, enzymes involved, genomes analysis and evolution. *FEMS Microbiology Reviews* 41(6): 941–962. https://doi.org/10.1093/femsre/fux049.

Jegorov A, Sedmera P, Maťha V, Šimek P, Zahradníčková H, Landa Z & Eyal J (1994). Beauverolides L and La from *Beauveria tenella* and *Paecilomyces fumosoroseus*. *Phytochemistry* 37(5): 1301–1303. https://doi.org/10.1016/S0031-9422(00)90402-3.

Jegorov A, Paizs B, Kuzma M, Zabka M, Landa Z, Sulc M, Barrow MP & Havlicek V (2004).

Extraribosomal cyclic tetradepsipeptides beauverolides: Profiling and modeling the fragmentation pathways. *Journal of Mass Spectrometry* 39(8): 949–960. https://doi.org/10.1002/jms.674.

Johnson MD & Perfect JR (2003). Caspofungin: First approved agent in a new class of antifungals. *Expert Opinion on Pharmacotherapy* 4(5): 807–823. https://doi.org/10.1517/14656566.4.5.807.

Justo A, Miettinen O, Floudas D, Ortiz-Santana B, Sjökvist E, Lindner D, Nakasone K, Niemelä T, Larsson KH, Ryvarden L, *et al.* (2017). A revised family-level classification of the Polyporales (Basidiomycota). *Fungal Biology* 121(9): 798–824. https://doi.org/10.1016/j.funbio.2017.05.010.

Kargbo RB (2020). Psilocybin therapeutic research: The present and future paradigm. *ACS Medicinal Chemistry Letters* 11(4): 399–402. https://doi.org/10.1021/acsmedchemlett.0c00048.

Kavanagh F, Hervey A & Robbins WJ (1951). Antibiotic substances from basidiomycetes: VIII. *Pleurotus multilus* (Fr.) Sacc. and *Pleurotus passeckerianus* Pilat. *Proceedings of the National Academy of Sciences* 37(9): 570–574. https://doi.org/10.1073/pnas.37.9.570.

Keller NP (2019). Fungal secondary metabolism: Regulation, function and drug discovery. *Nature Reviews Microbiology*. Nature Publishing Group 167–180. https://doi.org/10.1038/s41579-018-0121-1.

Kenis M, Hurley BP, Hajek AE & Cock MJW (2017). Classical biological control of insect pests of trees: Facts and figures. *Biological Invasions* 19(11): 3401–3417. https://doi.org/10.1007/s10530-017-1414-4.

Kepler RM, Luangsa-Ard JJ, Hywel-Jones NL, Quandt CA, Sung GH, Rehner SA, Aime MC, Henkel TW, Sanjuan T, Zare R, *et al.* (2017). A phylogenetically-based nomenclature for Cordycipitaceae (Hypocreales). *IMA Fungus* 8(2): 335–353. https://doi.org/10.5598/imafungus.2017.08.02.08.

Kijpornyongpan T, Schwartz A, Yaguchi A & Salvachúa D (2022). Systems biology-guided understanding of white-rot fungi for biotechnological applications: A review. *iScience* 25(7): 104640. https://doi.org/10.1016/j.isci.2022.104640.

Kim HW, Lee JW & Shim SH (2024). Biosynthesis, biological activities, and structure-activity relationships of decalin-containing tetramic acid derivatives isolated from fungi. *Natural Product Reports* 41(8): 1294–1317. https://doi.org/10.1039/d4np00013g.

Kornerup A & Wanscher JH (1978). *Methuen handbook of colour*. 3rd ed. Edited by D Pavey. London: Methuen & Co. Ltd.

Kou RW, Han R, Gao YQ, Li D, Yin X & Gao JM (2021). Anti-neuroinflammatory polyoxygenated lanostanoids from Chaga mushroom *Inonotus obliquus*. *Phytochemistry* 184: 112647. https://doi.org/10.1016/j.phytochem.2020.112647.

Krauss GJ & Nies DH (2015). *Ecological biochemistry: Environmental and interspecies interactions*. Edited by GJ Krauss and DH Nies Wiley. https://doi.org/10.1002/9783527686063.

Kristanti RA, Hadibarata T, Toyama T, Tanaka Y & Mori K (2011). Bioremediation of crude oil by white rot fungi *Polyporus* sp. S133. *Journal of Microbiology and Biotechnology* 21(9): 995–1000. https://doi.org/10.4014/jmb.1105.05047.

Krücken J, Holden-Dye L, Keiser J, Prichard RK, Townson S, Makepeace BL, Hübner MP, Hahnel SR, Scandale I, Harder A, *et al.* (2021). Development of emodepside as a possible adulticidal treatment for human onchocerciasis—The fruit of a successful industrial-academic collaboration. *PLoS Pathogens* 17(7 July): e1009682. https://doi.org/10.1371/journal.ppat.1009682.

Künzler K & Eichenberger W (1997). Betaine lipids and zwitterionic phospholipids in plants and fungi. *Phytochemistry* 46(5): 883–892. https://doi.org/10.1016/S0031-9422(97)81274-5.

Larriba E, Jaime MDLA, Carbonell-Caballero J, Conesa A, Dopazo J, Nislow C, Martín-Nieto J & Lopez-Llorca LV (2014). Sequencing and functional analysis of the genome of a nematode egg-parasitic fungus, *Pochonia chlamydosporia*. *Fungal Genetics and Biology* 65: 69–80. https://doi.org/10.1016/j.fgb.2014.02.002.

Larsen TO, Smedsgaard J, Nielsen KF, Hansen ME & Frisvad JC (2005). Phenotypic taxonomy and metabolite profiling in microbial drug discovery. *Natural Product Reports* 22(6): 672–695. https://doi.org/10.1039/b404943h.

Lee KF, Chen JH, Teng CC, Shen CH, Hsieh MC, Lu CC, Lee KC, Lee LY, Chen WP, Chen CC, *et al.* (2014). Protective effects of *Hericium erinaceus* mycelium and its isolated erinacine A against ischemia-injury-induced neuronal cell death via the inhibition of iNOS/p38 MAPK and nitrotyrosine. *International Journal of Molecular Sciences* 15(9): 15073–15089. https://doi.org/10.3390/ijms150915073.

Li D-W, Castañeda-Ruiz RF & LaMondia J (2016). Evolution of fungi and update on ethnomycology. in D-W Li (ed.) *Biology of Microfungi*. Springer, Cham 237–266. https://doi.org/10.1007/978-3-319-29137-6_11.

Li Y, Zhao XC, Wu LX, Wang Y, Xu A & Lin WF (2023). *Blackwellomyces kaihuaensis* and *Metarhizium putuoense* (Hypocreales), two new entomogenous fungi from subtropical forests in Zhejiang Province, eastern China. *Forests* 14(12): 2333. https://doi.org/10.3390/f14122333.

Liang M, Lyu HN, Ma ZY, Li EW, Cai L & Yin WB (2021). Genomics-driven discovery of a new cyclodepsipeptide from the guanophilic fungus *Amphichorda guana*. *Organic & Biomolecular Chemistry* 19(9): 1960–1964. https://doi.org/10.1039/D1OB00100K.

Liermann JC, Opatz T, Kolshorn H, Antelo L, Hof C & Anke H (2009). Omphalotins E-I, five oxidatively modified nematicidal cyclopeptides from *Omphalotus olearius*. *European Journal of Organic Chemistry* 2009(8): 1256–1262. https://doi.org/10.1002/ejoc.200801068.

Lin CH & Lane HY (2019). The role of N-methyl-D-aspartate receptor neurotransmission and precision medicine in behavioral and psychological symptoms of dementia. *Frontiers in Pharmacology*. Frontiers Media S.A. 540. https://doi.org/10.3389/fphar.2019.00540.

Lin X & Kück U (2022). Cephalosporins as key lead generation beta-lactam antibiotics. *Applied Microbiology and Biotechnology* 106(24): 8007–8020. https://doi.org/10.1007/s00253-022-12272-8.

Liu C, Guo H, Liu H, Yu J, Li S, Zhu T, Owusu AM & Li S (2022). Differential metabolomics reveals pathogenesis of *Pestalotiopsis kenyana* causing leaf spot disease of *Zanthoxylum schinifolium*. *Journal of Fungi* 8(11): 1208. https://doi.org/10.3390/jof8111208.

Liu SX, Ou-Yang SY, Lu YF, Guo CL, Dai SY, Li C, Yu TY & Pei YH (2023). Recent

advances on cyclodepsipeptides: Biologically active compounds for drug research. *Frontiers in Microbiology* 14: 1276928. https://doi.org/10.3389/fmicb.2023.1276928.

Lohr NJ, Molleston JP, Strauss KA, Torres-Martinez W, Sherman EA, Squires RH, Rider NL, Chikwava KR, Cummings OW, Morton DH, *et al.* (2010). Human ITCH E3 ubiquitin ligase deficiency causes syndromic multisystem autoimmune disease. *The American Journal of Human Genetics* 86(3): 447–453. https://doi.org/10.1016/j.ajhg.2010.01.028.

Lopez-Llorca LV, Olivares-Bernabeu C, Salinas J, Jansson HB & Kolattukudy PE (2002). Pre-penetration events in fungal parasitism of nematode eggs. *Mycological Research* 106(4): 499–506. https://doi.org/10.1017/S0953756202005798.

Lopez-Llorca LV, Maciá-Vicente JG & Jansson H-B (2008). Mode of action and interactions of nematophagous fungi. in *Integrated Management and Biocontrol of Vegetable and Grain Crops Nematodes*. Springer, Dordrecht 51–76. https://doi.org/10.1007/978-1-4020-6063-2_3.

Lovett B & St. Leger RJ (2017). The insect pathogens. *Microbiology Spectrum* 5(2): 10.1128. https://doi.org/10.1128/microbiolspec.funk-0001-2016.

Luo H, Mo M, Huang X, Li X & Zhang K (2004). *Coprinus comatus*: A basidiomycete fungus forms novel spiny structures and infects nematode. *Mycologia* 96(6): 1218–1224. https://doi.org/10.1080/15572536.2005.11832870.

Macías-Rubalcava ML, Hernández-Bautista BE, Jiménez-Estrada M, González MC, Glenn AE, Hanlin RT, Hernández-Ortega S, Saucedo-García A, Muria-González JM & Anaya AL (2008). Naphthoquinone spiroketal with allelochemical activity from the newly discovered endophytic fungus *Edenia gomezpompae*. *Phytochemistry* 69(5): 1185–1196. https://doi.org/10.1016/j.phytochem.2007.12.006.

Manzanilla-López RH, Esteves I, Finetti-Sialer MM, Hirsch PR, Ward E, Devonshire J, Hidalgo-Díaz L (2013). *Pochonia chlamydosporia*: Advances and challenges to improve its performance as a biological control agent of sedentary endo-parasitic nematodes. *Journal of Nematology* 45(1): 1–7.

Mapook A, Hyde KD, Hassan K, Kemkuignou BM, Čmoková A, Surup F, Kuhnert E, Paomephan P, Cheng T, de Hoog S, *et al.* (2022). Ten decadal advances in fungal biology leading towards human well-being. *Fungal Diversity* 116(1): 547–614. https://doi.org/10.1007/s13225-022-00510-3.

Marfori EC, Kajiyama S, Fukusaki EI & Kobayashi A (2002). Trichosetin, a novel tetramic acid antibiotic produced in dual culture of *Trichoderma harzianum* and *Catharanthus roseus callus*. *Zeitschrift fur Naturforschung C* 57(5–6): 465–470. https://doi.org/10.1515/znc-2002-5-611.

Matsuda D, Namatame I, Tomoda H, Kobayashi-Susumu S, Zocher R, Kleinkauf H & Omura S (2004). New beauveriolides produced by amino acid-supplemented fermentation of *Beauveria* sp. FO-6979. *Journal of Antibiotics* 57(1): 1–9. https://doi.org/10.7164/antibiotics.57.1.

de Mattos-Shipley KMJ, Ford KL, Alberti F, Banks AM, Bailey AM & Foster GD (2016). The good, the bad and the tasty: The many roles of mushrooms. *Studies in Mycology* 85: 125–157. https://doi.org/10.1016/j.simyco.2016.11.002.

Mayer A, Kilian M, Hoster B, Sterner O & Anke H (1999). In-vitro and in-vivo nematicidal activities of the cyclic dodecapeptide omphalotin A. *Pesticide Science* 55(1): 27–30.

https://doi.org/10.1002/(SICI)1096-9063(199901)55:1<27::AID-PS854>3.0.CO;2-K.

Mejias J, Truong NM, Abad P, Favery B & Quentin M (2019). Plant proteins and processes targeted by parasitic nematode effectors. *Frontiers in Plant Science* 10: 472968. https://doi.org/10.3389/fpls.2019.00970.

Mendoza-De Gives P (2022). Soil-borne nematodes: Impact in agriculture and livestock and sustainable strategies of prevention and control with special reference to the use of nematode natural enemies. *Pathogens* 11(6): 640. https://doi.org/10.3390/pathogens11060640.

Meyling NV & Eilenberg J (2007). Ecology of the entomopathogenic fungi *Beauveria bassiana* and *Metarhizium anisopliae* in temperate agroecosystems: Potential for conservation biological control. *Biological Control* 43(2): 145–155. https://doi.org/10.1016/j.biocontrol.2007.07.007.

Miyazaki K, Mizutani H, Katabuchi H, Fukuma K, Fujisaka S & Okamura H (1995). Activated (HLA-DR+) T-Lymphocyte subsets in cervical carcinoma and effects of radiotherapy and immunotherapy with sizofiran on cell-mediated immunity and survival. *Gynecologic Oncology* 56(3): 412–420. https://doi.org/10.1006/gyno.1995.1073.

Molnár I, Gibson DM & Krasnoff SB (2010). Secondary metabolites from entomopathogenic Hypocrealean fungi. *Natural Product Reports*. The Royal Society of Chemistry 1241–1275. https://doi.org/10.1039/c001459c.

Mongkolsamrit S, Noisripoom W, Tasanathai K, Khonsanit A, Thanakitpipattana D, Himaman W, Kobmoo N & Luangsa-ard JJ (2020). Molecular phylogeny and morphology reveal cryptic species in *Blackwellomyces* and *Cordyceps* (Cordycipitaceae) from Thailand. *Mycological Progress* 19(9): 957–983. https://doi.org/10.1007/s11557-020-01615-2.

Morgan-Jones G, White JF & Rodriguez-Kabana R (1984). Phytonematode pathology: Ultrastructural studies. II. Parasitism of *Meloidogyne arenaria* eggs and larvae by *Paecilomyces lilacinus*. *Nematropica* 14(1): 57–71. Available at: https://journals.flvc.org/nematropica/article/view/63829.

Moses JE, Commeiras L, Baldwin JE & Adlington RM (2003). Total synthesis of panepophenanthrin. *Organic Letters* 5(17): 2987–2988. https://doi.org/10.1021/ol0349817.

Moussa AY, Lambert C, Stradal TEB, Ashrafi S, Maier W, Stadler M & Helaly SE (2020). New peptaibiotics and a cyclodepsipeptide from *Ijuhya vitellina*: Isolation, identification, cytotoxic and nematicidal activities. *Antibiotics* 9(3): 132. https://doi.org/10.3390/antibiotics9030132.

Naghavi M, Vollset SE, Ikuta KS, Swetschinski LR, Gray AP, Wool EE, Robles Aguilar G, Mestrovic T, Smith G, Han C, *et al.* (2024). Global burden of bacterial antimicrobial resistance 1990–2021: A systematic analysis with forecasts to 2050. *The Lancet* 404(10459): 1199–1226. https://doi.org/10.1016/S0140-6736(24)01867-1.

Nakamura Y, Nguyen NH, Yoshinari T, Hachisu M, Nguyen PT & Shimizu K (2024). Identification of the oosporein biosynthesis gene cluster in an entomopathogenic fungus *Blackwellomyces cardinalis*. *Mycoscience* 65(2): 96–104. https://doi.org/10.47371/mycosci.2024.02.005.

Nandi S, Sikder R & Acharya K (2019). Secondary metabolites of mushrooms: A potential source for anticancer therapeutics with translational opportunities. in *Advancing Frontiers*

in Mycology & Mycotechnology. Singapore: Springer Singapore 563–598. https://doi.org/10.1007/978-981-13-9349-5_23.

Naranjo-Ortiz MA & Gabaldón T (2019). Fungal evolution: Major ecological adaptations and evolutionary transitions. *Biological Reviews* 94(4): 1443–1476. https://doi.org/10.1111/brv.12510.

Neumann K, Kehraus S, Gütschow M & König GM (2009). Cytotoxic and HLE-inhibitory tetramic acid derivatives from marine-derived fungi. *Natural Product Communications* 4(3): 347–354. https://doi.org/10.1177/1934578x0900400308.

Newman DJ & Cragg GM (2020). Natural products as sources of new drugs over the nearly four decades from 01/1981 to 09/2019. *Journal of Natural Products* 83(3): 770–803. https://doi.org/10.1021/acs.jnatprod.9b01285.

Nichols BW & Appleby RS (1969). The distribution and biosynthesis of arachidonic acid in algae. *Phytochemistry* 8(10): 1907–1915. https://doi.org/10.1016/S0031-9422(00)88075-9.

Niu XM (2017). Secondary metabolites from *Pochonia chlamydosporia* and other species of *Pochonia*. In Manzanilla-López R, Lopez-Llorca L (eds). Perspectives in sustainable nematode management through *Pochonia chlamydosporia* applications for root and rhizosphere health. *Sustainability in Plant and Crop Protection*. Springer, Cham. 131–168. https://doi.org/10.1007/978-3-319-59224-4_7

Noling JW & Becker JO (1994). The challenge of research and extension to define and implement alternatives to methyl bromide. *Journal of Nematology* 26(4S): 573–586. Available at: https://europepmc.org/articles/PMC2619561.

Nordbring-Hertz B, Jansson H-B & Tunlid A (2011). Nematophagous fungi. in *Encyclopedia of Life Sciences*. Wiley 1–13. https://doi.org/10.1002/9780470015902.a0000374.pub3.

Novak R (2011). Are pleuromutilin antibiotics finally fit for human use? *Annals of the New York Academy of Sciences* 1241(1): 71–81. https://doi.org/10.1111/j.1749-6632.2011.06219.x.

Oerke EC (2006). Crop losses to pests. *The Journal of Agricultural Science* 144(1): 31–43. https://doi.org/10.1017/S0021859605005708.

Oppong-Danquah E, Blümel M & Tasdemir D (2023). Metabolomics and microbiomics insights into differential surface fouling of three macroalgal species of *Fucus* (Fucales, Phaeophyceae) that co-exist in the German Baltic Sea. *Marine Drugs* 21(11): 595. https://doi.org/10.3390/md21110595.

Oriola AO & Kar P (2024). Naturally occurring xanthones and their biological implications. *Molecules* 29(17): 4241. https://doi.org/10.3390/molecules29174241.

Ortiz-Urquiza A & Keyhani NO (2013). Action on the surface: Entomopathogenic fungi versus the insect cuticle. *Insects* 4(3): 357–374. https://doi.org/10.3390/insects4030357.

Park MY, Jeon BJ, Kang JE & Kim BS (2020). Synergistic interactions of schizostatin identified from *Schizophyllum commune* with demethylation inhibitor fungicides. *Plant Pathology Journal* 36(6): 579–590. https://doi.org/10.5423/PPJ.OA.07.2020.0141.

Paukner S & Riedl R (2017). Pleuromutilins: Potent drugs for resistant bugs-mode of action and resistance. *Cold Spring Harbor Perspectives in Medicine* 7(1): a027110. https://doi.org/10.1101/cshperspect.a027110.

Pegler DN (1983). The genus *Lentinus*: A world monograph. *Kew Bulletin, additional series*.

Pinar O & Rodríguez-Couto S (2024). Biologically active secondary metabolites from white-rot fungi. *Frontiers in Chemistry* 12: 1363354. https://doi.org/10.3389/fchem.2024.1363354.

Pointing SB (2001). Feasibility of bioremediation by white-rot fungi. *Applied Microbiology and Biotechnology* 57(1–2): 20–33. https://doi.org/10.1007/s002530100745.

Polishook JD, Dombrowski AW, Tsou NN, Salituro GM & Curotto JE (1993). Preussomerin D from the endophyte *Hormonema dematioides*. *Mycologia* 85(1): 62–64. https://doi.org/10.1080/00275514.1993.12026246.

Prado PFV, Mendes CVC, Pires BA, Fiorin GL, Mieczkowski P, Pereira GAG, Teixeira PJPL & Thomazella DPT (2025). Unveiling molecular mechanisms of strobilurin resistance in the cacao pathogen *Moniliophthora perniciosa*. *iScience* 28(8): 113180. https://doi.org/10.1016/j.isci.2025.113180.

Prescott TAK, Hill R, Mas-Claret E, Gaya E & Burns E (2023). Fungal drug discovery for chronic disease: History, new discoveries and new approaches. *Biomolecules* 13(6): 986. https://doi.org/10.3390/biom13060986.

Rahman MU, Chen P, Zhang X & Fan B (2023). Predacious strategies of nematophagous fungi as bio-control agents. *Agronomy* 13(11): 2685. https://doi.org/10.3390/agronomy13112685.

Rajtar NN, Kielsmeier-Cook JC, Held BW, Toapanta-Alban CE, Ordonez ME, Barnes CW & Blanchette RA (2023). Diverse *Xylaria* in the Ecuadorian Amazon and their mode of wood degradation. *Botanical Studies* 64, 30. https://doi.org/10.1186/s40529-023-00403-x

Replansky T, Koufopanou V, Greig D & Bell G (2008). *Saccharomyces sensu stricto* as a model system for evolution and ecology. *Trends in Ecology and Evolution* 23(9): 494–501. https://doi.org/10.1016/j.tree.2008.05.005.

Riedling OL & Rokas A (2025). mGem: How many fungal secondary metabolites are produced by filamentous fungi? Conservatively, at least 1.4 million. *mBio* 16(4). https://doi.org/10.1128/mbio.01381-25.

Rokas A, Mead ME, Steenwyk JL, Raja HA & Oberlies NH (2020). Biosynthetic gene clusters and the evolution of fungal chemodiversity. *Natural Product Reports*. The Royal Society of Chemistry 868–878. https://doi.org/10.1039/c9np00045c.

Ross S, Bossis A, Guss J, Agin-Liebes G, Malone T, Cohen B, Mennenga SE, Belser A, Kalliontzi K, Babb J, *et al.* (2016). Rapid and sustained symptom reduction following psilocybin treatment for anxiety and depression in patients with life-threatening cancer: A randomized controlled trial. *Journal of Psychopharmacology* 30(12): 1165–1180. https://doi.org/10.1177/0269881116675512.

Roth MG, Westrick NM & Baldwin TT (2023). Fungal biotechnology: From yesterday to tomorrow. *Frontiers in Fungal Biology* 4: 1135263. https://doi.org/10.3389/ffunb.2023.1135263.

Rüegger A, Kuhn M, Lichti H, Loosli H-R, Huguenin R, Quiquerez C & von Wartburg A (1976). Cyclosporin A, a peptide metabolite from *Trichoderma polysporum* (LINK ex PERS.) *Rifai*, with a remarkable immunosuppressive activity. *Helvetica Chimica Acta* 59(4): 1075–1092. https://doi.org/10.1002/hlca.19760590412.

Rukachaisirikul V, Tansakul C, Saithong S, Pakawatchai C, Isaka M & Suvannakad R (2005). Hirsutane sesquiterpenes from the fungus *Lentinus connatus* BCC 8996. *Journal of Natural Products* 68(11): 1674–1676. https://doi.org/10.1021/np0502286.

Salomon S, Oliva O, Amato A, Bastien O, Michaud M & Jouhet J (2025). Betaine lipids: Biosynthesis, functional diversity and evolutionary perspectives. *Progress in Lipid Research* 97: 101320. https://doi.org/10.1016/j.plipres.2025.101320.

Samson RA, Houbraken J, Varga J & Frisvad JC (2009). Polyphasic taxonomy of the heat resistant ascomycete genus *Byssochlamys* and its *Paecilomyces* anamorphs. *Persoonia* 22: 14–27. https://doi.org/10.3767/003158509X418925.

Sasaki T, Takagi M, Yaguchi T, Miyadoh S, Okada T & Koyama M (1992). A new anthelmintic cyclodepsipeptide, PF1022A. *The Journal of Antibiotics* 45(5): 692–697. https://doi.org/10.7164/antibiotics.45.692.

Schlegel B, Härtl A, Dahse H-M, Gollmick FA, Gräfe U, Dörfelt H & Kappes B (2002). Hexacylinol, a new antiproliferative metabolite of *Panus rudis* HKI 0254. *The Journal of Antibiotics* 55(9): 814–817. https://doi.org/10.7164/antibiotics.55.814.

Schneider-Orelli O (1947). *Entomologisches Praktikum. Einführung in die land-und forstwirtschaftliche Insektenkunde.* 2., erw. A. Aarau : H. R. Sauerländer.

Schowalter TD (2022). *Insect Ecology: An Ecosystem Approach*. 5th ed. Elsevier. https://doi.org/10.1016/B978-0-323-85673-7.00019-8.

Schrey H, Lambert C & Stadler M (2025). Fungi: Pioneers of chemical creativity – Techniques and strategies to uncover fungal chemistry. *IMA Fungus* 16: e142462. https://doi.org/10.3897/imafungus.16.142462.

Schwartz RE, Sesin DF, Joshua H, Wilson KE, Kempf AJ, Goklen KA, Kuehner D, Gailliot P, Gleason C, White R, *et al.* (1992). Pneumocandins from *Zalerion arboricola*. I. Discovery and isolation. *The Journal of Antibiotics* 45(12): 1853–1866. https://doi.org/10.7164/antibiotics.45.1853.

Seephonkai P, Isaka M, Kittakoop P, Palittapongarnpim P, Kamchonwongpaisan S, Tanticharoen M & Thebtaranonth Y (2002). Evaluation of antimycobacterial, antiplasmodial and cytotoxic activities of preussomerins isolated from the lichenicolous fungus *Microsphaeropsis* sp. BCC 3050. *Planta Medica* 68(1): 45–48. https://doi.org/10.1055/s-2002-20055.

Sekizawa R, Ikeno S, Nakamura H, Naganawa H, Matsui S, Iinuma H & Takeuchi T (2002). Panepophenanthrin, from a mushroom strain, a novel inhibitor of the ubiquitin-activating enzyme. *Journal of Natural Products* 65(10): 1491–1493. https://doi.org/10.1021/np020098q.

Senthilarasu G (2015). The lentinoid fungi (*Lentinus* and *Panus*) from Western Ghats, India. *IMA Fungus* 6(1): 119–128. https://doi.org/10.5598/imafungus.2015.06.01.06.

Seong J, Shin J, Kim K & Cho BK (2021). Microbial production of nematicidal agents for controlling plant-parasitic nematodes. *Process Biochemistry* 108: 69–79. https://doi.org/10.1016/j.procbio.2021.06.006.

Shagufta & Ahmad I (2016). Recent insight into the biological activities of synthetic xanthone derivatives. *European Journal of Medicinal Chemistry* 116: 267–280. https://doi.org/10.1016/j.ejmech.2016.03.058.

Shah PA & Pell JK (2003). Entomopathogenic fungi as biological control agents. *Applied Microbiology and Biotechnology*. Springer Verlag 413–423. https://doi.org/10.1007/s00253-003-1240-8.

Shan R, Stadler M, Sterner O & Anke H (1996). New metabolites with nematicidal and antimicrobial activities from the ascomycete *Lachnum papyraceum* (Karst.) Karst: VIII. Isolation, structure determination and biological activities of minor metabolites structurally related to mycorrhizin A. *The Journal of Antibiotics* 49(5): 447–452. https://doi.org/10.7164/antibiotics.49.447.

Shankar A & Sharma KK (2022). Fungal secondary metabolites in food and pharmaceuticals in the era of multi-omics. *Applied Microbiology and Biotechnology* 106(9–10): 3465–3488. https://doi.org/10.1007/s00253-022-11945-8.

Sharma A, Sharma S & Yadav PK (2023). Entomopathogenic fungi and their relevance in sustainable agriculture: A review. *Cogent Food and Agriculture* 9(1). https://doi.org/10.1080/23311932.2023.2180857.

Singh S, Singh B & Singh AP (2015). Nematodes: A threat to sustainability of agriculture. *Procedia Environmental Sciences* 29: 215–216. https://doi.org/10.1016/j.proenv.2015.07.270.

Song JG, Ha LS, Ki DW, Choi DC, Lee IK & Yun BS (2021). Chemical constituents of the culture broth of *Panus rudis*. *Mycobiology* 49(6): 604–606. https://doi.org/10.1080/12298093.2021.2004663.

Sousa-Guimarães DK, Alves-Silva G, Bittencourt F, Camacho O, Menolli N, Góes-Neto A, Robledo GL & Drechsler-Santos ER (2024). A comprehensive phylogeny of *Panus* (Panaceae, Polyporales) and revisited Brazilian diversity. *Mycological Progress* 23(1): 1–28. https://doi.org/10.1007/s11557-024-01955-3.

Spiteller P (2008). Chemical defence strategies of higher fungi. *Chemistry - A European Journal* 14(30): 9100–9110. https://doi.org/10.1002/chem.200800292.

Stadler M, Anke H, Arendholz W-R, Hansske F, Anders U, Sterner O & Bergquist K-E (1993a). Lachnumon and lachnumol A, new metabolites with nematicidal and antimicrobial activities from the ascomycete *Lachnum papyraceum* (Karst.) Karst: I. Producing organism, fermentation, isolation and biological activities. *The Journal of Antibiotics* 46(6): 961–967. https://doi.org/10.7164/antibiotics.46.961.

Stadler M, Anke H, Karl-Erik B & Olov S (1993b). Lachnumon and lachnumol A, new metabolites with nematicidal and antimicrobial activities from the ascomycete *Lachnum papyraceum* (Karst.) Karst: II. Structural elucidation. *The Journal of Antibiotics* 46(6): 968–971. https://doi.org/10.7164/antibiotics.46.968.

Stadler M, Anke H, Shan R & Sterner O (1995a). New metabolites with nematicidal and antimicrobial activities from the ascomycete *Lachnum papyraceum* (Karst.) Karst: VI. Structure determination of non-halogenated metabolites structurally related to mycorrhizin A. *The Journal of Antibiotics* 48(2): 154–157. https://doi.org/10.7164/antibiotics.48.154.

Stadler M, Tichy H-V, Katsiou E & Hellwig V (2003). Chemotaxonomy of *Pochonia* and other conidial fungi with *Verticillium*-like anamorphs. *Mycological Progress* 2(2): 95–122. https://doi.org/10.1007/s11557-006-0048-1.

Stadler M, Anke H & Sterner O (1995b). Metabolites with nematicidal and antimicrobial

activities from the ascomycete *Lachnum papyraceum* (Karst.) Karst: V. Production, isolation and biological activities of bromine-containing mycorrhizin and lachnumon derivatives and four additional new bioactive metabolites. *The Journal of Antibiotics* 48(2): 149–153. https://doi.org/10.7164/antibiotics.48.149.

Sterner O, Etzel W, Mayer A & Anke H (1997). Omphalotin, a new cyclic peptide with potent nematicidal activity from *Omphalotus olearius*. II. Isolation and structure determination. *Natural Product Letters* 10(1): 33–38. https://doi.org/10.1080/10575639708043692.

Sum WC, Ebada SS, Clement Matasyoh J & Stadler M (2023). Recent progress in the evaluation of secondary metabolites from Basidiomycota. *Current Research in Biotechnology* 6: 100155. https://doi.org/10.1016/j.crbiot.2023.100155.

Sung GH, Hywel-Jones NL, Sung JM, Luangsa-Ard JJ, Shrestha B, Spatafora JW (2007). Phylogenetic classification of *Cordyceps* and the clavicipitaceous fungi. *Studies in Mycology* 57(1): 5–59. https://doi.org/10.3114/sim.2007.57.01.

Survase SA, Kagliwal LD, Annapure US & Singhal RS (2011). Cyclosporin A — A review on fermentative production, downstream processing and pharmacological applications. *Biotechnology Advances* 29(4): 418–435. https://doi.org/10.1016/j.biotechadv.2011.03.004.

Suryadi H, Judono JJ, Putri MR, Eclessia AD, Ulhaq JM, Agustina DN & Sumiati T (2022). Biodelignification of lignocellulose using ligninolytic enzymes from white-rot fungi. *Heliyon* 8(2): e08865. https://doi.org/10.1016/j.heliyon.2022.e08865.

Taji S, Yamada T, Wada SI, Tokuda H, Sakuma K & Tanaka R (2008). Lanostane-type triterpenoids from the sclerotia of *Inonotus obliquus* possessing anti-tumor promoting activity. *European Journal of Medicinal Chemistry* 43(11): 2373–2379. https://doi.org/10.1016/j.ejmech.2008.01.037.

Takamatsu S, Kim YP, Hayashi M, Hiraoka H, Natori M, Komiyama K & Omura S (1996). Macrosphelide, a novel inhibitor of cell-cell adhesion molecule. *Journal of Antibiotics* 49(1): 95–98. https://doi.org/10.7164/antibiotics.49.95.

Tejedor-Calvo E, Marco P, Fischer M & Creydt M (2024). Mass spectrometry-based non-targeted lipidome analysis and extraction of markers for the authentication of white and black truffle species and their origin determination. *Agriculture* 14(12): 2350. https://doi.org/10.3390/agriculture14122350.

Thongbai B, Rapior S, Hyde KD, Wittstein K & Stadler M (2015). *Hericium erinaceus*, an amazing medicinal mushroom. *Mycological Progress* 14(10): 1–23. https://doi.org/10.1007/s11557-015-1105-4.

Tihelka E, Cai C, Giacomelli M, Lozano-Fernandez J, Rota-Stabelli O, Huang D, Engel MS, Donoghue PCJ & Pisani D (2021). The evolution of insect biodiversity. *Current Biology* 31(19): R1299–R1311. https://doi.org/10.1016/j.cub.2021.08.057.

Tobert JA (2003). Lovastatin and beyond: The history of the HMG-CoA reductase inhibitors. *Nature Reviews Drug Discovery* 2(7): 517–526. https://doi.org/10.1038/nrd1112.

Toki S, Ando K, Yoshida M, Kawamoto I, Sano H & Matsuda Y (1992a). ES-242-1, a novel compound from *Verticillium* sp., binds to a site on N-methyl-D-aspartate receptor that is coupled to the channel domain. *The Journal of Antibiotics* 45(1): 88–93. https://doi.org/10.7164/antibiotics.45.88

Toki S, Tsukuda E, Nozawa M, Nonaka H, Yoshida M & Matsuda Y (1992b). The ES-242s, novel N-methyl-D-aspartate antagonists of microbial origin, interact with both the neurotransmitter recognition site and the ion channel domain. *Journal of Biological Chemistry* 267(21): 14884–14892. https://doi.org/10.1016/s0021-9258(18)42123-0.

Treseder KK & Lennon JT (2015). Fungal traits that drive ecosystem dynamics on land. *Microbiology and Molecular Biology Reviews* 79(2): 243–262. https://doi.org/10.1128/mmbr.00001-15.

Tsai-Teng T, Chin-Chu C, Li-Ya L, Wan-Ping C, Chung-Kuang L, Chien-Chang S, Chi-Ying HF, Chien-Chih C & Shiao YJ (2016). Erinacine A-enriched *Hericium erinaceus* mycelium ameliorates Alzheimer's disease-related pathologies in APPswe/PS1dE9 transgenic mice. *Journal of Biomedical Science* 23(1): 1–12. https://doi.org/10.1186/s12929-016-0266-z.

Umeyama A, Takahashi K, Grudniewska A, Shimizu M, Hayashi S, Kato M, Okamoto Y, Suenaga M, Ban S, Kumada T, *et al.* (2014). In vitro antitrypanosomal activity of the cyclodepsipeptides, cardinalisamides A-C, from the insect pathogenic fungus *Cordyceps cardinalis* NBRC 103832. *Journal of Antibiotics* 67(2): 163–166. https://doi.org/10.1038/ja.2013.93.

Vargas-Isla R, Capelari M, Menolli N, Nagasawa E, Tokimoto K & Ishikawa NK (2015). Relationship between *Panus lecomtei* and *P. strigellus* inferred from their morphological, molecular and biological characteristics. *Mycoscience* 56(6): 561–571. https://doi.org/10.1016/j.myc.2015.05.004.

Venkatesh G, Sakthi Priya P, Anithaa V, Dinesh GK, Velmurugan S, Abinaya S, Karthika P, Sivasakthivelan P, Soni R & Thennarasi A (2022). Role of entomopathogenic fungi in biocontrol of insect pests. In R Soni, DC Suyal, and R Goel (eds.) *Plant Protection: From Chemicals to Biologicals*. Berlin, Boston: De Gruyter 505–548. https://doi.org/10.1515/9783110771558-019.

Veve MP & Wagner JL (2018). Lefamulin: Review of a promising novel pleuromutilin antibiotic. *Pharmacotherapy* 38(9): 935–946. https://doi.org/10.1002/phar.2166.

Viehrig K, Surup F, Harmrolfs K, Jansen R, Kunze B & Müller R (2013). Concerted action of P450 plus helper protein to form the amino-hydroxy-piperidone moiety of the potent protease inhibitor crocapeptin. *Journal of the American Chemical Society* 135(45): 16885–16894. https://doi.org/10.1021/ja4047153.

Wang B, Kang Q, Lu Y, Bai L & Wang C (2012). Unveiling the biosynthetic puzzle of destruxins in *Metarhizium* species. *PNAS* 109(4): 1287–1292. https://doi.org/10.1073/pnas.1115983109.

Wang S-X, Zhao R-L, Guo C, Chen B-S, Dai H-Q, Liu G-Q & Liu H-W (2020). New meroterpenoid compounds from the culture of mushroom *Panus lecomtei*. *Chinese Journal of Natural Medicines* 18(4): 268–272. https://doi.org/10.1016/S1875-5364(20)30033-9.

Wang X, Gong X, Li P, Lai D & Zhou L (2018). Structural diversity and biological activities of cyclic depsipeptides from fungi. *Molecules*. Multidisciplinary Digital Publishing Institute 169. https://doi.org/10.3390/molecules23010169.

Wang X, Gao Y Le, Zhang ML, Zhang HD, Huang JZ & Li L (2020). Genome mining and biosynthesis of the Acyl-CoA: Cholesterol acyltransferase inhibitor beauveriolide I and

III in *Cordyceps militaris*. *Journal of Biotechnology* 309: 85–91. https://doi.org/10.1016/j.jbiotec.2020.01.002.

Wang Y, Bian Z & Wang Ya (2022). Biofilm formation and inhibition mediated by bacterial quorum sensing. *Applied Microbiology and Biotechnology* 106(19–20): 6365–6381. https://doi.org/10.1007/S00253-022-12150-3.

Wang YL, Li LF, Li DX, Wang B, Zhang K & Niu X (2015). Yellow pigment aurovertins mediate interactions between the pathogenic fungus *Pochonia chlamydosporia* and its nematode host. *Journal of Agricultural and Food Chemistry* 63(29): 6577–6587. https://doi.org/10.1021/acs.jafc.5b02595.

Weber HA & Gloer JB (1991). The preussomerins: Novel antifungal metabolites from the coprophilous fungus *Preussia isomera* Cain. *Journal of Organic Chemistry* 56(14): 4355–4360. https://doi.org/10.1021/jo00014a007.

Wennrich JP, Holzenkamp C, Kolařík M, Maier W, Mándi A, Kurtán T, Ashrafi S, Ebada SS & Stadler M (2024). Dactylfungins and tetralones: Bioactive metabolites from a nematode-associated *Laburnicola nematophila*. *Journal of Natural Products* 87(7): 1860–1871. https://doi.org/10.1021/acs.jnatprod.4c00623.

Wennrich JP, Ebada SS, Sepanian E, Holzenkamp C, Khalid SJ, Schrey H, Maier W, Mándi A, Kurtán T, Ashrafi S, *et al.* (2024). Omnipolyphilins A and B: Chlorinated cyclotetrapeptides and naphtho-α-pyranones from the plant nematode-derived fungus *Polyphilus sieberi*. *Journal of Agricultural and Food Chemistry* 72(13): 6998–7009. https://doi.org/10.1021/acs.jafc.4c00572.

Willis K (2018). *State of the World's Fungi 2018*. Edited by K. Willis. Kew Publishing. Available at: https://kew.iro.bl.uk/concern/reports/e30de436-455d-410e-8605-8c533a0398ce?locale=en.

Wittstein K, Cordsmeier A, Lambert C, Wendt L, Sir EB, Weber J, Wurzler N, Petrini LE & Stadler M (2020). Identification of *Rosellinia* species as producers of cyclodepsipeptide PF1022 A and resurrection of the genus *Dematophora* as inferred from polythetic taxonomy. *Studies in Mycology* 96(1): 1–16. https://doi.org/10.1016/j.simyco.2020.01.001.

World Health Organization (2025). *Global antibiotic resistance surveillance report 2025*. Available at: https://www.who.int/publications/i/item/9789240116337.

Wu J & Yu H-Q (2007). Biosorption of 2,4-dichlorophenol by immobilized white-rot fungus *Phanerochaete chrysosporium* from aqueous solutions. *Bioresource Technology* 98(2): 253–259. https://doi.org/10.1016/j.biortech.2006.01.018.

Yan L, Banuelos CA, Mawji NR, Patrick BO, Sadar MD & Andersen RJ (2021). Structure–activity relationships for the marine natural product sintokamides: Androgen receptor N-terminus antagonists of interest for treatment of metastatic castration-resistant prostate cancer. *Journal of Natural Products* 84(3): 797–813. https://doi.org/10.1021/acs.jnatprod.0c00921.

Yang F, Zhao M, Zhou L, Zhang M, Liu J & Marchioni E (2021). Identification and differentiation of wide edible mushrooms based on lipidomics profiling combined with principal component analysis. *Journal of Agricultural and Food Chemistry* 69(34): 9991–10001. https://doi.org/10.1021/acs.jafc.1c02269.

Yang SW, Mierzwa R, Terracciano J, Patel M, Gullo V, Wagner N, Baroudy B, Puar M, Chan

TM, McPhail AT, *et al.* (2006). Chemokine receptor CCR-5 inhibitors produced by *Chaetomium globosum*. *Journal of Natural Products* 69(7): 1025–1028. https://doi.org/10.1021/np060121y.

Yang SW, Mierzwa R, Terracciano J, Patel M, Gullo V, Wagner N, Baroudy B, Puar M, Chan TM & Chu M (2007). Sch 213766, a novel chemokine receptor CCR-5 inhibitor from *Chaetomium globosum*. *Journal of Antibiotics* 60(8): 524–528. https://doi.org/10.1038/ja.2007.67.

Yue L, Chen J, Tuo Y, Qi Z, Liu Y, He XL, Zhang B, Hu J & Li Y (2024). Taxonomy and phylogeny of *Panus* (Polyporales, Panaceae) in China and its relationship with allies. *MycoKeys* 105: 267–294. https://doi.org/10.3897/mycokeys.105.121025.

Zhang L, Fasoyin OE, Molnár I & Xu Y (2020). Secondary metabolites from Hypocrealean entomopathogenic fungi: Novel bioactive compounds. *Natural Product Reports* 37(9): 1181–1206. https://doi.org/10.1039/c9np00065h.

Zhang Y, Li S, Li H, Wang R, Zhang KQ & Xu J (2020). Fungi–nematode interactions: Diversity, ecology, and biocontrol prospects in agriculture. *Journal of Fungi*. Multidisciplinary Digital Publishing Institute 1–24. https://doi.org/10.3390/jof6040206.

Zhao D, Han X, Wang D, Liu M, Gou J, Peng Y, Liu J, Li Y, Cao F & Zhang C (2019). Bioactive 3-decalinoyltetramic acids derivatives from a marine-derived strain of the fungus *Fusarium equiseti* D39. *Frontiers in Microbiology* 10:1285. https://doi.org/10.3389/fmicb.2019.01285.

Zhao F, Mai Q, Ma J, Xu M, Wang X, Cui T, Qiu F & Han G (2015). Triterpenoids from *Inonotus obliquus* and their antitumor activities. *Fitoterapia* 101: 34–40. https://doi.org/10.1016/j.fitote.2014.12.005.

Zhao L & Zheng L (2023). A review on bioactive anthraquinone and derivatives as the regulators for ROS. *Molecules* 28(24): 8139. https://doi.org/10.3390/molecules28248139.

Zheng W, Miao K, Liu Y, Zhao Y, Zhang M, Pan S & Dai Y (2010). Chemical diversity of biologically active metabolites in the sclerotia of *Inonotus obliquus* and submerged culture strategies for up-regulating their production. *Applied Microbiology and Biotechnology* 87(4): 1237–1254. https://doi.org/10.1007/s00253-010-2682-4.

7 Appendix

7.1 Biological Activities of Secondary Metabolites from *Murispora* sp.

Table 2. Antimicrobial activity (MIC) of compounds **9**–**17** isolated from *Murispora* sp. (JKI 72806).

Test Microorganism	MIC (µg/mL)									Reference (µg/mL)
	9	**10**	**11**	**12**	**13**	**14**	**15**	**16**	**17**	
S. aureus	n.i.	n.i.	n.i.	**66.6**	**33.3**	n.i.	n.i.	n.i.	n.i.	0.21[G]
M. smegmatis	n.i.	n.i.	n.i.	n.i.	n.i.	n.i.	n.i.	n.i.	n.i.	1.70[K]
B. subtilis	n.i.	n.i.	n.i.	**16.6**	**8.3**	n.i.	n.i.	n.i.	n.i.	16.6[O]
A. baumannii	n.i.	n.i.	n.i.	n.i.	n.i.	n.i.	n.i.	n.i.	n.i.	0.52[C]
P. aeruginosa	n.i.	n.i.	n.i.	n.i.	n.i.	n.i.	n.i.	n.i.	n.i.	0.21[G]
E. coli	n.i.	n.i.	n.i.	n.i.	n.i.	n.i.	n.i.	n.i.	n.i.	0.42[G]
C. violaceum	n.i.	n.i.	n.i.	n.i.	n.i.	n.i.	n.i.	n.i.	n.i.	1.70[G]
C. albicans	n.i.	n.i.	n.i.	n.i.	n.i.	n.i.	n.i.	n.i.	n.i.	8.3[N]
S. pombe	n.i.	n.i.	n.i.	**8.3**	**8.3**	n.i.	n.i.	n.i.	n.i.	8.30[N]
M. hiemails	n.i.	n.i.	n.i.	n.i.	n.i.	n.i.	n.i.	n.i.	**66.6**	8.30[N]
R. toruloides	n.i.	n.i.	n.i.	**16.6**	**16.6**	n.i.	n.i.	n.i.	n.i.	4.20[N]
W. anomalus	n.i.	n.i.	n.i.	**66.6**	n.i.	n.i.	n.i.	n.i.	n.i.	16.6[N]

n.i.: No inhibition (>66.6 µg/mL).
[G]: Gentamycin; [O]: Oxytetracycline; [N]: Nystatin; [C]: Ciprofloxacin; [K]: Kanamycin.

Table 3. Cytotoxicity (IC_{50}) of compounds **9**–**17** isolated from *Murispora* sp. (JKI 72806).

Test Cell Line	IC_{50} (µM)									Epothilone B (nM)
	9	**10**	**11**	**12**	**13**	**14**	**15**	**16**	**17**	
L929	n.a.	n.a.	n.a.	n.a.	n.a.	n.a.	n.a.	n.a.	n.a.	0.65
KB3.1	n.a.	n.a.	n.a.	n.a.	n.a.	n.a.	n.a.	n.a.	n.a.	0.17

n.a.: No significant activity

Table 4. Nematicidal activity of compounds **9**–**17** isolated from *Murispora* sp. (JKI 72806).

Compound	Corrected mortality rate [%]			Positive control
	100 µg/mL	50 µg/mL	10 µg/mL	
9	n.a.	n.a.	n.a.	
10	n.a.	n.a.	n.a.	
11	n.a.	n.a.	n.a.	
12	**52.5** ± **1.7**	n.a.	n.a.	
13	**52.4** ± **3.4**	n.a.	n.a.	93.8 ± 5.1
14	n.a.	n.a.	n.a.	
15	n.a.	n.a.	n.a.	
16	n.a.	n.a.	n.a.	
17	n.a.	n.a.	n.a.	

n.a.: no significant activity (mortality rate <50 %)
Positive control: Ivermectin (1 µg/mL).
The mortality rate in the negative control (MeOH) was 4.5±4.1%, and was used to calculate the corrected mortality using the Schneider-Orelli's formula.

7.2 Biological Activities of Secondary Metabolites from an Undescribed Genus of Pleosporales

Table 5. Antimicrobial activity (MIC) of compounds **18**–**35** isolated from four strains (JKI 73016, JKI 72728, JKI 73278, JKI 73275) from an undescribed genus of Pleosporales.

Test Microorganism	MIC (µg/mL)																		Reference (µg/mL)
	18	**19**	**20**	**21**	**22**	**23**	**24**	**25**	**26**	**27**	**28**	**29**	**30**	**31**	**32**	**33**	**34**	**35**	
S. aureus	n.d.	n.d.	**33.3**	**66.6**	n.i.	n.i.	**66.6**	n.i.	n.d.	n.i.	n.i.	n.d.	n.i.	n.i.	n.i.	n.i.	**33.3**	**33.3**	0.21[G]
M. smegmatis	n.d.	n.d.	n.i.	n.i.	n.d.	n.i.	n.d.	n.i.	n.d.	n.i.	**66.6**	n.d.	n.d.	n.i.	n.i.	n.i.	**16.6**	n.i.	1.70[K]
B. subtilis	n.d.	n.d.	**8.3**	**16.6**	n.i.	n.i.	**33.3**	n.i.	n.d.	n.i.	**33.3**	n.d.	n.i.	n.i.	n.i.	n.i.	**66.6**	**8.3**	16.6[O]
A. baumannii	n.d.	n.d.	n.i.	n.i.	n.d.	n.i.	n.d.	n.d.	n.d.	n.i.	n.i.	n.d.	n.d.	n.d.	n.i.	n.i.	n.i.	n.i.	0.52[C]
P. aeruginosa	n.d.	n.d.	n.i.	n.i.	n.d.	n.i.	n.d.	n.d.	n.d.	n.i.	n.i.	n.d.	n.d.	n.d.	n.i.	n.i.	n.i.	n.i.	0.21[G]
E. coli	n.d.	n.d.	n.d.	n.d.	n.d.	n.d.	n.d.	n.d.	n.d.	n.d.	n.d.	n.d.	n.d.	n.d.	n.i.	n.i.	n.i.	n.i.	0.42[G]
C. violaceum	n.d.	n.d.	n.i.	n.i.	n.d.	n.i.	n.d.	n.d.	n.d.	n.i.	n.i.	n.d.	n.d.	n.d.	n.i.	n.i.	n.i.	n.i.	1.70[G]
C. albicans	n.d.	n.d.	n.i.	n.i.	n.i.	n.i.	n.i.	n.i.	n.d.	n.i.	n.i.	n.d.	n.i.	n.d.	n.i.	n.i.	n.i.	n.i.	8.3[N]
S. pombe	n.d.	n.d.	n.i.	n.i.	n.d.	n.i.	n.d.	n.i.	n.d.	n.i.	n.i.	n.d.	n.d.	n.d.	n.i.	n.i.	n.i.	n.i.	8.30[N]
M. hiemails	n.d.	n.d.	n.i.	**66.6**	n.i.	n.i.	**33.3**	**66.6**	n.d.	n.i.	n.i.	n.d.	n.i.	n.i.	**66.6**	n.i.	**33.3**	n.i.	8.30[N]
R. toruloides	n.d.	n.d.	n.i.	n.i.	n.d.	n.i.	n.d.	**66.6**	n.d.	n.i.	n.i.	n.d.	n.d.	n.d.	n.i.	n.i.	n.i.	n.i.	4.20[N]
W. anomalus	n.d.	n.d.	n.i.	n.i.	n.d.	n.i.	n.d.	n.i.	n.d.	n.i.	n.i.	n.d.	n.d.	n.d.	n.i.	n.i.	n.i.	n.i.	16.6[N]

n.i.: No inhibition (>66.6 µg/mL). n.d.: Not determined.
[G]: Gentamycin; [O]: Oxytetracycline; [N]: Nystatin; [C]: Ciprofloxacin; [K]: Kanamycin.

Table 6. Cytotoxicity (IC_{50}) of compounds **18**–**35** isolated from four strains (JKI 73016, JKI 72728, JKI 73278, JKI 73275) from an undescribed genus of Pleosporales.

Test Cell Line	IC_{50} (µM)																		Epothilone B (nM)
	18	**19**	**20**	**21**	**22**	**23**	**24**	**25**	**26**	**27**	**28**	**29**	**30**	**31**	**32**	**33**	**34**	**35**	
L929	n.d.	n.d.	**0.66**	**1.98**	n.a.	n.a.	**0.94**	**65.81**	n.d.	n.a.	**0.81**	n.d.	n.a.	n.a.	n.a.	n.a.	**8.23**	n.a.	1.77
KB3.1	n.d.	n.d.	**9.01**	**19.78**	n.a.	n.a.	**1.95**	**32.90**	n.d.	n.a.	**2.30**	n.d.	n.a.	n.a.	n.a.	n.a.	**49.98**	n.a.	0.13
A431	n.d.	n.d.	**4.37**	**7.97**	n.d.	n.d.	n.d.	n.d.	n.d.	n.d.	**0.36**	n.d.	n.d.	n.d.	n.d.	n.d.	**7.06**	n.d.	0.26
MCF-7	n.d.	n.d.	**4.64**	**8.52**	n.d.	n.d.	n.d.	n.d.	n.d.	n.d.	**0.45**	n.d.	n.d.	n.d.	n.d.	n.d.	**6.17**	n.d.	0.28
A549	n.d.	n.d.	n.d.	**21.97**	n.d.	n.d.	**1.67**	n.d.	n.d.	n.d.	**1.71**	n.d.	n.d.	n.d.	n.d.	n.d.	**55.86**	n.d.	0.05
SKOV3	n.d.	n.d.	n.d.	n.d.	n.d.	n.d.	n.d.	n.d.	n.d.	n.d.	n.d.	n.d.	n.d.	n.d.	n.d.	n.d.	**32.34**	n.d.	0.75
PC-3	n.d.	n.d.	**3.00**	**8.79**	n.d.	n.d.	n.d.	n.d.	n.d.	n.d.	**0.99**	n.d.	n.d.	n.d.	n.d.	n.d.	n.d.	n.d.	0.24

n.a.: No significant activity. n.d.: Not determined.

Table 7. Nematicidal activity of compounds **18**–**35** isolated from four strains (JKI 73016, JKI 72728, JKI 73278, JKI 73275) from an undescribed genus of Pleosporales.

Compound	Corrected mortality rate [%]			Positive control
	100 µg/mL	**50 µg/mL**	**10 µg/mL**	
18–**35**	n.a.	n.a.	n.a.	93.8 ± 5.1

Compounds **18**–**35** were tested individually; all showed no significant activity.
n.a.: no significant activity (mortality rate <50 %). Positive control: Ivermectin (1 µg/mL).
The mortality rate in the negative control (MeOH) was 4.5±4.1%, and was used to calculate the corrected mortality using the Schneider-Orelli's formula.

7.3 Publications of the Dissertation

Roman numerals within the text correspond to the following publications.

I. **Llanos-López NA**, Ebada SS, Vasco-Palacios AM, Sánchez-Giraldo LM, López L, Rojas LF, Mándi A, Kurtán T, Marin-Felix Y (**2023**). Panapophenanthrin, a rare oligocyclic diterpene from *Panus strigellus*. *Metabolites* 13(7):848. https://doi.org/10.3390/metabo13070848.

II. Phutthacharoen K†, **Llanos-López NA**†, Toshe R, Noisripoom W, Khonsanit A, Luangsa-Ard JJ, Hyde KD, Ebada SS, Stadler M (**2024**). Bioactive bioxanthracene and cyclodepsipeptides from the entomopathogenic fungus *Blackwellomyces roseostromatus* BCC56290. *Antibiotics* 13(7):585. https://doi.org/10.3390/antibiotics13070585.

III. **Llanos-López NA**†, Wennrich J-P†, Miled J, Ashrafi S, Maier W, Surup S, Stadler M (**2025**). Polydosetins & pullularins – Bioactive tetramic acids & cyclodepsipeptides from the endophytic and nematophagous fungus *Polydomus karssenii*. *Natural Products and Bioprospecting* (accepted).

IV. Wennrich J-P, Sepanian E, Ebada SS, **Llanos-López NA**, Ashrafi S, Maier W, Kurtán T, Stadler M (**2023**). Bioactive naphtho-α-pyranones from two endophytic fungi of the genus *Polyphilus*. *Antibiotics* 12(8):1273. https://doi.org/10.3390/antibiotics12081273.

V. Phutthacharoen K, Toshe R, Khalid SJ, **Llanos-López NA**, Wennrich J-P, Schrey H, Ebada SS, Hyde KD, Stadler M (**2024**). Lachnuoic acids A–F: Ambuic acid congeners from a saprotrophic *Lachnum* species. *Chemistry & Biodiversity* 21(4):e2024003. https://doi.org/10.1002/cbdv.202400385.

VI. Wennrich J-P, Schmidt K, Ashrafi S, **Llanos-López NA**, Kaspara F, Stradal T, Held J, de Carvalho LP, Maier W, Surup F, Stadler M (**2025**). Pochoniatoxin, a cytotoxic pentacyclic metabolite from the nematode-associated fungus *Pochonia chlamydosporia*. *ACS Omega*. (submitted).

† these authors contributed equally to this work

Publication I

Panapophenanthrin, a Rare Oligocyclic Diterpene from *Panus strigellus*

Natalia A. Llanos-López[1,2], Sherif Saeed Ebada[1,3,*], Aída M. Vasco-Palacios[4], Laura M. Sánchez-Giraldo[5], Lina López[6], Luisa F. Rojas[6], Attila Mándi[7], Tibor Kurtán[7] and Yasmina Marin-Felix[1,2,*]

[1] Department of Microbial Drugs, Helmholtz Centre for Infection Research (HZI) and German Centre for Infection Research (DZIF), DZIF Partner Site Hannover-Braunschweig, Inhoffenstrasse 7, 38124 Braunschweig, Germany.

[2] Institute of Microbiology, Technische Universität Braunschweig, Spielmannstraße 7, 38106 Braunschweig, Germany.

[3] Department of Pharmacognosy, Faculty of Pharmacy, Ain Shams University, Cairo 11566, Egypt.

[4] Grupo de Microbiología Ambiental and Grupo BioMicro, Escuela de Microbiología, Universidad de Antioquia, Calle 70 No. 52-21, 050010 Medellín, Colombia.

[5] Grupo de Investigación de Biotecnología Industrial, Facultad de Ciencias, Universidad Nacional de Colombia Sede Medellín, Calle 59A No. 63-20, 050034 Medellín, Colombia.

[6] Grupo de Biotransformación, Escuela de Microbiología, Universidad de Antioquia, Calle 70 No. 52-21, 050010 Medellín, Colombia.

[7] Department of Organic Chemistry, University of Debrecen, P.O. Box 400, 4002 Debrecen, Hungary.

* Corresponding author.

Metabolites 2023, 13(7): 848. https://doi.org/10.3390/metabo13070848.

metabolites

MDPI

Article

Panapophenanthrin, a Rare Oligocyclic Diterpene from *Panus strigellus*

Natalia A. Llanos-López [1,2], Sherif Saeed Ebada [1,3,*], Aída M. Vasco-Palacios [4], Laura M. Sánchez-Giraldo [5], Lina López [6], Luisa F. Rojas [6], Attila Mándi [7], Tibor Kurtán [7] and Yasmina Marin-Felix [1,2,*]

1 Department of Microbial Drugs, Helmholtz Centre for Infection Research (HZI) and German Centre for Infection Research (DZIF), DZIF Partner Site Hannover-Braunschweig, Inhoffenstrasse 7, 38124 Braunschweig, Germany; natalia.llanos@helmholtz-hzi.de
2 Institute of Microbiology, Technische Universität Braunschweig, Spielmannstraße 7, 38106 Braunschweig, Germany
3 Department of Pharmacognosy, Faculty of Pharmacy, Ain Shams University, Cairo 11566, Egypt
4 Grupo de Microbiología Ambientaland Grupo BioMicro, Escuela de Microbiología, Universidad de Antioquia, Calle 70 No. 52-21, 050010 Medellin, Colombia; aida.vasco@udea.edu.co
5 Grupo de Investigación de Biotecnología Industrial, Facultad de Ciencias, Universidad Nacional de Colombia Sede Medellín, Calle 59A No. 63-20, 050034 Medellin, Colombia; laumsanchezgir@unal.edu.co
6 Grupo de Biotransformación, Escuela de Microbiología, Universidad de Antioquia, Calle 70 No. 52-21, 050010 Medellin, Colombia; linam.lopez@udea.edu.co (L.L.); lfernanda.rojas@udea.edu.co (L.F.R.)
7 Department of Organic Chemistry, University of Debrecen, P.O. Box 400, 4002 Debrecen, Hungary; mandi.attila@science.unideb.hu (A.M.); kurtan.tibor@science.unideb.hu (T.K.)
* Correspondence: sherif.elsayed@helmholtz-hzi.de or sherif_elsayed@pharma.asu.edu.eg (S.S.E); yasmina.marinfelix@helmholtz-hzi.de (Y.M.-F.)

Abstract: During the course of our search for biologically active secondary metabolites from fungal cultures, a new oligocyclic diterpenoidal derivative, panapophenanthrin (**1**), was isolated from *Panus strigellus*. In addition, two known metabolites, panepophenanthrin (**2**) and dihydrohypnophilin (**3**), were also obtained. The chemical structures of the isolated compounds were elucidated based on extensive 1D and 2D NMR spectral analyses together with high-resolution electrospray ionization mass spectrometry (HR-ESI-MS). The absolute configuration was determined through TDDFT-ECD calculations. All of the compounds were assessed for their antimicrobial and cytotoxic activities. Compounds **1** and **3** showed moderate to weak activities in the performed antimicrobial assays, while compound **1** exhibited potent cytotoxic activity against the mammalian cell lines mouse fibroblast (L929) and human endocervical adenocarcinoma (KB3.1).

Keywords: basidiomycota; antimicrobial; cytotoxicity; secondary metabolites; white rot fungi

Citation: Llanos-López, N.A.; Ebada, S.S.; Vasco-Palacios, A.M.; Sánchez-Giraldo, L.M.; López, L.; Rojas, L.F.; Mándi, A.; Kurtán, T.; Marin-Felix, Y. Panapophenanthrin, a Rare Oligocyclic Diterpene from *Panus strigellus*. *Metabolites* **2023**, *13*, 848. https://doi.org/10.3390/metabo13070848

Academic Editor: Michał Tomczyk

Received: 9 June 2023
Revised: 3 July 2023
Accepted: 11 July 2023
Published: 13 July 2023

1. Introduction

White rot fungi (WRF) are a broad class of wood-decaying basidiomycetes that have the ability to degrade lignin, a complex and recalcitrant component of plant cell walls [1]. These have been extensively studied for their capacity to break down and remediate organic contaminants, such as pharmaceutically active compounds (PhACs)—e.g., metoprolol and its recalcitrant metabolite metoprolol acid—due to their wide substrate spectrum and their capability to synthesize enzymatic complexes [2–4]. Other pollutants—including polychlorinated biphenyls (PCBs), polycyclic aromatic hydrocarbons (PAHs), petroleum hydrocarbons, and pesticides—have also been shown to be degraded by WRF [5–7].

The genus *Panus* belongs to the family Polyporaceae [8], and many of its studied species have been identified as WRF. This genus is defined by its dimitic hyphal system, with unbranched skeletal hyphae and lacking any binding processes, which makes it thin but tough [8]. It is also characterized by its agaricoid habit in the Polyporales [9]. Based on their morphological characteristics, Pegler combined both genera *Lentinus* and *Panus* into

one large genus, *Lentinus* [10]. However, recent studies, including morphological, biological, and phylogenetic species concepts, have provided evidence to segregate it into two genera [11–13]. Studies also show that this group of lentinoid fungi needs further studies to elucidate the phylogenetic relationships between its sections. *Panus* includes species with skeletal hyphae (thick-walled, typically unbranched), lacking hyphal pegs, with metuloids and gloecystidia, and hymenophoral trama, mostly of a radiate construction [14]. Species of *Panus* are mainly widespread in tropical and subtropical regions, and typically grow on dead wood, downed logs, and tree stumps, playing a vital role in the decomposition of the organic material [8,9,15]. In Colombia, six species of *Panus* have been reported, including *P. conchatus*, *P. neostrigosus*, *P. rudis*, *P. similis*, *P. tephroleucus*, and *P. strigellus* [16]. Moreover, some of the species of *Panus* are edible and eaten in various cultures, including indigenous communities in the Amazon [17,18].

Although WRF have been extensively studied for their bioremediation capacities, little attention has been given to explore their potential for producing secondary metabolites. Different species of *Panus* have been found to produce diverse secondary metabolites, such as epoxy compound derivatives of quinones [19,20], sesquiterpenes [21], and other bioactive substances [22]; however, there are relatively few studies on their pharmacological properties and potential health benefits. Panepoxydone, a compound previously reported in *Lentinus crinitus*, was also found in *P. conchatus* and *P. rudis* and can interfere with the NF-κB mediated signal, which promotes tumor growth by inhibiting the phosphorylation of IκBα [19,23]. Another example is hexacyclinol, isolated from the fungal strain *P. rudis* HKI 0254, which exhibited antiproliferative activity on L-929 cells [24].

The genus *Panus* is a promising source of biologically active secondary metabolites due to its diverse chemical profile and potential therapeutic applications. Furthermore, the limited research conducted on this genus makes it a valuable source for the discovery of novel compounds. To explore this potential, we studied *P. strigellus* for the production of bioactive compounds. Our study led to the identification of a new polyhydro-4-oxa-monoepoxyphenanthrylen-1,7-dione derivative (**1**), along with the two known compounds, panepophenanthrin (**2**) [25], and a hirsutane sesquiterpenoidal congener, dihydrohypnophilin (**3**) [26,27]. The current paper provides a detailed report of the structural elucidation, antimicrobial activity, and cytotoxicity of the isolated compounds.

2. Materials and Methods

2.1. General Experimental Procedures

Nuclear magnetic resonance (NMR) spectra were recorded using an Avance III 500 MHz spectrometer equipped with a BBFO (plus) SmartProbe (^{1}H 500 MHz, ^{13}C 125 MHz; Bruker, Billerica, MA, USA) and an Avance III 700 MHz spectrometer equipped with a 5 mm TCI cryoprobe (^{1}H 700 MHz, ^{13}C 175 MHz; Bruker, Billerica, MA, USA) (sample temperature: 298 K). The NMR data were referenced to selected chemical shifts δ of $CDCl_3$ (^{1}H, δ = 7.27 ppm; ^{13}C, δ = 77.2 ppm) and DMSO-*d6* (^{1}H, δ = 2.50 ppm; ^{13}C, δ = 39.51 ppm).

Electrospray ionization mass (ESI-MS) spectra were recorded with an UltiMate® 3000 Series uHPLC (Thermo Fisher Scientific; Waltman, MA, USA) employing a C18Acquity® UPLC BEH column (2.1 × 50 mm, 1.7 µm; Waters, Milford, MA, USA) (temperature of the column: 40 °C), connected to an amaZon® speed ESI-Iontrap-MS (Bruker; Billerica, MA, USA). The following parameters were used to set up the HPLC system: solvent A: Deionized H_2O + 0.1% formic acid (FA) (*v*/*v*), solvent B: acetonitrile (MeCN) + 0.1% FA (*v*/*v*) as the mobile phase; gradient: 5% B for 0.5 min, increasing to 100% B in 19.5 min and maintaining isocratic conditions at 100% B for 5 min; flow rate: 0.6 mL/min, and Diode-Array Detection (DAD) at 190–600 nm. The crude extracts and pure compounds were dissolved in a solution of acetone and methanol (1:1) to achieve a concentration of 4.5 mg/mL and 1 mg/mL, respectively. High-resolution electrospray ionization mass spectrometry (HR-ESI-MS) spectra were obtained with an Agilent 1200 Infinity Series HPLC–UV system (Agilent Technologies, Böblingen, Germany) with the same conditions as for ESI-MS spectra, connected to a maXis® ESI-TOF mass spectrometer

(Bruker; Daltonics, Bremen, Germany)) (scan range 100–2500 *m/z*, capillary voltage 4500 V, dry temperature 200 °C).

Optical rotations (OR) were recorded in chloroform or DMSO (Uvasol, Merck; Darmstadt, Germany) using a MCP-150 polarimeter (Anton Paar; Seelze, Germany) at 20 °C. UV/Vis spectra measurements were carried out using the UV-Vis spectrophotometer UV-2450 (Shimadzu; Kyoto, Japan), while electronic circular dichroism (ECD) spectra were collected with a J-815 spectropolarimeter (Jasco, Pfungstadt, Germany).

2.2. Fungal Isolation

The specimen was collected in the municipality of Santa Fe de Antioquia, located in the department of Antioquia, Colombia (6.56° N 75.83° W, 571 masl), with an average temperature of 28 °C. Sporomes of *Panus* were collected using an opportunistic approach of convenience sampling [28]. Macromorphological characters were described, including the fresh color, according to the Methuen Handbook of Colour [29]. Specimens were dried in a food dehydrator and placed in plastic bags for transport. All collections were deposited in the University of Antioquia herbarium (HUA). Isolation and culture were performed using small fragments of the pileus. The obtained pure cultures were preserved in potato dextrose agar medium (PDA agar, Himedia, Mumbai, India) at 4 °C until the beginning of the experiments. The strain was deposited in the Microorganism Collection of the School of Microbiology CM-EM-UdeA (CM-UDEA-H9, voucher basidiomata 2574a AMV).

2.3. DNA Extraction, PCR Amplification and Sequencing

DNA of *P. strigellus* was extracted from a 1-week-old colony growing on yeast malt agar (YM agar, malt extract 10 g/L, yeast extract 4 g/L, D-glucose 4 g/L, agar 20 g/L, pH 6.3 before autoclaving) according to the Fungal gDNA Miniprep Kit EZ-10 Spin Column kit protocol (NBS Bio-logicals, Cambridgeshire, UK). The polymerase chain reaction (PCR) was performed to amplify partial sequences of DNA regions, i.e., the internal transcribed spacer region (ITS) using the standard primers ITS1F [30] and ITS4 [31], and the 28S large subunit (LSU) with the primers LR0R and LR7 [32]. The PCR products were purified and sequenced using the Sanger Cycle Sequencing method at Microsynth Seqlab GmbH (Göttingen, Germany). Consensus sequences were obtained using the Geneious® 7.1.9 program [33]. Afterward, the sequences were compared to the available reference data using the Basic Local Alignment Search Tool (BLAST, https://blast.ncbi.nlm.nih.gov/Blast.cgi accessed on 7 June 2023) to achieve the identification of the fungus as *P. strigellus*. The ITS sequence shows affinities to *P. strigellus* (99.76% nucleotide similarity with JQ955727, and 99.05% with MT669136 and JQ955724), while the LSU sequence showed 99.25% nucleotide similarity with *P. conchatus* (ON417226) and 99.17% with *P. lecomtei* (KP135233). However, the morphological study of the voucher specimen, 2574a AMV, from which the strain was isolated, is conclusive with the tropical species *P. strigellus*. The sequences generated in this study were deposited in GenBank (ITS: OR160301, LSU: OR165097).

2.4. Fermentation and Extraction

The fungal strain was subjected to submerged culture in shaker flasks. A 5-L fermentation was carried out in twenty-five shaker flasks of 500 mL Erlenmeyer shape culture flasks containing 200 mL of YM medium (10 g/L malt extract, 4 g/L d-glucose, 4 g/L yeast extract, pH 6.3 before autoclaving). For the inoculum, a well-grown mycelium on an YM agar plate was cut into small pieces using a cork borer (1 cm × 1 cm) and six plugs were inoculated in each flask. The cultures were incubated under shake conditions in the dark at 140 rpm and 23 °C. The fermentation was monitored by checking the concentration of free glucose with Medi-Test glucose (Macherey-Nagel, Düren, Germany). The free glucose was fully consumed after 11 days, and the fermentation was terminated after 3 days of glucose depletion.

To extract the secondary metabolites from the culture, the supernatant and mycelium were first separated through vacuum filtration. The supernatant was decanted with an equal amount of ethyl acetate in a separatory funnel. The organic phase obtained was filtered

through anhydrous sodium sulfate and the permeate was evaporated to dryness in vacuo at 40 °C with a rotary evaporator (Heidolph Instruments GmbH and Co. KG, Schwabach, Germany; pump: Vacuubrand GmbH and Co. KG, Wertheim am Main, Germany) to obtain the crude extract. To extract the secondary metabolites from the mycelium, it was initially soaked with acetone and sonicated for 30 min at 40 °C in an ultrasonic bath (Sonorex Digital 10 P, Bandelin Electronic GmbH and Co. KG, Berlin, Germany); the acetone was evaporated in vacuo at 40 °C, and the resulting aqueous phase was decanted with an equal amount of ethyl acetate. To obtain the crude extract, the organic phase was filtered through anhydrous sodium sulfate and then evaporated to dryness. The process was conducted twice, yielding 2565 mg of supernatant extract and 1824 mg of mycelium extract.

*2.5. Isolation of Compounds **1**–**3***

For a further separation of the compounds, 904 mg of the supernatant extract were dissolved in methanol, portioned in 4 × 226 mg, and fractionated using a preparative reverse phase HPLC (Büchi, Pure C-850, 2020, Flawil, Switzerland). A Gemini® 10 µm C18 110 Å column (250 × 50 mm; Phenomenex, Torrance, CA, USA) was used as the stationary phase. Deionized H_2O + 0.1% formic FA (*v*/*v*) (solvent A) and acetonitrile (MeCN) + 0.1% FA (*v*/*v*) (solvent B) were used as the mobile phase with a flow rate of 40 mL/min. The separation was carried out with an elution gradient started with isocratic conditions at 5% solvent B for 8 min, followed by a gradual increase to 20% B in 5 min, then an increase from 20% B to 30% B in 30 min, 30% B to 42%B in 30 min, 42% B to 100% B in 5 min, and finally isocratic conditions at 100% B for 5 min. UV detection was performed at 210, 254, 300, and 350 nm and eight fractions (F1–F8) were collected based on the observed peaks. The purity of the fractions was checked using HPLC-DAD-ESI-MS.

Fraction F5 (74.8 mg) was further separated using the same equipment and mobile phase as before, but with a flow rate of 20 mL/min and using a Gemini® 10 µm C18 110 Å column (250 × 21.2 mm; Phenomenex, Torrance, CA, USA) as the stationary phase. For F5, the gradient was operated with isocratic conditions at 10% B for 5 min, followed by an increase from 10% B to 20% B in 10 min, from 20% B to 25% B in 20 min, 25% B to 40% B in 15 min, 40% B to 100% B in 5 min, and a final isocratic step of 100% B for 5 min. Ten sub-fractions (G1–G10) were collected from this separation. Compound **1** (0.59 mg, t_R = 32–33 min) was obtained from G5 (19.8 mg) through preparative reverse phase HPLC (Büchi, Pure C-850, 2020, Flawil, Switzerland) with a Synergi™ 10 µm Polar-RP 80 Å column (250 × 50 mm; Phenomenex, Torrance, CA, USA). The aforementioned solvents A and B were employed as the mobile phase with a flow rate of 20 mL/min and a gradient of 5% B for 3 min, then an increase from 5% B to 15% B in 18 min, 15% B to 100% B in 25 min, and finally isocratic conditions at 100% B for 5 min. Sub-fraction G6 (17.7 mg) was further separated using the same instruments and conditions as G5, beginning with isocratic conditions at 5% B for 3 min, afterward an increase to 50% B in 25 min, then an increase to 100% B in 8 min, finished with isocratic conditions at 100% B for 3 min. Four sub-fractions (H1–H4) were obtained from this separation. A total of 10.34 mg of H4 were further purified through preparative reverse phase HPLC (Büchi, Pure C-850, 2020, Flawil, Switzerland) using a Luna® 5 µm C18 110 Å column (250 × 21.2 mm; Phenomenex, Torrance, CA, USA) as the stationary phase, and the same solvents, A and B, as the mobile phase with a flow rate of 15 mL/min. The gradient was operated with isocratic conditions at 10% B for 3 min, then an increase from 10% B to 25% B in 36 min, from 25% B to 100% B in 3 min, and a final isocratic step of 100% B for 3 min. From this separation, compound **2** (3.49 mg, t_R = 27.5–28.5 min) was isolated.

Fraction F6 (50.2 mg) was fractionated using a preparative reverse phase HPLC (Büchi, Pure C-850, 2020, Flawil, Switzerland). A Gemini® 10 µm C18 110 Å column (250 × 21.2 mm; Phenomenex, Torrance, CA, USA) was employed as the stationary phase. Solvents A and B were used as the mobile phase with a flow rate of 20 mL/min. For the separation, the elution gradient started with isocratic conditions at 25% B for 5 min, followed by an increase to 45% B in 20 min, then an increase to 100% B in 10 min, and ended with isocratic conditions at 100% B for 5 min. Three sub-fractions (J1–J3) were collected and J3 (21 mg)

was further separated to obtain compound **3** (4.51 mg, t_R = 19.5–20.5 min) using the same equipment and XBridge 5 µm C18 column (250 × 19 mm; Waters, Milford, MA, USA) as the stationary phase. Solvents A and B were employed as the mobile phase with a flow rate of 20 mL/min. In order to separate sub-fraction J3, the elution gradient was initiated by maintaining the isocratic conditions at 5% B for 3 min, followed by an increase to 20% B in 2 min, 20% B to 30% B in 30 min, 30% B to 100% B in 5 min, and ending with isocratic conditions at 100% B for 3 min. Further details about the purification data are available in Supplementary Materials (Figure S12).

2.5.1. Panapophenanthrin (**1**)

White solid powder; 0.59 mg; $[\alpha]_D^{20}$ –7 (c 0.04, chloroform); UV/Vis (MeOH): λ_{max} (log ε) = 246 (0.1), 202.0 (0.3) nm; ECD (MeOH, λ (nm) (Δε), c 4.97 × 10^{-4} M): 322 (−1.88), 306 (+3.06), 206 (−7.98); NMR data (^{1}H NMR: 500 MHz, ^{13}C NMR: 125 MHz) see Table 1; HR-(+)ESIMS: m/z 403.1750 $[M+H]^+$ (calcd. 403.1751 for $C_{22}H_{27}O_7^+$), 425.1568 $[M+Na]^+$ (calcd. 425.1571 for $C_{22}H_{26}NaO_7^+$), 827.3248 $[2M+Na]^+$ (calcd. 827.3249 for $C_{44}H_{52}NaO_{14}^+$); t_R = 6.72 min (HR-LC-ESIMS). $C_{22}H_{26}O_7$ (402.11 g/mol).

Table 1. ^{1}H and ^{13}C NMR data of **1**.

Pos.	δ_H (Multi, *J* [Hz]) [a]	δ_C, Type [b,e]	δ_H (Multi, *J* [Hz]) [c]	δ_C, Type [d,e]
1		201.2, CO		202.9, CO
2	5.13 (br s, 1H)	64.0, CH	5.17 (br s, 1H)	64.5, CH
3	3.58 (m, *J* = 1.6 Hz, 1H)	55.7, CH	3.50 (m, overlapped, 1H)	57.8, CH
3a	3.66 (dd, *J* = 3.6, 1.3 Hz, 1H)	60.4, CH	3.61 (dd, *J* = 3.8, 1.2 Hz, 1H)	62.5, CH
5		81.3, C		83.0, C
5a	3.52 (t, *J* = 3.7 Hz, 1H)	50.3, CH	3.50 (t, *J* = 3.2 Hz, 1H)	50.0, CH
6	6.52 (dd, *J* = 4.1, 2.8 Hz, 1H)	134.4, CH	6.31 (dd, *J* = 4.8, 2.8 Hz, 1H)	133.2, CH
6a		133.3, C		136.6, C
7		193.9, CO		198.0, CO
8	8.08 (d, *J* = 2.0 Hz, 1H)	129.5, CH	8.56 (s, 1H)	130.9, CH
9		165.2, C		170.3, C
10	4.29 (t, *J* = 5.7 Hz, 1H)	68.6, CH	4.12 (d, *J* = 5.7 Hz, 1H)	70.5, CH
10a	2.65 (ddd, *J* = 11.0, 5.7, 2.8 Hz, 1H)	44.8, CH	2.59 (ddt, *J* = 11.2, 5.7, 2.8 Hz, 1H)	45.9, CH
10b	2.38 (dd, *J* = 11.0, 1.6 Hz, 1H)	47.5, CH	2.46 (dt, *J* = 11.2, 1.6 Hz, 1H)	48.4, CH
10c		59.6, C		61.5, C
11	5.10 (d, *J* = 10.0 Hz, 1H)	80.3, CH	5.56 (d, *J* = 9.9 Hz, 1H)	80.8, CH
12	5.03 (dt, *J* = 10.0, 1.4 Hz, 1H)	120.0, CH	4.98 (dt, *J* = 9.9, 1.4 Hz, 1H)	123.1, CH
13		142.8, C		140.0, C
14	1.78 (d, *J* = 1.4 Hz, 3H)	18.5, CH_3	1.76 (d, *J* = 1.4 Hz, 3H)	19.1, CH_3
15	1.76 (d, *J* = 1.4 Hz, 3H)	26.4, CH_3	1.71 (d, *J* = 1.4 Hz, 3H)	26.6, CH_3
16	1.48 (s, 3H)	28.3, CH_3	1.42 (s, 3H)	30.2, CH_3
17	1.09 (s, 3H)	23.7, CH_3	1.06 (s, 3H)	25.9, CH_3

Measured in chloroform-*d* at [a] 500 (for ^{1}H) and [b] 125 (for ^{13}C) MHz. Measured in methanol-d_4: acetone-d_6 (3:1) at [c] 500 (for ^{1}H) and [d] 125 (for ^{13}C) MHz. [e] Assigned based on HMBC and HSQC spectra.

2.5.2. Panepophenanthrin (**2**)

White solid powder; 3.49 mg; $[\alpha]_D^{20}$ +57 (*c* 1.0, DMSO); UV/Vis (MeOH): λ_{max} (log ε) = 256 (0.1), 203.0 (0.2) nm; NMR data (^{1}H NMR: 500 MHz, ^{13}C NMR: 125 MHz in DMSO-d_6) see Supplementary Material Table S1; HR-(+)ESIMS: *m/z* 443.1674 $[M+Na]^+$ (calcd. 443.1676

for $C_{22}H_{28}NaO_8^+$), 863.3460 $[2M+Na]^+$ (calcd. 863.3461 for $C_{44}H_{56}NaO_{16}^+$); t_R = 3.90 min (HR-LC-ESIMS). $C_{22}H_{28}O_8$ (420.12 g/mol).

2.5.3. Dihydrohypnophilin (**3**)

White solid powder; 4.51 mg; $[\alpha]_D^{20}$ +155 (*c* 0.1, chloroform); UV/Vis (MeOH): λ_{max} (log ε) = 202.0 (0.3) nm; NMR data (^{1}H NMR: 500 MHz, ^{13}C NMR: 125 MHz in chloroform-*d*) see Supplementary Material Table S2; HR-(+)ESIMS: *m/z* 233.1532 $[M\text{-}H_2O+H]^+$ (calcd. 233.1536 for $C_{15}H_{21}O_2^+$), *m/z* 251.1637 $[M+H]^+$ (calcd. 273.1461 for $C_{15}H_{22}NaO_3^+$), 501.3208 $[2M+H]^+$ (calcd. 501.3211 for $C_{30}H_{45}O_6^+$), 523.3027 $[2M+Na]^+$ (calcd. 523.3030 for $C_{30}H_{22}NaO_6^+$); t_R = 5.20 min (HR-LC-ESIMS). $C_{15}H_{22}O_3$ (250.12 g/mol).

2.6. Antimicrobial Assay

The Minimum Inhibitory Concentration (MIC) of the isolated compounds was determined following the method described by Charria-Girón et al. [34]. Compounds **2** and **3** were tested against the fungi *Schizosaccharomyces pombe, Pichia anomala, Mucor hiemalis Candida albicans*, and *Rhodotorula glutinis*; the Gram-positive bacteria *Bacillus subtilis, Mycobacterium smegmatis*, and *Staphylococcus aureus*; and the Gram-negative bacteria *Acinetobacter baumanii, Chromobacterium violaceum, Escherichia coli*, and *Pseudomonas aeruginosa.* Compound **1** was tested against *M. hiemalis, B. subtilis, E. coli, Ps. aeruginosa*, and *S. aureus.* A serial dilution assay was performed in 96-well microtiter plates, using MYC medium (1% bactopeptone, 1% yeast extract, 2% glycerol, pH 6.3) for fungi and adjusted at OD_{548} nm to 0.1. MHB medium (Müller-Hinton Broth: SNX927.1, Carl Roth GmbH, Karlsruhe, Germany) was used for bacteria and most of the cell suspensions were adjusted at OD_{600} nm to 0.1. Ciprofloxacin, oxytetracycline, kanamycin, and gentamycin were used as positive controls against bacterial pathogens, while nystatin was used as the positive control against fungi. The MIC was determined as the lowest concentration of a compound needed to prevent the visible growth of the test organism under specific conditions.

2.7. Cytotoxicity Assay

The in vitro cytotoxicity of the isolated metabolites was evaluated against the two mammalian cell lines, KB 3.1 (human endocervical adenocarcinoma) and L929 (mouse fibroblasts), in a 96-well microtiter plate. The IC_{50} was determined using the colorimetric tetrazolium dye MTT (3-(4,5-dimethylthiazol-2-yl)-2,5-diphenyltetrazolium bromide) assay with epothilone B as a positive control, following the experimental procedure described by Charria-Girón et al. [34]. The half-maximum inhibitory concentration (IC_{50})—the concentration at which cell growth inhibition reached 50% compared to the control—was calculated.

2.8. Computational Section

Mixed torsional/low-mode conformational searches were carried out by means of the Macromodel 10.8.011 software, using the MMFF with an implicit solvent model for $CHCl_3$ and applying a 21 kJ/mol energy window [35]. Geometry re-optimizations of the resultant conformers (ωB97X/TZVP PCM/MeOH) and TDDFT-ECD (B3LYP/TZVP PCM/MeOH, BH&HLYP/TZVP PCM/MeOH, CAM-B3LYP/TZVP PCM/MeOH and PBE0/TZVP PCM/MeOH) calculations were performed with the Gaussian 09 package [36]. ECD spectra were generated as sums of Gaussians with 4200 cm^{-1} width at half-height, using dipole-velocity-computed rotational strength values [37]. Boltzmann distributions were estimated from the DFT energies. Visualization of the results was performed using the MOLEKEL 5.4 software package [38].

3. Results and Discussion

*3.1. Isolation and Identification of Compounds (**1**–**3**)*

Compound **1** was purified as a white solid powder that revealed a quasi-molecular ion peak at *m/z* 403.1750 $[M+H]^+$ (calculated 403.1751) and at *m/z* 425.1568 $[M+Na]^+$ (calculated

425.1571), establishing its molecular formula as $C_{22}H_{26}O_7$ and indicating its inclusion of ten degrees of unsaturation. The ^{13}C NMR and HSQC spectral data of **1** (Table 1) unveiled the presence of twenty-two different carbon resonances that can be distinguished into seven quaternary carbon atoms, including two ketocarbonyl groups at δ_C 201.2 (C-1) and δ_C 193.9 (C-7) and three olefinic carbons at δ_C 165.2 (C-9), δ_C 142.8 (C-13), and at δ_C 133.3 (C-6a), along with two aliphatic quaternary carbons at δ_C 81.3 (C-5) and δ_C 59.6 (C-10c). In addition, the ^1H, ^{13}C NMR, and HSQC spectral data of **1** (Table 1) revealed the presence of three olefinic protons at δ_H 5.03 (dt, J = 10.1, 1.5 Hz, H-12; δ_C 120.0), δ_H 6.52 (dd, J = 4.1, 2.8 Hz, H-6; δ_C 134.4), and a downfield proton at δ_H 8.08 (d, J = 2.0 Hz, H-8; δ_C 129.5), together with eight aliphatic methines, four methyls recognized into two allylic methyls at δ_H 1.78 and δ_H 1.76 that were directly correlated to two carbons at δ_C 18.5 (C-14) and δ_C 26.4 (C-15), respectively, and two singlet methyl groups at δ_H 1.09 (H_3-17; δ_C 23.7) and δ_H 1.48 (H_3-16; δ_C 28.3). By comparing the obtained results with the reported literature and the NMR data obtained for **2** (see Supplementary Material Table S1), compound **1** was suggested to be a related derivative to panepophenanthrin (**2**) and hexacyclinol, previously reported from different strains of the fungus *P. rudis* [16,17]. A careful investigation of the 2D NMR spectral data of **1** and **2** gave sufficient proofs interpreting the differences in their depicted chemical structures (Figure 1). The ^1H-^1H COSY and HSQC spectra of **1** (Figure 2, see Supplementary Materials Figures S4 and S6) revealed four spin systems: the first comprises one olefinic proton (H-6) and one aliphatic methine proton at δ_H 3.52 (t, J = 3.7 Hz, H-5a; δ_C 50.3); the second extends over three methine protons at δ_H 4.29 (t, J = 5.2 Hz, H-10; δ_C 68.6), δ_H 2.65 (ddd, J = 11.0, 5.7, 2.8 Hz, H-10a; δ_C 44.8), and at δ_H 2.38 (dd, J = 11.0, 1.6 Hz, H-10b; δ_C 47.5); the third was defined among the other three aliphtic methines at δ_H 5.13 (br s, H-2; δ_C 64.0), δ_H 3.58 (m, J = 1.6 Hz, H-3; δ_C 55.7), and at δ_H 3.66 (dd, J = 3.6, 1.3 Hz, H-3a; δ_C 60.4); and the fourth spin system was distinguished between one oxygenated aliphatic methine at δ_H 5.10 (d, J = 10.0 Hz, H-11; δ_C 80.3), H-12, and also exhibiting long range correlations to two allyl methyl groups (Me-14 and Me-15). The HMBC spectrum of **1** (Figure 2) revealed key correlations from H-6 and H-8 to C-6a, whereas H-6 revealed a HMBC correlation to the ketocarbonyl carbon at C-7, and H-8 revealed a key correlation to C-9, indicating the inclusion of ring A to *α*,*β*-unsaturated carbonyl moiety. Further key HMBC correlations were identified from H-3, along with long range correlations from H-11 to a ketocarbonyl carbon at C-1 and in addition to the key correlations from the two singlet methyl groups (Me-16 and Me-17) to C-5 (δ_C 81.3) and C-5a (δ_C 50.3). Based on the aforementioned results, compound **1** was identified as a new polyhydro-4-oxa-monoepoxyphenanthrylen-1,7-dione related to panepophenanthrin (**2**) and hexacyclinol that was trivially named as panapophenanthrin.

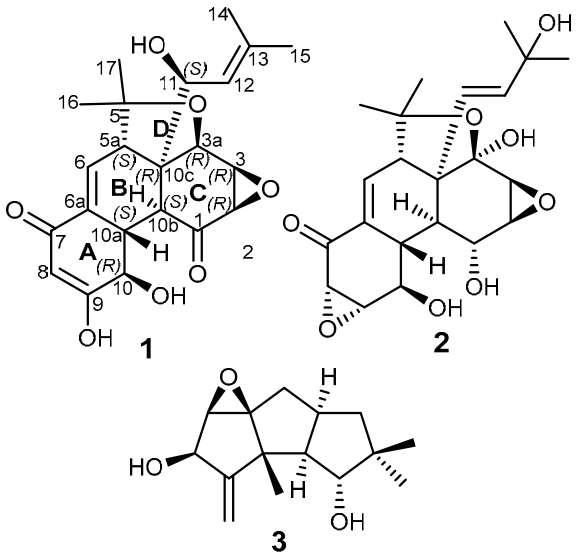

Figure 1. Chemical structures of **1**–**3**.

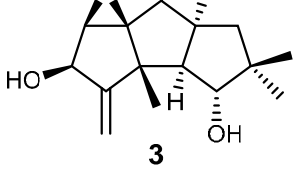

3

Figure 1. Chemical structures of **1**–**3**.

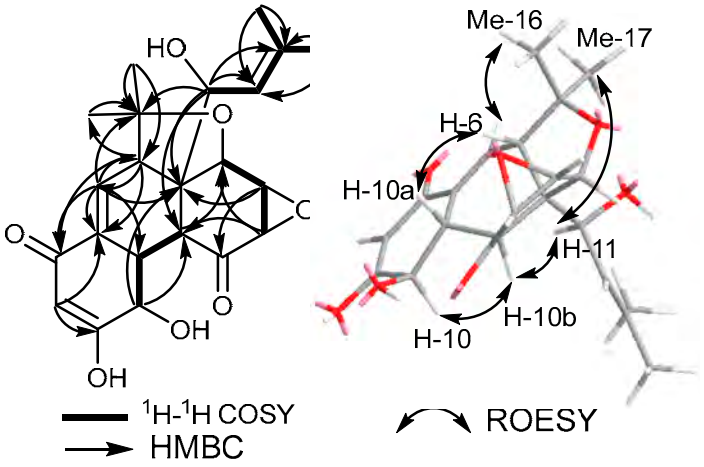

Figure 2. Key COSY, HMBC and ROESY correlations of **1**.

The relative stereochemistry of **1** was determined based on its ROESY spectrum (Figure 2), which revealed key NOE correlations between H-10, H-10b, H-11, and Me-17, indicating that they are facing the same plane of the molecule; on the other hand, other NOE correlations were noticed among H-6, H-10a, and Me-16, supporting their presence toward an opposite plane of the molecule.

In order to elucidate the absolute configuration, the TDDFT-ECD approach was applied on the (2*R*,3*R*,3a*R*,5a*S*,10*R*,10a*S*,10b*S*,10c*R*,11*S*) enantiomer of **1** [39,40]. The initial Merck Molecular Force Field (MMFF) conformational search resulted in two conformer clusters with a 21 kJ/mol energy window, the ωB97X/TZVP [41] PCM/MeOH re-optimization of which yielded conformers A and B with Boltzmann populations of 95.3% and 4.7%, respectively. These conformers differed only in the orientation of the C-10c substituent. The Boltzmann-averaged ECD spectra calculated (Figure 3) at various levels reproduced all the transitions of the experimental spectrum, allowing the determination of the absolute configuration as (2*R*,3*R*,3a*R*,5a*S*,10*R*,10a*S*,10b*S*,10c*R*,11*S*).

The relative stereochemistry of **1** was determined based on its ROESY spectrum (Figure 2), which revealed key NOE correlations between H-10, H-10b, H-11, and Me-17, indicating that they are facing the same plane of the molecule; on the other hand, other NOE correlations were noticed among H-6, H-10a, and Me-16, supporting their presence toward an opposite plane of the molecule.

In order to elucidate the absolute configuration, the TDDFT-ECD approach was applied on the (2*R*,3*R*,3a*R*,5a*S*,10*R*,10a*S*,10b*S*,10c*R*,11*S*) enantiomer of **1** [39,40]. The initial Merck Molecular Force Field (MMFF) conformational search resulted in two conformer clusters with a 21 kJ/mol energy window, the ωB97X/TZVP [41] PCM/MeOH re-optimization of which yielded conformers A and B with Boltzmann populations of 95.3% and 4.7%, respectively. These conformers differed only in the orientation of the C-10c substituent. The Boltzmann-averaged ECD spectra calculated (Figure 3) at various levels reproduced all the transitions of the experimental spectrum, allowing the determination of the absolute configuration as (2*R*,3*R*,3a*R*,5a*S*,10*R*,10a*S*,10b*S*,10c*R*,11*S*).

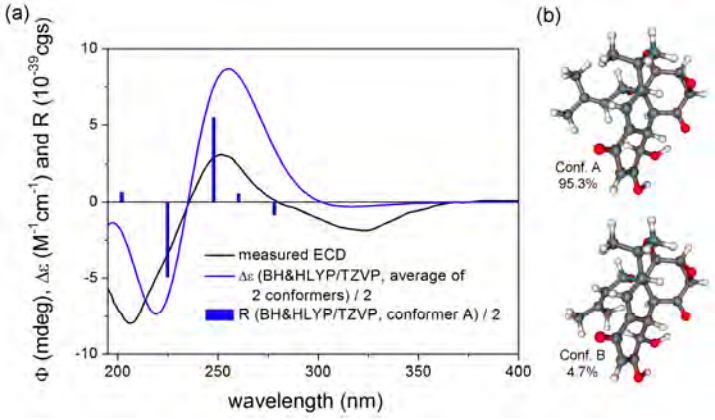

Figure 3. **(a)** Experimental ECD spectrum of **1** in MeOH compared with the BH&HLYP/TZVP PCM/MeOH ECD spectrum of (2*R*,3*R*,3a*R*,5a*S*,10*R*,10a*S*,10b*S*,10c*R*,11*S*)-**1** calculated for the ωB97X/TZVP PCM/MeOH conformers. (**b**) Low-energy ωB97X/TZVP PCM/MeOH conformers of (2*R*,3*R*,3a*R*,5a*S*,10*R*,10a*S*,10b*S*,10c*R*,11*S*)-**1**.

3.2. *Biological Assays*

To assess the antimicrobial activity of compounds 1–3, a serial dilution assay was conducted against several Gram-positive and Gram-negative bacteria, as well as fungal strains, namely: *Schizosaccharomyces pombe, Pichia anomala, Mucor hiemalis Candida albicans, Rhodotorula glutinis, Bacillus subtilis, Mycobacterium smegmatis, Staphylococcus aureus, Acinetobacter baumanii, Chromobacterium violaceum, Escherichia coli,* and *Pseudomonas aeruginosa*. The results obtained (Table 2) revealed that panapophenanthrin (**1**) and dihydrohypnophilin (**3**), rather than panepophenanthrin (**2**), have only moderate to weak antimicrobial activities, with MICs ranging between 33.3 and 66.6 µg/mL. Compound **1** exhibited moderate activity against the Gram-positive bacterium *B. subtilis*, with a MIC value of 33.3

results obtained (Table 2) revealed that panapophenanthrin (**1**) and dihydrohypnophilin (**3**), rather than panepophenanthrin (**2**), have only moderate to weak antimicrobial activities, with MICs ranging between 33.3 and 66.6 µg/mL. Compound **1** exhibited moderate activity against the Gram-positive bacterium *B. subtilis*, with a MIC value of 33.3 µg/mL, compared to oxytetracyclin, which was used as the positive control. In addition, **1** inhibited the growth of the Gram-positive bacterium *S. aureus* at 66.7 µg/mL, indicating weak activity in comparison to the positive control, gentamycin. Compound **2** was inactive against all of the organisms tested. It is important to note that **1** exhibited antimicrobial activity despite being a derivative of **2**, while **2** demonstrated inactivity. This intriguing result highlights a difference in the biological properties between the two compounds. However, it is difficult to identify the functional group responsible for the observed activity in **1** based on the structural differences with compound **2**. Therefore, further studies are needed to determine the group contributing to the antimicrobial activity of **1**. On the other hand, compound **3** showed weak activity against *B. subtilis*, with a MIC value of 66.7 µg/mL, compared to the positive control. However, it was inactive against the remaining organisms tested.

Table 2. Minimum inhibitory concentration (MIC) of compounds **1**–**3** against test organisms.

	MIC (µg/mL)			
Test Organism	**1**	**2**	**3**	**Reference**
Schizosaccharomyces pombe	n.t	-	-	4.2 [N]
Pichia anomala	n.t	-	-	8.3 [N]
Mucor hiemalis	-	-	-	4.2 [N]
Candida albicans	n.t	-	-	4.2 [N]
Rhodotorula glutinis	n.t	-	-	2.1 [N]
Acinetobacter baumanii	n.t	-	-	0.52 [C]
Escherichia coli	-	-	-	0.83 [G]
Bacillus subtilis	33.3	-	66.6	16.6 [O]
Mycobacterium smegmatis	n.t	-	-	1.7 [K]
Staphylococcus aureus	66.6	-	-	0.21 [G]
Pseudomonas aeruginosa	-	-	-	0.21 [G]
Chromobacterium violaceum	n.t	-	-	0.83 [G]

(-): no inhibition observed, n.t: not tested, [C]: Ciprobay 2.54 mg/mL, [G]: Gentamycin 1 mg/mL, [K]: Kanamycin 1 mg/mL, [N]: Nystatin 10 mg/mL, [O]: Oxytetracyclin 1 mg/mL.

Compound **2** was originally isolated from the fermented broth of *P. rudis* FO 8994 [25] and it has been extensively studied for its capacity to inhibit the ubiquitin-activating enzyme (E1) [25,42,43]. It was the first reported inhibitor of E1 from a natural source. The enzyme E1 plays an indispensable role in the ubiquitin-proteasome pathway (UPP), which regulates diverse cellular processes through the degradation of targeted proteins [42,43]. The abnormal functioning of this pathway has been associated with neurodegenerative disease and human cancers [44,45]. Moreover, **2** has generated significant interest among synthetic chemists owing to its unique molecular architecture, distinguished by a densely substituted tetracyclic core. This core structure is notable for its 11 contiguous stereocenters, including two quaternaries [42]. The unique structural characteristics of this molecule, together with its significant biological activity, have prompted extensive studies on its total synthesis [42,43,46,47]. Compound **2**, along with its related derivative **1**, belong to a general class of related epoxyquinoid natural products that are synthesized through Diels–Alder-type dimerization [43]. This group of molecules exhibits a degree of structural complexity spanning from the lower order epoxyquinols—including (+)-isoepoxydon, (+)-epiepoformin, and (+)-bromoxone—to its acetylated derivative [47]. Compounds from this

class have been previously isolated from phylogenetically diverse organisms, such as fungi, bacteria, and worms, inhabiting a wide range of terrestrial and marine ecosystems [47].

Compound **3**, a sesquiterpene with a hirsutane skeleton, was first isolated from the fungus *L. crinitus* [26]. It is structurally related to the hirsutic acid C and is characterized by the presence of an α-methylene ketone moiety [26]. In a prior study conducted by Abate and Abraham (1994), the compound was tested against different microorganisms, revealing activity against *Bacillus cereus* and spores of *Aspergillus flavus*, *Aspergillus niger*, and *Mucor rouxii* [26].

On the other hand, panapophenanthrin (**1**) exhibited potent cytotoxic activity against two mammalian cell lines—mouse fibroblast (L929) and human endocervical adenocarcinoma (KB3.1)—compared to its related derivative **2** (Table 3). This imparts a possible role for their structural differences in eliciting cytotoxic activity. Dihydrohypnophilin (**3**) revealed very weak to no cytotoxic activity against the tested cell lines.

Table 3. Cytotoxic activity (IC_{50}) of compounds **1**–**3** against mammalian cell lines.

	IC_{50} (μM)			
Cell Lines	**1**	**2**	**3**	**Epothilone B**
L929	13.2	*	103.9	6.5×10^{-4}
KB3.1	17.9	*	**	1.73×10^{-5}

(*): Slight inhibition of cell proliferation, (**): no cytotoxic activity observed.

Although compound **3** showed weak cytotoxic activity in our experiment, Abate and Abraham previously reported an IC_{50} of 2.4 g/mL of **3** against the L929 cell line [26]. Moreover, prior studies have reported the strong activity of **3** against the malarial parasite *Plasmodium falciparum,* and cytotoxic activity against the human small lung cancer (NCI-H187) cell line and the derived cells from the kidney of an African green monkey (Vero) [27].

To the best of our knowledge, compound **2** has solely been reported from *P. rudis*, highlighting its possible significance in the genus. Compound **3**, on the other hand, has only been isolated from other genera, but all belonging to the family Polyporaceae, such as *L. crinitus* [26], *L. conatus* [27], *L. strigosus* [48], and *Cerrena* sp. A593 [49]. However, the boundaries between *Lentinus* and *Panus* remain unclear, and species of both genera are still awaiting proper classification based on polyphasic studies [13,14]. Therefore, it is possible that the compounds reported have been associated with the incorrect genus due to this problem. Further research is needed to explore the chemical diversity and biological activities of secondary metabolites from both genera, as well as to understand their evolutionary differentiation.

4. Conclusions

In the current study, three compounds—including one novel compound and two known compounds—were isolated from the submerged culture of *P. strigellus.* The novel compound was named panapophenanthrin (**1**), while the known compounds were identified as panepophenanthrin (**2**) and dihydrohypnophilin (**3**). Our results provide new insights into the chemical diversity of the fungus *P. strigellus.* According to our research findings, compounds **1** and **2** belong to a rare category of oligocyclic terpenoidal metabolites that are only known from the genus *Panus*. The discovery of this novel compound highlights the potential of the genus *Panus* as a source of bioactive substances. In addition, this finding shows the importance of studying unexplored tropical species for the discovery of novel natural products. Further studies are needed to fully characterize the bioactivity of these compounds and to explore their potential applications.

Supplementary Materials: The following supporting information can be downloaded at: https://www.mdpi.com/article/10.3390/metabo13070848/s1, Table S1: ^{1}H and ^{13}C NMR data of panepophenanthrin (2); Table S2: ^{1}H and ^{13}C NMR data of dihydrohypnophilin (3); Figures S1

and S2: HPLC chromatogram and LR-/HRESIMS spectra of **1**; Figures S3–S6: 1D/2D NMR spectra of **1** in chloroform-*d*; Figures S7–S11: 1D/2D NMR spectra of **1** in methanol-d_4:acetone-d_6 (3:1) at 500 (for ^{1}H) and 125 (for ^{13}C) MHz. Figure S12: Flow chart of the purification procedure.

Author Contributions: Conceptualization N.A.L.-L. and Y.M.-F.; methodology, N.A.L.-L., S.S.E., A.M.V.-P., L.M.S.-G. and L.L.; formal analysis, N.A.L.-L., S.S.E. and Y.M.-F.; TDDFT-ECD, A.M. and T.K.; software, S.S.E.; resources, A.M.V.-P.; writing—original draft preparation, N.A.L.-L., S.S.E. and A.M.V.-P.; writing—review and editing, N.A.L.-L., S.S.E. and Y.M.-F.; project administration, Y.M.-F. and L.F.R.; funding acquisition, L.F.R. All authors have read and agreed to the published version of the manuscript.

Funding: Financial support by a personal PhD stipend from the German Academic exchange service DAAD to N.A.L.-L. is immensely acknowledged (program ID 57552340). Y.M.-F. is supported by the Deutsche Forschungsgemeinschaft (DFG)—Project-ID490821847, acronym: COPFUN. Furthermore, S.S.E. is grateful for the Georg-Forster Fellowship for Experienced Researchers stipend (Ref 3.4-1222288-EGY-GF-E), received from the Alexander von Humboldt Foundation, Germany. This research also had support from the Exploration of Collections of Colombian producers for new biologically active secondary metabolites with a focus on scalable and reproducible fermentation processes, Contract 80740-056 of 2019, granted by the Ministerio de Ciencia Tecnología e Innovación, and the contract for access to genetic resources and derived products, No 126-13/05/2016, Otrosi No. 12, granted by the Ministerio de Ambiente y Desarrollo Sostenible de la República de Colombia. T.K. and A.M. thank the National Research Development and Innovation Office for their financial support (Grant numbers FK-134653, K-138672). A.M.V.-P. was supported by Fondo Primer Proyecto Universidad de Antioquia, Project: Exploración de la capacidad antimicrobiana de especies de macrohongos nativas de la Amazonía Colombiana, Project ID 2020-33675.

Institutional Review Board Statement: Not applicable.

Informed Consent Statement: Not applicable.

Data Availability Statement: The DNA sequences are deposited in GenBank (https://www.ncbi.nlm.nih.gov/genbank/ (accessed on 8 June 2023)) and all other relevant data are included in the Supplementary Information.

Acknowledgments: The authors want to thank Wera Collisi for conducting the bioassays, Christel Kakoschke for recording the NMR data, and Esther Surges for recording the HPLC-MS data. We would also like to thank the research group Biotecnología Industrial (Universidad Nacional de Colombia) for their support. The Governmental Information-Technology Development Agency (KIFÜ) is acknowledged for CPU time.

Conflicts of Interest: The authors declare no conflict of interest.

Sample Availability: Samples of compounds **2** and **3** are available from the authors. Sample of compound **1** is not available from the authors, due to consumption for structure elucidation and bioassays.

References

1. Suryadi, H.; Judono, J.J.; Putri, M.R.; Eclessia, A.D.; Ulhaq, J.M.; Agustina, D.N.; Sumiati, T. Biodelignification of lignocellulose using ligninolytic enzymes from white-rot fungi. *Heliyon* **2022**, *8*, e08865. [CrossRef] [PubMed]
2. Chen, L.; Zhang, X.; Zhang, M.; Zhu, Y.; Zhuo, R. Removal of heavy-metal pollutants by white rot fungi: Mechanisms, achievements, and perspectives. *J. Clean Prod.* **2022**, *354*, 131681. [CrossRef]
3. Jaén-Gil, A.; Castellet-Rovira, F.; Llorca, M.; Villagrasa, M.; Sarrà, M.; Rodríguez-Mozaz, S.; Barceló, D. Fungal treatment of metoprolol and its recalcitrant metabolite metoprolol acid in hospital wastewater: Biotransformation, sorption and ecotoxicological impact. *Water Res.* **2019**, *152*, 171–180. [CrossRef] [PubMed]
4. Harms, H.; Schlosser, D.; Wick, L.Y. Untapped potential: Exploiting fungi in bioremediation of hazardous chemicals. *Nat. Rev. Microbiol.* **2011**, *9*, 177–192. [CrossRef] [PubMed]
5. Kristanti, R.A.; Hadibarata, T.; Toyama, T.; Tanaka, Y.; Mori, K. Bioremediation of crude oil by white rot fungi *Polyporus* sp. S133. *J. Microbiol. Biotechnol.* **2011**, *21*, 995–1000. [CrossRef]
6. Kumar, A.; Yadav, A.N.; Mondal, R.; Kour, D.; Subrahmanyam, G.; Shabnam, A.A.; Khan, S.A.; Yadav, K.K.; Sharma, G.K.; Cabral-Pinto, M.; et al. Myco-Remediation: A mechanistic understanding of contaminants alleviation from natural environment and future prospect. *Chemosphere* **2021**, *284*, 131325. [CrossRef]
7. Wu, J.; Yu, H.-Q. Biosorption of 2,4-dichlorophenol by immobilized white-rot fungus *Phanerochaete chrysosporium* from aqueous solutions. *Bioresour. Technol.* **2007**, *98*, 253–259. [CrossRef]

8. Corner, E.J.H. The agaric genera *Lentinus*, *Panus*, and *Pleurotus*, with particular reference to Malaysian species. *Nova Hedwig.* **1981**, *69*, 1–169.
9. Vargas-Isla, R.; Capelari, M.; Menolli, N.; Nagasawa, E.; Tokimoto, K.; Ishikawa, N.K. Relationship between *Panus lecomtei* and *P. strigellus* inferred from their morphological, molecular and biological characteristics. *Mycoscience* **2015**, *56*, 561–571. [CrossRef]
10. Pegler, D.N. *The Genus Lentinus: A World Monograph*; Coode, M., Ed.; Kew Bulletin Additional Series X: London, UK, 1983.
11. Nuñez, M.; Ryvarden, L. Polyporus (Basidiomycotina) and Related Genera. *Synop. Fungorum* **1995**, *10*, 1–85.
12. Grand, E.A. *Systematics and Species Concepts in the Genera Lentinus Fr. and Panus Fr., with Emphasis on the Lentinus tigrinus, L. Crinitus and Panus Lecomtei Complexes*; Univ. Tennessee Press: Knoxville, TN, USA, 2004.
13. Hibbett, D.S.; Vilgalys, R. Phylogenetic relationships of *Lentinus* (basidiomycotina) inferred from molecular and morphological characters. *Syst. Bot.* **1993**, *18*, 409–433. [CrossRef]
14. Seelan, J.S.S.; Justo, A.; Nagy, L.G.; Grand, E.A.; Redhead, S.A.; Hibbett, D. Phylogenetic relationships and morphological evolution in *Lentinus*, *Polyporellus* and *Neofavolus*, emphasizing southeastern Asian taxa. *Mycologia* **2015**, *107*, 460–474. [CrossRef]
15. Senthilarasu, G. The Lentinoid Fungi (*Lentinus* and *Panus*) from Western Ghats, India. *IMA Fungus* **2015**, *6*, 119–128. [CrossRef] [PubMed]
16. Cossu, T.A.; Lücking, R.; Vargas-Estupiñán, N.; Carretero, J.; Vasco-Palacios, A.M.; Moncada, B.; Kirk, P.M.; Almeida, R.F.; Gaya, E.; Coca, L.F.; et al. Annotated checklist of fungi of Colombia. In *Catalogue of Fungi of Colombia*; Kew Publishing, Royal Botanic Gardens: Key, UK, 2022; pp. 209–424.
17. Prance, G.T. The mycological diet of the Yanomam Indians. *Mycologia* **1973**, *65*, 248–250. [CrossRef] [PubMed]
18. Vasco-Palacios, A.M.; Suaza, S.C.; Castanõ-Betancur, M.; Franco-Molano, A.E. Conocimiento Etnoecólogico de Los Hongos Entre Los Indígenas Uitoto, Muinane y Andoke de La Amazonía Colombiana. *Acta Amaz.* **2008**, *38*, 17–30. [CrossRef]
19. Nandi, S.; Sikder, R.; Acharya, K. Secondary metabolites of mushrooms: A potential source for anticancer therapeutics with translational opportunities. In *Advancing Frontiers in Mycology & Mycotechnology*; Springer: Singapore, 2019; pp. 563–598.
20. Song, J.-G.; Ha, L.S.; Ki, D.-W.; Choi, D.-C.; Lee, I.-K.; Yun, B.-S. Chemical constituents of the culture broth of *Panus rudis*. *Mycobiology* **2021**, *49*, 604–606. [CrossRef]
21. Ding, J.-H.; Li, Z.-H.; Feng, T.; Liu, J.-K. A new cadinane sesquiterpenoid from cultures of the basidiomycete *Panus conchatus*. *Nat. Prod. Res.* **2018**, *32*, 2333–2337. [CrossRef]
22. Wang, S.-X.; Zhao, R.-L.; Guo, C.; Chen, B.-S.; Dai, H.-Q.; Liu, G.-Q.; Liu, H.-W. New meroterpenoid compounds from the culture of mushroom *Panus lecomtei*. *Chin. J. Nat. Med.* **2020**, *18*, 268–272. [CrossRef]
23. Erkel, G.; Anke, T.; Sterner, O. Inhibition of NF-KB activation by panepoxydone. *Biochem. Biophys. Res. Commun.* **1996**, *226*, 214–221. [CrossRef]
24. Schlegel, B.; Härtl, A.; Dahse, H.-M.; Gollmick, F.A.; Gräfe, U.; Dörfelt, H.; Kappes, B. Hexacylinol, a new antiproliferative metabolite of *Panus rudis* HKI 0254. *J. Antibiot.* **2002**, *55*, 814–817. [CrossRef]
25. Sekizawa, R.; Ikeno, S.; Nakamura, H.; Naganawa, H.; Matsui, S.; Iinuma, H.; Takeuchi, T. Panepophenanthrin, from a mushroom strain, a novel inhibitor of the ubiquitin-activating enzyme. *J. Nat. Prod.* **2002**, *65*, 1491–1493. [CrossRef]
26. Abate, D.; Abraham, W.-R. Antimicrobial metabolites from *Lentinus crinitus*. *J. Antibiot.* **1994**, *47*, 1348–1350. [CrossRef] [PubMed]
27. Rukachaisirikul, V.; Tansakul, C.; Saithong, S.; Pakawatchai, C.; Isaka, M.; Suvannakad, R. Hirsutane Sesquiterpenes from the Fungus *Lentinus connatus* BCC 8996. *J. Nat. Prod.* **2005**, *68*, 1674–1676. [CrossRef]
28. O'Dell, T.E.; Lodge, D.J.; Mueller, G.M. Approaches to Sampling Macrofungi. In *Biodiversity of Fungi: Inventory and Monitoring Methods*; Elsevier Academic Press: Amsterdam, The Netherland, 2004; pp. 163–168.
29. Kornerup, A.; Wanscher, J.H. *Methuen Handbook of Colour*, 3rd ed.; Don Pavey, Ed.; Methuen & Co., Ltd.: London, UK, 1978.
30. Gardes, M.; Bruns, T.D. ITS Primers with Enhanced Specificity for Basidiomycetes-Application to the Identification of Mycorrhizae and Rusts. *Mol. Ecol.* **1993**, *2*, 113–118. [CrossRef]
31. White, T.J.; Bruns, T.; Lee, S.; Taylor, J. Amplification and Direct Sequencing of Fungal Ribosomal Genes for Phylogenetics. In *PCR Protocols: A Guide to Methods and Applications*; Gelfand, M., Sninsky, J.I., White, T.J., Eds.; Academic Press: New York, NY, USA, 1990; pp. 315–322.
32. Vilgalys, R.; Hester, M. Rapid Genetic Identification and Mapping of Enzymatically Amplified Ribosomal DNA from Several *Cryptococcus* Species. *J. Bacteriol.* **1990**, *172*, 4238–4246. [CrossRef]
33. Kearse, M.; Moir, R.; Wilson, A.; Stones-Havas, S.; Cheung, M.; Sturrock, S.; Buxton, S.; Cooper, A.; Markowitz, S.; Duran, C.; et al. Geneious Basic: An Integrated and Extendable Desktop Software Platform for the Organization and Analysis of Sequence Data. *Bioinformatics* **2012**, *28*, 1647–1649. [CrossRef] [PubMed]
34. Charria-Girón, E.; Stchigel, A.M.; Čmoková, A.; Kolařík, M.; Surup, F.; Marin-Felix, Y. *Amesia hispanica* sp. nov., Producer of the Antifungal Class of Antibiotics Dactylfungins. *J. Fungi* **2023**, *9*, 463. [CrossRef]
35. MacroModel. Schrödinger LLC. Available online: http://www.schrodinger.com/MacroModel (accessed on 10 May 2023).
36. Frisch, M.J.; Trucks, G.W.; Schlegel, H.B.; Scuseria, G.E.; Robb, M.A.; Cheeseman, J.R.; Scalmani, G.; Barone, V.; Mennucci, B.; Petersson, G.A.; et al. *Gaussian 09, Revision E.01*; Gaussian Inc.: Wallingford, CT, USA, 2013.
37. Stephens, P.J.; Harada, N. ECD Cotton Effect Approximated by the Gaussian Curve and Other Methods. *Chirality* **2010**, *22*, 229–233. [CrossRef]
38. Varetto, U. *MOLEKEL, 5.4*; Swiss National Supercomputing Centre: Manno, Switzerland, 2009.

39. Mándi, A.; Kurtán, T. Applications of OR/ECD/VCD to the Structure Elucidation of Natural Products. *Nat. Prod. Rep.* **2019**, *36*, 889–918. [CrossRef] [PubMed]
40. Superchi, S.; Scafato, P.; Gorecki, M.; Pescitelli, G. Absolute Configuration Determination by Quantum Mechanical Calculation of Chiroptical Spectra: Basics and Applications to Fungal Metabolites. *Curr. Med. Chem.* **2018**, *25*, 287–320. [CrossRef]
41. Chai, J.-D.; Head-Gordon, M. Systematic Optimization of Long-Range Corrected Hybrid Density Functionals. *J. Chem. Phys.* **2008**, *128*, 084106. [CrossRef] [PubMed]
42. Moses, J.E.; Commeiras, L.; Baldwin, J.E.; Adlington, R.M. Total Synthesis of Panepophenanthrin. *Org. Lett.* **2003**, *5*, 2987–2988. [CrossRef] [PubMed]
43. Lei, X.; Johnson, R.P.; Porco Jr, J.A. Total Synthesis of the Ubiquitin-Activating Enzyme Inhibitor (+)-Panepophenanthrin. *Angew. Chem. Int. Ed.* **2003**, *42*, 3913–3917. [CrossRef]
44. Lohr, N.J.; Molleston, J.P.; Strauss, K.A.; Torres-Martinez, W.; Sherman, E.A.; Squires, R.H.; Rider, N.L.; Chikwava, K.R.; Cummings, O.W.; Morton, D.H.; et al. Human ITCH E3 Ubiquitin Ligase Deficiency Causes Syndromic Multisystem Autoimmune Disease. *Am. J. Hum. Genet.* **2010**, *86*, 447–453. [CrossRef]
45. Duan, S.; Pagano, M. Ubiquitin Ligases in Cancer: Functions and Clinical Potentials. *Cell Chem. Biol.* **2021**, *28*, 918–933. [CrossRef]
46. Mehta, G.; Islam, K. Enantioselective Total Synthesis of Epoxyquinone Natural Products (−)-Phyllostine, (+)-Epoxydon, (+)-Epiepoxydon and (−)-Panepophenanthrin: Access to Versatile Chiral Building Blocks through Enzymatic Kinetic Resolution. *Tetrahedron Lett.* **2004**, *45*, 7683–7687. [CrossRef]
47. Comméiras, L.; Moses, J.E.; Adlington, R.M.; Baldwin, J.E.; Cowley, A.R.; Baker, C.M.; Albrecht, B.; Grant, G.H. Total Synthesis of the Epoxyquinol Dimer (+)-Panepophenanthrin: Application of a Diastereospecific Biomimetic Diels–Alder Dimerisation. *Tetrahedron* **2006**, *62*, 9892–9901. [CrossRef]
48. Cota, B.B.; Rosa, L.H.; Fagundes, E.M.S.; Martins-Filho, O.A.; Correa-Oliveira, R.; Romanha, A.J.; Rosa, C.A.; Zani, C.L. A Potent Trypanocidal Component from the Fungus *Lentinus strigosus* Inhibits Trypanothione Reductase and Modulates PBMC Proliferation. *Mem. Inst. Oswaldo Cruz* **2008**, *103*, 263–270. [CrossRef] [PubMed]
49. Xie, J.-Q.; Chen, Y.-C.; Sun, Z.-H.; Liu, H.-X.; Li, S.-N.; Li, H.-H.; Gao, X.-X.; Zhang, W.-M. Sesquiterpenoids of Endophytic Fungus *Cerrena* sp. from *Pogostemon cablin* and Their Cytotoxic Activities. *Zhongguo Zhong Yao Za Zhi* **2017**, *42*, 1693–1698. [PubMed]

Publication II

Bioactive Bioxanthracene and Cyclodepsipeptides from the Entomopathogenic Fungus *Blackwellomyces roseostromatus* BCC56290

Kunthida Phutthacharoen[1,2,†], **Natalia A. Llanos-López[1,3,†]**, Rita Toshe[1,3], Wasana Noisripoom[4], Artit Khonsanit[4], Janet Jennifer Luangsa-ard[4], Kevin D. Hyde[2,5], Sherif S. Ebada[1,6,*] and Marc Stadler[1,3,*]

[1] Department of Microbial Drugs, Helmholtz Centre for Infection Research GmbH (HZI), Inhoffenstraße 7, 38124 Braunschweig, Germany.

[2] Center of Excellence in Fungal Research, Mae Fah Luang University, Chiang Rai 57100, Thailand.

[3] Institute of Microbiology, Technische Universität Braunschweig, Spielmannstraße 7, 38106 Braunschweig, Germany.

[4] National Center for Genetic Engineering and Biotechnology (BIOTEC), National Science and Technology Development Agency (NSTDA), 113 Thailand Science Park, Phahonyothin Rd., Khlong Nueng, Khlong Luang, Pathum Thani 12120, Thailand.

[5] School of Science, Mae Fah Luang University, Chiang Rai 57100, Thailand.

[6] Department of Pharmacognosy, Faculty of Pharmacy, Ain Shams University, Cairo 11566, Egypt.

* Corresponding author.

† these authors contributed equally to this work.

Antibiotics 2024, 13(7): 585. https://doi.org/10.3390/antibiotics13070585.

antibiotics

MDPI

Article

Bioactive Bioxanthracene and Cyclodepsipeptides from the Entomopathogenic Fungus *Blackwellomyces roseostromatus* BCC56290

Kunthida Phutthacharoen [1,2,†], Natalia A. Llanos-López [1,3,†], Rita Toshe [1,3], Wasana Noisripoom [4], Artit Khonsanit [4], Janet Jennifer Luangsa-ard [4], Kevin D. Hyde [2,5], Sherif S. Ebada [1,6,*] and Marc Stadler [1,3,*]

1 Department of Microbial Drugs, Helmholtz Centre for Infection Research GmbH (HZI), Inhoffenstraße 7, 38124 Braunschweig, Germany; 6071105503@lamduan.mfu.ac.th (K.P.); natalia.llanos@helmholtz-hzi.de (N.A.L.-L.); ritatoshe840@gmail.com (R.T.)
2 Center of Excellence in Fungal Research, Mae Fah Luang University, Chiang Rai 57100, Thailand; kdhyde3@gmail.com
3 Institute of Microbiology, Technische Universität Braunschweig, Spielmannstraße 7, 38106 Braunschweig, Germany
4 National Center for Genetic Engineering and Biotechnology (BIOTEC), National Science and Technology Development Agency (NSTDA), 113 Thailand Science Park, Phahonyothin Rd., Khlong Nueng, Khlong Luang, Pathum Thani 12120, Thailand; wasana.noi@biotec.or.th (W.N.); artit.kho@biotec.or.th (A.K.); jajen@biotec.or.th (J.J.L.-a.)
5 School of Science, Mae Fah Luang University, Chiang Rai 57100, Thailand
6 Department of Pharmacognosy, Faculty of Pharmacy, Ain Shams University, Cairo 11566, Egypt
* Correspondence: sherif.elsayed@helmholtz-hzi.de or sherif_elsayed@pharma.asu.edu.eg (S.S.E.); marc.stadler@helmholtz-hzi.de (M.S.); Tel.: +49-531-6181-4240 (M.S.)
† The authors equally contributed to this work.

Abstract: In the course of our ongoing research targeting the identification of potential biocontrol agents from entomopathogenic fungi (EPF), we explored a solid-state rice fungal extract of *Blackwellomyces roseostromatus* BCC56290 derived from infected lepidopteran larvae. Chemical and biological prospections afforded four unprecedentedly reported natural products differentiated into a dimeric naphthopyran bioxanthracene ES-242 derivative (**1**) and three cyclodepsipeptides (**2**–**4**) in addition to two known cyclodepsipeptides, cardinalisamides B (**5**) and C (**6**). Chemical structures of the isolated compounds were elucidated through comprehensive 1D/2D NMR and HR-ESI-MS data together with comparisons to the reported literature. The absolute configuration of the isolated cyclodepsipeptides was determined using Marfey's method. All isolated compounds were assessed for their antimicrobial, cytotoxic, and nematicidal activities with some compounds revealing significant activities.

Keywords: insect pathogen; Hypocreales; Ascomycota; beauveriolides

check for updates

Citation: Phutthacharoen, K.; Llanos-López, N.A.; Toshe, R.; Noisripoom, W.; Khonsanit, A.; Luangsa-ard, J.J.; Hyde, K.D.; Ebada, S.S.; Stadler, M. Bioactive Bioxanthracene and Cyclodepsipeptides from the Entomopathogenic Fungus *Blackwellomyces roseostromatus* BCC56290. *Antibiotics* **2024**, *13*, 585. https://doi.org/10.3390/antibiotics13070585

Academic Editor: Marc Maresca

Received: 25 May 2024
Revised: 15 June 2024
Accepted: 22 June 2024
Published: 24 June 2024

1. Introduction

Entomopathogenic fungi constitute a subgroup of soil-dwelling trophic fungi, infecting insects, majorly classified under the order Hypocreales, class Sordariomycetes, phylum Ascomycota [1]. The Hypocrealean Entomopathogenic Fungi (HEPF) comprise several genera including *Beauveria*, *Cordyceps*, and *Isaria* (family Cordycipitaceae) in addition to *Metarhizium* (family Clavicipitaceae) [2]. Species of *Beauveria* and *Metarhizium* serve as the most commercially applied biocontrol agents (BCAs) [3]. In addition, the HEPF revealed an immanent capacity to produce secondary metabolites (SMs) of diverse structural and pharmacological features including some marketed pharmaceuticals and/or agrochemicals [2,4,5]. The diversity in the HEPF parvome of SMs, ranging from molecules below 200 Da up to cyclic polypeptide (>1200 Da) [1], was reflected in a broad range of bioactivities mitigating the pathologic stresses affecting the hepatic, cardiovascular, immune,

and nervous systems [2,4,5]. Among the other genera of the family Cordycipitaceae is the genus *Blackwellomyces* whose species were reported to infect the larvae of coleopteran and lepidopteran insects in particular *B. calendulinus* and *B. minutus* [6–8]. To the best of our knowledge, few SMs were reported from the genus *Blackwellomyces cardinalis* including the antitrypanosomal cyclohexadepsipeptides, cardinalisamides A–C [9], and oosporein, a bibenzoquinone derivative with potent antimicrobial, antifungal and insecticidal activities [10] whose biosynthetic gene cluster was recently described [11].

Along the course of our ongoing research targeting anti-infective secondary metabolites from HEPF, we came across the fungal strain *Blackwellomyces roseostromatus* BCC56290 derived from a soil-buried lepidopteran larva in Thailand. The current study reports the chemical and biological characterization of fungal secondary metabolites purified from its solid-state rice culture extract.

2. Results and Discussion

2.1. Isolation and Identification of 1–6

The solid-state rice culture of *B. roseostromatus* was subjected to chromatographic workup schemes starting with vacuum liquid chromatography followed by preparative HPLC isolations of the promising fractions. These procedures afforded four previously undescribed natural products (**1**–**4**) and two known cyclohexdepsipeptides (**5** and **6**) (Figure 1).

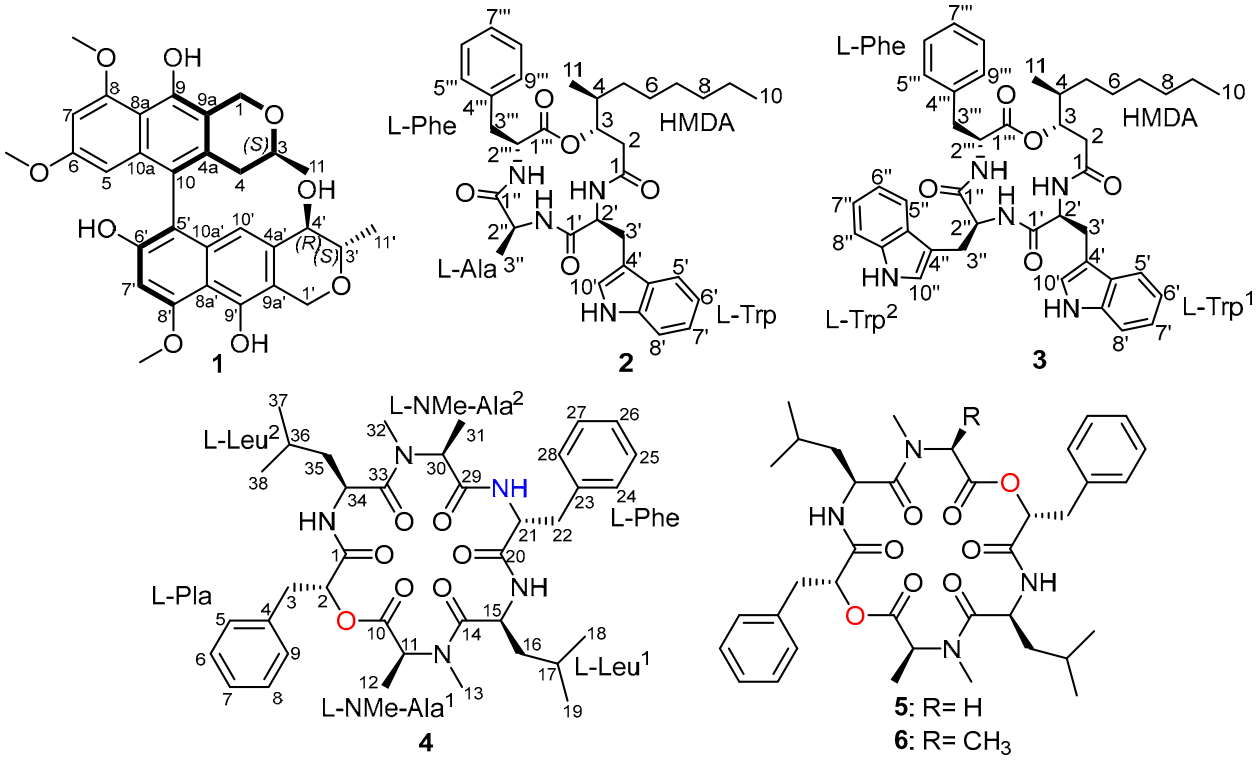

Figure 1. Chemical structures of **1**–**6**.

Compound **1** was obtained as a pale yellow amorphous solid. Its molecular formula was established as $C_{31}H_{32}O_9$ based on the acquired HR-ESI-MS spectrum that revealed a protonated molecular ion peak at m/z 549.2110 $[M + H]^+$ (calculated 549.2119) and a sodium adduct peak at m/z 571.1939 $[M + Na]^+$ (calculated 571.1939) and hence indicating sixteen degrees of unsaturation. The ^{13}C NMR spectral data and the HSQC spectrum of **1** (Table 1, Figure S7) displayed the presence of thirty-one carbon resonances with twenty of them recognized as sp^2 differentiated into sixteen unprotonated and three methine carbon atoms. The assigned twenty sp^2 carbons accounted for ten degrees of unsaturation, thus indicating that compound **1** comprises six rings in its structure. A literature review of **1** suggested its chemical structure to be an analog of ES-242-3, a group of bioxanthracene

Table 1. ^{1}H and ^{13}C NMR data of ES-242-3 (**1**).

Pos.	δ_C [a,c] Type	δ_H [b] Multi (*J* [Hz])	Pos.	δ_C [a,c] Type	δ_H [b] Multi (*J* [Hz])
1	64.3, CH_2	α 4.66 d (15.4) β 5.00 d (15.4)	1′	64.1, CH_2	α 4.59 d (15.2) β 4.82 d (15.2)
3	69.9, CH	3.64 m	3′	74.9, CH	3.31 overlapped
4	34.2, CH_2	α 1.96 dd (16.7, 10.9) β 2.20 dd (16.7, 3.0)	4′	69.6, CH	3.99 t (8.4)
4a	134.1, C		4a′	139.2, C	
5	98.3, CH	6.04 d (2.2)	5′	110.2, C	
6	156.7, C		6′	152.0, C	
7	96.3, CH	6.56 d (2.2)	7′	97.3, CH	6.73 s
8	157.3, C		8′	156.2, C	
8a	108.8, C		8a′	108.1, C	
9	148.1, C		9′	148.2, C	

derivatives previously reported from fungal strains of the two genera *Verticillium* [12,13] and *Cordyceps* [14,15] with a novel *N*-methyl-D-aspartate (NMDA) receptor antagonistic activity [16]. The ^{1}H–^{1}H COSY spectrum of **1** (Figure 2) revealed the presence of two different spin systems. The first spin system extends from one aliphatic oxygenated methine proton at δ_H 3.64 (m, H-3) to a doublet methyl group at δ_H 1.06 (d, J = 6.2, H_3-11) together with two diastereotopic methylene proton signals at δ_H 1.96 (dd, J = 16.7, 10.9 Hz, H-4α) and 2.20 (dd, J = 16.7, 3.0 Hz, H-4β) which were correlated via the HSQC spectrum to one sp^3 secondary carbon atom at δ_C 34.2 (C-4). The second spin system was recognized between two oxygenated methine proton signals at δ_H 3.99 (t, J = 8.4 Hz, H-4′) and δ_H 3.31 (overlapped, H-3′) and extending to a doublet methyl group at δ_H 1.18 (d, J = 6.0 Hz, H_3-11′). In addition, the ^{1}H–^{1}H COSY spectrum of **1** (Figure 2) revealed a long-range ^{4}J correlation between two *meta*-coupled aromatic protons at δ_H 6.04 (d, J = 2.2 Hz, H-5) and 6.56 (d, J = 2.2 Hz, H-7). The HMBC and HSQC spectra of **1** (Figures 2, S6 and S7) revealed the presence of three singlet methoxy groups at δ_H 3.46 (6-OCH_3; δ_C 54.9), 4.04 (8-OCH_3; δ_C 56.5) and 4.05 (8′-OCH_3; δ_C 56.1) that revealed clear HMBC correlations to three oxygenated aromatic carbon atoms at δ_C 156.7, 157.3 and 156.2 ascribed to C-6, C-8 and C-8′, respectively. The relative stereochemistry of **1** was deduced through its ROESY spectrum (Figure 2) that revealed clear ROE correlations from H-3 to the pseudo-axial proton H-1α at δ_H 4.66 (d, J = 15.4 Hz) and from H_3-11′ to the pseudo-axial proton H-4′ at δ_H 3.99 (t, J = 8.4 Hz) indicating cofacial orientations of each pair. In addition, the ROESY spectrum (Figure 2) revealed key correlations from H-7′ to 8′-OCH_3 and from H-7 to both 6-OCH_3 and 8-OCH_3 confirming the chemical structure of **1** as an ES-242 derivative.

Table 1. ^{1}H and ^{13}C NMR data of ES-242-9 (**1**).

Pos.	δ_C, [a,c] Type	δ_H [b] Multi (*J* [Hz])	Pos.	δ_C, [a,c] Type	δ_H [b] Multi (*J* [Hz])
1	64.3, CH_2	α 4.66 d (15.4) β 5.00 d (15.4)	1′	64.1, CH_2	α 4.59 d (15.2) β 4.82 d (15.2)
3	69.9, CH	3.64 m	3′	74.9, CH	3.31 overlapped
4	34.2, CH_2	α 1.96 dd (16.7, 10.9) β 2.20 dd (16.7, 3.0)	4′	69.6, CH	3.99 t (8.4)
4a	134.1, C		4a′	139.2, C	
5	98.3, CH	6.04 d (2.2)	5′	110.2, C	
6	156.7, C		6′	152.0, C	
7	96.3, CH	6.56 d (2.2)	7′	97.3, CH	6.73 s
8	157.3, C		8′	156.2, C	
8a	108.8, C		8a′	108.1, C	
9	148.1, C		9′	148.3, C	
9a	114.3, C		9a′	113.8, C	
10	122.0, C		10′	111.9, CH	6.57 d (1.2)
10a	134.9, C		10a′	135.0, C	
11	21.6, CH_3	1.06 d (6.2)	11′	18.6, CH_3	1.18 d (6.0)
6-OCH_3	54.9, CH_3	3.46 s	4′-OH	-	5.19 d (8.0)
8-OCH_3	56.5, CH_3	4.04 s	6′-OH	-	9.20 br s
9-OH	-	9.49 s	8′-OCH_3	56.1, CH_3	4.05 s
			9′-OH	-	9.46 s

Measured in DMSO-d_6 [a] at 125 MHz/ [b] at 500 MHz. [c] Assignment confirmed by HMBC and HSQC spectra.

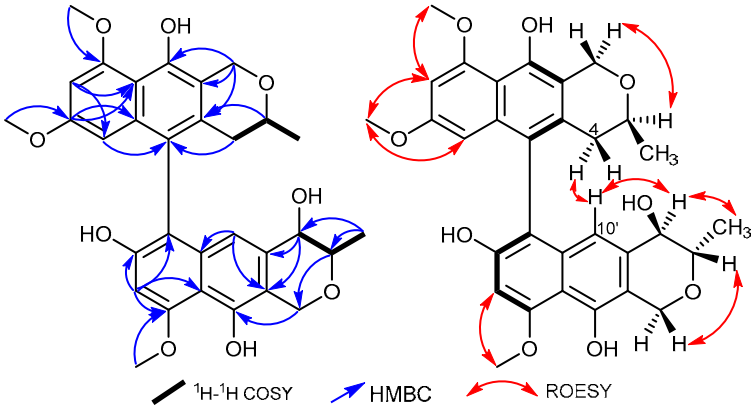

Figure 2. Key ^{1}H–^{1}H COSY, HMBC and ROESY correlations of **1**.

According to the obtained results, the axial chirality of **1** was suggested to be either a 6′-*O*-desmethyl derivative of FS-242-8 [14] or 4-deoxy-6′-*O*-desmethyl derivative of its atropisomer [15]. To distinguish between the two suggested atropisomers, the ROE correlation from H_2-4 to H-10′ was examined and an intense ROE cross-peak was noticed from the pseudoaxial proton H-4α to H-10′ indicating the axial chirality at the C-10/C-5′ to be as depicted in **1** (Figure 1). Based on the obtained results, compound **1** was identified as a previously undescribed naphthopyran bioxanthracene derivative that was named FS-242-9.

Compound **2** was isolated as a yellowish-white amorphous solid. The HR-ESI-MS spectrum of **2** revealed a protonated molecular ion peak and a sodium adduct at *m*/*z* 589.3388 $[M + H]^+$ (calculated 589.3384) and 611.3207 $[M + Na]^+$ (calculated 611.3204), respectively. Thus, its molecular formula was established as $C_{34}H_{44}N_4O_5$ indicating fifteen degrees of unsaturation. The ^{1}H NMR spectral data of **2** in DMSO-d_6 (Table 2, Figure S11) revealed characteristic features of a peptide through the presence of three exchangeable amide NH signals (δ_H 7.31–8.51) together with three amino acid α-proton signals (δ_H 3.82–4.62) and two diastereotopic β-methylene groups (δ_H 3.02/3.12, 2.86/2.92). In addition, the ^{1}H NMR spectral data of **2** also revealed one deshielded pyrrole NH proton at δ_H 10.86 (d, J = 2.4 Hz) and two doublet methyl groups at δ_H 1.11 (d, J = 6.9 Hz) and 0.75 (d, J = 6.9 Hz), respectively. Thus, its molecular formula was established as $C_{34}H_{44}N_4O_5$ indicating fifteen degrees of unsaturation. The ^{1}H NMR spectral data of **2** in DMSO-d_6 (Table 2, Figure S11) revealed characteristic features of a peptide through the presence of three exchangeable amide NH signals (δ_H 7.31–8.51) together with three amino acid α-proton signals (δ_H 3.82–4.62) and two diastereotopic β-methylene groups (δ_H 3.02/3.12, 2.86/2.92). In addition, the ^{1}H NMR spectral data of **2** also revealed one deshielded pyrrole NH proton at δ_H 10.86 (d, J = 2.4 Hz) and two doublet methyl groups at δ_H 1.11 (d, J = 6.9 Hz) and 0.75 (d, J = 6.9 Hz). The ^{1}H–^{1}H COSY spectrum revealed a spin system extending over four aromatic protons at δ_H 7.51 (H-5′)/6.97 (H-6′)/7.06 (H-7′)/7.32 (H-8′), a second spin system over three proton signals at δ_H 7.19 (H-5″, 9″)/7.21 (H-6″, 8″)/7.26 (H-7″) integrated for five protons in addition to a spin system from one α-proton at δ_H 3.82 (p, J = 6.9 Hz, H-2″) to a doublet methyl group at δ_H 1.11 (d, J = 6.9 Hz, H_3-3″) and an amide NH at δ_H 8.47 (d, J = 7.3 Hz). These structural features indicated that **2** is a peptide comprising three amino acids suggested to be tryptophan (Trp), alanine (Ala), and phenylalanine (Phe). In addition, the ^{1}H–^{1}H COSY spectrum revealed an additional spin system extending from a diastereotopic methylene group at δ_H 2.34/2.46 (H_2-2) over two methines protons at δ_H 4.83 (H-9) and δ_H 1.91 (H-4)/δ_H 0.75 (d, J = 6.9 Hz, H_3-11) then five methylene groups ending by a triplet methyl group at δ_H 0.85 (t, J = 6.9 Hz, H_3-10) indicating the presence of a 3-hydroxy-4-methyldecanoyl moiety (HMDA). A literature search of **2** revealed its structural similarity to beauveriolides, cyclic tetradepsipeptides previously reported from entomopathogenic fungi of the genera *Beauveria* [17–19], *Cordyceps* [20,21] and *Isaria fumosorosea* (formerly *Paecilomyces fumosoroseus*) [18,22]. By careful comparison with the reported literature [17–22] alongside the HMBC spectrum of **2** (Figure 3), its amino acid sequence was determined as HMDA-Trp-Ala-Phe based on the key correlations from H-3 to C-1 (δ_C 170.3)/C-1‴ (δ_C 168.7); from H-2′ at δ_H 4.21 (q, J = 7.6 Hz, αH-Trp) to C-1/C-1′ (δ_C 171.4); from H-2″ at δ_H 3.82 (p, J = 6.9 Hz, αH-Ala) to C-1′/C-1″ (δ_C 170.7); and from H-2‴ at δ_H 4.62 (dd, J = 9.1, 7.8 Hz, αH-Phe) to C-1″/C-1‴.

Table 2. ^{1}H and ^{13}C NMR data of beauveriolides T (**2**) and U (**3**).

Pos.	2		3	
	δ_C, [a,c] Type	δ_H [b] Multi (*J* [Hz])	δ_C, [a,c] Type	δ_H [b] Multi (*J* [Hz])
HMDA				
1	170.3, CO		170.3, CO	
2	35.8, CH_2	*α* 2.34 dd (13.8, 9.2) *β* 2.46 dd (13.8, 4.2)	35.6, CH_2	*α* 2.37 dd (14.5, 8.3) *β* 2.41 dd (14.5, 4.7)
3	76.1, CH	4.83 ddd (9.7, 5.8, 4.2)	76.1, CH	4.85 td (7.4, 4.9)
4	35.2, CH	1.91 ddd (9.8, 5.9, 2.4)	34.9, CH	2.01 m
5	31.0, CH_2	*α* 0.96 m; *β* 1.34 m	31.1, CH_2	*α* 0.95 m; *β* 1.36 m
6	26.5, CH_2	*α* 1.12 overlapped *β* 1.28 overlapped	26.4, CH_2	*α* 1.12 overlapped *β* 1.29 overlapped
7	31.3, CH_2	1.23 m	31.3, CH_2	1.23 m
8	29.0, CH_2	1.23 m	29.0, CH_2	1.23 m
9	22.1, CH_2	1.25 m	22.2, CH_2	1.25 m
10	14.0, CH_3	0.85 t (6.9)	14.0, CH_3	0.84 t (6.8)
11	15.3, CH_3	0.75 d (6.9)	15.4, CH_3	0.75 d (6.9)
Trp/Trp[1]				
1′	171.4, CO		170.2, CO	
2′	55.9, CH	4.21 q (7.6)	56.5, CH	4.18 overlapped
3′	25.6, CH_2	*α* 3.02 dd (14.5, 7.9) *β* 3.12 dd (14.5, 7.6)	25.6, CH_2	*α* 3.07 dd (15.3, 7.1) *β* 3.11 overlapped
4′	109.8, C		110.0, C	
4a′	127.0, C		127.1, C	
5′	118.0, CH	7.51 d (8.0)	118.2, CH	7.48 dd (8.0)
6′	118.1, CH	6.97 ddd (8.0, 6.9, 1.0)	118.4, CH	6.98 overlapped
7′	120.8, CH	7.06 ddd (8.0, 6.9, 1.2)	121.0, CH	7.07 m
8′	111.2, CH	7.32 d (8.0)	111.5, CH	7.35 d (8.1)
8a′	136.0, C		136.1, C	
9′-NH	-	10.86 d (2.4)	-	10.83 d (2.5)
10′	123.3, CH	7.11 d (2.4)	123.6, CH	7.10 d (2.5)
NH	-	8.51 d (7.4)	-	8.43 d (7.7)
Ala/Trp[2]				
1″	170.7, CO		171.9, CO	
2″	48.6, CH	3.82 p (6.9)	54.2, CH	4.15 overlapped
3″	15.4, CH_3	1.11 d (6.9)	25.0, CH_2	*α* 2.94 dd (14.8, 7.1) *β* 3.25 dd (14.7, 7.1)
4″			111.0, C	
4a″			127.4, C	
5″			118.3, CH	7.47 d (7.9)
6″			118.2, CH	6.95 overlapped
7″			120.8, CH	7.04 m
8″			111.3, CH	7.32 d (8.2)
8a″			136.0, C	
9″-NH			-	10.69 d (2.4)
10″			123.0, CH	6.81 d (2.4)
NH	-	8.47 d (7.3)	-	8.30 d (7.5)
Phe				
1‴	168.7, CO		169.1, CO	

Table 2. *Cont.*

Pos.	δ_C, [a,c] Type	δ_H [b] Multi (*J* [Hz])	δ_C, [a,c] Type	δ_H [b] Multi (*J* [Hz])
2‴	54.8, CH	4.62 dd (9.1, 7.8)	55.0, CH	4.60 q (8.0)
3‴	37.6, CH_2	*α* 2.86 dd (13.9, 7.5) *β* 2.92 dd (13.9, 8.0)	37.3, CH_2	2.90 q (6.5)
4‴	136.7, C		136.8, C	
5‴, 9‴	128.6, CH	7.19 overlapped	128.8, CH	7.18 overlapped
6‴, 8‴	126.5, CH	7.21 overlapped	126.7, CH	7.21 overlapped
7‴	128.1, CH	7.26 t (7.1)	128.3, CH	7.24 t (7.1)
NH		7.31 d (8.8)		7.77 d (8.7)

Measured in DMSO-d_6 [a] at 125 MHz/ [b] at 500 MHz. [c] Assignment confirmed by HMBC and HSQC spectra.

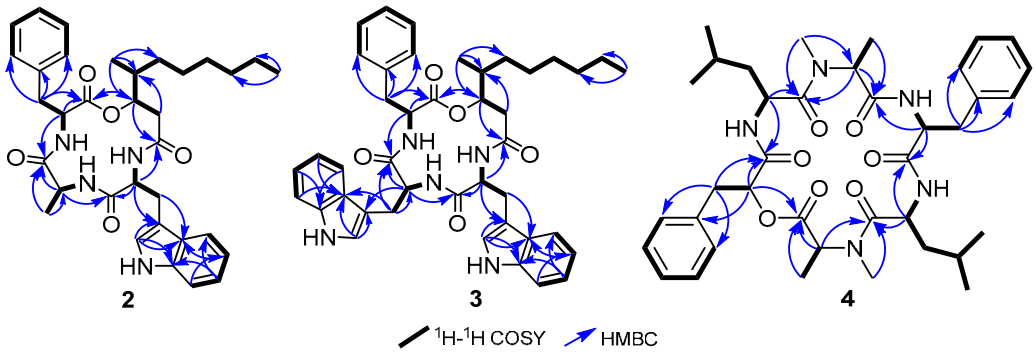

Figure 3. Key ^{1}H–^{1}H COSY and HMBC correlations of **2**–**4**.

Compound **3** was purified as a yellowish-white amorphous solid. Its HR-ESI-MS revealed a protonated molecular ion peak at *m*/*z* 704.3806 $[M + H]^+$ (calculated 704.3806 for $C_{42}H_{50}N_5O_5^+$) and a sodium adduct at *m*/*z* 726.3627 $[M + Na]^+$ (calculated 726.3626 for $C_{42}H_{49}N_5NaO_5^+$). Therefore, the molecular formula of **3** was determined as $C_{42}H_{49}N_5O_5$ indicating twenty-one degrees of unsaturation exceeding those in **2** by six degrees. The ^{1}H NMR and the ^{1}H–^{1}H COSY spectral data of **3** in DMSO-d_6 (Table 2, Figures 3 and S21) revealed comparable characteristic features for **2** apart from the emergence of proton signals ascribed to a second Trp residue such as a deshielded pyrrole NH proton at δ_H 10.69 (d, *J* = 2.4 Hz) that revealed a key cross peak to an olefinic proton at δ_H 6.81 (d, *J* = 2.4 Hz, H-10′) in addition to the presence of a second spin system among four olefinic protons at δ_H 7.47 (H-4′), 6.95 (H-5′), 7.04 (H-7′), 7.32 (H-8′) in comparing the 1D (^{1}H and ^{13}C) NMR data and the key HMBC correlations of **2** and **3** (Table 2, Figures 3, S14 and S22), compound **3** was found to have a second Trp residue replacing Ala in **2** and hence has the amino acid sequence as HMDA-Trp^1-Trp^2-Phe. As for **2**, the absolute configurations of amino acid residues were determined to be 3*S*,4*S*-HMDA-L-Trp^1-L-Trp^2-L-Phe based on the common biosynthetic origin of beauveriolides [20], and the results of Marfey's method (Figures S45–S46). Based on the aforementioned results, compound **3** was recognized as a previously undescribed cyclic tetradepsipeptide and was named beauveriolide U.

Compound **4** was obtained as a yellowish-brown amorphous solid with its molecular formula established as $C_{38}H_{53}N_5O_7$ indicating fifteen degrees of unsaturation based on its HR-ESI-MS that revealed a protonated molecular ion peak at *m*/*z* 692.4023 $[M + H]^+$ (calculated 692.4018) and a sodium adduct at *m*/*z* 714.3836 $[M + Na]^+$ (calculated 714.3837). The 1D (^{1}H/^{13}C) NMR spectral data of **4** (Table 3, Figure S27) exhibited the characteristic features of a peptide including the presence of three exchangeable amide NH signals (δ_H 7.42–7.92) together with two *N*-methyl moieties at δ_H 3.12 (δ_C 37.6) and 3.16 (δ_C 36.5) in addition to five amino acid *α*-proton signals (δ_H 3.47–4.93), and four diastereotopic *β*-methylene groups (δ_H 3.19/3.34, 2.90/3.15, 1.57/1.64, 1.47/1.53). The ^{1}H–^{1}H COSY spectrum of **4** (Figure 3) revealed two comparable spin systems each extending over a set of three aromatic protons signals at δ_H 7.15/7.27/7.18 and at δ_H 7.28/7.20/7.21 with each having a total integration index of five suggesting the presence of two monosubstituted aromatic

of three aromatic protons signals at δ_H 7.15/7.27/7.18 and at δ_H 7.28/7.20/7.21 with each having a total integration index of five suggesting the presence of two monosubstituted aromatic rings. In addition, the ^1H–^1H COSY spectrum of **4** (Figure 3) revealed two pairs of comparable spin systems, one pair represents two leucine residues by spin systems extending from α-proton signals (δ_H 4.93/4.81) to two diastereotopic methylene groups (δ_H 1.57/1.64 or δ_H 1.47/1.53) then to two methine protons (δ_H 1.58/1.45) and ending either by pair of two doublet methyl groups (δ_H 0.84–0.89). The second pair of comparable spin systems revealed clear COSY cross-peaks between two overlapping α-proton signals at δ_H 3.48 to two doublet methyl groups at δ_H 1.32/1.19 with each having a coupling constant of 7.0 Hz. Based on the obtained results and by searching the reported literature, compound **4** was found to be structurally related to cardinalisamide C (**6**) [9], a symmetric cyclohexadepsipeptide isolated from *Blackwellomyces cardinalis* (aka *C. cardinalis*) NBRC 103832, an entomopathogenic fungus derived from an infected lepidopteran larva. A careful comparison of the $^1H/^{13}C$ NMR and HR-ESI-MS spectral data of **4** and cardinalisamide C (**6**) revealed that compound **4** lacks symmetry in **6** due to the replacement of one oxygen atom by nitrogen resulting from having one phenyllactic acid (Pla) and one Phe residue in **4** instead of having two Pla residues in **6**. This structural difference led to the asymmetry of **4**. The amino acid sequence in **4** was determined by acquiring its HMBC spectrum (Figures 3 and S30) that revealed key correlations from an oxygenated methine proton at δ_H 5.05 (dd, J = 10.5, 3.9 Hz, H-2) to two carbonyl carbon atoms at δ_C 168.0 (C-1) and 170.0 (C-10): from an α-proton at δ_H 4.93 (dt, J = 9.5, 7.0 Hz, H-15) to C-10 and C14 (δ_C 171.2); from H-21 and H-30 to C-20 (δ_C 169.8) and C-29 (δ_C 170.2); and from H-34 to C-29 and C-33 (δ_C 171.8). Accordingly, compound **4** was found to be a cyclohexadepsipeptide composed of Pla-NMe-Ala^1-Leu^1-Phe-NMe-Ala^2-Leu^2. According to the results of Marfey's analysis (Figures S46–S48) and based on the taxonomic proximity with common biosynthetic origin, the absolute configurations of the amino acid residues in **4** were deduced to be all in L-configuration. In conclusion, compound **4** was determined to be a previously undescribed cyclohexadepsipeptide and it was given a trivial name cardinalisamide D.

Table 3. ^1H and ^{13}C NMR data of cardinalisamide D (**4**).

Pos.	δ_C, [a,c] Type	δ_H [b] Multi (*J* [Hz])	Pos.	δ_C, [a,c] Type	δ_H [b] Multi (*J* [Hz])
L-Pla			L-Phe		
1	168.0, CO		20	169.8, CO	
2	74.0, CH	5.05 dd (10.5, 3.9)	21	55.8, CH	4.03 ddd (11.7, 8.0, 3.4)
3	37.4, CH_2	α 2.90 dd (14.1, 10.5) β 3.15 overlapped	22	34.2, CH_2	α 3.19 overlapped β 3.34 overlapped
4	137.2, C		23	139.5, C	
5, 9	129.1, CH	7.15 m (2H)	24, 28	129.2, CH	7.28 m (2H)
6, 8	128.0, CH	7.27 m (2H)	25, 27	126.3, CH	7.20 m (2H)
7	125.9, CH	7.18 m (1H)	26	128.8, CH	7.21 m (1H)
L-NMe-Ala^1			21-NH	-	7.92 d (7.9)
10	170.0, CO		L-NMe-Ala^2		
11	58.0, CH	3.48 q (7.0)	29	170.2, CO	
12	13.2, CH_3	1.19 d (7.0)	30	60.8, CH	3.48 q (7.0)
13	36.5, CH_3	3.16 s	31	12.8, CH_3	1.32 d (7.0)
L-Leu^1			32	37.6, CH_3	3.12 s
14	171.2, CO		L-Leu^2		
15	45.8, CH	4.93 dt (9.5, 7.0)	33	171.8, CO	
16	40.4, CH_2	α 1.57 overlapped β 1.64 overlapped	34	46.1, CH	4.81 td (8.2, 6.3)

Table 3. *Cont.*

Pos.	δ_C, [a,c] Type	δ_H [b] Multi (*J* [Hz])	Pos.	δ_C, [a,c] Type	δ_H [b] Multi (*J* [Hz])
17	23.5, CH	1.58 overlapped	35	39.6, CH_2	α 1.47 overlapped β 1.53 overlapped
18	21.5–23.0, CH_3	0.84–0.89 overlapped	36	24.0, CH	1.45 overlapped
19	21.5–23.0, CH_3	0.84–0.89 overlapped	37	21.5–23.0, CH_3	0.84–0.89 overlapped
15-NH	-	7.85 d (9.6)	38	21.5–23.0, CH_3	0.84–0.89 overlapped
			34-NH	-	7.42 d (8.9)

Measured in DMSO-d_6 [a] at 125 MHz/ [b] at 500 MHz. [c] Assignment confirmed by HMBC and HSQC spectra.

Compounds **5** and **6** were isolated similarly as yellowish-brown amorphous solids with their molecular formulas determined as $C_{37}H_{50}N_4O_8$ and $C_{38}H_{52}N_4O_8$ through their HR-ESI-MS spectra (Figures S34 and S40). A literature search of **5**/**6** and by comparing their $^1H/^{13}C$ NMR spectra to the reported literature [9], they were identified as cardinalisamides B and C, respectively.

2.2. Biological Assays

In our search for novel biological natural products with anti-infective activity, several bioassays were performed. All the isolated compounds **1**–**6** were assessed for their cytotoxic, antimicrobial, and nematicidal activity against a panel of different cell lines, Gram-positive/negative bacterial, fungal pathogens, and *Caenorhabditis elegans*, respectively. In cytotoxicity (MTT) assay, the obtained results (Table 4) revealed that among the tested compounds, only cardinalisamides B (**5**) and C (**6**) revealed significant pancytotoxic activities against almost all tested human cancer cell lines with IC_{50} values between 2.2 and 13.9 µM in spite of being relatively non-toxic against normal fibroblast (L929) cell line which gives a positive indication for their safety. The antimicrobial activity assay was conducted against a panel of twelve different bacterial and fungal pathogens (Table S1), however, none of the tested compounds proved to be active. According to the reported literature, related ES-242 derivatives revealed moderate to potent antimalarial activity against *Plasmodium falciparum* (K1, multidrug-resistant strain) at IC_{50} values between 3.3 and 12 µM [15]. Herein, the nematicidal activity assay results (Figure 4, Table S2) revealed that only ES-242-9 (**1**) and cardinalisamide C (**6**) exhibited significant effects against *C. elegans* with corrected mortality rates of 51.1 and 53.6% at 100 µg/mL, respectively. Being neither cytotoxic nor antimicrobial in the conducted assays, ES-242-9 (**1**) could be a suitable candidate for further assessment to develop a nematicidal agent. In the literature, cardinalisamides B (**5**) and (**6**) were first reported to have an almost equipotent in vitro antitrypanosomal activity against *Trypanosoma brucei*, with IC_{50} values of 12.8 and 12.5 µM, respectively [9].

The two previously undescribed beauveriolides T (**2**) and U (**3**) revealed no activity in any of the conducted assays. These cyclodepsipeptides belong to the class of beauveriolides, which are abundantly biosynthesized by HEPF [17–19]. Beauveriolides were first isolated from the insect pathogenic fungus *Beauveria bassiana* in 1977 [17]. Although various related derivatives have been reported to exhibit pharmacological properties, such as calmodulin (CaM) inhibition [23], and protective effects on HEI-OC1 cells [24], as well as stimulating glucose uptake in cultured rat L6 myoblasts [24], to the best of our knowledge, none has shown antimicrobial or nematicidal activities.

Table 4. Cytotoxic (IC_{50} in μM) activity results of **1–6** against mammalian cells.

	IC_{50} (μM)						Positive Control
Test Cell Line	**1**	**2**	**3**	**4**	**5**	**6**	**Epothilone B (nM)**
L929 (murine)	**	*	*	**	**	26.0	0.65
KB3.1 (cervix)	29.2	*	*	36.2	2.2	8.4	0.17
PC-3 (prostate)	n.t.	n.t.	n.t.	n.t.	2.5	7.5	0.09
MCF-7 (breast)	n.t.	n.t.	n.t.	n.t.	6.9	13.9	0.07
SKOV-3 (ovary)	n.t.	n.t.	n.t.	n.t.	25.0	12.3	0.09
A431 (skin)	n.t.	n.t.	n.t.	n.t.	4.3	8.5	0.06
A549 (lung)	n.t.	n.t.	n.t.	n.t.	11.5	11.1	0.05

(*): Slight inhibition of cell proliferation, (**): no cytotoxic activity observed, n.t.: not tested.

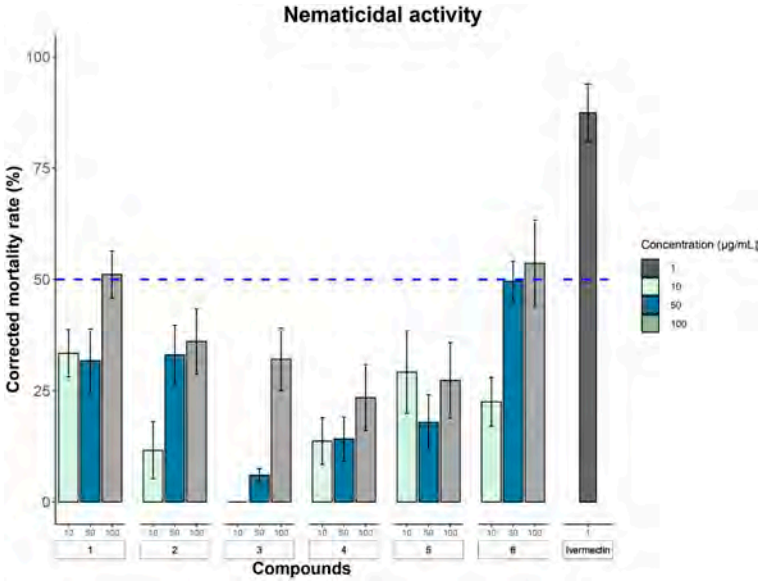

Figure 4. Bioassay of compounds **1**–**6** against *Caenorhabditis elegans*. Corrected mortality rate of compounds **1**–**6** (10 μg mL^{-1}, 50 μg mL^{-1}, and 100 μg mL^{-1}) against *C. elegans* after 18 h of treatment. A solution of ivermectin (1 μg mL^{-1}) was used as a positive control. The data were corrected using Schneider-Orelli's formula based on the negative control as methanol and are shown as the mean ± SD (n ≥ 3). The blue dash line characterizes the IC_{50}.

3. Materials and Methods

3.1. General Experimental Procedures

Optical rotation values were measured on a PerkinElmer 241 polarimeter at 20 °C (Anton Paar GmbH, Graz, Austria). UV spectra were acquired using a Shimadzu UV/VIS spectrophotometer UV-2450 (Shimadzu®, Kyoto, Japan). High resolution electrospray ionization mass spectra (HR-ESI-MS) were measured on an Agilent 1200 Infinity Series HPLC-UV system (Agilent Technologies®, Santa Clara, CA, USA) equipped with a C_{18} Acquity UPLC BEH column (50 × 2.1 mm, 1.7 μm; Waters, Milford, MA, USA), solvent A: H_2O + 0.1% formic acid (FA) (*v*/*v*); solvent B: acetonitrile (MeCN) + 0.1% FA (*v*/*v*), gradient: 5% B for 0.5 min increasing to 100% B in 19.5 min, holding at 100% B for 5 min, a flow rate of 0.6 mL min^{-1}, UV/Vis detection 190–600 nm) connected to a Time-Of-Flight mass spectrometer (ESI-TOF-MS, Maxis, Bruker, Billerica, MA, USA) (scan range 100–2500 *m*/*z*, rate 2 Hz, capillary voltage 4500 V, dry temperature 200 °C). NMR spectra were recorded with an Avance III 500 spectrometer (Bruker®, Billerica, MA, USA, ^{1}H-NMR: 500 MHz, and ^{13}C-NMR: 125 MHz) dissolving compounds in deuterated DMSO-d_6.

3.1. General Experimental Procedures

Optical rotation values were measured on a PerkinElmer 241 polarimeter at 20 °C (Anton Paar GmbH, Graz, Austria). UV spectra were acquired using a Shimadzu UV/VIS spectrophotometer UV-2450 (Shimadzu®, Kyoto, Japan). High resolution electrospray ionization mass spectra (HR-ESI-MS) were measured on an Agilent 1200 Infinity Series HPLC-UV system (Agilent Technologies®, Santa Clara, CA, USA) equipped with a C_{18} Acquity UPLC BEH column (50 × 2.1 mm, 1.7 μm; Waters, Milford, MA, USA), solvent A: H_2O + 0.1% formic acid (FA) (*v*/*v*); solvent B: acetonitrile (MeCN) + 0.1% FA (*v*/*v*), gradient: 5% B for 0.5 min increasing to 100% B in 19.5 min, holding at 100% B for 5 min, a flow rate of 0.6 mL min^{-1}, UV/Vis detection 190–600 nm) connected to a Time-Of-Flight mass spectrometer (ESI-TOF-MS, Maxis, Bruker, Billerica, MA, USA) (scan range 100–2500 *m*/*z*, rate 2 Hz, capillary voltage 4500 V, dry temperature 200 °C). NMR spectra were recorded with an Avance III 500 spectrometer (Bruker®, Billerica, MA, USA, ^{1}H-NMR: 500 MHz, and ^{13}C-NMR: 125 MHz) dissolving compounds in deuterated DMSO-d_6.

3.2. Fungal Material

Blackwellomyces sp. BCC56290 (Cordycipitaceae, Hypocreales, Sordariomycetes, Ascomycota) found on lepidopteran larva buried in soil in October 2012, by Artit Khonsanit, Kanoksri Tasanathai, Prasert Srikitikulchai, Rachada Promharn and Wasana Noisripoom

3.2. Fungal Material

Blackwellomyces sp. BCC56290 (Cordycipitaceae, Hypocreales, Sordariomycetes, Ascomycota) found on lepidopteran larva buried in soil in October 2012, by Artit Khonsanit, Kanoksri Tasanathai, Prasert Srikitikulchai, Rachada Promharn and Wasana Noisripoom in Chiang Mai Province, Kanlayaniwatthana District, Ban Chan Upriver Forest Nature Trail, located at coordinates 18°59′15″N and 98°17′09″E. The pure culture was deposited in the BIOTEC culture collection (BCC). Combined analyses of ITS, *LSU*, *EF1*, and *RPB1* sequences (GenBank accession numbers ITS = PP709052, *LSU* = PP711712, *EF1* = PP735441, and *RPB1* = PP735443) confirmed that *Blackwellomyces* sp. BCC56290 is nested within the type specimen of *B. roseostromatus* BCC91358 [7], confirming its identity (Maximum Likelihood phylogenetic tree inferred from 117 taxa of Cordycipitaceae based on combined ITS, *LSU*, *EF1* and *RPB1* sequence data, see Supplementary Figure S49). Fungal specimen was dried in a food dehydrator and deposited in the BIOTEC Bangkok Herbarium (BBH), Thailand Science Park, Pathum Thani Province, Thailand.

3.3. Fermentation, Extraction and Isolation

We evaluated the antiviral activities of *Blackwellomyces* species such as *B. aurantiacus*, *B. calendulinus*, *B. minutus*, and *B. roseostromatus*, against SARS-CoV-2 and CHIKV infections including the inhibitory effect on 3CLpro activity, cytotoxicity of the extracts to Vero E6, Huh7, and HEK293 cells used in the assays and found that *B. roseostromatus* BCC56290 extract inhibited CHIKV infection. We therefore chose this fungus due to our previous findings against the virus. Fermentation of the selected strain *B. roseostromatus* BCC56290 was grown on solid-state rice media (fermentations completed in 10 × 1000 mL Erlenmeyer flasks containing 180 g of rice in 180 mL distilled water) and inoculated with 10 pieces of fully grown 7 mm mycelial plugs. The rice cultures were incubated on static conditions in white light/dark cycles in the laboratory, under room temperature, until full growth of the mycelia was achieved (31 days from inoculation). Thereafter, the cultures were soaked overnight in acetone (500 mL) and extracted thrice under sonication. The solvent was evaporated to yield an aqueous phase (400 mL) that was extracted thrice with ethyl acetate in a ratio of 1:1 (*v*/*v*). The organic phase was filtered through anhydrous sodium sulfate and evaporated on a rotary evaporator to dryness. The extracts were transferred into vials and dried under nitrogen and thereafter their weights were determined.

The crude extract (4.43 g) was dissolved in 3.0 mL of MeOH and loaded on silica gel by trituration using mortar and pestle and then left to dry overnight. The loaded air-dried extract was applied on the top of a column dry-packed with silica gel. A vacuum liquid chromatography (VLC) procedure was initiated by applying a gradient elution starting with 100% *n*-hexane, *n*-hexane/EtOAc (7:3, 1:1, and 3:7) and 100% EtOAc. Then, the gradient was switched to 100% DCM, DCM/MeOH (9:1, 8:2, 1:1) and ended by washing with 100% MeOH (*v*/*v*) affording ten fractions (F1–F10).

Fraction 3 (F3, 179 mg, *n*-hexane/EtOAc (1:1)) was further purified using preparative reversed-phase liquid chromatography (PLC 2020, Gilson, Middleton, Wisconsin, USA) equipped with a Gemini C_{18} column (50 × 21 mm, 10 µm, Phenomenex, Aschaffenburg, Germany) as a stationary phase. Deionized water (Milli-Q, Millipore, Schwalbach, Germany) supplemented with 0.1% formic acid (FA) (solvent A) and acetonitrile (MeCN) with 0.1% FA (solvent B) were used as the mobile phase. The elution gradient used for fractionation started using 20% of solvent B (MeCN + 0.1% FA) and 80% of solvent A (deionized water + 0.1% FA) for 5 min. Then, the gradient continued from 20 to 40% of solvent B over 10 min and from 40 to 100% of solvent B over 30 min ending by holding 100% of solvent B for 10 min, the flow rate was set to 15 mL/min, and UV detection was carried out at 210, 225, 275, and 330 nm to yield **1** (1.6 mg, t_R = 11.0 min), **5** (2.0 mg, t_R = 18.0 min), and **6** (2.1 mg, t_R = 21.0 min).

Fractions 4 (F4, *n*-hexane/EtOAc (3:7)) and 5 (F5, 100% EtOAc) were pooled and concentrated under reduced pressure yielding 157 mg. Afterward, the combined fraction was subjected to preparative HPLC separations adopting the same conditions and gradient

elution as for F3 to obtain **4** (4.1 mg, t_R = 17.0 min), **2** (1.5 mg, t_R = 19.0 min), and **3** (3.8 mg, t_R = 20.0 min).

Spectral data (see also Figures S1–S48)

ES-242-9 (**1**): Pale yellow amorphous solid; $[\alpha]_D^{20}$ +32.0° (*c* 0.1, acetone); UV/Vis (MeOH): λ_{max} (log ε) = 201 (4.91), 239 (4.91), 293.5 (4.07), 309 (4.04), 346 (3.95) nm; NMR data (^{1}H NMR: 500 MHz, ^{13}C NMR: 125 MHz in DMSO-d_6) see Table 1; HR-(+)ESI-MS: *m*/*z* 549.2110 $[M + H]^+$ (calcd. 549.2119 for $C_{31}H_{33}O_9^+$), 571.1939 $[M + Na]^+$ (calcd. 571.1939 for $C_{31}H_{32}NaO_9^+$); t_R = 9.66 min (LC-ESI-MS). $C_{31}H_{32}O_9$ (548.20 g/mol).

Beauveriolide T (**2**): Yellowish-white amorphous solid; $[\alpha]_D^{20}$ –66.7° (*c* 0.06, DMSO); UV/Vis (MeOH): λ_{max} (log ε) = 194 (4.21), 202 (4.44), 218.5 (4.43), 279.5 (3.71), 289.5 (3.63) nm; NMR data (^{1}H NMR: 500 MHz, ^{13}C NMR: 125 MHz in DMSO-d_6) see Table 2; HR-(+)ESI-MS: *m*/*z* 589.3388 $[M + H]^+$ (calcd. 589.3384 for $C_{34}H_{45}N_4O_5^+$), 611.3207 $[M + Na]^+$ (calcd. 611.3204 for $C_{34}H_{44}N_4NaO_5^+$); t_R = 13.15 min (LC-ESI-MS). $C_{34}H_{44}N_4O_5$ (588.33 g/mol).

Beauveriolide U (**3**): Yellowish-white amorphous solid; $[\alpha]_D^{20}$ –51.0° (*c* 0.1, acetone); UV/Vis (MeOH): λ_{max} (log ε) = 201 (5.01), 218 (4.92), 262.5 (4.27) nm; NMR data (^{1}H NMR: 500 MHz, ^{13}C NMR: 125 MHz in DMSO-d_6) see Table 2; HR-(+)ESI-MS: *m*/*z* 704.3806 $[M + H]^+$ (calcd. 704.3806 for $C_{42}H_{50}N_5O_5^+$), 726.3627 $[M + Na]^+$ (calcd. 726.3626 for $C_{42}H_{49}N_5NaO_5^+$); t_R = 14.23 min (LC-ESI-MS). $C_{42}H_{49}N_5O_5$ (703.41 g/mol).

Cardinalisamide D (**4**): Yellowish-brown amorphous solid; $[\alpha]_D^{20}$ –136.0° (*c* 0.1, acetone); UV/Vis (MeOH): λ_{max} (log ε) = 194 (4.65), 203 (4.97) nm; NMR data (^{1}H NMR: 500 MHz, ^{13}C NMR: 125 MHz in DMSO-d_6) see Table 3; HR-(+)ESI-MS: *m*/*z* 692.4023 $[M + H]^+$ (calcd. 692.4018 for $C_{38}H_{54}N_5O_7^+$), 714.3836 $[M + Na]^+$ (calcd. 714.3837 for $C_{38}H_{53}N_5NaO_7^+$); t_R = 12.91 min (LC-ESI-MS). $C_{38}H_{53}N_5O_7$ (691.45 g/mol).

Cardinalisamide B (**5**): Yellowish-brown amorphous solid; $[\alpha]_D^{20}$ –93.0° (*c* 0.1, acetone); UV/Vis (MeOH): λ_{max} (log ε) = 204 (4.83) nm; NMR data (^{1}H NMR: 500 MHz, ^{13}C NMR: 125 MHz in DMSO-d_6) comparable to those reported in the literature [19,20]; HR-(+)ESI-MS: *m*/*z* 679.3709 $[M + H]^+$ (calcd. 679.3701 for $C_{37}H_{51}N_4O_8^+$), 701.3521 $[M + Na]^+$ (calcd. 701.3521 for $C_{37}H_{50}N_4NaO_8^+$); t_R = 13.58 min (LC-ESI-MS). $C_{37}H_{50}N_4O_8$ (678.42 g/mol).

Cardinalisamide C (**6**): Yellowish-brown amorphous solid; $[\alpha]_D^{20}$ –129.0° (*c* 0.1, acetone); UV/Vis (MeOH): λ_{max} (log ε) = 201 (4.86), 256.5 (4.13) nm; NMR data (^{1}H NMR: 500 MHz, ^{13}C NMR: 125 MHz in DMSO-d_6) comparable to those reported in the literature [19,20]; HR-(+)ESI-MS: *m*/*z* 693.3866 $[M + H]^+$ (calcd. 693.3867 for $C_{38}H_{53}N_4O_8^+$), 715.3676 $[M + Na]^+$ (calcd. 715.3677 for $C_{38}H_{52}N_4NaO_8^+$); t_R = 14.68 min (LC-ESI-MS). $C_{38}H_{52}N_4O_8$ (692.45 g/mol).

3.4. Derivatization with Marfey's Reagent and Elucidation of Amino Acid Configurations

Determination of amino acid stereochemistry of beauveriolide U (**3**) and cardinalisamide D (**4**) was conducted using Marfey's method, following the experimental procedure outlined by Viehrig et al. [25]. For the hydrolysis, 500 µL of 6 N HCl was added to 0.5 mg of the compound and incubated at 90 °C for 18 h. The resulting hydrolysate was evaporated under vacuum conditions and suspended in 200 µL of Milli-Q water. Subsequently, 20 µL of 1 M $NaHCO_3$ and 100 µL of acetone containing 1% derivatization agent Nα-(2,4-dinitro-5-fluorophenyl)-l-alaninamide (FDAA) were added. The mixture was incubated at 40 °C for 40 min and evaporated to dryness under vacuum. Finally, the residual product was diluted in 1 mL MeOH and analyzed using an HPLC system connected to an amaZon speed ESI-MS as described before. The $_L$- or $_D$- configuration of the amino acids was determined by comparing the observed retention times with those of authentic amino acids subjected to the same derivatization procedure. The retention times (in minutes) of the FDAA-derivatized amino acids were as follows: alanine ($_L$-: 5.61, $_D$-: 6.40), tryptophan ($_L$-: 7.82, $_D$-: 8.41; leucine ($_L$-: 8.07, $_D$-: 9.0), and phenylalanine ($_L$-: 8.01, $_D$-: 8.81).

3.5. Cytotoxicity Assay

In vitro cytotoxic activity of the isolated compounds was tested by applying the MTT (3-(4,5-dimethylthiayol-2-yl)-2,5-diphenyltetrazolium bromide) assay as previously reported [26,27]. The mammalian cell lines used in the tests were sourced from DSMZ

and included mouse fibroblasts (L929) and endocervical adenocarcinoma (KB3.1), human lung carcinoma (A549), breast adenocarcinoma (MCF-7), human ovarian cancer (SKOV-3), prostate carcinoma (PC-3), and epidermoid carcinoma cells (A431). Epothilone B was used as the positive control.

3.6. Antimicrobial Assay

The antimicrobial activity of the isolated secondary metabolites was determined using our established protocol [26,27], against clinically relevant microorganisms obtained from the German Collection of Microorganisms and Cell Cultures (DSMZ, Braunschweig, Germany). These included *Staphylococcus aureus* (DSM 346), *Bacillus subtilis* (DSM 10), *Acinetobacter baumanii* (DSM 30008), *Escherichia coli* (DSM 1116), *Chromobacterium violaceum* (DSM 30191), *Pseudomonas aeruginosa* (PA14), *Mycolicibacterium smegmatis* (ATCC 700084), *Candida albicans* (DSM 1665), *Mucor hiemalis* (DSM 2656), *Rhodotorula glutinis* (DSM 10134), *Schizosaccharomyces pombe* (DSM 70572) and *Pichia anomala* (DSM 6766). Nystatin was used as an antifungal positive control whereas oxytetracycline, ciprofloxacin, gentamicin, and kanamycin were used as positive controls against Gram-positive and Gram-negative bacteria.

3.7. Nematicidal Activity

The nematicidal activity assay was conducted following a previously described procedure with slight modifications [28,29]. *C. elegans* was cultured on nematode growth medium (NGM) containing 3 g NaCl, 20 g agar, 2.5 g peptone, 1 mL 1 M $CaCl_2$, 25 mL of 1 M (pH 6.0) KPO_4, 1 mL 1 M $MgSO_4$, and 1 mL cholesterol (5 mg/mL in ethanol) per liter of medium. Plates were coated with *Escherichia coli* strain OP50, which served as the food source for nematodes. Synchronization of the nematode population was performed using a high egg density plate (~120 h). The plate was rinsed three times with 4 mL of 0.9% NaCl solution and then transferred to a 15 mL falcon tube. The nematode suspension was centrifuged at 1000 rpm for 3 min, and the supernatant was discarded. This procedure was repeated until a clear nematode suspension was obtained. After the last washing step, 2 mL of the suspension was mixed with 5 mL of bleaching solution (1 mL sodium hypochlorite solution, 0.5 mL 5 M NaOH, and 3.5 mL Milli-Q water). The solution was gently shaken for approximately 5 min to break down the nematode tissue, and monitored under the microscope. The reaction was stopped by adding 7 mL 0.9% NaCl solution when traces of adults were still visible. Subsequently, the suspension was centrifuged at 2500 rpm for 2 min and washed 3 times as previously described. After the final washing step, the supernatant was removed, and the volume was adjusted to 7 mL with 0.9% NaCl solution. The nematode egg suspension was incubated at 23 °C on a rotary shaker at 80 rpm for 18 h. The hatched nematodes were transferred to a fresh NGM plate supplemented with *E.coli* OP50. After 50–70 h, the J4 and adult *C. elegans* were washed from the plate as mentioned above. The nematode concentration was determined and diluted to approximately 1000 nematodes/mL.

Pure compounds were tested at concentrations of 10, 50, and 100 µg/mL in 48-well microtiter plates. The compounds, dissolved in MeOH, were added to the well plate and subsequently dried under nitrogen. After complete evaporation of the solvent, 300 µL of the nematode suspension (1000 nematodes/mL) was added to the compounds. Each treatment was replicated three times. MeOH was used as the negative control while 1 µg/mL Ivermectin served as the positive control. Nematodes were monitored 15 min after inoculation, and the plates were incubated at 24 °C and 150 rpm for 18 h. After incubation, both alive and dead nematodes were counted in three replicates under a stereomicroscope, and the mortality rate was calculated. Erect and non-moving nematodes were considered dead. A compound was deemed active if it resulted in mortality rates of at least 50% at a concentration of 100 µg/mL (lethal dose, 50%). The observed percentage of dead nematodes was corrected by considering the natural mortality observed in the negative control, using the Schneider-Orelli formula [30].

4. Conclusions

In this study, we explored, both chemically and biologically, the total mycelial extract derived from a solid-state rice culture of the entomopathogenic fungus *B. roseostromatus* BCC56290. Chemically, six secondary metabolites were successfully distinguished including four unprecedentedly reported natural products, namely one bioxanthracene ES-242-9 (**1**), three cyclodepsipeptides (**2**–**4**) together with two known congeners, cardinalisamides B (**5**) and C (**6**). Among the different bioassays conducted, compounds **5** and **6** revealed significant cytotoxic activity against the tested cell lines with minor or no toxicity against the normal cells that might have a positive impact on their specificity toward cancerous cells. In the antimicrobial assay, none of the isolated compounds revealed significant activity against any tested bacterial or fungal pathogens. In nematicidal activity against *C. elegans*, both ES-242-9 (**1**) and **6** revealed comparable mortality rates, however, revealing neither cytotoxic nor antimicrobial activity by **1** supports its potential as a candidate for further development of a biocontrol agent.

Supplementary Materials: The following supporting information can be downloaded at: https://www.mdpi.com/article/10.3390/antibiotics13070585/s1, Figures S1–S8. HPLC, LR-/HR-ESI-MS, 1D/2D NMR spectra of **1**; Figures S9–S16. HPLC, LR-/HR-ESI-MS, 1D/2D NMR spectra of **2**; Figures S17–S24. HPLC, LR-/HR-ESI-MS, 1D/2D NMR spectra of **3**; Figures S25–S32. HPLC, LR-/HR-ESI-MS, 1D/2D NMR spectra of **4**; Figures S33–S38. HPLC, LR-/HR-ESI-MS, 1D/2D NMR spectra of **5**; Figures S39–S44. HPLC, LR-/HR-ESI-MS, 1D/2D NMR spectra of **6**; Figures S45–S48. HPLC, LR-ESI-MS of advanced Marefy's method for compounds **3** and **4**. Figure S49. Maximum likelihood phylogenetic tree inferred from 117 taxa of Cordycipitaceae based on combined ITS, LSU, EF1, and RPB1 sequence data. Tables S1 and S2: Antimicrobial and nematicidal activity assays of **1**–**6**.

Author Contributions: Conceptualization: K.P., S.S.E. and M.S.; fungal isolation and identification: A.K., W.N. and J.J.L.-a.; methodology: K.P., N.A.L.-L., R.T. and S.S.E.; formal analysis: K.P., N.A.L.-L., R.T. and S.S.E.; data curation and structure elucidation: S.S.E.; nematicidal activity: N.A.L.-L.; writing—original draft preparation: K.P., A.K., N.A.L.-L. and S.S.E.; writing—review and editing: K.D.H., S.S.E. and M.S.; project administration: M.S.; funding acquisition, M.S. All authors have read and agreed to the published version of the manuscript.

Funding: This research benefitted from funding by the European Union's Horizon 2020 Research Infrastructure and Staff Exchange Program (RISE) under the Marie Skłodowska-Curie grant agreement No. 101008129, project acronym "Mycobiomics". K.P. is grateful for a Royal Golden Jubilee PhD stipend from the Thailand Research fund (Grant no PHD/002/2560). Financial support by a personal PhD stipend from the German Academic Exchange Service (DAAD) to N.A.L.-L. (Program ID 57552340) is gratefully acknowledged. S.S.E. immensely acknowledges the Alexander von Humboldt (AvH) foundation for granting him the Georg-Forster Fellowship for Experienced Researchers stipend (Ref 3.4-1222288-EGY-GF-E). Financial support by the National Science and Technology Development Agency (NSTDA) through Grant No. P21-50844 is acknowledged.

Data Availability Statement: Data are contained within the article and Supplementary Materials. The authors provide the raw NMR files upon request.

Acknowledgments: All Authors thank A. Skiba, S. Reinecke, C. Kakoschke, E. Surges, and W. Collisi for their eminent technical and advisory assistance, in acquiring HR-ESI-MS, NMR spectroscopy, antimicrobial and cytotoxicity assays.

Conflicts of Interest: The authors declare no conflicts of interest.

References

1. Venkatesh, G.; Sakthi Priya, P.; Anithaa, V.; Dinesh, G.K.; Velmurugan, S.; Abinaya, S.; Karthika, P.; Sivasakthivelan, P.; Soni, R.; Thennarasi, A. Role of entomopathogenic fungi in biocontrol of insect pests. In *Plant Protection*; Soni, R., Suyal, D.C., Goel, R., Eds.; De Gruyter: Berlin, Germany, 2022; pp. 505–548.
2. Zhang, L.; Fasoyin, O.E.; Molnár, I.; Xu, Y. Secondary metabolites from hypocrealean entomopathogenic fungi: Novel bioactive compounds. *Nat. Prod. Rep.* **2020**, *37*, 1181–1206. [CrossRef]
3. Shah, P.A.; Pell, J.K. Entomopathogenic fungi as biological control agents. *Appl. Microbiol. Biotechnol.* **2003**, *61*, 413–423. [CrossRef]

4. Gibson, D.M.; Donzelli, B.G.G.; Krasnoff, S.B.; Keyhani, N.O. Discovering the secondary metabolite potential encoded within entomopathogenic fungi. *Nat. Prod. Rep.* **2014**, *31*, 1287–1305. [CrossRef] [PubMed]
5. Molnár, I.; Gibson, D.M.; Krasnoff, S.B. Secondary metabolites from entomopathogenic Hypocrealean fungi. *Nat. Prod. Rep.* **2010**, *27*, 1241–1275. [CrossRef] [PubMed]
6. Kepler, R.M.; Luangsa-Ard, J.J.; Hywel-Jones, N.L.; Quandt, C.A.; Sung, G.H.; Rehner, S.A.; Aime, M.C.; Henkel, T.W.; Sanjuan, T.; Zare, R.; et al. A phylogenetically-based nomenclature for Cordycipitaceae (Hypocreales). *IMA Fungus* **2017**, *8*, 335–353. [CrossRef] [PubMed]
7. Mongkolsamrit, S.; Noisripoom, W.; Tasanathai, K.; Khonsanit, A.; Thanakitpipattana, D.; Himaman, W.; Kobmoo, N.; Luangsa-ard, J.J. Molecular phylogeny and morphology reveal cryptic species in *Blackwellomyces* and *Cordyceps* (Cordycipitaceae) from Thailand. *Mycol. Prog.* **2020**, *19*, 957–983. [CrossRef]
8. Li, Y.; Zhao, X.C.; Wu, L.X.; Wang, Y.; Xu, A.; Lin, W.F. *Blackwellomyces kaihuaensis* and *Metarhizium putuoense* (Hypocreales), two new entomogenous fungi from subtropical forests in Zhejiang Province, Eastern China. *Forests* **2023**, *14*, 2333. [CrossRef]
9. Umeyama, A.; Takahashi, K.; Grundniewska, A.; Shimizu, M.; Hayashi, S.; Kato, M.; Okamoto, Y.; Suenaga, M.; Ban, S.; Kumada, T.; et al. In vitro antitrypanosomal activity of the cyclodepsipeptides, cardinalisamides A–C, from the insect pathogenic fungus *Cordyceps cardinalis* NBRC 103832. *J. Antibiot.* **2014**, *67*, 163–166, Erratum in *J. Antibiot.* **2014**, *67*, 487. [CrossRef]
10. Feng, P.; Shang, Y.; Cen, K.; Wang, C. Fungal biosynthesis of the bibenzoquinone oosporein to evade insect immunity. *Proc. Natl. Acad. Sci. USA* **2015**, *112*, 11365–11370. [CrossRef]
11. Nakamura, Y.; Nguyen, N.-H.; Yoshinari, T.; Hachisu, M.; Nguyen, P.-T.; Shimizu, K. Identification of the oosporein biosynthesis gene cluster in an entomopathogenic fungus *Blackwellomyces cardinalis*. *Mycoscience* **2024**, *65*, 96–104. [CrossRef]
12. Toki, S.; Ando, K.; Yoshida, M.; Kawamoto, I.; Sano, H.; Matsuda, Y. ES-242-1, a novel compound from *Verticillium* sp., binds to a site on *N*-methyl-D-aspartate receptor that is coupled to the channel domain. *J. Antibiot.* **1992**, *45*, 88–93. [CrossRef] [PubMed]
13. Toki, S.; Ando, K.; Kawamoto, I.; Sano, H.; Yoshida, M.; Matsuda, Y. ES-242-2, -3, -4, -5, -6, -7, and -8, novel bioxanthracenes produced by *Verticillium* sp., which act on the *N*-methyl-D-aspartate receptor. *J. Antibiot.* **1992**, *45*, 1047–1054. [CrossRef] [PubMed]
14. Isaka, M.; Kongsaeree, P.; Thebtaranonth, Y. Bioxanthracenes from the insect pathogenic fungus *Cordyceps pseudomilitaris* BCC 1620. *J. Antibiot.* **2001**, *54*, 36–43. [CrossRef] [PubMed]
15. Isaka, M.; Srisanoh, U.; Lartpornmatulee, N.; Boonruangprapa, T. ES-242 derivatives and cycloheptapeptides from *Cordyceps* sp. Strains BCC 16173 and BCC 16176. *J. Nat. Prod.* **2007**, *70*, 1601–1604. [CrossRef] [PubMed]
16. Toki, S.; Tsukuda, E.; Nozawa, M.; Nonaka, H.; Yoshida, M.; Matsuda, Y. The ES-242s, novel *N*-methyl-D-aspartate antagonists of microbial origin, interact with both the neurotransmitter recognition site and the ion channel domain. *J. Biol. Chem.* **1992**, *267*, 14884–14892. [CrossRef] [PubMed]
17. Elsworth, J.F.; Grove, J.F. Cyclodepsipeptides from *Beauveria bassiana* Bals. Part 1. Beauverolides H and I. *J. Chem. Soc. Perkin 1.* **1977**, *3*, 270–273. [CrossRef]
18. Jegorov, A.; Sedmera, P.; Matha, V.; Simek, P.; Zahradnickova, H.; Landa, Z.; Eyal, J. Beauverolides L and La from *Beauveria tenella* and *Paecilomyces fumosoroseus*. *Phytochemistry* **1994**, *37*, 1301–1303. [CrossRef]
19. Matsuda, D.; Namatame, I.; Tomoda, H.; Kobayashi, S.; Zocher, R.; Kleinkauf, H.; Omura, S. New beauveriolides produced by amino acid-supplemented fermentation of *Beauveria* sp. FO-6979. *J. Antibiot.* **2004**, *57*, 1–9. [CrossRef]
20. Wang, X.; Gao, Y.L.; Zhang, M.L.; Zhang, H.D.; Huang, J.Z.; Li, L. Genome mining and biosynthesis of the Acyl-CoA: Cholesterol acyltransferase inhibitor beauveriolide I and III in *Cordyceps militaris*. *J. Biotechnol.* **2020**, *309*, 85–91. [CrossRef]
21. Helaly, S.E.; Kuephadungphan, W.; Phainuphong, P.; Ibrahim, M.A.A.; Tasanathai, K.; Mongkolsamrit, S.; Luangsa-ard, J.J.; Phongpaichit, S.; Rukachaisirikul, V.; Stadler, M. Pigmentosins from *Gibellula* sp. as antibiofilm agents and a new glycosylated asperfuran from *Cordyceps javanica*. *Beilstein J. Org. Chem.* **2019**, *15*, 2968–2981. [CrossRef]
22. Jegorov, A.; Paizs, B.; Kuzma, M.; Zabka, M.; Landa, Z.; Sulc, M.; Barrow, M.P.; Havlicek, V. Extraribosomal cyclic tetradepsipeptides beauverolides: Profiling and modeling the fragmentation pathways. *J. Mass Spectrom.* **2004**, *39*, 949–960. [CrossRef] [PubMed]
23. Madariaga-Mazon, A.; Gonzalez-Andrade, M.; Toriello, C.; Navarro-Barranco, H.; Mata, R. Potent anti-calmodulin activity of cyclotetradepsipeptides isolated from *Isaria fumosorosea* using a newly designed biosensor. *Nat. Prod. Commun.* **2015**, *10*, 113–116. [CrossRef] [PubMed]
24. Zhou, Y.F.; Hu, K.; Wang, F.; Tang, J.W.; Zhang, L.; Sun, H.D.; Cai, X.H.; Puno, P.T. 3-Hydroxy-4-methyldecanoic acid-containing cyclotetradepsipeptides from an endolichenic *Beauveria* sp. *J. Nat. Prod.* **2021**, *84*, 1244–1253. [CrossRef] [PubMed]
25. Viehrig, K.; Surup, F.; Harmrolfs, K.; Jansen, R.; Kunze, B.; Müller, R. Concerted action of P450 plus helper protein to form the amino-hydroxy-piperidone moiety of the potent protease inhibitor crocapeptin. *J. Am. Chem. Soc.* **2013**, *135*, 16885–16894. [CrossRef]
26. Sum, W.C.; Mitschke, N.; Schrey, H.; Wittstein, K.; Kellner, H.; Stadler, M.; Matasyoh, J.C. Antimicrobial and cytotoxic cyathane-xylosides from cultures of the basidiomycete *Dentipellis fragilis*. *Antibiotics* **2022**, *11*, 1072. [CrossRef]
27. Sum, W.C.; Ebada, S.S.; Kirchenwitz, M.; Wanga, L.; Decock, C.; Stradal, T.E.B.; Matasyoh, J.C.; Mándi, A.; Kurtán, T.; Stadler, M. Neurite outgrowth-inducing drimane-type sesquiterpenoids isolated from cultures of the polypore *Abundisporus violaceus* MUCL 56355. *J. Nat. Prod.* **2023**, *86*, 2457–2467. [CrossRef]

28. Wennrich, J.-P.; Ebada, S.S.; Sepanian, E.; Holzenkamp, C.; Khalid, S.J.; Schrey, H.; Maier, W.; Kurtán, T.; Ashrafi, S.; Stadler, M. Omnipolyphilins A and B: Novel chlorinated cyclotetrapeptides and naphtho-α-pyranones from two plant nematode-derived fungi *Polyphilus sieberi*. *J. Agric. Food Chem.* **2024**, *72*, 6998–7009. [CrossRef] [PubMed]
29. Phutthacharoen, K.; Toshe, R.; Khalid, S.J.; Llanos-López, N.A.; Wennrich, J.-P.; Schrey, H.; Ebada, S.S.; Hyde, K.D.; Stadler, M. Lachnuoic Acids A–F: Ambuic acid congeners from a saprotrophic *Lachnum* species. *Chem. Biodiver.* **2024**, *21*, e202400385. [CrossRef]
30. Schneider-Orelli, O. *Entomologisches Praktikum. Einführung in Die Land-Und Forstwirtschaftliche Insektenkunde*, 2nd ed.; H. R. Sauerländer: Aarau, Switzerland, 1947.

Publication III

Polydosetins & Pullularins – Bioactive Tetramic Acids & Cyclodepsipeptides from the Endophytic and Nematophagous Fungus *Polydomus karssenii*

Natalia A. Llanos-López[1,2,†], Jan-Peer Wennrich[1,2,†,‡], Janette Miled[1,2], Samad Ashrafi[3,4], Wolfgang Maier[3], Frank Surup[1,2], and Marc Stadler[1,2,*]

[1] Department of Microbial Drugs, Helmholtz Centre for Infection Research (HZI) and German Centre for Infection Research (DZIF), DZIF Partner Site Hannover-Braunschweig, Germany, Inhoffenstrasse 7, 38124 Braunschweig, Germany.

[2] Institute of Microbiology, Technische Universität Braunschweig, Spielmannstraße 7, 38106 Braunschweig, Germany.

[3] Institute for Epidemiology and Pathogen Diagnostics, Julius Kühn Institut (JKI) - Federal Research Centre for Cultivated Plants, Messeweg 11–12, 38104 Braunschweig, Germany.

[4] Department of Zoology and Entomology, University of the Free State, Bloemfontein 9300, South Africa.

‡ Present address: Laboratory of Fungal Genetics and Metabolism, Institute of Microbiology of the Czech Academy of Sciences, Prague 14220, Czechia.

* Corresponding author.

† these authors contributed equally to this work.

Natural Products and Bioprospecting (accepted).

Polydosetins & Pullularins – Bioactive Tetramic Acids & Cyclodepsipeptides from the Endophytic and Nematophagous Fungus *Polydomus karssenii*

Natalia A. Llanos-López[1,2,#], Jan-Peer Wennrich[1,2,‡,#], Janette Miled[1,2], Samad Ashrafi[3,4], Wolfgang Maier[3], Frank Surup[1,2], and Marc Stadler[1,2,*]

1 Department of Microbial Drugs, Helmholtz Centre for Infection Research (HZI) and German Centre for Infection Research (DZIF), DZIF Partner Site Hannover-Braunschweig, Germany, Inhoffenstrasse 7, 38124 Braunschweig, Germany

2 Institute of Microbiology, Technische Universität Braunschweig, Spielmannstraße 7, 38106 Braunschweig, Germany

3 Institute for Epidemiology and Pathogen Diagnostics, Julius K hn Institut (JKI) - Federal Research Centre for Cultivated Plants, Messeweg 11–12, 38104 Braunschweig, Germany

4 Department of Zoology and Entomology, University of the Free State, Bloemfontein 9300, South Africa

‡ Present address: Laboratory of Fungal Genetics and Metabolism, Institute of Microbiology of the Czech Academy of Sciences, Prague 14220, Czechia

* Correspondence: marc.stadler@helmholtz-hzi.de (M.S)

\# These authors contributed equally

Abstract

In course of investigating the endophytic and nematode-associated fungus *Polydomus karssenii* for the production of secondary metabolites, seven previously undescribed natural products were isolated from liquid and solid-state fermentations. 1D and 2D NMR spectroscopy, together with HR-ESI-MS data, enabled the elucidation of the planar structures of 3-decalinoyltetramic acids polydosetins A–E (**1**–**5**) and cyclodepsipeptides pullularins G and H (**6** and **7**). The relative configurations of the decalin moiety of **1**–**5** were determined based on ROESY correlations and ^{1}H–^{1}H coupling constants. The configuration of the side chains was established through a detailed *J*-resolved analysis (Murata's method) in combination with chemical shift comparison to model compounds. Absolute stereochemistry of **1**–**5** was assigned based on ECD data, and confirmed by Mosher's method utilizing **3**. Finally, the absolute configuration of amino acid residues in **6** and **7** was determined through advanced Marfey's method. Bioassays revealed that compounds **1**, **3**, **5**, and **7** were active against Gram-positive bacteria, **5** and **7** exhibited antifungal activity, and **1** and **2** showed nematicidal effects. These results underscore the untapped chemical potential of *P. karssenii* and highlight the importance of exploring nematode-associated fungi as sources of new natural products with potential antimicrobial and nematicidal properties.

Keywords

Polydomus; tetramic acids; cyclodepsipeptides; antimicrobial; nematicidal

1 Introduction

Natural products constitute a rich reservoir of structurally diverse molecules with therapeutic potential, and fungi serve as an invaluable source of these bioactive compounds [1]. Several fungi have been extensively studied for the production of secondary metabolites, including common soil molds such as *Aspergillus* and *Penicillium* in filamentous fungi, while the majority of the fungal kingdom remains largely unexplored [2,3]. Among these are nematode-associated fungi, of which only a few species have been studied to date, including *Laburnicola nematophila* and *Polyphilus sieberi* [4,5]. Both species produce bioactive secondary metabolites. Dactylfungin derivatives from *L. nematophila* exhibit activity against azole-resistant *Aspergillus fumigatus*, while talaroderxine D from *P. sieberi* inhibits the formation of *Staphylococcus aureus* biofilms [4,5]. The broader biosynthetic potential of nematode-associated fungi remains a promising but understudied group for natural product discovery.

The nematode-associated genus *Polydomus* was recently introduced by Ashafi et al. (2023) as a monophyletic lineage within the family Phaeosphaeriaceae (Pleosporales, Dothideomycetes) [6]. *Polydomus karssenii*, isolated from eggs of the cereal cyst nematode *Heterodera filipjevi* and from the plant *Microthlaspi perfoliatum*, is a fungus with a bifunctional lifestyle, functioning both as a plant-inhabiting dark-septate endophyte and as a nematode parasite [6]. Prior to its formal description, the metabolites ophiotine, xanthomide Z, arthrichitin, and arthrichitins B and C were isolated from a single strain of *P. karssenii*, of which ophiotine showed nematicidal activity [7]. A subsequent metabolite profile study across multiple strains of this species revealed the production of a nearly identical set of secondary metabolites among the studied strains [6]. However, the chemical diversity of *P. karssenii* remains only partially explored, and the majority of its compounds have yet to be purified and structurally characterized.

Here, we report the isolation and characterization of seven previously undescribed tetramic acids and cyclodepsipeptides obtained from two strains of *P. karssenii*. One strain (JKI 73120) was isolated as an endophytic fungus from the roots of *M. perfoliatum*, whereas the other strain (DSM 111209) was obtained as the infecting fungal agent of eggs of the plant-parasitic nematode *H. filipjevi*. In this study, we also evaluated the antimicrobial, cytotoxic, and nematicidal activities of the newly discovered secondary metabolites.

2 Materials and methods

2.1 Chromatography and spectral methods

Crude extracts from *P. karssenii* strains JKI 73120 and DSM 111209 were diluted to a concentration of 4.5 mg/mL in a solution of methanol (MeOH) and acetone (1:1), while fractions and pure compounds were diluted to a concentration of 1 mg/mL in the same solution. The samples were analyzed using an analytical HPLC system (UltiMate® 3000 series uHPLC, Thermo Fisher Scientific®, MA, USA) coupled to an ion trap mass spectrometer (amaZon speed™, Bruker, Billerica, MA, USA), operating in both positive and negative ionization modes. Pure compounds were further analyzed by high-resolution mass spectrometry (HR-ESI-MS) at a concentration of 0.1 mg/mL in the same solvent system, using a trapped ion mobility quadrupole time-of-flight mass spectrometer (timsTOF Pro 2, Bruker Daltonics, Bremen, Germany) coupled to an Agilent 1290 series HPLC-UV system (Agilent Technologies, Santa Clara, CA, USA). Both systems employed a C18 Acquity® UPLC BEH column (2.1 x 50 mm, 1.7 µm; Waters, Milford, MA, USA) (temperature of the column: 40 °C) as the stationary phase. The mobile phase consisted of MilliQ water + 0.1% formic acid (FA) as solvent A, and acetonitrile (MeCN) + 0.1% FA as solvent B, with an injection volume of 2 µL. The gradient elution started at 5% B for 0.5 min, then increased to 100% B over 19.5 min, and was maintained at 100% B for 5 min at a flow rate of 0.6 mL/min. UV-Vis spectral data were detected using a Diode-Array Detector (DAD) at 210 nm and 190–600 nm.

UV/Vis, electronic circular dichroism (ECD), and optical rotation (OR) spectra of the pure compounds were recorded in methanol Uvasol® using a Shimadzu UV-2450 UV-Vis spectrophotometer (Shimadzu, Kyoto, Japan), a Jasco J-815 spectropolarimeter (JASCO, Pfungstadt, Germany), and an Anton Paar MCP-150 polarimeter (Anton Paar OptoTec GmbH, Seelze, Germany), respectively.

Nuclear magnetic resonance (NMR) spectra were recorded using a Bruker Avance III 500 MHz spectrometer (Bruker Daltonics®, Bremen, Germany; ^{1}H-NMR: 500 MHz, ^{13}C-NMR: 125 MHz), a Bruker Avance III 600 MHz spectrometer (^{1}H-NMR: 600 MHz, ^{13}C-NMR: 150 MHz), and a Bruker Avance III 700 MHz spectrometer (^{1}H-NMR: 700 MHz, ^{13}C-NMR: 175 MHz). Chemical shifts were referenced to the solvent peaks DMSO–d_6 (δ_H 2.50, δ_C 39.51), acetone–d_6 (δ_H 2.05, δ_C 29.32), CH_3OH–d_4 (δ_H 3.31, δ_C 49.15), pyridine–d_5 (δ_H 7.22, δ_C 123.87), or $CHCl_3$–d (δ_H 7.27, δ_C 77.00).

2.2 Origin of fungal strains

The morphological characteristics and multilocus phylogeny of *P. karssenii* strains JKI 73120 and DSM 111209 were previously described in detail by Ashrafi et al. (2023). Strain JKI 73120 was isolated as an endophyte from the roots of *M. perfoliatum*, whereas strain DSM 111209 was obtained from infected eggs of the plant-parasitic nematode *H. filipjevi*. The strains were maintained on yeast malt agar (YM agar, malt extract 10 g/L, yeast extract 4 g/L, D-glucose 4 g/L, agar 20 g/L, pH 6.3 before autoclaving) at 23 °C in the dark. Both strains are preserved in the fungal strain collection of the Julius Kühn-Institut (JKI) in Braunschweig, Germany, while DSM 111209 is also deposited at the Leibniz Institute DSMZ in Braunschweig, Germany.

2.3 Cultivation of *P. karssenii* strains and extraction

Precultures of *P. karssenii* strains JKI 73120 and DSM 111209 were prepared in individual 250 mL Erlenmeyer flasks, each containing 100 mL of Q6 ½ medium (D-glucose 2.5 g/L, glycerol 10 g/L, cottonseed flour 5 g/L; pH 7.2 before autoclaving). Each flask was inoculated with three 0.25 cm² mycelial plugs grown on YM 6.3 agar. Cultivation was carried out over five days at 23 °C and 140 rpm in the dark. The resulting precultures were homogenized using an Ultra-Turrax (T25 easy clean digital, IKA) equipped with an S25 N-25F dispersing tool at 5000 rpm for 30 seconds.

For the scale-up fermentation aimed at secondary metabolite production, strain JKI 73120 was subjected to solid-state fermentation in autoclaved brown rice-based (BRFT) and whole oat-based (WOFT) media. Each medium was prepared with 100 mL of a solution containing KH_2PO_4 (0.5 g/L), sodium tartrate (0.5 g/L), and yeast extract (1 g/L), along with 28 g of cereal substrate. The cultivation was carried out in twelve 500 mL Erlenmeyer flasks per medium, each flask inoculated with 6 mL of the preculture and incubated for 2, 4, and 6 weeks (four flasks for each time point) at room temperature. The cultivation was terminated after 2, 4, and 6 weeks, and each flask was harvested with 3 × 250 mL of acetone, thoroughly mixed, and processed according to the previously described protocol [8]. The resulting extracts were defatted through liquid–liquid partitioning with *n*-heptane and MeOH. Both phases were evaporated until dryness and analyzed using HPLC-DAD/MS.

Strain DSM 111209 was cultivated in liquid Q6 ½ medium, using twelve 1-L flasks filled with 400 mL of medium and inoculated with 2 mL of preculture. The cultures were incubated at 23 °C and 140 rpm in the dark. Fermentation progress was monitored by measuring the free glucose concentration using Medi-Test Glucose test strips (Macherey-Nagel, Düren, Germany). Complete glucose consumption occurred after 8 days, and fermentation ended 2 days after glucose was depleted. The mycelium and supernatant were separated by filtration, and both phases were extracted according to the previously established method [8]. Secondary metabolites from the supernatant were recovered using 2% (*m/v*) of AmberLite™ XAD16N adsorbent resin (Sigma-Aldrich, Deisenhofen, Germany) as previously described [8].

2.4 Isolation of compounds 1-7

2.4.1 Isolation of compounds from *P. karssenii* strain JKI 73120

The methanol extracts from strain JKI 73120, cultivated in BRFT and WOFT for 2–6 weeks (see Section 2.3), were combined based on similar HPLC-DAD/MS profiles, yielding 3.2 g of crude material. This extract was fractionated using normal-phase flash chromatography, followed by multiple rounds of preparative reversed-phase (RP) HPLC, which resulted in the isolation of compounds **2**, **3**, and **6**. Similarly, the *n*-heptane extracts (3.6 g) from both media, which also exhibited comparable metabolite profiles, were combined and subjected to normal-phase flash chromatography. Major pooled fractions were subsequently purified by preparative and semipreparative RP-HPLC, yielding compounds **3**, **5**, and **7**. Details of chromatographic conditions, gradient elutions, retention times, and yields are provided in the Supplementary Information (Scheme S1, Tables S3–S11).

2.4.2 Isolation of compounds from *P. karssenii* strain DSM 111209

The mycelium extract (877 mg) obtained from the fermentation of strain DSM 111209 in Q6 ½ medium (see Section 2.3) was subjected to flash chromatography separation using a Büchi C-850 Flash Prep system (Büchi Labortechnik AG, Flawil, Switzerland) operating in normal-phase mode. Separation was performed on a 12 g silica cartridge (FlashPure ID Silica, Büchi). Three solvents served as the mobile phase: solvent A was *n*-heptane with 0.1% FA, solvent B contained 63% *n*-heptane, 35.5% TBME, and 1.5% MeOH with 0.1% FA, and solvent C was MeOH with 0.1% FA. The flow rate was maintained at 60 mL/min. The gradient was programmed as follows: isocratic elution at 0% AB for 3 min, followed by a linear gradient to 100% AB over 15 min, and then an isocratic hold at 100% AB for 3 min. The mobile phase was switched to a BC system, starting with 50% BC for 2 min, followed by a linear gradient to 100% BC over 1 min, and maintained at 100% BC for 5 min. Fractions were monitored using UV detection at wavelengths of 210, 254, 300, and 350 nm and collected based on their chromatographic profiles. This separation yielded a fraction of 420 mg with a retention time (t_R) of 22.1–23.7 min and was further purified by RP-HPLC on the same equipment, employing a Gemini 10 µm C18 110 Å column (250 x 50 mm, Phenomenex) as the stationary phase. A binary solvent system, flowing at 50 mL/min, consisting of solvent A (MilliQ water + 0.1% FA) and solvent B (MeCN + 0.1% FA) was used. A two-stage gradient program was implemented: starting with 50% B held isocratically for 5 min, followed by a linear gradient to 100% B over 40 min, which was then maintained for 10 min. From this separation, a fraction of 60 mg with a t_R = 42.1–45.2 min was collected and further separated to obtain compounds **1** (8 mg, t_R = 17.1 min) and **4** (6.1 mg, t_R = 23.1 min) by preparative RP-HPLC (PLC 2050, Gilson). Separation was performed using a Luna 5 µm C18 110 Å column (250 × 21.2 mm; Phenomenex). The mobile phase (solvents A and B) was maintained at a flow rate of 20 mL/min. The separation was eluted with 65% B for 5 min, then ramped linearly to 90% B over 40 min, followed by a rapid increase to 100% B over 2 min, which was maintained for an additional 10 min.

In parallel with the purification of the mycelial extract, the crude extract from the supernatant (248 mg), recovered using XAD16N adsorbent resin (Section 2.3), was subjected to fractionation. The Büchi C-850 Flash Prep system, configured in reversed-phase mode, was utilized for the separation with a Gemini 10 µm C18 110 Å column (250 x 50 mm, Phenomenex). Solvents A and B were used, with the flow rate set to 50 mL/min. The following gradient was applied: 50% B for 5 min, a linear increase to 100% B over 40 min, and then held at 100% B for 10 min. Two subfractions were collected: 5 mg (t_R = 34.0–34.6 min) and 40 mg (t_R = 35.1–39.8 min), which underwent further separation. Compound **2** (4.81 mg, t_R = 17.1 min) was purified from the first subfraction using a semipreparative RP-HPLC system (1200 Infinity Series, Agilent Technologies Deutschland GmbH, Böblingen, Germany). The system was equipped with an XBridge BEH 5 µm C18 column (250 × 10 mm; Waters, Eschborn, Germany). The mobile phase consisted of solvents A and B, maintained at a flow rate of 5 mL/min. The chromatographic profile consisted of an initial isocratic step at 50% B for 3 min, followed by a linear gradient to 70% B over 16 min, a 2-minute increase to 100% B, and a final isocratic step at 100% B for 3 min. From the second subfraction, compound

1 (6.84 mg, t_R = 24.8 min) was isolated using a preparative RP-HPLC system (PLC 2050, Gilson), equipped with a Luna 5 µm C18 110 Å column (250 × 21.2 mm; Phenomenex). Solvents A and B were employed with a flow rate of 20 mL/min. The gradient elution started with an isocratic condition at 60% B for 30 min, followed by a linear increase to 100% B over 5 min, and was maintained at 100% B for 10 min. A detailed description of the separation conditions is provided in the Supporting Information appendix (Scheme S2, Tables S12–S17).

Polydosetin A (**1**): brown solid; $[\alpha]^{20}_D$ −4.2 (*c* 0.1, MeOH); UV/Vis (MeOH): λmax (log ε) = 289 (0.4), 202 (0.7) nm; ECD (MeOH, λ (nm) (Δε), c = 4.34 × 10−4 M): 273 (−10.31), 252 (−6.60), 235 (−7.38), 223 (−5.48), 200 (−51.21); ^{1}H NMR (700 MHz, CH_3OH–d_4): see table 2; ^{1}H NMR data (700 MHz, aceton–d_6; 500 MHz, chloroform–*d*; 700 MHz, pyridine–d_5; 700 MHz, DMSO–d_6): see Table S2; ^{13}C NMR (175 MHz, CH_3OH–d_4): see table 1; ^{13}C NMR data (175 MHz, aceton–d_6; 125 MHz, chloroform–*d*; 175 MHz, pyridine–d_5; 175 MHz, DMSO–d_6): see Table S1;; HRESI-MS: *m/z* 462.2460 $[M+H]^+$ (calcd. 462.2492 for $C_{25}H_{36}NO_7$), 484.2277 $[M+Na]^+$ (calcd. 484.2311 for $C_{25}H_{35}NNaO_7$).

Polydosetin B (**2**): yellow solid; $[\alpha]^{20}_D$ −4.0 (*c* 0.1, MeOH); UV/Vis (MeOH): λmax (log ε) = 288 (0.4), 204 (0.6) nm; ECD (MeOH, λ (nm) (Δε), c = 4.47 × 10−4 M): 279 (−9.03), 250 (−3.58), 234 (−4.99), 223 (−4.21), 198 (−42.95); ^{1}H NMR (500 MHz, CH_3OH–d_4): see Table 2; ^{13}C NMR (125 MHz, CH_3OH–d_4): see Table 1; HRESI-MS: *m/z* 448.2309 $[M+H]^+$ (calcd. 448.2335 for $C_{24}H_{34}NO_7$), 470.2124 $[M+Na]^+$ (calcd. 470.2155 for $C_{24}H_{33}NNaO_7$, 895.4497 $[2M+H]^+$ (calcd. 895.4592 for $C_{48}H_{67}N_2O_{14}$).

Polydosetin C (**3**): yellow amorphous solid; $[\alpha]^{20}_D$ −2.3 (*c* 0.1, MeOH); UV/Vis (MeOH): λmax (log ε) = 288 (0.2), 251 (0.2) nm, 202 (0.5) nm; ECD (MeOH, λ (nm) (Δε), c = 4.21 × 10−4 M): 278 (−7.72), 253 (−4.55), 234 (−5.46), 224 (−3.37), 199 (−34.72), 194 (−26.41); ^{1}H NMR (700 MHz, CH_3OH–d_4): see Table 2; ^{13}C NMR (125 MHz, CH_3OH–d_4): see Table 1; HRESI-MS: *m/z* 476.2618 $[M+H]^+$ (calcd. 476.2643 for $C_{26}H_{38}NO_7$), 498.2432 $[M+Na]^+$ (calcd. 498.2468 for $C_{26}H_{37}NNaO_7$), 951.5112 $[2M+H]^+$ (calcd. 951.5218 for $C_{52}H_{75}N_2O_{14}$.

Polydosetin D (**4**): yellow solid; $[\alpha]^{20}_D$ −3.6 (*c* 0.1, MeOH); UV/Vis (MeOH): λmax (log ε) = 288 (0.4), 254 (0.3) nm, 203 (0.7) nm; ECD (MeOH, λ (nm) (Δε), c = 4.49 × 10−4 M): 272 (−8.62), 253 (−0.06), 241 (−5.43), 223 (−4.20), 199 (−47.43); ^{1}H NMR (500 MHz, CH_3OH–d_4): see Table 2; ^{13}C NMR (125 MHz, CH_3OH–d_4): see Table 1; HRESI-MS: *m/z* 446.1941 $[M+H]^+$ (calcd. 446.2543 for $C_{25}H_{36}NO_6$), 468.1829 $[M+Na]^+$ (calcd. 468.2362 for $C_{25}H_{35}NNaO_6$).

Polydosetin E (**5**): yellow oily; $[\alpha]^{20}_D$ −5.3 (*c* 0.1, MeOH); UV/Vis (MeOH): λmax (log ε) = 288 (0.4), 254 (0.3) nm, 203 (0.7) nm; ECD (MeOH, λ (nm) (Δε), c = 2.33 × 10−4 M): 273 (−7.99), 245 (−3.94), 244 (−16.49), 230 (−3.38), 200 (−46.10); ^{1}H NMR (500 MHz, CH_3OH–d_4): see Table 2; ^{13}C NMR (125 MHz, CH_3OH–d_4): see Table 1; HRESI-MS: *m/z* 430.2584 $[M+H]^+$ (calcd. 430.2593 for $C_{25}H_{36}NO_5$), 452.2399 $[M+Na]^+$ (calcd. 452.2413 for $C_{25}H_{35}NNaO_5$), 859.5050 $[2M+H]^+$ (calcd. 859.5109 for $C_{50}H_{71}N_2O_{10}$).

Pullularin G (**6**): yellow solid; $[\alpha]^{20}_D$ −4.2 (*c* 0.1, MeOH); UV/Vis (MeOH): λmax (log ε) = 278 (0.02), 201 (0.5) nm; ECD (MeOH, λ (nm) (Δε), c = 2.44 × 10−4 M): 285 (−2.17), 260 (−0.90), 228 (−36.69), 210 (−14.83), 208 (−15.55), 194 (+53.26); ^{1}H NMR (500 MHz, DMSO–d_6) & ^{13}C NMR (125 MHz, DMSO–d_6): see Table 3; HRESI-MS: *m/z* 818.4650 $[M+H]^+$ (calcd. 818.4704 for $C_{45}H_{64}N_5O_9$), 840.4467 $[M+Na]^+$ (calcd. 840.4523 for $C_{45}H_{63}N_5NaO_9$).

Pullularin H (**7**): yellow solid; $[\alpha]^{20}_D$ +2.8 (*c* 0.1, MeOH);); UV/Vis (MeOH): λmax (log ε) = 280 (0.02), 202 (0.4) nm; ECD (MeOH, λ (nm) (Δε), c = 2.54 × 10−4 M): 285 (−2.09), 268 (−1.41), 230 (−35.35), 210 (−14.29), 208 (−14.98), 194 (+51.31); ^{1}H NMR (700 MHz, DMSO–d_6) & ^{13}C NMR (175 MHz, DMSO–d_6): see Table 3; HRESI-MS: *m/z* 788.4555 $[M+H]^+$ (calcd. 788.4598 for $C_{44}H_{62}N_5O_8$), 810.4368 $[M+Na]^+$ (calcd. 810.4418 for $C_{44}H_{61}N_5NaO_8$).

2.5 Advanced Marfey's analysis of compounds 6 and 7

The stereochemistry of the amino acid residues in pullularins G and H (**6** and **7)** was determined using Marfey's method, adapted from Viehrig et al. [9]. For hydrolysis, **6** and **7** (0.1 mg each) were treated separately with 500 µL of 6 N HCl and heated at 90 °C for 18 h. The hydrolysates were dried under vacuum and dissolved in 200 µL of Milli-Q water. To each solution, 20 µL of 1 M $NaHCO_3$ and 100 µL of acetone containing 1% derivatization agent Nα-(2,4-dinitro-5-fluorophenyl)-L-alaninamide (FDAA) were added. The mixtures were incubated at 40 °C for 40 min and then evaporated to dryness under vacuum. The residues were suspended in 1 mL of MeOH and analyzed by LC-ESI-MS under the same conditions as previously described. The enantiomeric configuration of the amino acids was determined by comparing their retention times with those of authenticated $_L$- and $_D$-amino acid standards derivatized in parallel. The standards included $_L$-proline, $_D$-proline, N-methyl-$_L$-leucine, N-methyl-$_D$-leucine, N-methyl-$_L$-isoleucine, $_L$-serine, and $_{DL}$-serine.

2.6 Derivatization of 3 with *R*- and *S*-MTPA-chloride

Polydosetin C (**3**, 2 mg) was dissolved in 0.7 mL dry pyridine–d_5 and treated with *R*–MTPA chloride to obtain the *S*–MTPA ester of **3**. After stirring at 25 °C for 18 h, the mixture was directly subjected to NMR analysis. ^{1}H NMR of 3-*S*-MTPA ester (700 MHz, pyridine–d_5) similar to **3**, but: δ_H 6.16 (dd, J = 6.2, 4.1 Hz, H–6'), 5.24 (d, J = 6.2 Hz, H–7'), 5.24 (d, J = 6.2 Hz, H–7'), 4.50 (d, J = 4.1 Hz, H–5') ppm.

The *R*–MTPA ester of **3** was obtained analogously by using *S*–MTPA chloride, with ^{1}H NMR data (700 MHz, pyridine–d_5) similar to **3**, but: δ_H 6.24 (dd, J = 6.0, 3.5 Hz, H–6'), 5.15 (d, J = 6.0 Hz, H–7'), 5.24 (d, J = 6.2 Hz, H–7'), 4.71 (d, J = 3.5 Hz, H–5') ppm.

2.7 Antimicrobial assay

Antimicrobial activity was assessed using a serial dilution assay to determine the minimum inhibitory concentration (MIC) following a previously established procedure [10]. Compounds **1**–**7** were tested against the fungi *Schizosaccharomyces pombe* (DSM 70572), *Wickerhamomyces anomalus* (DSM 6766), *Mucor hiemalis* (DSM 2656), *Candida albicans* (DSM 1665), and *Rhodosporidium toruloides* (DSM 10134); the Gram-positive bacteria *Bacillus subtilis* (DSM 10), *Mycobacterium smegmatis* (ATCC 700084), and *Staphylococcus aureus* (DSM 346); and the Gram-negative bacteria *Acinetobacter baumannii* (DSM 30008), *Chromobacterium violaceum* (DSM 30191), *Escherichia coli* (DSM 1116), and *Pseudomonas aeruginosa* (DSM 19882). Ciprofloxacin, oxytetracycline, kanamycin, and gentamycin were used as positive controls for bacterial strains, while nystatin served as the positive control for fungal strains.

2.8 Cytotoxicity assay

The in vitro cytotoxic activity of compounds **1**–**7** was evaluated using the colorimetric tetrazolium dye MTT (3-(4,5-dimethylthiazol-2-yl)-2,5-diphenyltetrazolium bromide) assay as previously described [10]. The mammalian cell lines used in this study were obtained from the DSMZ and included mouse fibroblasts (L929) and endocervical adenocarcinoma cells (KB3.1). Epothilone B was employed as the positive control. The half-maximal inhibitory concentration (IC_{50}), corresponding to 50% inhibition of cell growth relative to the control, was calculated.

2.9 Nematode assay against *Caenorhabditis elegans*

2.9.1 Nematode culture and synchronization

Synchronization of the nematode population was performed according to a previously described method with minor modifications [11]. *C. elegans* (N2 wild-type strain, obtained from the Caenorhabditis Genetics Center) was cultured monoxenically on nematode growth medium (NGM; per liter: 3 g NaCl, 2.5 g peptone, 20 g agar,

1 mL 1 M $CaCl_2$, 25 mL 1 M [pH 6.0] KPO_4, 1 mL 1 M $MgSO_4$, and 1 mL cholesterol [5 mg/mL in ethanol]) seeded with *E. coli* OP50 as the food source. Plates were incubated at 19 °C for ~120 h until a high density of eggs was achieved. For synchronization, nematodes and eggs were rinsed from the plates three times with 5 mL 0.9% NaCl into a 15 mL Falcon tube, centrifuged at 600 rpm for 3 min, and the supernatant was discarded. This procedure was repeated until a clear suspension of nematodes was obtained. After the last washing step, the pellet suspended in 2 mL 0.9% NaCl was mixed with 5 mL of bleaching solution (1 mL sodium hypochlorite solution, 0.5 mL 5 M NaOH, and 3.5 mL Milli-Q water). The mixture was incubated for 3 min with gentle swirling and monitored microscopically until adult worms were digested, leaving eggs intact. The reaction was stopped by adding 8 mL 0.9% NaCl, followed by centrifugation at 2500 rpm for 2 min. Eggs were washed three times with 13 mL 0.9% NaCl using centrifugation at 2500 rpm for 2 min each time. If adult residues remained, the bleaching process was repeated with 1 mL bleaching solution for 1 min, followed by washing as described above. After the final wash, the egg suspension was adjusted to 2 mL, diluted with 5 mL 0.9% NaCl, and transferred to a 50 mL Falcon tube. Eggs were incubated in a horizontal position on a shaker at 23 °C and 80 rpm for 18 h to allow hatching. The hatched larvae were centrifuged at 600 rpm for 3 min, the supernatant discarded, and the pellet transferred to fresh NGM plates seeded with *E. coli* OP50. Plates were incubated at 19 °C for 48 h to reach the fourth larval (L4) and adult stages. Nematodes were then rinsed from the plates as described above and adjusted with 0.9% NaCl to a final concentration of 1000 nematodes/mL.

2.9.2 Nematode assay procedure

The nematicidal activity of compounds **1**–**7** was evaluated against *C. elegans* following a previously described method [11]. Test compounds were dissolved in MeOH at a stock concentration of 0.15 mg/mL. Aliquots of 200 µL, 100 µL, and 20 µL were transferred into a 48-well microtiter plate to yield final assay concentrations of 100 µg/mL, 50 µg/mL, and 10 µg/mL, respectively. MeOH (100 µL) served as a negative control, while ivermectin (1 µg/mL) was used as the positive control. Compounds were tested in triplicate, and controls in six replicates. Following solvent evaporation under nitrogen, 300 µL of synchronized nematode suspension (1000 nematodes/mL) was added to each well, and the plates were incubated at 23 °C and 150 rpm for 18 h. After incubation, live (motile) and dead (erect and immobile) nematodes were counted from a 30 µL drop, in triplicate, and mortality rates were calculated. The observed mortality rate was corrected using the Schneider-Orelli formula [12]. Compounds were classified as active if they induced ≥50% mortality at 100 µg/mL.

3 Results and discussion

The solid-state cultures of *P. karssenii* strain JKI 73120 grown in BRFT and WOFT media were fractionated using chromatographic techniques, starting with normal-phase flash chromatography and followed by preparative and semipreparative RP-HPLC of the fractions of interest. This procedure led to the isolation of five previously undescribed natural products: the tetramic acids **2**, **3**, and **5**, and the cyclodepsipeptides **6** and **7**. In parallel, fermentation extracts of strain DSM 111209 cultivated in liquid Q6 ½ medium were subjected to the same fractionation workflow, resulting in the isolation of three new tetramic acids, **1**, **2**, and **4**.

3.1 Structure elucidation of polydosetins A–E (1–5)

Compound **1** was assigned the molecular formula $C_{25}H_{35}NO_5$ based on its quasimolecular ion peak cluster at *m/z* 462.2485 in the HRESIMS spectrum, corresponding to 9 degrees of unsaturation. Initial ^1H and ^{13}C NMR spectra recorded in $CHCl_3$–*d* showed broad, poorly resolved signals that impeded interpretation. Therefore, additional NMR spectra were also acquired in CH_3OH–d_4, acetone–d_6, pyridine–d_5 and DMSO–d_6 (see Tables S1and S2), with acetone–d_6 providing the most informative dataset. Still several signals were notably broad or duplicated, likely due to tautomerism or conformational exchange. ^1H and HSQC NMR spectra revealed the presence of five methyl groups, three methylene groups, two olefinic methines, and six aliphatic methines, of which two were

oxymethines and one was an azamethine. The ^{13}C NMR spectrum further displayed three unsaturated ketones/oxyolefins (C–1, C–2', C–4'), one carboxylic carbon (C–8'), three sp²-hybridized quaternary carbons (C–10, C–13, C–3'), and one sp³-hybridized nonprotonated carbon. COSY and HMBC correlations allowed the assembly of two substructures: a) a bicyclic decalin part, substituted at C–3 with a 1-methylprop-1-enyl group, and b) a 4-amino-2,3,5-trihydroxypentanoyl moiety (see Figure S39 for details). It was not possible to connect these two subunits, since no HMBC correlations were observed between those subunits, nor were HMBC correlations observed to two nonprotonated carbons (C–2', C–3'). However, a literature search involving these fragments suggested that **1** belongs to the class of decanoyltetramic acids [13]. This compound class is known to undergo multi-sided tautomeric exchange, which leads to signal broadening and often to the absence of expected NMR signals and 2D NMR correlations [14]. Based on all spectroscopic data, the planar structure of **1** was proposed as shown in Figure 1, for which we suggest the name polydosetin A.

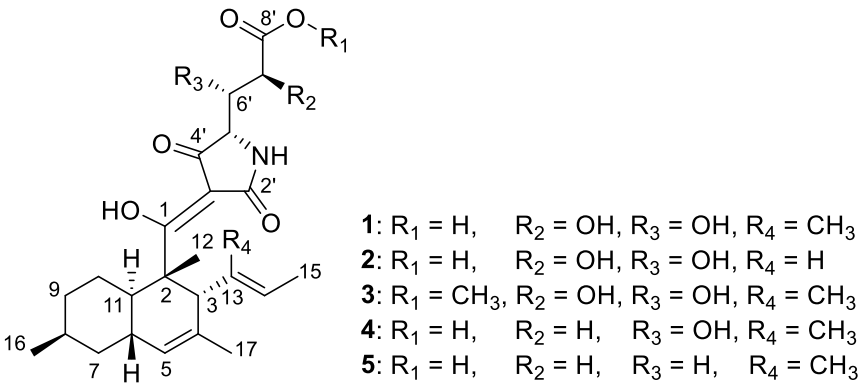

Figure 1. Chemical structures of polydosetin A–E (**1**–**5**)

We utilized a multitude of methods to assign the stereochemistry of all asymmetric centers of **1**. The absolute configurations at C–2 and C–5′ were determined by the comparison of ECD spectroscopic data with those of the known data of structurally related compounds trichosetin and *epi*-trichosetin; minima at both 230 and 280 nm indicate a 2*S*,5'*S* configuration [15]. The ROESY correlations between H_3–12 and H–3, as well as between H_3–12 and H–6, specified that the stereocenters C–2, C–3, and C–6 are conserved relative to hymenosetin (Figure 2). The large coupling constant of $^3J_{H6H11}$ = 10.2 Hz, observed in the pseudo triplet of H–11, confirmed the *trans* configuration of these protons. A detailed comparison of the ^{13}C NMR chemical shifts with those of hymenosetin indicated a high degree of similarity, thereby confirming that the stereogenic centers possess a common configuration. However, comparative analysis of the ^{13}C NMR chemical shifts with those of the closely related hymenosetin [16], CJ-1576 [17], and colposetin [18] revealed significant shift differences at C–8 and C–16, suggesting an inversed stereochemistry at this position. Since the C–6 and C–8 signals overlapped in acetone–d_6, impeding the investigation, ROESY correlations were analyzed in methanol–d_4. Strong 1,3-diaxial ROESY correlations between H_3–16, H–6, and H–10b confirmed the assumed 8*S* configuration. The relative configuration of C–6'/C–7 was assigned by a *J*-based configurational analysis. Despite the measurement of HSQC-Hecade and *J*-HMBC NMR experiments in multiple solvents, only the coupling constants $^3J_{H6',H7'}$ = 6.0 Hz, $^2J_{H7',C6'}$ = 5.0 Hz and $^2J_{H6',C7'}$ = 1.9 Hz could be extracted from data obtained in acetone–d_6. Because the ^3J(H6′,H7′) coupling constant is classified as 'medium' in the sense of Matsumori et al. (1999) [19], a straightforward analysis based on a single rotamer is not possible. Rather, the observed data indicate an equilibrium of conformations. Nevertheless, the combination of a 'large' ^2J(H7',C6') and a 'small' ^2J(H6',C7') provides a clear diagnostic signature for the dihydroxy configuration as *erythro*. As only ^3J(H5′,H6′) = 2.0 Hz and ^2J(H5′,C6′) = 3.8 Hz were observed, the *J*-based analysis could not be extended to C–5 and therefore did not allow a direct correlation with the C–5 absolute configuration determined by ECD data.

However, NMR data have been reported for all diastereomers of synthetic 3,4-dihydroxyglutamic acid, which can be regarded as a reliable model compound [20,21]. Based on this comparison, the observed 'small' ^{3}J(H5′,H6′) and 'medium' ^{3}J(H6′,H7′) coupling constants are characteristic for the 5′S,6′S,7′S configuration.

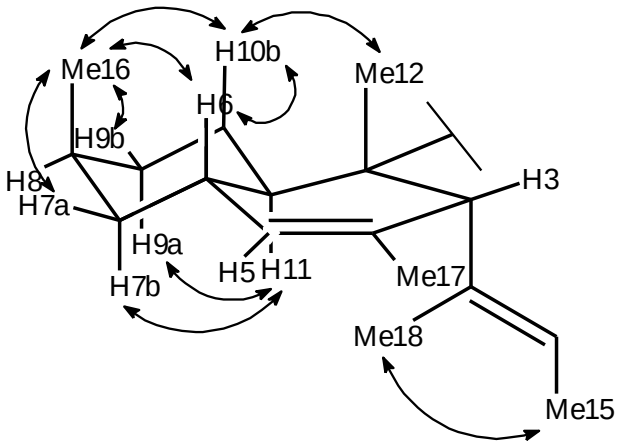

Figure 2. Key ROESY correlations utilized for the structure elucidation of **1**.

Polydosetin B (**2**) was isolated as a co-metabolite alongside A and exhibited a quasimolecular ion cluster at *m/z* 448.2335 in the HRESIMS spectrum, consistent with a molecular formula of $C_{24}H_{33}NO_7$, indicating one methyl group less than A. Comparative analysis of the NMR data revealed nearly identical chemical shifts and coupling patterns to those of A, with a notable absence of the methyl group C–18, confirming B as the 13-demethyl derivative of **1**. The loss of the C–18 methyl group resulted in subtle deshielding effects at adjacent positions (particularly at C–12 and C–14, see Table 1), but the overall connectivity and stereochemical configuration remained conserved. ROESY and HMBC data supported an identical planar structure to **1**, minus the C-13 substituent. ROESY correlations between H–13 and H_3–15 as well as H–3 and H–14 indicate an unchanged *E* configuration of the $\Delta^{13,14}$ double bond. Thus, polydosetin B (**2**) was unambiguously identified as the 13-demethyl derivative of **1**.

Polydosetin C (**3**) was identified as a structural analogue of **1**, showing a quasimolecular ion cluster at *m/z* 476.2640 in the HRESIMS spectrum, corresponding to a molecular formula of $C_{26}H_{37}NO_7$, indicating the presence of an additional oxygen atom. Comparison of the ^{1}H and ^{13}C NMR spectra of C with those of A revealed high overall similarity, with the most prominent difference being the appearance of a methoxy singlet (δ_H 3.77 ppm, δ_C 52.7 ppm), consistent with a methoxy group. HMBC correlations from the methoxy protons to C–8′ confirmed that the substitution occurred at this position and unambiguously identified C as the 8′–O-methyl derivative of **1**. Polydosetin C (**3**) was used to confirm the stereoconfiguration using a Mosher's method experiment. The $\Delta\delta^{SR}$ chemical shift pattern of the MTPA derivatives of **3**, showing negative values for H-5′ (- 0.21 ppm) and H-6′ (- 0.08 ppm), along with a positive value for H-7′ (+ 0.09 ppm), is characteristic of the *anti*-1,2 Type C arrangement and thus validates our analysis [22].

Compounds D and E (**4** and **5**) were isolated as additional structural analogues of **1**, displaying quasimolecular ion peaks at *m/z* 446.1941 and 430.2584, corresponding to molecular formulae consistent with the loss of one and two oxygen atoms, respectively, relative to **1**. NMR spectral comparison revealed that both compounds shared the same overall core structure as **1**, but differed in the substitution pattern of the side chain.

In **4**, the absence of the C–7′ oxymethine signal was evident in the ^{1}H NMR and HSQC spectra, replaced by an aliphatic methylene resonance (δ_H 2.13 & 1.84 ppm, δ_C 38.6 ppm). COSY and HMBC correlations confirmed the intact side chain, and no other significant changes were observed. Polydosetin E (**5**) exhibited the additional absence of the C–6′ oxymethine signal, confirming it as the 6′,7′-didehydroxy derivative of **1**. In this compound,

both C–6′ and C–7′ appeared as aliphatic methines, and HMBC data supported the uninterrupted carbon chain. The rest of the molecule—including the tetramic acid core and its stereochemical features—remained unchanged in both derivatives.

Table 1. ^{13}C NMR data of polydosetins A–E in CH_3OH–d_4.

pos	**1**[a]	**2**[b]	**3**[a]	**4**[b]	**5**[b]
1	201.6, C	201.5, C	201.4, C	203.3, C	202.8, C
2	49.6, C	51.2, C	52.2, C	52.6, C	52.5, C
3	57.5, CH	50.6, CH	57.5, CH	57.5, CH	57.3, CH
4	133.0, C	133.8, C	133.1, C	132.9, C	132.9, C
5	128.2, CH	127.1, CH	128.2, CH	128.2, CH	128.3, CH
6	33.7, CH	34.3, CH	33.8, CH	33.7, CH	33.7, CH
7	41.2, CH_2	41.2, CH_2	41.3, CH_2	41.2, CH_2	41.3, CH_2
8	29.5, CH	29.5, CH	29.5, CH	29.5, CH_2	29.5, CH
9	34.1, CH_2	33.9, CH_2	34.1, CH_2	34.1, CH_2	34.1, CH_2
10	24.5, CH_2	24.0, CH_2	24.5, CH_2	24.4, CH_2	24.5, CH_2
11	43.2, CH	42.5, CH	43.2, CH	43.2, CH_2	43.3, CH
12	15.7, CH_3	14.4, CH_3	15.7, CH_3	15.6, CH_3	15.7, CH_3
13	136.0, C	132.4, CH	136.3, C	136.4, C	136.5, C
14	125.9, CH	128.9, CH	125.7, CH	125.6, CH	125.4, CH
15	13.8, CH_3	18.2, CH_3	13.8, CH_3	13.8, CH_3	13.7, CH_3
16	19.4, CH_3	19.4, CH_3	19.4, CH_3	19.4, CH_3	19.4, CH_3
17	23.0, CH_3	22.7, CH_3	23.2, CH_3	23.0, CH_3	23.0, CH_3
18	14.7, CH_3		14.6, CH_3	14.6, CH_3	14.4, CH_3
2’	n.o.	n.o.	181.5, C	n.o.	n.o.
3’	n.o.	101.2, C	102.5, C	n.o.	n.o.
4’	n.o.	n.o.	193.9, C	195.3, C	194.5, C
5’	63.2, CH	n.o.	63.7, CH	n.o.	60.9, CH
6’	72.8, CH	72.9, CH	73.0, CH	69.0, CH	28.2, CH_2
7’	74.5, CH	74.5, CH	74.4, CH	38.6, CH_2	30.2, CH_2
8’	176.0, C	176.0, C	174.8, C	177.5, C	176.6, C
8’–CH_3			52.7, CH_3		

n.o. not observed, [a] 700 MHz, [b] 500 MHz

Table 2. ^{1}H NMR data of polydosetins A–E in CH_3OH–d_4.

Pos	**1**[a]	**2**[b]	**3**[b]	**4**[b]	**5**[b]
3	3.30, br s	3.32, m	3.32, m	3.32, m	3.35, m
5	5.22, s	5.23, s	5.22, s	5.23, s	5.23, s
6	2.07, m	2.08, m	2.06, m	2.08, m	2.07, m
7	1.64, m	1.61, m	1.64, m	1.65, m	1.65, m
	1.47, m	1.44, m	1.48, m	1.48, m	1.48, m
8	2.07, m	2.08, m	2.07, m	2.08, m	2.07, m
9	1.69, m	1.73, m	1.69, m	1.69, m	1.68, m
	1.54, br d (13.0)	1.55, m		1.55, m	1.54, m
10	1.62, m	1.78, m	1.61, m	1.63, m	1.61, m
	1.22, m	1.24, m		1.24, m	1.22, m
11	1.89, br t (10.2)	1.70, m	1.89, br t (10.4)	1.90, m	1.90, m
12	1.49, s	1.44, s	1.48, s	1.49, s	1.49, s
13		5.13, m			
14	5.25, br s	5.27, m	5.25, br s	5.25, m	5.24, m
15	1.46, m	1.55, br d (6.7)		1.46, m	1.47, m
16	1.05, d (7.3)	1.04, d (7.3)		1.05, d (7.3)	1.05, d (7.3)
17	1.50, br s	1.58, m	1.50, br s	1.51, m	1.51, m
18	1.46, m		1.46, br s	1.46, m	1.46, m
1’NH	n.o.	n.o.	4.63, br s	n.o.	n.o.

5’	n.o.	3.90, br s	4.00, br s	3.98, br s	3.90, br t (4.7)
6’	4.17, dd (6.0,2.0)	4.17, dd (6.3,2.0)	4.13, dd (7.5,2.0)	4.28, dd (9.6, 3.4)	2.13, m 1.88, m
7’	4.23, d (6.0)	4.23, d (6.3)	4.22, d (7.5)	2.13, m 1.84, m	2.36, m
8’OMe			3.77, s		

n.o. not observed, [a] 175 MHz, [b] 125 MHz

The polydosetins A–E (**1**–**5**) exhibit several unusual structural features: The relative configuration at C–8 to the other stereocenters of the decalin part is particularly noteworthy, as this relatedness has only been observed once in a single related metabolite, the minor compound conipyridoin F [23]. In addition, incorporation of a glutamic acid unit is highly uncommon in tetramic acids; with gabusectin, only one decanoyltetramic acid derivative has been described as being derived from glutamic acid to date [24].

Finally, our results demonstrate that straightforward chemical shift analysis provides a reliable tool for establishing the relative configuration of this class of compounds, offering a practical alternative to more elaborate approaches.

3.2 Structure elucidation of pullularins G and H

The molecular formula of pullularin G (**6**) was established as $C_{45}H_{63}N_5O_9$ based on the high-resolution electrospray ionization mass spectrum (HRESIMS), which displayed a molecular ion cluster at *m/z* 818.4650. This composition corresponds to 16 degrees of unsaturation.

Initial analysis of the ^{1}H, ^{13}C, and HSQC NMR spectra indicated that compound **6** possesses a peptidic nature, as evidenced by the presence of five characteristic azamethine signals and six carboxyl carbons resonating between δ_C 165–172 ppm.

Detailed interpretation of COSY and HMBC correlations allowed the identification of the constituent amino acid residues, namely proline, serine, isoleucine, tyrosine, and leucine. In addition, signals consistent with a 3-phenyl-lactic acid moiety were observed. Structural refinements revealed specific modifications: both the leucine and isoleucine residues were found to be *N*-methylated, while the tyrosine residue carried a prenyl substituent attached to the *para*-oxygen atom of its phenolic group (see Figure 4).

The sequence of the amino acid residues was established by analyzing long-range HMBC correlations between neighboring units, which enabled the complete assembly of the planar structure. All amino acids were determined to have L-configuration (Figures S58−S61)

The molecular formula of compound **7** was established as $C_{44}H_{61}N_5O_8$ based on its HRESIMS data (molecular ion cluster at *m/z* 788.4555). The NMR spectra of **7** were largely highly similar to those of pullularin G (**6**), confirming a close structural relationship. However, careful analysis revealed two key differences: (i) the terminal oxymethylene group of the serine residue in **6** was replaced by a methyl group in **7**, thus **7** contains an alanine instead of the serine. (ii) The detection of an additional methylene unit in the former valin spin system indicated the substitution by isoleucine. These modifications account for the observed changes in both the molecular composition and the NMR spectroscopic data.

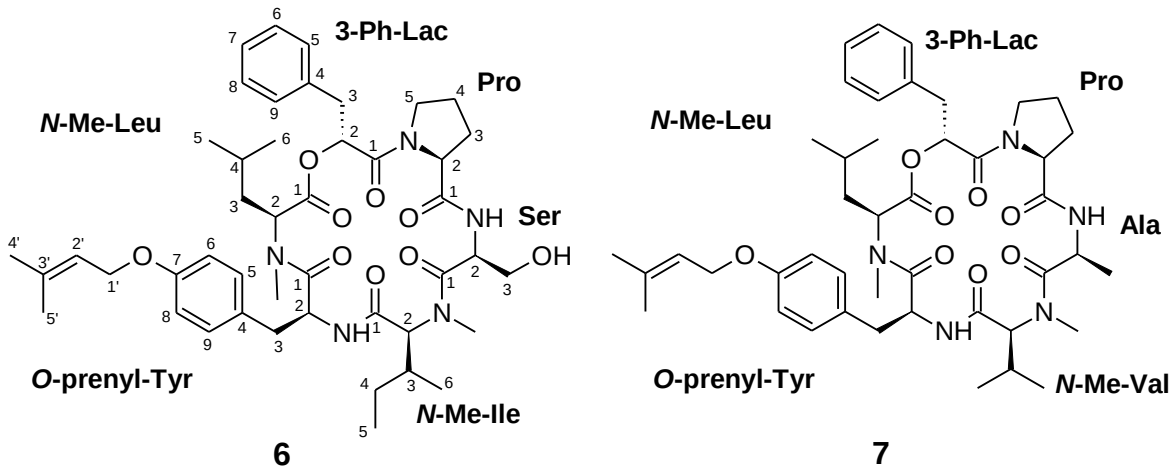

397

398 Figure 4. Chemical structures of pullularins G–H (**6**–**7**)

399

400 Table 3. NMR data of pullularins G (^{1}H 500 MHz, ^{13}C 125 MHz) and H (^{1}H 700 MHz, ^{13}C 175 MHz) in DMSO-
401 d_6.

	6		**7**	
pos	δ_C, mult.	δ_H, mult.	δ_C, mult.	δ_H, mult.
3-Ph-Lac			3-Ph-Lac	
1	165.3, C		165.3, C	
2	71.3, CH	5.61, ps t (7.0)	71.1, CH	5.61, ps t (7.0)
3	36.1, CH_2	3.06, dd (13.3, 7.5)	36.1, CH_2	3.06, dd (13.3, 7.4)
		2.86, dd (13.3, 6.7)		2.83, dd (13.3, 6.7)
4	136.6, C		136.3, C	
5,9	129.7, CH	7.21, m	129.7, CH	7.20, m
6,8	128.2, CH	7.24, m	128.1, CH	7.24, m
7	126.4, CH	7.17, m	126.4, CH	7.17, m
Pro			Pro	
1	172.4, C		171.7, C	
2	58.3, CH	4.47, m	58.2, CH	4.32, dd (8.7, 2.5)
3	29.4, CH_2	2.04, m	29.1, CH_2	2.05, m
		1.69, m		1.67, m
4	23.9, CH_2	1.79, m	23.8, CH_2	1.79, m
5	45.8, CH_2	3.66, m	45.7, CH_2	3.68, m
		3.23, m		3.25, m
Ser			Ala	
1	171.2, C		173.7, C	
2	52.6, CH	4.47, m	44.4, CH	4.69, m
3	61.3, CH_2	3.56, m	17.1, CH_3	1.23, d (6.7)
2-NH		9.20, br s		8.87, d (4.1)
N-Me-Ile			*N*-Me-Val	
1	168.0, C		168.1, C	
2	64.8, CH	4.56, d (10.7)	65.0, CH	4.54, d (10.8)
3	32.0, CH	2.05, m	25.6, CH	2.50, m
4	24.2, CH_2	1.28, m	19.5, CH_3	0.99, d (6.4)
		0.91, m		
5	12.0, CH_3	0.92, t (7.3)	18.5, CH_3	0.81, d (6.9)
6	16,3, CH_3	0.93, d (6.4)		
2-*N*-Me	28.5, CH_3	2.48, s	28.4, CH_3	2.52, m
O-preny-Tyr				
1	167.6, C		167.6, C	
2	51.9, CH	4.68, ddd (9.9,8.4,6.7)	51.9, CH	4.67, m

3	36.6, CH_2	2.86, dd (13.1 10.3)	36.6, CH_2	2.87, dd (13.1 10.3)
		2.48, m		2.50, m
4	129.7, C		129.7, C	
5,9	129.9, CH	7.01, br d (8.8)	129.9, CH	7.02, br d (8.8)
6,8	114.1, CH	6.76, br d (8.8)	114.1, CH	6.76, br d (8.8)
7	156.8, C		156.8, C	
1’	64.1, CH_2	4.42, m	64.1, CH_2	4.43, d (6.7)
2’	120.1, CH	5.37, m	120.1, CH	5.58, tspt (6.7, 1.4)
3’	136.8, C		136.8, C	
4’	25.4, CH_3	1.71, br s	25.4, CH_3	1.72, br s
5’	18.0, CH_3	1.67, br s	17.9, CH_3	1.67, br s
N-Me-Leu			*N*-Me-Leu	
1	169.4, C		169.3, C	
2	61.2, CH	3.48, dd (8.7, 5.3)	61.2, CH	3.44, dd (8.6, 5.4)
3	37.2, CH_2	1.42, m	37.1, CH_2	1.43, m
		1.27, m		1.27, m
4	23.9, CH	1.03, m	23.9, CH	1.02, m
5	21.8, CH_3	0.73, d (6.6)	21.8, CH_3	0.72, d (6.6)
6	22.9, CH_3	0.58, d (6.6)	22.9, CH_3	0.57, d (6.6)
2-*N*-Me	37.4, CH_3	2.99, s	37.4, CH_3	2.98, s

3.3 Bioassays

In our search for novel bioactive natural products, we evaluated the antimicrobial activities of the tetramic acid derivatives polydosetins A–E (**1**–**5**) and the cyclodepsipeptides pullularins G and H (**6** and **7**), isolated from the two studied strains of *P. karssenii*. The compounds were tested against a panel of Gram-positive and Gram-negative bacteria, as well as various fungal strains. The antimicrobial assay results (Table S19) revealed that compounds **1**, **3**, **5**, and **7** (Table 4) displayed activity against the Gram-positive bacterium *B. subtilis*, with polydosetin C (**3**) being the most potent, showing a MIC value of 16.6 µg/mL. Compound **3** also exhibited moderate activity against *S. aureus* (33.3 µg/mL), while **7** showed weak activity against *S. aureus* (66.6 µg/mL) and *M. smegmatis* (66.6 µg/mL). However, none of the tested compounds showed inhibition against Gram-negative bacteria at the tested concentrations (MIC >66.6 µg/mL). In addition, polydosetin E (**5**) demonstrated antifungal activity against *C. albicans*, *R. toruloides*, and *M. hiemalis*, showing the strongest activity against *M. hiemalis* (16.6 µg/mL). In comparison, compound **3** also exhibited activity against *M. hiemalis*, but with a MIC value of 66.6 µg/mL. Polydosetins A–E (**1**–**5**) belong to the 3-decalinoyltetramic acids (3-DTAs) class and only a few of them have been reported to affect Gram-negative bacteria; examples include pyrrospirones C, F, and I, which can inhibit the growth of *E. coli* [13,25]. These findings correlate with the literature, which establishes that 3-DTAs exhibit significant antimicrobial activities, particularly against Gram-positive bacteria, including methicillin-resistant *S. aureus* (MRSA) and *B. subtilis* [13]. This lack of activity could be explained by the fact that the outer membrane barrier of Gram-negative bacteria restricts penetration of 3-DTAs unless their structures incorporate sufficiently lipophilic (decalin-based or other hydrophobic) groups, which may improve outer membrane passage [13]. However, further studies are needed to explain this mechanism. Similar observations have been reported for cyclodepsipeptides, which have demonstrated a broad spectrum of activity against various Gram-positive bacteria, especially *B. subtilis* and *Mycobacterium* spp. [26–29].

Table 4. Antimicrobial activities of compounds **1**, **3**, **5**, and **7** in the serial dilution assay. All other compounds (**2**, **4**, and **6**) were devoid of significant effects up to concentrations of 66.6 µg/mL.

Test Microorganism	MIC (µg/mL)				Positive control (µg/mL)
	1	**3**	**5**	**7**	
Staphylococcus aureus	n.i	**33.3**	n.i	**66.6**	0.21[G]
Mycobacterium smegmatis	n.i	n.i	n.i	**66.6**	1.70[K]
Bacillus subtilis	**66.6**	**16.6**	**66.6**	**66.6**	16.6[O]
Candida albicans	n.i	n.i	**66.6**	n.i	8.3[N]
Mucor hiemails	n.i	**66.6**	**16.6**	n.i	8.30[N]
Rhodosporidium toruloides	n.i	n.i	**66.6**	n.d	4.20[N]

n.i: No inhibition (>66.6 µg/mL). n.d: Not determined.
[G]: Gentamycin; [O]: Oxytetracycline; [N]: Nystatin; [K]: Kanamycin.

On the other hand, methylation of the carboxylic acid group in the studied tetramic acids can significantly affect their biological activity. Compound **3**, which is the 8′–O-methyl derivative of **1**, showed a wider range of antimicrobial effects (as shown in Table 4). This indicates that methylation can enhance antimicrobial properties. Similar results have been observed in structure–activity relationship (SAR) studies, where replacing a methyl group in enol ethers with a hydroxyl group caused a notable decrease in bioactivity [30]. However, there are limited direct comparisons between methylated esters and free carboxylic acids across different compounds. Despite this, small chemical modifications like methylation can have a significant impact on the biological activity of these compounds.

All the compounds were tested for their cytotoxic effects (Table S18) on two mammalian cell lines: mouse fibroblasts (L929) and endocervical adenocarcinoma cells (KB3.1). Only polydosetin E (**5**) and pullularin H (**7**) (Table 5) showed cytotoxic effects against KB3.1 cells, exhibiting weak activity with IC_{50} values of 24.1 and 53.6 µM, respectively. These findings suggest that the studied cyclodepsipeptides and tetramic acids generally have a favorable safety profile. This aligns with previous research evaluating the cytotoxicity of certain 3-DTAs, where most derivatives exhibited moderate cytotoxicity against various cancer cell lines, showing no significant difference between *trans*- and *cis*-decalin isomers [31]. Only a limited number of 3-DTAs have been reported to exhibit strong cytotoxic activity against various cell lines [13]. On the other hand, numerous studies have reported diverse cytotoxic properties of cyclodepsipeptides against a wide range of cell lines, highlighting their potential as valuable candidates for further investigation in anticancer drug discovery and development [26,29].

Table 5. Cytotoxicity results of compounds **5** and **7**. All other compounds (**1**–**4** and **6**) were devoid of significant effects up to concentrations of 66.6 µM.

Test Cell Line	IC_{50} (µM)		Positive Control Epothilone B (nM)
	5	**7**	
L929	**	*	0.65
KB3.1	**53.6**	**24.1**	0.17

(*): Slight inhibition of cell proliferation, (**): No cytotoxic activity observed.

As part of our ongoing search for bioactive molecules, compounds **1**–**7** were tested for nematicidal activity. The nematode assay revealed that only polydosetins A and B (**1** and **2**) (Table 6) exhibited significant activity against *C. elegans*, with corrected mortality rates of 57.6% and 83.1% at 100 µg/mL, respectively. These results suggest

that the presence of hydroxyl groups at positions C–6′ and C–7′, combined with a carboxylic acid at C–8′, could play a key role in enhancing nematode mortality. Compounds lacking these features did not demonstrate significant activity (Table S20). Interestingly, compound **2** is the only metabolite among those studied that has a hydrogen atom at C–13 instead of a methyl group. Moreover, it was the only compound that was detected in both *P. karssenii* strains, JKI 73120 and DSM 111209. These findings suggest that the absence of methylation at C–13 in 3-DTAs may enhance nematicidal activity and that compound **2** could play a key role in the ecological function of the studied strains. Nevertheless, further investigations are required to confirm this relationship. In addition, compounds **1** and **2** showed no cytotoxicity in the conducted assays, supporting their potential as promising, safe candidates for nematicidal agent development. To the best of our knowledge, this is the first report of 3-DTAs with nematicidal activity, and only a few other tetramic acids have been previously described with this property [32,33].

Table 6. Results of the nematode assay of compounds **1** and **2** against *C. elegans*.

Compound	Corrected mortality rate [%]			Positive control
	100 µg/mL	50 µg/mL	10 µg/mL	
1	57.6 ± 10.8	n. a.	n. a.	93.4 ± 4.1
2	83.1 ± 5.2	n. a.	n. a.	

n.a.: no significant activity (mortality rate <50 %), Positive control: ivermectin (1 µg/mL).
The mortality rate in the negative control (MeOH) was 14.7±3.5%, and was used to calculate the corrected mortality using the Schneider-Orelli's formula.

Although none of the tested cyclodepsipeptides showed nematicidal activity, the nematicidal compound ophiotine was previously isolated from *P. karssenii* DSM106825, prior to its formal identification and taxonomic classification [6,7]. Ophiotine caused 59% mortality in the host nematode *H. filipjevi* at a concentration of 10 µg/mL [7]. In addition, certain fungal cyclodepsipeptides, particularly those related to the PF1022 series, represent an important class of compounds with proven nematicidal properties, some of which have already been developed into commercial anthelmintics [26,34]. The cyclodepsipeptide PF1022A, originally isolated from the endophytic fungus *Rosellinia* sp., exhibits nematicidal activity against *Ascaridia galli* in chickens [35,36]. Its mode of action is complex and involves at least two targets: a latrophilin-like receptor and a Ca^{2+}-activated K^{+} channel [26,37]. A semisynthetic derivative of PF1022A, emodepside, is a pharmacologically active anthelmintic agent used in the treatment of both gastrointestinal and extraintestinal nematodes. Its mechanism of action is similar to that of PF1022A, involving targeted disruption of the nematode neuromuscular function [26,38].

Cyclodepsipeptides are a diverse class of cyclic peptide natural products characterized by the replacement of one or more amino acid residues in the peptide backbone with hydroxy acids [26,29,39]. This modification results in the formation of at least one ester bond, often called a lactone linkage, within the core ring [26,29,39]. They are biosynthesized by non-ribosomal peptide synthetases (NRPS) combined with either polyketide synthase (PKS) or fatty acid synthase enzyme systems [26]. Cyclodepsipeptides are widely found in bacteria, fungi, plants, algae, sponges, and other marine organisms [26,40]. Among the fungal kingdom, these metabolites are mainly reported from the ascomycetous genera *Fusarium*, *Beauveria*, *Isaria*, *Trichoderma*, *Acremonium*, *Aspergillus*, *Penicillium*, and *Rosellinia*, many of which are endophytic in at least part of their lifecycle [26,29]. Fungal cyclodepsipeptides exhibit a wide range of biological activities, including cytotoxic, phytotoxic, antimicrobial, antiviral, anthelmintic, insecticidal, antimalarial, antitumor, and enzyme-inhibitory effects [26,41]. Besides PF1022A, other cyclodepsipeptides with pharmaceutical applications include enniatins, which are produced by *Fusarium* spp. [42]. Fusafungine, a mixture of enniatins, was previously employed as an antibacterial nasal spray for the

treatment of rhinosinusitis; however, it was withdrawn by the European Medicines Agency in 2016 due to the identification of enniatins as potential mycotoxins with associated health risks [26,43]. Fungal cyclodepsipeptides are a diverse group of bioactive compounds with significant potential for drug development. Their distinctive structures and wide-ranging biological activities make them promising candidates for therapeutic applications in human health, veterinary medicine, and crop protection, highlighting the importance of continued research on this class of natural products [29,41]. The biological role of the cyclodepsipeptides pullularins G and H (**6** and **7**) in *P. karssenii* remains unknown, and further research through various bioassays is required to determine their activity and potential applications.

Tetramic acids comprise a diverse class of natural products characterized by a pyrrolidine-2,4-dione core [44]. These compounds are widely distributed in marine and terrestrial organisms, including bacteria, actinobacteria, cyanobacteria, fungi, and sponges [44,45]. Tetramic acids display a wide range of bioactivities, including antitumor, antibacterial, antifungal, antiprotozoal, and antiviral effects [44,45]. In addition, certain derivatives, such as macrocidins, function as herbicides [46], while others exhibit antibiofilm activity against bacteria such as *S. aureus* [47,48]. More than 270 tetramic acid derivatives have been described, exhibiting remarkable structural diversity arising from variations in acylation, hydroxylation, esterification, and cyclization [44,49]. The biosynthesis of tetramic acids and related 2-pyridones typically involves polyketide synthase-nonribosomal peptide synthetase (PKS-NRPS) hybrid machineries [48]. Comparative analyses of biosynthetic gene clusters (BGCs) involved in the tetramic acid/2-pyridone biosynthesis have revealed that, in addition to the core PKS–NRPS hybrid genes, these clusters may also contain varying numbers of oxidoreductases, tailoring genes, transporters, transcription factors, and other regulatory elements [50]. This genomic complexity underlies the remarkable structural diversity and evolutionary dynamics of these biosynthetic pathways [48,51].

Tetramic acids can be classified into eight groups based on their structural features and biosynthetic pathways. These groups include simple 3-acyl-tetramic acids, 3-oligoenoyltetramic acids, 3-decalinoyltetramic acids (3-DTAs), 3-spirotetramic acids, macrocyclic tetramic acids, N-acylated tetramic acids, α-cyclopiazonic acid-type tetramic acids, and other tetramic acids [45]. Polydosetins A–E (**1**–**5**) belong to the 3-DTAs class, which are primarily produced by filamentous fungi and are widespread among ascomycetes. [31,52]. This class of compounds exhibits diverse biological activities, including antibacterial, antifungal, antiviral, and antihyperlipidemic properties [31]. The structural diversity of these compounds is generated through fungal biosynthetic pathways involving PKS-NRPS and decalin synthase [13,31]. The polyketide moiety forms the decalin ring via an intramolecular Diels-Alder cycloaddition, while the heterocyclic pyrrolidine-2-one moiety, derived from amino acids, connects to the polyketide-derived decalin ring [13].

Several 3-DTAs share structural similarities with compounds **1**–**5**, including equisetin, trichosetin, beauversetin, Sch 210972, and Sch 213766. These compounds exhibit diverse bioactivities, ranging from antimicrobial effects to anti-HIV properties, highlighting their potential as lead compounds in drug discovery [13]. Equisetin was the first identified member of the 3-DTAs class derived from fungi. It was first isolated in 1974 from *Fusarium equiseti* [53]. Equisetin exhibits phytotoxicity [54] and has been reported as an inhibitor of human immunodeficiency virus type 1 (HIV-1) integrase [55]. Additionally, it shows cytotoxic activity against all NCI-60 cell lines, particularly against human leukemic lymphoblast CCRF-CEM cells [55]. Trichosetin, a derivative of equisetin, was initially isolated from dual cultures of *Trichoderma harzianum* and *Catharanthus roseus* [56]. It is also produced by *F. oxysporum* and has shown antimicrobial activity against *S. aureus* (MRSA) and *B. subtilis* [15,56]. Beauversetin, a phomasetin-type 3-DTA, was first reported from *Beauveria bassiana* isolated from the marine sponge *Myxilla incrustans* [57]. Beauversetin has shown moderate cytotoxic activity against a panel of six cell lines [57]. Sch 210972 and Sch 213766 are also phomasetin-type 3-DTAs and were isolated from the fungus *Chaetomium globosum* [58,59]. These compounds displayed inhibitory activities in a CCR-5 membrane binding

assay, suggesting their potential as inhibitors of the chemokine receptor CCR-5, considered a therapeutic target for antiviral agents [58,59]. The diverse biological activities of the 3-DTAs discussed above, which share structural similarities with polydosetins A–E (**1**–**5**), suggest that these compounds may have additional activities beyond those reported here and therefore merit further investigation. Moreover, the mode of action of 3-DTAs compounds is not well understood, highlighting an important area for future research.

4 Conclusions

The current study evaluated the potential of the endophytic and nematode-associated fungus *P. karssenii* strains JKI 73120 and DSM 111209 to produce secondary metabolites. Building on previous research by Helaly et al. (2018), which reported five compounds from this fungus, we herein report seven additional metabolites that are novel to science, the tetramic acids polydosetins A–E (**1**–**5**) and the cyclodepsipeptides pullularins G and H (**6** and **7**). Bioactivity tests revealed that compounds **1**, **3**, **5**, and **7** demonstrated antimicrobial effects against Gram-positive bacterial strains, with compounds **3** and **5** also exhibiting activity against fungi. Importantly, the tetramic acids **1** and **2**, belonging to the 3-DTA class, are the first compounds in this class reported to exhibit nematicidal activity. Hydroxyl groups at positions C–6′ and C–7′, together with a carboxylic acid at C–8′, may play a key role in increasing nematode mortality. Additionally, the absence of methylation at C–13, as observed in compound **2**—which was the only metabolite produced by both studied strains—may further enhance nematicidal activity. Compounds **1** and **2** showed no cytotoxicity, highlighting their potential as biocontrol agents. These findings emphasize the impressive chemical diversity of nematode-associated fungi and their potential as sources of bioactive compounds for developing novel strategies to control nematodes and microbial pathogens.

Supplementary Information

The online version contains supplementary material available at xxxx

Acknowledgements

The authors want to thank Wera Collisi for conducting the cytotoxicity and antimicrobial assays, Kirsten Harmrolfs and Esther Surges for performing the NMR spectroscopic measurements, and Aileen Gollasch for recording HRESIMS data. N.A.L.-L.is grateful for a PhD stipend grant (program ID 57552340) from the German Academic Exchange Service (DAAD). We express our sincere gratitude to the late Soleiman Helaly and the Alexander von Humboldt Foundation, supporting him with a scholarship. This work was supported by funds of the Landwirtschaftliche Rentenbank, Germany. *C. elegans* strain N2 was provided by the Caenorhabditis Genetics Center (CGC), which is funded by the National Institute of Health (NIH) Office of Research Infrastructure Programs (P40 OD010440). Funding from the European Union's Horizon 2020 research and innovation program (RISE) under the Marie Skłodowska-Curie grant agreement No. 101008129, project acronym "Mycobiomics" to M.S. and J-P. W. is also gratefully acknowledged

Author contributions

Conceptualization: N.A.L.-L., J.-P.W., and M.S.; fungal isolation and identification: S. A. and W. M.; methodology, N.A.L.-L., J.-P. W., and J.M.; data curation and interpretation: N.A.L.-L., F.S, and J.-P.W.; visualization: N.A.L-L and F.S.; writing—original draft preparation: N.A.L.-L. and F.S.; writing—review and editing: N.A.L.-L. and M.S.; project administration: M. S.; funding acquisition: M. S. All authors have read and agreed on the published version of the manuscript.

Data availability

The data that support the findings of this study are available in the supplementary information of this article.

Declarations

Ethics approval and consent to participate

Not applicable.

Consent for publication

Not applicable.

Competing interests

The authors declare no conflicts of interest.

5 References

[1] Alberti F, Foster GD, Bailey AM. Natural products from filamentous fungi and production by heterologous expression. Appl Microbiol Biotechnol 2017;101:493–500. https://doi.org/10.1007/s00253-016-8034-2.

[2] Hyde KD, Xu J, Rapior S, Jeewon R, Lumyong S, Niego AGT et al.. The amazing potential of fungi: 50 ways we can exploit fungi industrially. Fungal Divers 2019;97:1–136. https://doi.org/10.1007/s13225-019-00430-9.

[3] Schrey H, Lambert C, Stadler M. Fungi: Pioneers of chemical creativity – Techniques and strategies to uncover fungal chemistry. IMA Fungus 2025;16:e142462. https://doi.org/10.3897/imafungus.16.142462.

[4] Wennrich JP, Ebada SS, Sepanian E, Holzenkamp C, Khalid SJ, Schrey H, Maier W, Mándi A, Kurtán T, Ashrafi S, Stadler M. Omnipolyphilins A and B: Chlorinated cyclotetrapeptides and naphtho-α-pyranones from the plant nematode-derived fungus *Polyphilus sieberi*. J Agric Food Chem 2024;72:6998–7009. https://doi.org/10.1021/acs.jafc.4c00572.

[5] Wennrich JP, Holzenkamp C, Kolařík M, Maier W, Mándi A, Kurtán T, Ashrafi S, Ebada SS, Stadler M. Dactylfungins and tetralones: Bioactive metabolites from a nematode-associated *Laburnicola nematophila*. J Nat Prod 2024;87:1860–71. https://doi.org/10.1021/acs.jnatprod.4c00623.

[6] Ashrafi S, Wennrich JP, Becker Y, Maciá-Vicente JG, Brißke-Rode A, Daub M, Thünen T, Dababat AA, Finckh MR, Stadler M, Maier W. *Polydomus karssenii* gen. nov. sp. nov. is a dark septate endophyte with a bifunctional lifestyle parasitising eggs of plant parasitic cyst nematodes (*Heterodera* spp.). IMA Fungus 2023;14:1–20. https://doi.org/10.1186/s43008-023-00113-w.

[7] Helaly SE, Ashrafi S, Teponno RB, Bernecker S, Dababat AA, Maier W, Stadler M. Nematicidal cyclic lipodepsipeptides and a xanthocillin derivative from a phaeosphariaceous fungus parasitizing eggs of the plant parasitic nematode *Heterodera filipjevi*. J Nat Prod 2018;81:2228–34. https://doi.org/10.1021/acs.jnatprod.8b00486.

[8] Wennrich JP, Sepanian E, Ebada SS, Llanos-Lopez NA, Ashrafi S, Maier W, Kurtán T, Stadler M. Bioactive naphtho-α-pyranones from two endophytic fungi of the Genus *Polyphilus*. Antibiotics 2023;12:1273. https://doi.org/10.3390/antibiotics12081273.

[9] Viehrig K, Surup F, Harmrolfs K, Jansen R, Kunze B, Müller R. Concerted action of P450 plus helper protein to form the amino-hydroxy-piperidone moiety of the potent protease inhibitor crocapeptin. J Am Chem Soc 2013;135:16885–94. https://doi.org/10.1021/ja4047153.

[10] Harms K, Surup F, Stadler M, Stchigel AM, Marin-felix Y. Morinagadepsin, a depsipeptide from the fungus *Morinagamyces vermicularis* gen. Et comb. nov. Microorganisms 2021;9:1191. https://doi.org/10.3390/microorganisms9061191.

[11] Phutthacharoen K, Llanos-López NA, Toshe R, Noisripoom W, Khonsanit A, Luangsa-ard JJ, Hyde KD, Ebada SS, Stadler M. Bioactive bioxanthracene and cyclodepsipeptides from the entomopathogenic fungus *Blackwellomyces roseostromatus* BCC56290. Antibiotics 2024;13:585. https://doi.org/10.3390/antibiotics13070585.

[12] Schneider-Orelli O. Entomologisches Praktikum. Einführung in die land-und forstwirtschaftliche Insektenkunde. 2., erw. A. Aarau : H. R. Sauerländer; 1947.

[13] Kim HW, Lee JW, Shim SH. Biosynthesis, biological activities, and structure-activity relationships of decalin-containing tetramic acid derivatives isolated from fungi. Nat Prod Rep 2024;41:1294–317. https://doi.org/10.1039/d4np00013g.

[14] Jeong YC, Moloney MG. Synthesis of and tautomerism in 3-acyltetramic acids. J Org Chem 2011;76:1342–54. https://doi.org/10.1021/jo102304y.

[15] Inokoshi J, Shigeta N, Fukuda T, Uchida R, Nonaka K, Masuma R, Tomoda H. Epi-trichosetin, a new undecaprenyl pyrophosphate synthase inhibitor, produced by *Fusarium oxysporum* FKI-4553. J Antibiot (Tokyo) 2013;66:549–54. https://doi.org/10.1038/ja.2013.44.

[16] Halecker S, Surup F, Kuhnert E, Mohr KI, Brock NL, Dickschat JS, Junker C, Schulz B, Stadler M. Hymenosetin, a 3-decalinoyltetramic acid antibiotic from cultures of the ash dieback pathogen, *Hymenoscyphus pseudoalbidus*. Phytochemistry 2014;100:86–91. https://doi.org/10.1016/j.phytochem.2014.01.018.

[17] Demir Ö, Zeng H, Schulz B, Schrey H, Steinert M, Stadler M, Surup F. Bioactive compounds from an endophytic *Pezicula* sp. showing antagonistic effects against the Ash Dieback pathogen. Biomolecules 2023;13:1632. https://doi.org/10.3390/biom13111632.

[18] Primahana G, Narmani A, Surup F, Teponno RB, Arzanlou M, Stadler M. Five tetramic acid derivatives isolated from the Iranian fungus *Colpoma quercinum* CCTU A372. Biomolecules 2021;11:783. https://doi.org/10.3390/biom11060783.

[19] Matsumori N, Kaneno D, Murata M, Nakamura H, Tachibana K. Stereochemical determination of acyclic structures based on carbon-proton spin-coupling constants. A method of configuration analysis for natural products. J Org Chem 1999;64:866–76. https://doi.org/10.1021/jo981810k.

[20] Oba M, Koguchi S, Nishiyama K. A concise diastereoselective synthesis of (2S,3S,4R)-3,4-dihydroxyglutamic acid. Tetrahedron Lett 2001;42:5901–2. https://doi.org/10.1016/S0040-4039(01)01120-0.

[21] Oba M, Koguchi S, Nishiyama K. Asymmetric synthesis of 3,4-dihydroxyglutamic acids via enantioselective reduction of cyclic *meso*-imide. Tetrahedron 2004;60:8089–92. https://doi.org/10.1016/j.tet.2004.06.109.

[22] Seco JM, Quiñoá E, Riguera R. Assignment of the absolute configuration of polyfunctional compounds by NMR using chiral derivatizing agents. Chem Rev 2012;112:4603–41. https://doi.org/10.1021/cr2003344.

[23] Han J, Liu C, Li L, Zhou H, Liu L, Bao L, Chen Q, Song F, Zhang L, Li E, Liu L, Pei Y, Jin C, Xue Y, Yin W, Ma Y, Liu H. Decalin-containing tetramic acids and 4-hydroxy-2-pyridones with antimicrobial and cytotoxic activity from the fungus *Coniochaeta cephalothecoides* collected in tibetan plateau (Medog). J Org Chem 2017;82:11474–86. https://doi.org/10.1021/acs.joc.7b02010.

[24] Kaur A, Rogers KD, Swenson DE, Dowd PF, Wicklow DT, Gloer JB. Bioactive natural products from fungicolous Hawaiian isolates: secondary metabolites from a *Phialemoniopsis* sp. Mycology 2014;5:120–9. https://doi.org/10.1080/21501203.2014.931309.

[25] Song T, Chen M, Chai W, Zhang Z, Lian XY. New bioactive pyrrospirones C−I from a marine-derived fungus *Penicillium* sp. ZZ380. Tetrahedron 2018;74:884–91. https://doi.org/10.1016/j.tet.2018.01.015.

[26] Wang X, Gong X, Li P, Lai D, Zhou L. Structural diversity and biological activities of cyclic depsipeptides from fungi. Molecules 2018;23:169. https://doi.org/10.3390/molecules23010169.

[27] Haritakun R, Sappan M, Suvannakad R, Tasanathai K, Isaka M. An antimycobacterial cyclodepsipeptide from the entomopathogenic fungus *Ophiocordyceps communis* BCC 16475. J Nat Prod 2010;73:75–8. https://doi.org/10.1021/np900520b.

[28] Liang M, Lyu HN, Ma ZY, Li EW, Cai L, Yin WB. Genomics-driven discovery of a new cyclodepsipeptide from the guanophilic fungus *Amphichorda guana*. Org Biomol Chem 2021;19:1960–4. https://doi.org/10.1039/D1OB00100K.

[29] Liu SX, Ou-Yang SY, Lu YF, Guo CL, Dai SY, Li C, Yu TY, Pei YH. Recent advances on cyclodepsipeptides: biologically active compounds for drug research. Front Microbiol 2023;14:1276928. https://doi.org/10.3389/fmicb.2023.1276928.

[30] Yan L, Banuelos CA, Mawji NR, Patrick BO, Sadar MD, Andersen RJ. Structure-activity relationships for the marine natural product sintokamides: Androgen receptor N-terminus antagonists of interest for

treatment of metastatic castration-resistant prostate cancer. J Nat Prod 2021;84:797–813. https://doi.org/10.1021/acs.jnatprod.0c00921.

[31] Kato N, Ebihara K, Nogawa T, Futamura Y, Inaba K, Okano A, Aono H, Fujikawa Y, Inoue H, Matsuda K, Osada H, Niwa R, Takahashi S. cis-Decalin-containing tetramic acids as inhibitors of insect steroidogenic glutathione S-transferase Noppera-bo. PLoS One 2023;18:e0290851. https://doi.org/10.1371/journal.pone.0290851.

[32] Nguyen VT, Yu NH, Lee Y, Hwang IM, Bui HX, Kim JC. Nematicidal activity of cyclopiazonic acid derived from *Penicillium commune* against root-knot nematodes and optimization of the culture fermentation process. Front Microbiol 2021;12:726504. https://doi.org/10.3389/fmicb.2021.726504.

[33] Lee HR, Lee SC, Lee JE, Seo SM, Jeong YC, Jung CS, Moloney MG, Park IK. Nematicidal activity of 3-acyltetramic acid analogues against pine wood nematode, *Bursaphelenchus xylophilus*. Molecules 2017;22:1568. https://doi.org/10.3390/molecules22091568.

[34] Ohyama M, Okada Y, Takahashi M, Sakanaka O, Matsumoto M, Atsumi K. Structure-activity relationship of anthelmintic cyclooctadepsipeptides. Biosci Biotechnol Biochem 2011;75:1354–63. https://doi.org/10.1271/bbb.110129.

[35] Sasaki T, Takagi M, Yaguchi T, Miyadoh S, Okada T, Koyama M. A new anthelmintic cyclodepsipeptide, PF1022A. J Antibiot (Tokyo) 1992;45:692–7. https://doi.org/10.7164/antibiotics.45.692.

[36] Wittstein K, Cordsmeier A, Lambert C, Wendt L, Sir EB, Weber J, Wurzler N, Petrini LE, Stadler M. Identification of *Rosellinia* species as producers of cyclodepsipeptide PF1022 A and resurrection of the genus *Dematophora* as inferred from polythetic taxonomy. Stud Mycol 2020;96:1–16. https://doi.org/10.1016/j.simyco.2020.01.001.

[37] Krücken J, Harder A, Jeschke P, Holden-Dye L, O'Connor V, Welz C, Von Samson-Himmelstjerna G. Anthelmintic cyclcooctadepsipeptides: Complex in structure and mode of action. Trends Parasitol 2012;28:385–94. https://doi.org/10.1016/j.pt.2012.06.005.

[38] Krücken J, Holden-Dye L, Keiser J, Prichard RK, Townson S, Makepeace BL, Hübner MP, Hahnel SR, Scandale I, Harder A, Kulke D. Development of emodepside as a possible adulticidal treatment for human onchocerciasis-The fruit of a successful industrial-academic collaboration. PLoS Pathog 2021;17:e1009682. https://doi.org/10.1371/journal.ppat.1009682.

[39] Farah HI, Supratman U, Hidayat AT, Maharani R. An Overview of the Synthesis of Biologically Active Cyclodepsipeptides. ChemistrySelect 2022;7:e202103470. https://doi.org/10.1002/slct.202103470.

[40] Gogineni V, Hamann MT. Marine natural product peptides with therapeutic potential: Chemistry, biosynthesis, and pharmacology. Biochim Biophys Acta - Gen Subj 2018;1862:81–196. https://doi.org/10.1016/j.bbagen.2017.08.014.

[41] Sivanathan S, Scherkenbeck J. Cyclodepsipeptides: A rich source of biologically active compounds for drug research. Molecules 2014;19:12368–420. https://doi.org/10.3390/molecules190812368.

[42] Lopes Hasuda A, Bracarense APFRL. Toxicity of the emerging mycotoxins beauvericin and enniatins: A mini-review. Toxicon 2024;239:107534. https://doi.org/10.1016/j.toxicon.2023.107534.

[43] Taevernier L, Detroyer S, Veryser L, De Spiegeleer B. Enniatin-containing solutions for oromucosal use: Quality-by-design *ex-vivo* transmucosal risk assessment of composition variability. Int J Pharm 2015;491:144–51. https://doi.org/10.1016/j.ijpharm.2015.06.029.

[44] Mo X, Gulder TAM. Biosynthetic strategies for tetramic acid formation. Nat Prod Rep 2021;38:1555–66. https://doi.org/10.1039/d0np00099j.

[45] Jiang M, Chen S, Li J, Liu L. The biological and chemical diversity of tetramic acid compounds from marine-derived microorganisms. Mar Drugs 2020;18:114. https://doi.org/10.3390/md18020114.

[46] Graupner PR, Carr A, Clancy E, Gilbert J, Bailey KL, Derby JA, Gerwick BC. The macrocidins: Novel cyclic tetramic acids with herbicidal activity produced by *Phoma macrostoma*. J Nat Prod 2003;66:1558–61. https://doi.org/10.1021/np030193e.

[47] Toshe R, Khalid SJ, Kemkuignou BM, Charria-Girón E, Eckhardt P, Sandargo B, Nuchthien K, Luangsa-

Ard JJ, Opatz T, Schrey H, Ebada SS, Stadler M. Antibiofilm and cytotoxic metabolites from the entomopathogenic fungus *Samsoniella aurantia*. Beilstein J Org Chem 2025;21:327–39. https://doi.org/10.3762/bjoc.21.23.

[48] Charria-Girón E, Zeng H, Gorelik TE, Pahl A, Truong KN, Schrey H, Surup F, Marin-Felix Y. Arcopilins: A new family of *Staphylococcus aureus* biofilm disruptors from the soil fungus *Arcopilus navicularis*. J Med Chem 2024;67:15029–40. https://doi.org/10.1021/acs.jmedchem.4c00585.

[49] Bai WJ, Lu C, Wang X. Recent advances in the total synthesis of tetramic acid-containing natural products. J Chem 2016;2016:8510278. https://doi.org/10.1155/2016/8510278.

[50] Wongkanoun S, Charria-Girón E, Cedeño-Sanchez M, Chainuwong B, Somrithipol S, Kuhnert E, Srikitikulchai P, Pornputtapong N, Surup F, Luangsa-ard J, Stadler M. *Hypoxylon luteogranulatum* (Hypoxylaceae, Xylariales), a novel species from Thailand with distinct chemical and ecological traits. Mycology 2025:1–19. https://doi.org/10.1080/21501203.2024.2435979.

[51] Halo LM, Heneghan MN, Yakasai AA, Song Z, Williams K, Bailey AM, Cox RJ, Lazarus CM, Simpson TJ. Late stage oxidations during the biosynthesis of the 2-pyridone tenellin in the entomopathogenic fungus *Beauveria bassiana*. J Am Chem Soc 2008;130:17988–96. https://doi.org/10.1021/ja807052c.

[52] Halecker S, Surup F, Kuhnert E, Mohr KI, Brock NL, Dickschat JS, Junker C, Schulz B, Stadler M. Hymenosetin, a 3-decalinoyltetramic acid antibiotic from cultures of the ash dieback pathogen, *Hymenoscyphus pseudoalbidus*. Phytochemistry 2014;100:86–91. https://doi.org/10.1016/j.phytochem.2014.01.018.

[53] Burmeister HR, Bennett GA, Vesonder RF, Hesseltine CW. Antibiotic produced by *Fusarium equiseti* NRRL 5537. Antimicrob Agents Chemother 1974;5:634–9. https://doi.org/10.1128/AAC.5.6.634.

[54] Zhao D, Han X, Wang D, Liu M, Gou J, Peng Y, Liu J, Li Y, Cao F, Zhang C. Bioactive 3-decalinoyltetramic acids derivatives from a marine-derived strain of the fungus *Fusarium equiseti* D39. Front Microbiol 2019;10:458965. https://doi.org/10.3389/fmicb.2019.01285.

[55] Hazuda D, Blau CU, Felock P, Hastings J, Pramanik B, Wolfe A, Bushman F, Farnet C, Goetz M, Williams M, Silverman K, Lingham R, Singh S. Isolation and characterization of novel human immunodeficiency virus integrase inhibitors from fungal metabolites. Antivir Chem Chemother 1999;10:63–70. https://doi.org/10.1177/095632029901000202.

[56] Marfori EC, Kajiyama S, Fukusaki EI, Kobayashi A. Trichosetin, a novel tetramic acid antibiotic produced in dual culture of *Trichoderma harzianum* and *Catharanthus roseus callus*. Z Naturforsch C 2002;57:465–70. https://doi.org/10.1515/znc-2002-5-611.

[57] Neumann K, Kehraus S, Gütschow M, König GM. Cytotoxic and HLE-inhibitory tetramic acid derivatives from marine-derived fungi. Nat Prod Commun 2009;4:347–54. https://doi.org/10.1177/1934578x0900400308.

[58] Yang SW, Mierzwa R, Terracciano J, Patel M, Gullo V, Wagner N, Baroudy B, Puar M, Chan TM, Chu M. Sch 213766, a novel chemokine receptor CCR-5 inhibitor from *Chaetomium globosum*. J Antibiot (Tokyo) 2007;60:524–8. https://doi.org/10.1038/ja.2007.67.

[59] Yang SW, Mierzwa R, Terracciano J, Patel M, Gullo V, Wagner N, Baroudy B, Puar M, Chan TM, McPhail AT, Chu M. Chemokine receptor CCR-5 inhibitors produced by *Chaetomium globosum*. J Nat Prod 2006;69:1025–8. https://doi.org/10.1021/np060121y.

Publication IV

Bioactive Naphtho-α-Pyranones from Two Endophytic Fungi of the Genus *Polyphilus*

Jan-Peer Wennrich[1,2], Ellen Sepanian[1], Sherif S. Ebada[1,3,*], **Natalia A. Llanos-Lopez[1,2]**, Samad Ashrafi[4,5], Wolfgang Maier[4], Tibor Kurtán[6] and Marc Stadler[1,2,*]

[1] Department of Microbial Drugs, Helmholtz Centre for Infection Research (HZI), Inhoffenstrasse 7, 38124 Braunschweig, Germany.

[2] Institute of Microbiology, Technische Universität Braunschweig, Spielmannstraße 7, 38106 Braunschweig, Germany.

[3] Department of Pharmacognosy, Faculty of Pharmacy, Ain Shams University, Cairo 11566, Egypt.

[4] Institute for Epidemiology and Pathogen Diagnostics, Julius Kühn Institute (JKI)—Federal Research Centre for Cultivated Plants, Messeweg 11-12, 38104 Braunschweig, Germany.

[5] Institute for Crop and Soil Science, Julius Kühn Institute (JKI)—Federal Research Centre for Cultivated Plants, Bundesallee 58, 38116 Braunschweig, Germany.

[6] Department of Organic Chemistry, University of Debrecen, P.O. Box 400, 4002 Debrecen, Hungary.

* Corresponding author.

Antibiotics 2023, 12(8): 1273. https://doi.org/10.3390/antibiotics12081273.

antibiotics

MDPI

Article

Bioactive Naphtho-α-Pyranones from Two Endophytic Fungi of the Genus *Polyphilus*

Jan-Peer Wennrich [1,2], Ellen Sepanian [1], Sherif S. Ebada [1,3,*], Natalia A. Llanos-Lopez [1], Samad Ashrafi [4,5], Wolfgang Maier [4], Tibor Kurtán [6] and Marc Stadler [1,2,*]

1 Department of Microbial Drugs, Helmholtz Centre for Infection Research (HZI), Inhoffenstrasse 7, 38124 Braunschweig, Germany; jan-peer.wennrich@helmholtz-hzi.de (J.-P.W.); ellen.sepanian@gmail.com (E.S.); natalia.llanos@helmholtz-hzi.de (N.A.L.-L.)
2 Institute of Microbiology, Technische Universität Braunschweig, Spielmannstraße 7, 38106 Braunschweig, Germany
3 Department of Pharmacognosy, Faculty of Pharmacy, Ain Shams University, Cairo 11566, Egypt
4 Institute for Epidemiology and Pathogen Diagnostics, Julius Kühn Institute (JKI)—Federal Research Centre for Cultivated Plants, Messeweg 11-12, 38104 Braunschweig, Germany; samad.ashrafi@julius-kuehn.de (S.A.); wolfgang.maier@julius-kuehn.de (W.M.)
5 Institute for Crop and Soil Science, Julius Kühn Institute (JKI)—Federal Research Centre for Cultivated Plants, Bundesallee 58, 38116 Braunschweig, Germany
6 Department of Organic Chemistry, University of Debrecen, P.O. Box 400, 4002 Debrecen, Hungary; kurtan.tibor@science.unideb.hu
* Correspondence: sherif.elsayed@helmholtz-hzi.de or sherif_elsayed@pharma.asu.edu.eg (S.S.E.); marc.stadler@helmholtz-hzi.de (M.S.); Tel.: +49-531-6181-4240 (M.S.)

Abstract: In the course of our survey to study the metabolic potential of two species of a new helotialean genus *Polyphilus*, namely *P. frankenii* and *P. sieberi*, their crude extracts were obtained using different cultivation techniques, which led to the isolation and characterization of two new naphtho-α-pyranone derivatives recognized as a monomer (**1**) and its 6,6′-homodimer (**2**) together with two known diketopiperazine congeners, outovirin B (**3**) and (3*S*,6*S*)-3,6-dibenzylpiperazine-2,5-dione (**4**). The structures of isolated compounds were determined based on extensive 1D and 2D NMR and HRESIMS. The absolute configuration of new naphtho-α-pyranones was determined using a comparison of their experimental ECD spectra with those of related structural analogues. 6,6′-binaphtho-α-pyranone talaroderxine C (**2**) exhibited potent cytotoxic activity against different mammalian cell lines with IC_{50} values in the low micromolar to nanomolar range. In addition, talaroderxine C unveiled stronger antimicrobial activity against *Bacillus subtilis* rather than *Staphylococcus aureus* with MIC values of 0.52 μg mL^{-1} (0.83 μM) compared to 66.6 μg mL^{-1} (105.70 μM), respectively.

Keywords: *Polyphilus*; Helotiales; Ascomycota; naphthopyranones; antimicrobial

Citation: Wennrich, J.-P.; Sepanian, E.; Ebada, S.S.; Llanos-Lopez, N.A.; Ashrafi, S.; Maier, W.; Kurtán, T.; Stadler, M. Bioactive Naphtho-α-Pyranones from Two Endophytic Fungi of the Genus *Polyphilus*. *Antibiotics* **2023**, *12*, 1273. https://doi.org/10.3390/antibiotics12081273

Academic Editor: Manuel Simões

Received: 17 July 2023
Revised: 29 July 2023
Accepted: 31 July 2023
Published: 2 August 2023

1. Introduction

Naphtho-α-pyranones comprise a unique class of fungal metabolites that have been reported as monomers, such as semiviriditoxin [1–3], semivioxanthin [1–3], and penicitor A [4] and its 7-*O*-methyl derivative [5]. In addition, naptho-α-pyranone dimers have been firstly reported as "mycotoxins", such as viriditoxin [6] followed by several other symmetric dimers featuring either 6,6′-linkages, such as asteromine [7], talaroderxines [8], pigmentosins [9,10], and aschernaphtopyrone A [11], or 8,8′-linkages, such as vioxanthin [12,13], mycopyranone [14], aschernaphtopyrone B [11], and lichenocholin A [15].

A rare 5,8′-linkage was also recently reported in lulworthinone obtained from a marine-derived fungus: *Lulworthia medusa* [16]. Several members of the dimer class have been reported to exhibit potential antibacterial activity. In particular, viriditioxin has been reported to inhibit FtsZ, which is essential for bacterial cell division [17]. Based on the fact

been reported to exhibit potential antibacterial activity. In particular, viriditioxin has been reported to inhibit FtsZ, which is essential for bacterial cell division [17]. Based on the fact that antibiotic resistance is an exacerbating problem, the need for new antimicrobial agents remains an unmet demand.

During our ongoing research targeting the discovery of new fungal metabolites with potential antimicrobial activities, in this study, we investigated the root endophytic representatives of the recently described fungal genus *Polyphilus*, namely *P. frankenii* and *P. sieberi* [18]. The chemical exploration resulted in the isolation and identification of a monomer (**1**) and its symmetric 6,6′-homodimer (**2**) (Figure 1) together with two known metabolites identified as outovirin B (**3**) [19] and (3*S*,6*S*)-3,6-dibenzylpiperazine-2,5-dione (**4**) [20]. In this study, we report the isolation and structure elucidation of two new naphtho-*α*-pyranone derivatives together with their antimicrobial and cytotoxic activity, which were recorded in our routine assays.

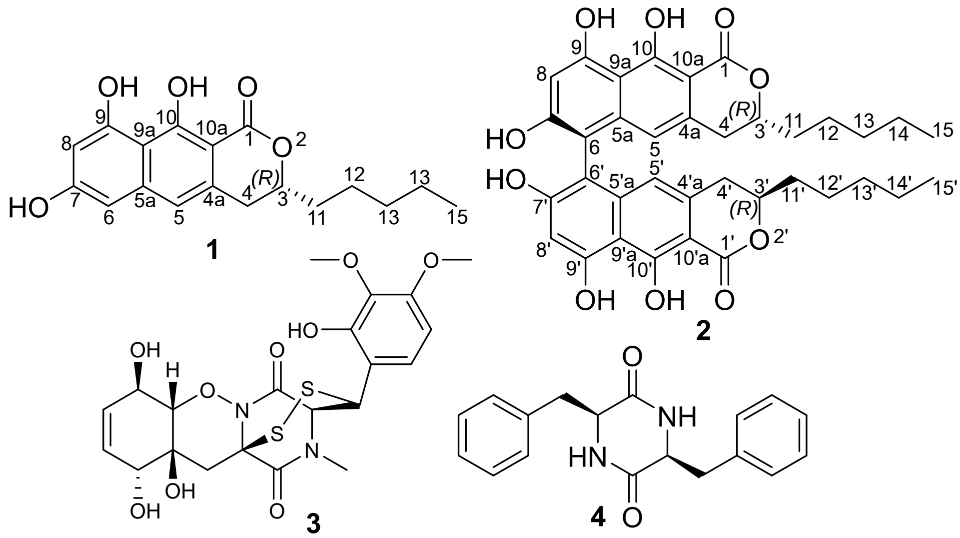

Figure 1. Chemical structures of **1**–**4**.

2. Results and Discussion

*2.1. Isolation and Identification of Compounds (**1** and **2**)*

Compound **1** was purified as a white solid powder, and its molecular formula was established to be $C_{18}H_{20}O_5$ based on its HRESIMS spectrum, which revealed pseudomolecular ion peaks at *m/z* 317.1386 $[M+H]^+$ (calculated for 317.1384) and at *m/z* 339.1202 $[M+Na]^+$ (calculated for 339.1203), indicating the existence of nine degrees of unsaturation. The ^{13}C NMR spectral data of **1** (Table 1) displayed the presence of fifteen carbon resonances that can be differentiated into eight quaternary carbon atoms recognized as one carbonyl at δ_C 170.7 (C-1) and seven olefinic (two oxygenated) carbon atoms at δ_C 162.8 (C-10), 161.0 (C-7), 160.7 (C-9), 140.6 (C-5a), 133.9 (C-4a), 107.2 (C-9a) and 98.8 (C-10a). In addition, the ^{13}C NMR spectrum of **1** also revealed the presence of four tertiary (one aliphatic and three olefinic) carbon atoms at δ_C 114.5 (C-5), 101.5 (C-8), 101.4 (C-6), and 79.3 (C-3) along with four methylenes (δ_C 34.0 (C-11), 32.3 (C-4), 31.0 (C-13), 22.5 (C-14)) and one methyl carbon along δ_C 13.7 (C-15). By comparing the obtained results with the reported literature, compound **1** was suggested to be a naphtho-pyrone derivative related to those reported as fungal metabolites, such as pernicopyrone A [4,5], semiviriditoxin [1,2], and semivioxanthin [3]. Further structural features of **1** were concluded using 2D NMR spectra including ^1H-^1H COSY, HMBC, and HSQC. The ^1H-^1H COSY spectrum of **1** revealed two main spin systems, with one extending over two *meta*-positioned aromatic protons at δ_H 6.51 (H-6) and 6.47 (H-8) while the second spin system was found to begin at a methylene group at δ_H 2.88/δ_H 3.00 (H_2-4) and extended to an aliphatic oxygenated methine group at δ_H 4.58 (H-3), thus extending over four methylenes forming an aliphatic side chain at δ_H 1.68/δ_H 1.74 (H_2-11), δ_H 1.41/δ_H 1.46 (H_2-12), and δ_H 1.31 (H_2-14 and H_2-13), and ending with a terminal triplet methyl group at δ_H 0.88 (H_3-15) to confirm the presence of

the *n*-pentyl side chain. The HMBC spectrum of **1** (Figure 2) revealed key correlations from H_2-4 to four carbon atoms ascribed to C-10a (δ_C 98.8), C-4a (δ_C 133.9), C-3 (δ_C 79.3), and C-11 (δ_C 34.0), whereas additional HMBC correlations from H_2-11 to C-3 confirmed that the *n*-pentyl side chain was present at C-3. Further key HMBC correlations (Figure 2) were also observed in the aromatic protons from H-5, H-6, and H-8 to C-9a (δ_C 107.2) and from H-5 and H_2-4 to C-10a, which confirmed the depicted structure of **1** as a naphthopyrone derivative. The ECD spectrum of **1** (see Supplementary Materials: Figure S9) showed negative Cotton effects (CEs) at 219 nm and 267 nm, a weaker positive one at 242 nm, and a broad positive plateau within the range of 280-400. This ECD spectrum was a near mirror image of that of (*S*)-7-*O*-methylpenicitor A [5], which differed only in the C-9 and C-14 methoxy groups, and its absolute configuration (AC) was determined using ECD calculations and single-crystal X-ray diffraction analysis. Due to the mirror image ECD curves, the AC of **1** was assigned as (*R*), and as a new naphthopyrone derivative, it was given the trivial name semitalaroderxine C.

Table 1. ^{1}H and ^{13}C NMR data of **1** and **2**.

	1			**2**	
Pos.	**δ_H (Multi, *J*(Hz)) [a]**	**δ_C, Type [b,c]**	**Pos.**	**δ_H (Multi, *J*(Hz)) [a]**	**δ_C, Type [b,c]**
1		170.7, CO	1/1′		170.6, CO
3	4.58, m	79.3, CH	3/3′	4.50, m	79.4, CH
4	α 2.88, dd, (15.6, 11.1) β 3.00, br d, (15.6)	32.3, CH_2	4/4′	α 2.72, dd, (16.2, 11.0) β 2.81, dd, (16.5, 3.1)	32.5, CH_2
4a		133.9, C	4a/4′a		133.6, C
5	6.82, s	114.5, CH	5/5′	6.20, s	112.7, CH
5a		140.6, C	5a/5′a		139.9, C
6	6.31, s	101.4, CH	6/6′		107.7, C
7		161.0, C, C	7/7′		157.8, C
8	6.47, s	101.5, CH	8/8′	6.57, s	101.6, CH
9		160.7, C	9/9′		158.9, C
9a		107.2, C	9a/9′a		107.7, C
10		162.6, C	10/10′		163.2, C
10a		98.8, C	10a/10′a		98.7, C
11	α 1.68, m β 1.74, m	34.0, CH_2	11/11′	α 1.57, ddd, (14.2, 10.8, 5.6) β 1.66, m	34.1, CH_2
12	α 1.41, m; β 1.46, m	24.0, CH_2	12/12′	1.36, m (2H)	23.9, CH_2
13	1.31, m, 2H	31.0, CH_2	13/13′	1.23, m (2H)	31.0, CH_2
14	1.31, m, 2H	22.0, CH_2	14/14′	1.25, m (2H)	22.0, CH_2
15	0.88, t, (7.0)	13.9, CH_3	15/15′	0.84, t (6.8, 3H)	13.9, CH_3
7-O*H*	10.11, br s		7-O*H*	10.17, br s	
9-O*H*	9.66, br s		9-O*H*	9.65, s	
10-O*H*	13.35, br s		10-O*H*	13.43, br s	

Measured in DMSO-d_6 [a] at 500 MHz/[b] at 125 MHz. [c] Assigned based on HMBC and HSQC spectra.

nm and 267 nm, a weaker positive one at 242 nm, and a broad positive plateau within the range of 280-400. This ECD spectrum was a near mirror image of that of (*S*)-7-*O*-methylpenicitor A [5], which differed only in the C-9 and C-14 methoxy groups, and its absolute configuration (AC) was determined using ECD calculations and single-crystal X-ray diffraction analysis. Due to the mirror image ECD curves, the AC of **1** was assigned as (*R*), and as a new naphthopyrone derivative, it was given the trivial name semitalaroderxine C.

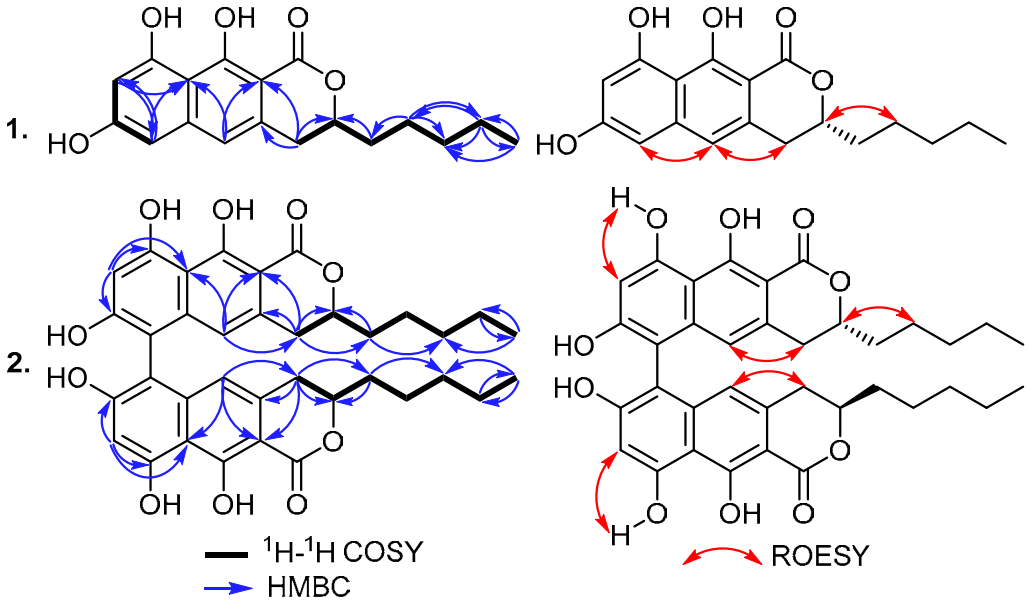

Figure 2. Key COSY, HMBC, and ROESY correlations of **1** and **2**.

Compound **2** was isolated as a white solid powder that revealed in a pseudomolecular ion peak at *m*/*z* 631.2541 $[M+H]^+$ (calculated for 631.2538) its HRESIMS spectrum, confirming its molecular formula as $C_{36}H_{38}O_{10}$ and indicating its inclusion of eighteen degrees of unsaturation. Intriguingly, by comparing the molecular formulas of **1** and **2**, it could be obviously observed that **2** is a symmetric dimer of the two monomers of **1**. This assumption was further confirmed using ^{13}C NMR spectral data (Table 1), which revealed only eighteen carbon resonances (instead of thirty-six), each of which was assigned to two electromagnetically equivalent carbon atoms in the two monomers. The ^{1}H NMR spectral data of **2** (Table 1) displayed an identical set of proton resonances to those of **1**, except in the absence of one aromatic proton at δ_H 6.31 (H-6) in **1** and hence suggesting that compound **2** is a 6,6′-binaphthopyrone dimer of semitalaroderxine C (**1**). Based on the obtained results and by searching the reported literature, compound **2** was found to be related to the previously reported 6,6′-binaphthopyrone dimers, talaroderxines A and B, that were reported from a soil-derived fungus *Talaromyces derxii* [8] and pigmentosins A/B [10,21].

Table 1. ^{1}H and ^{13}C NMR data of **1** and **2**.

	1				**2**			
Pos.	δ_H **(Multi; *J* (Hz))** [a]	δ_C	**Type** [b,c]	**Pos.**	δ_H **(Multi; *J* (Hz))** [a]	δ_C	**Type** [b,c]
1		170.7	CO	1/1′		170.6	CO
3	4.58, m	79.3	CH	3/3′	4.57, m	79.4	CH
4	α 2.88, dd, (15.6; 11.1) β 3.00, br d, (15.6)	32.3	CH_2	4/4′	α 2.72, dd, (16.2; 11.0) β 2.81, dd, (16.3; 3.1)	32.5	CH_2
4a		133.9	C	4a/4′a		133.6	C
5	6.82, s	114.5	CH	5/5′	6.20, s	112.7	CH
5a		140.6	C	5a/5′a		139.9	C
6		101.4	CH	6/6′		107.7	C
7		161.0	C	7/7′		157.8	C
8	6.47, s	101.5	CH	8/8′	6.57, s	101.6	CH

The major structural difference between **2** and talaroderxines A/B was the presence of *n*-pentyl in **2** instead of the *n*-propyl side chain in talaroderxines A/B. Since compound **2** is the 6,6′-linked axially chiral homodimer of **1**, the (3*S*,3′*S*) absolute configuration of the central chirality elements was deduced on the basis of their common biosynthetic origin. The (a*S*) axial chirality of **2**, arising from the hindered rotation around the C-6-C-6′ biaryl axis, was determined by comparing its experimental ECD spectrum (see Supplementary Materials Figure S18) with those of related 6,6′-linked *bis*-naphthopyrone pigmentosins A and B [10] and talaroderxine A [8]. Compound **2** showed an intense positive exciton-coupled couplet centered at 260 nm (268 nm ($\Delta\varepsilon$: +16.58); 252 nm ($\Delta\varepsilon$: −14.15)), which was a mirror image of the negative couplet of (a*R*)-pigmentosins A and B and (a*R*)-talaroderxine B [8–10]. Compound **2** was identified as a new 6,6′-linked *bis*-naphthopyrone homodimer with (a*S*) axial chirality, which was named talaroderxine C.

2.2. Biological Assays

Due to the limited amounts of compounds **1**, **3**, and **4**, only talaroderxine C (**2**) was subjected to antimicrobial and cytotoxicity assays. Against all tested microorganisms, talaroderxine C disclosed potent antimicrobial activity against *Bacillus subtilis* with a minimal inhibitory concentration (MIC) of 0.52 µg/mL (0.83 µM). In the case of *Staphylococcus aureus*, it revealed moderate activity with an MIC of 66.6 µg/mL (105.70 µM). In addition, the obtained results of the cytotoxicity (3-(4,5-dimethylthiayol-2-yl)-2,5-diphenyltetrazolium

bromide, MTT) assay (Table 2) revealed that talaroderxine C (**2**) exhibits pan-cytotoxic activity against all tested cell lines, with IC_{50} values falling within the low micromolar to nanomolar range. In particular, against breast adenocarcinoma (MCF-7) cells, talaroderxine C revealed a high potency (IC_{50} = 68 nM). Nevertheless, outovirin B (**3**) is structurally recognized as a gliovirin-like compound [22] that was reported to exhibit selective antifungal and anti-inflammatory [23] and antitrypanosomal [24] and antimycobacterial [25] activities.

Table 2. Cytotoxic (IC_{50} in μM) activity results of talaroderxine C (**2**).

Compound	IC_{50}					
	L929	**KB3.1**	**A431**	**A549**	**PC-3**	**MCF-7**
Talaroderxine C (**2**) in μM	1.19	10.32	2.38	2.06	8.73	0.068
Epothilone B in nM	0.65	0.17	0.065	0.053	0.091	0.075

3. Materials and Methods

3.1. General Experimental Procedures

UV measurements were performed using a Shimadzu UV-VIS spectrophotometer UV-2450 (Shimadzu®, Kyoto, Japan), and ECD spectra were obtained using a Jasco J-815 spectropolarimeter (JASCO®, Pfungstadt, Germany). Optical rotation values were measured using a PerkinElmer 241 polarimeter at 20 °C (Anton-Paar Opto Tec GmbH, Seelze, Germany). High-resolution electrospray ionization mass spectra (HR-ESI-MS) were acquired using an Agilent 1200 Infinity Series HPLC-UV system (Agilent Technologies®, Santa Clara, CA, USA), utilizing a C_{18} Acquity UPLC BEH column (2.1 × 50 mm, 1.7 μm: Waters, Milford, MA, USA); solvent A: H_2O + 0.1% formic acid; solvent B: acetonitrile (MeCN) + 0.1% formic acid; gradient: 5% B for 0.5 min increasing to 100% B in 19.5 min and maintaining 100% B for 5 min at a flow rate of 0.6 mL min^{-1} (UV/Vis detection 190–600 nm) connected to a time-of-flight mass spectrometer (ESI-TOF-MS, Maxis, Bruker, Billerica, MA, USA) (scan range: 100–2500 m/z; rate 2: Hz; capillary voltage: 4500 V; dry temperature: 200 °C). NMR spectra were recorded using an Avance III 500 spectrometer (Bruker®, Billerica, MA, USA; ^{1}H-NMR: 500 MHz; ^{13}C-NMR: 125 MHz), dissolving compounds in deuterated methanol-d_4 and deuterated DMSO-d_6.

3.2. Fermentation, Extraction, and Isolation

The two fungal species explored in this study namely, *P. frankenii* strain V16 (DSM 106521) and *P. sieberi* strain Ref052 (DSM 106515) were recognized as endophytic fungi associated with the roots of *Pinus sylvetris* and *Asclepias syriaca* collected from Villerupt (France) and Bugac (Hungary), respectively. The fungi were maintained on a YM6.3 agar (D-glucose: 4 g L^{-1}; malt extract: 10 g L^{-1}: yeast extract: 4 g L^{-1}; agar: 20 g L^{-1}; pH adjusted to 6.3 and sterilized by autoclaving) at 23 °C. To prepare seed cultures for the following larger-scale cultivation, five mycelia plugs measuring 25 mm^2 were transferred to a 500 mL Erlenmeyer shaking flask containing 200 mL of Q6/2 media (D-glucose: 2.5 g L^{-1}; glycerine: 10 g L^{-1}; cotton seed flour: 5 g L^{-1}; pH: 7.2) and incubated at 23 °C and 140 min^{-1}. After achieving a sufficient amount of biomass, the culture broth was homogenized using Ultra-Turrax (T25 easy clean digital, IKA) equipped with an S25 N-25F dispersing tool at 10,000 rpm for 10 s. This seed culture was used for all following cultivations as an inoculum for YM6.3, BRFT, and WOFT media (K_2HPO_4: 0.5 g L^{-1}; sodium tartrate: 0.5 g L^{-1}; yeast extract: 1 g L^{-1}; 100 mL of solution was added to 28 g brown rice or whole oat and autoclaved).

3.2.1. Solid State Fermentation

Six Erlenmeyer culture flasks with BRFT and WOFT were inoculated with 6 mL of homogenized seed culture, mixed under sterile conditions, and incubated at room temperature for two, three, and four weeks in the dark. After the planned incubation time, the cultures were stopped by adding 250 mL of acetone, mixed with a spatula, and kept

in an ultrasonic bath for 30 min at 40 °C for extraction. The liquid was separated from the solid phase via filtration. The extraction was repeated twice using fresh acetone. The filtrate was evaporated under a vacuum at 40 °C in a rotary evaporator, and the remaining aqueous phase was filled up to 50 mL with distilled water and extracted with EtOAc (1:1) in a separatory funnel three times. The organic phase (EtOAc) was separated, evaporated under reduced pressure, and then dissolved again in 5 mL of MeOH and extracted again with 45 mL of heptane. Extraction was performed in a separatory funnel twice with fresh heptane. Both fractions (heptane and methanol) were evaporated to dryness.

3.2.2. Liquid Fermentation

In this study, 0.5% of the homogenized inoculum was transferred into twelve 2 L Erlenmeyer culture flasks containing 400 mL of YM6.3 medium. The content of glucose was monitored using test stripes (Medi-Test Glucose, Machery-Nagel®, Düren, Germany). Incubation was terminated after five days of glucose depletion. Mycelia and supernatant were separated using a Büchner funnel and a vacuum pump. The extraction of metabolites of the mycelia followed the procedure of solid-state fermentation. The culture broth was mixed with 2% AmberLite™ XAD™ 16N polymeric absorbent and stirred for 4 h on a magnetic stirrer. The extraction of metabolites was carried out with acetone under stirring. Afterward, the purification scheme followed the same steps as described above for solid-state extraction.

3.2.3. Analytical HPLC

The extracts obtained were dissolved in Acetone:MeOH (1:1) and adjusted to a concentration of 4.5 mg mL^{-1}. An injection volume of 2 µL was applied to an UltiMate® 3000 Series uHPLC (Thermo Fisher Scientific®, Waltman, MA, USA). Mass spectrometry was performed with a connected amaZon® speed ESI Iontrap MS (Amazon, Bruker). HRESIMS measurements were performed with sample concentrations of 1 mg mL^{-1} with an Agilent 1200 series HPLC-UV system in combination with an ESI-TOF-MS (Maxis, Bruker). The conditions were identical to the methods described before [26].

3.2.4. Isolation of Compounds

The mycelial extract of *Polyphilus sieberi* Ref052 (DSM 106515) cultivated in YM6.3 media (86 mg) was separated with a Reveleris® X2 flash chromatography system using a FlashPure ID Silica 12 g cartridge. The mobile phase consisted of three solvent mixtures supplemented with 0.1% formic acid: solvent A (heptane 100%), solvent B (heptane 58%, TBME 40%, and MeOH 2%), and solvent C (Acetone 37.5%, DCM 37.5%, and MeOH 25%); flow rate: 30 mL min^{-1}; gradient: 3 min B at 0%, increasing to 100% B in 10 min, maintaining 100% B for 5 min, switching to solvent mixture B and C, starting from 0% C and increasing to 100% C in 10 min, and maintaining 100% C for 10 min. All the following flash chromatographic separations were performed, implementing the same conditions. The separation led to the purification of **1** (1.1 mg; t_R = 8.5 min).

The second *Polyphilus frankenii* V16 (DSM 106521) strain was cultivated in BRFT and WOFT media. Due to the high similarity observed in ESI-MS profiles for 2–4 weeks, the extracts were combined to yield a crude extract (672 mg) and subjected to the Reveleris© X2 equipped with a FlashPure ID Silica 24 g cartridge. Further purification steps of the resulting fraction 5 (49.2 mg, t_R = 13.5 min) were carried out on a Büchi Pure C-850 FlashPrep equipped with a Gemini C18 (250 × 21.2 mm, 10 µm; Phenomenex) (solvent A: H_2O + 0.1% formic acid; solvent B: MeCN + 0.1% formic acid; flow rate: 20 mL min^{-1}; gradient: 5 min maintaining 40% B, increasing B to 90% in 50 min, increasing to 100% B in 5 min, and maintaining 100% B for 10 min) led to the isolation of **2** (15.8 mg, t_R = 53.4 min). The mycelial extract of the cultivation in YM6.3 media was weighed at 35 mg, and it was purified on a Gilson PLC 2250 equipped with a Gemini C18 (250 × 21.2 mm, 10 µm; Phenomenex, Torrance, CA, USA) (solvent A: H_2O + 0.1% formic acid; solvent B: MeCN + 0.1% formic acid; flow rate: 20 mL min^{-1}; gradient: 10 min maintaining 5% B, increasing

B to 50% in 45 min, increasing to 100% B in 10 min, and maintaining 100% B for 10 min. This led to the isolation of known metabolites **3** (0.2 mg; t_R = 17.3 min) and **4** (0.2 mg; t_R = 27.5 min).

3.2.1 Semitalaroderxine C (**1**): white solid powder; 0.59 mg; $[\alpha]_D^{20}$ –7.5 (*c* 0.04, chloroform); UV/Vis (MeOH): λ_{max} (log ε) = 193.5 (0.8), 200.0 (0.9), 220.5 (1.0), 261.0 (2.7), 314.5 (0.2), 369.5 (0.6) nm; ECD ($c = 3.16 \times 10^{-4}$ M; MeOH) λ [nm], (Δε) 373 (1.4), 310 (1.0), 268 (−3.2), 243 (1.1), 218 (−4.6), 196 (4.2); NMR data (^{1}H NMR: 500 MHz, ^{13}C NMR: 125 MHz in DMSO-d_6) see Table 1; HR-(+)ESIMS: *m*/*z* 299.1277 $[M–H_2O+H]^+$ (calcd. 299.1278 for $C_{18}H_{19}O_4^+$), *m*/*z* 317.1386 $[M+H]^+$ (calcd. 317.1384 for $C_{18}H_{21}O_5^+$), 339.1203 $[M+Na]^+$ (calcd. 339.1203 for $C_{18}H_{20}NaO_5^+$), 655.2516 $[2M+Na]^+$ (calcd. 655.2514 for $C_{36}H_{40}NaO_{10}^+$).

3.2.2 Talaroderxine C (**2**): white solid powder; 3.49 mg; $[\alpha]_D^{20}$ +57.5 (*c* 1.0, DMSO-d_6); UV/Vis (MeOH): λ_{max} (log ε) = 223.0 (0.1), 265.5 (0.1), 376.5 (0.04) nm; ECD ($c = 3.17 \times 10^{-4}$ M; MeOH) λ [nm], (Δε) 268 (82.9), 252 (−70.7); NMR data (^{1}H NMR: 500 MHz, ^{13}C NMR: 125 MHz in DMSO-d_6) see Table 1; HR-(+)ESIMS: *m*/*z* 631.2541 $[M+H]^+$ (calcd. 631.2538 for $C_{36}H_{39}O_{10}^+$).

3.3. Antimicrobial Assay

Due to the limited amounts of compounds **1**, **3**, and **4**, only talaroderxine C (**2**) was assessed for their antimicrobial activity based on their minimum inhibitory concentration (MIC), following our previously reported protocol [26], against five pathogenic fungi, including *Candida albicans* DSM 1665, *Mucor hiemails* DSM 2656, *Pichia anomala* DSM 6766, *Rhodotorula glutinis* DSM 10134, and *Schizosaccharomyces pombe* DSM 70572; three Gram-positive bacteria, including *Bacillus subtilis* DSM 10, *Mycobacterium smegmatis* DSM ATCC 700084, and *Staphylococcus aureus* DSM 436; and four Gram-negative bacteria, including *Chromobacterium violaceum* DSM 30191, *Acinetobacter baumanii* DSM 30008, *Escherichia coli* DSM 1116, and *Pseudomonas aeruginosa* DSM PA14. Nystatin was used as an antifungal positive control, whereas oxytetracycline, ciprofloxacin, gentamycin, and kanamycin were used as positive controls against Gram-positive and Gram-negative bacteria.

3.4. Cytotoxicity Assay

The cytotoxicity (IC_{50}) of Talaroderxine C (**2**) was also tested using the MTT (3-(4,5-dimethylthiayol-2-yl)-2,5-diphenyltetrazolium bromide) test, following the experimental procedure described by Charria-Girón et al. [27]. These compounds were tested against seven mammalian cell lines, including human endocervical adenocarcinoma KB 3.1, breast cancer MCF-7, lung cancer A549, ovary cancer SK-OV-3, prostate cancer PC-3, squamous cancer A431, and mouse fibroblasts L929. Epothilone B was used as the positive control.

4. Conclusions

This represents the first study of secondary metabolites from the fungal genus *Polyphilus*. In summary, semitalaroderxine C (**1**), talaroderxine C (**2**), outovirin B (**3**), and (3*S*,6*S*)-3,6-dibenzylpiperazine-2,5-dione (**4**) could be isolated and elucidated where **1** and **2** are recognized among naphtha-*α*-pyranone congeners that are well-known for a vast array of bioactivities. Talaroderxine C showed potent antimicrobial activity against *Bacillus subtilis* with an MIC of 0.52 µg/mL. In addition, it exhibited pan-cytotoxic activity against all tested cell lines, with IC_{50} values falling in the low micromolar to nanomolar range. Talaroderxine C (**2**) showed high potency (IC_{50} = 68 nM), particularly against breast adenocarcinoma (MCF-7) cells. Due to the limited amounts of **3** and **4**, antimicrobial and cytotoxic activity assays were not determined, but the gliovirin-like compound [22], outovirin B (**3**), was reported to exhibit selective antifungal and anti-inflammatory [23] along with antitrypanosomal [24] and antimycobacterial [25] activities.

The strains of the genus *Polyphilus* arose from an attempt to find nematode antagonistic fungi that can be used as ecologically friendly alternatives to toxic chemicals and soil fumigants. Such biocontrol agents may turn out to be a valid alternative, especially as they are supposed to be host-specific and do not kill harmless organisms in the soil. However,

the results of the current study, which showed that *Polyphilus* strains can produce rather toxic secondary metabolites, should give rise to deprioritizing them over other strains that were encountered concurrently and that were devoid of toxic metabolites. Mycopesticides, which are mostly used against insects, already have an annual market share of ca. USD 550 million [28], and this is bound to increase further in the future. Nematode antagonists will probably obtain their share as they are one of the only environmentally friendly alternatives to chemical pesticides.

Supplementary Materials: The following supporting information can be downloaded at https://www.mdpi.com/article/10.3390/antibiotics12081273/s1. Tables S1 and S2: 2D NMR data of semi-talaroderxine C (**1**) and talaroderxine C (**2**); Figures S1–S4: LC-ESI-MS spectra of sole four-weeks mycelia extracts of *P. sieberi* or *P. frankenii* in different solid or liquid media; Figures S5–S14: HPLC, UV, LR-/HRESIMS, 1D/2D NMR, and ECD spectra of **1**; Figures S15–S24: HPLC, UV, LR-/HRESIMS, 1D/2D NMR, and ECD spectra of **2**; Figures S25–S30: HPLC and LR-/HRESIMS 1D/2D NMR spectra of **3**; Figures S31–S38: HPLC and LR-/HRESIMS 1D/2D NMR spectra of **4**.

Author Contributions: Conceptualization: J.-P.W., S.S.E. and M.S.; culture characterization: S.A. and W.M.; methodology and investigation: J.-P.W., E.S. and N.A.L.-L.; data curation and interpretation: J.-P.W., S.S.E. and T.K.; visualization: J.-P.W. and S.S.E.; writing—original draft preparation: J.-P.W. and S.S.E.; writing—review and editing: all authors. All authors have read and agreed to the published version of the manuscript.

Funding: This work was supported by funds from Landwirtschaftliche Rentenbank, Germany (Project "MycoNem").

Institutional Review Board Statement: Not applicable.

Informed Consent Statement: Not applicable.

Data Availability Statement: All data are available in the manuscript or the SI.

Acknowledgments: S. Pfütze, E. Charria-Girón, and F. Surup are acknowledged for their expert advisory assistance. A. Skiba, S. Reinecke, C. Kakoschke, E. Surges, and W. Collisi are thanked for their expert technical assistance. D.G. Knapp, D. Blaudez, M. Chalot, and G.M. Kovács are acknowledged for collecting and depositing the fungal strains. T. Kurtán thanks the financial support from the National Research Development and Innovation Office (Grant number K-138672). The Georg-Forster Fellowship for Experienced Researchers stipend (Ref 3.4-1222288-EGY-GF-E) that Alexander von Humboldt (AvH) Foundation granted to S.S. Ebada is gratefully acknowledged. Financial support by a personal PhD stipend from the German Academic exchange service DAAD to N.A.L.-L. is immensely acknowledged (program ID 57552340).

Conflicts of Interest: The authors declare no conflict of interest.

References

1. Ayer:, W.A.; Craw, P.A.; Nozawa, K. Two 1*H*-naphtho [2,3-c]pyran-1-one metabolites from the fungus *Paecilomyces variotii*. *Can. J. Chem.* **1991**, *69*, 189–191. [CrossRef]
2. Liu, J.; Li, F.; Kim, E.L.; Hong, J.; Jung, H.J. Viriditoxin, from a jellyfish-derived fungus, is antibiotic to fish pathogens. *Nat. Prod. Sci.* **2013**, *19*, 61–65.
3. Elix, J.A.; Wardlaw, J.H. Pigmentosin A, a new naphthopyrone from the lichen *Hyptotrachyna immaculata*. *Aust. J. Chem.* **2004**, *57*, 681–683. [CrossRef]
4. Kong, F.D.; Zhou, L.M.; Ma, Q.Y.; Huang, S.Z.; Wang, P.; Dai, H.F.; Zhao, Y.X. Metabolites with Gram-negative bacteria quorum sensing inhibitory activtiy from the marine animal endogenic fungus *Penicillium* sp. SCS-KFDo8. *Arch. Pharm. Res.* **2017**, *40*, 25–31. [CrossRef]
5. Luo, X.-W.; Gao, C.-H.; Han, F.-H.; Chen, X.-Q.; Lin, X.-P.; Zhou, X.-F.; Wang, J.-J.; Liu, Y.-H. A new naphthopyranone from the sponge-associated fungus *Penicillium* sp. XWSo2F62. *Magn. Reson. Chem.* **2019**, *57*, 982–986. [CrossRef]
6. Suzuki, K.; Nozawa, K.; Nakajima, S.; Kawai, K. Structure revision of mycotoxin, viriditoxin, and its derivatives. *Chem. Pharm. Bull.* **1990**, *38*, 3180–3181. [CrossRef]
7. Arnone, A.; Assante, G.; Montorsi, M.; Nasini, G. Asteromine, a bioactive secondary metabolite from a strain of *Mycosphaerella asteroma*. *Phytochemistry* **1995**, *38*, 595–597. [CrossRef]
8. Suzuki, K.; Nozawa, K.; Nakajima, S.; Udagawa, S.; Kawai, K. Isolation and structures of antibacterial binaphtho-α-pyrones, talaroderxines A and B, from *Talaromyces derxii*. *Chem. Pharm. Bull.* **1992**, *40*, 1116–1119. [CrossRef]

9. Tan, N.P.H.; Donner, C.D. Total synthesis and confirmationn of the absolute stereochemistry of semiviriditoxin, a naphthopyranone metabolite from the fungus *Paecilomyces variotii*. *Tetrahedron* **2009**, *65*, 4007–4012. [CrossRef]
10. Helaly, S.E.; Kuephadungphan, W.; Phainuphong, P.; Ibrahim, M.A.A.; Tasanathai, K.; Mongkolsamrit, S.; Luangsa-ard, J.J.; Phongpaichit, S.; Rukachaisirikul, V.; Stadler, M. Pigmentosins from *Gibellula* sp. as antibiofilm agents and a new glycosylated asperfuran from *Cordyceps javanica*. *Beilstein J. Org. Chem.* **2019**, *15*, 2968–2981. [CrossRef]
11. Isaka, M.; Yangchum, A.; Rachtawee, P.; Komwijit, S.; Lutthisungneon, A. Hopane-type triterpenes and binaphthopyrones from the scale insect pathogenic fungus *Aschersonia paraphysata* BCC 11964. *J. Nat. Prod.* **2010**, *73*, 688–692. [CrossRef] [PubMed]
12. Bode, S.E.; Drochner, D.; Müller, M. Synthesis, biosynthesis and absolute configuration of vioxanthin. *Angew. Chem. Int. Ed.* **2007**, *46*, 5916–5920. [CrossRef] [PubMed]
13. Blank, F.; Ng, A.S.; Just, G. Metabolites of pathogenic fungi. V. Isolation and tentative structures of vioxanthin and viopurpurin, two coloured metabolites from *Trichophyton violaceum*. *Can. J. Chem.* **1966**, *44*, 2873–2879. [CrossRef]
14. Rivera-Chávez, J.; Caesar, L.K.; Garcia-Salazar, J.J.; Raja, M.A.; Cech, N.B.; Pearce, C.J.; Oberlies, N.H. Mycopyranone: A 8,8′-binaphthopyranone with potent anti-MRSA activity from the fungus *Phialemoniopsis* sp. *Tetrahedron Lett.* **2019**, *60*, 594–597. [CrossRef]
15. He, H.; Bigelis, R.; Yang, H.Y.; Chang, L.-P.; Singh, M.P. Lichenicolins A and B, new bisnaphthopyrones from an unidentified lichenicolous fungus, strain *LL*-RB0668. *J. Antibiot.* **2005**, *58*, 731–736. [CrossRef] [PubMed]
16. Jenssen, M.; Rainsford, P.; Juskewitz, E.; Andersen, J.H.; Hansen, E.H.; Isaksson, J.; Rämä, T.; Hansen, K.Ø. Lulworthinone, a new dimeric naphthopyrone from a marine fungus in the family Lulworthiaceae with antibacterial activity against clinical methicillin-resistant *Staphylococcus aureus* isolates. *Front. Microbiol.* **2021**, *12*, 730740. [CrossRef]
17. Wang, J.; Galgoci, A.; Kodali, S.; Herath, K.B.; Jayasuriya, H.; Dorso, K.; Vicente, F.; González, A.; Cully, D.; Bramhill, D.; et al. Discovery of a small molecule that inhibits cell division by blocking FtsZ, a novel therapeutic target of antibiotics. *J. Biol. Chem.* **2003**, *278*, 44424–44428. [CrossRef]
18. Ashrafi, S.; Knapp, D.G.; Blaudez, D.; Chalot, M.; Maciá-Vicente, J.G.; Zagyva, I.; Dababat, A.A.; Maier, W.; Kovács, G.M. Inhabiting plant roots, nematodes and truffles-*Polyphilus*, a new helotialean genus two globally distributed species. *Mycologia* **2018**, *110*, 286–299. [CrossRef]
19. Kajula, M.; Ward, J.M.; Turpenien, A.; Tejesvi, M.V.; Hokkanen, J.; Tolonen, A.; Häkkänen, H.; Picart, P.; Ihalainen, J.; Sahl, H.-G.; et al. Bridged epipolythiodiketopiperazines from *Penicillium raciborskii*, an endophytic fungus of *Rhododendron tomentosum* Harmaja. *J. Nat. Prod.* **2016**, *79*, 685–690. [CrossRef]
20. Tang, R.; Zhou, D.; Kimishima, A.; Setiawan, A.; Arai, M. Selective cytotoxicity of marine-derived fungal metabolite (3*S*,6*S*)-3,6-dibenzylpiperazine-2,5-dione against cancer cells adapted to nutrient starvation. *J. Antibiot.* **2020**, *73*, 873–875. [CrossRef]
21. Grove, C.I.; Di Maso, M.J.; Jaipuri, F.A.; Kim, M.B.; Shaw, J.T. Synthesis of 6,6′-binaphthopyran-2-one natural products: Pigmentosin A, talaroderxines A and B. *Org. Lett.* **2012**, *14*, 4338–4341. [CrossRef]
22. Yamazaki, H.; Rotinsulu, H.; Narita, R.; Takahashi, R.; Namikoshi, M. Induced production of halogenated epidithiodiketopiperazines by a marine-derived *Trichoderma* cf. *brevicompactum* with sodium halides. *J. Nat. Prod.* **2015**, *78*, 2319–2321. [CrossRef]
23. Stipanovic, R.D.; Howell, C.R. The structure of gliovirin, a new antibiotic from *Gliocladium virens*. *J. Antibiot.* **1982**, *35*, 1326–1330. [CrossRef] [PubMed]
24. Iwatsuki, M.; Otoguro, K.; Ishiyama, A.; Namatame, M.; Nishihara-Tukashima, A.; Hashida, J.; Nakashima, T.; Masuma, R.; Takahashi, Y.; Yamada, H.; et al. In vitro antitrypanosomal activity of 12-low-molecular-weight antibiotics and observations of structure/activity relationships. *J. Antibiot.* **2010**, *63*, 619–622. [CrossRef] [PubMed]
25. Seephonkai, P.; Kongsaeree, S.; Prabpai, S.; Isaka, M.; Thebtaranonth, Y. Transformation of an irregularly bridged epidithiodiketopiperazine to trichodermamide A. *Org. Lett.* **2006**, *8*, 3073–3075. [CrossRef]
26. Chepkirui, C.; Cheng, T.; Matasyoh, J.; Decock, C.; Stadler, M. An unprecedented spiro[furan-2,1′-indene]-3-one derivative and other nematicidal and antimicrobial metabolites from *Sanghuangporus* sp. (Hymenochaetaceae, Basidiomycota) collected in Kenya. *Phytochem. Lett.* **2018**, *25*, 141–146. [CrossRef]
27. Charria-Girón, E.; Stchigel, A.M.; Čmoková, A.; Kolařík, M.; Surup, F.; Marin-Felix, Y. *Amesia hispanica* sp. nov., producer of the antifungal class of antibiotics dactylfungins. *J. Fungi* **2023**, *9*, 463. [CrossRef] [PubMed]
28. Niego, A.G.T.; Lambert, C.; Mortimer, P.; Thongklang, N.; Rapior, S.; Grosse, M.; Schrey, H.; Charria-Girón, E.; Walker, A.; Stadler, M. The contribution of fungi to the global economy. *Fungal Divers.* **2023**, *in press*. [CrossRef]

Publication V

Lachnuoic Acids A−F: Ambuic Acid Congeners from a Saprotrophic *Lachnum* Species

Kunthida Phutthacharoen[1,2], Rita Toshe[1,3], Syeda J. Khalid[1,3,] **Natalia A. Llanos-López[1,3]**, Jan-Peer Wennrich[1,3], Hedda Schrey[1,3], Sherif S. Ebada[1,4,*], Kevin D. Hyde[2,5], and Marc Stadler[1,3,*]

[1] Department of Microbial Drugs, Helmholtz Centre for Infection Research GmbH (HZI), Inhoffenstraße 7, 38124 Braunschweig, Germany.

[2] Center of Excellence in Fungal Research, Mae Fah Luang University, Chiang Rai 57100, Thailand.

[3] Institute of Microbiology, Technische Universität Braunschweig, Spielmannstraße 7, 38106 Braunschweig, Germany.

[4] Department of Pharmacognosy, Faculty of Pharmacy, Ain Shams University,11566 Cairo, Egypt.

[5] School of Science, Mae Fah Luang University, Chiang Rai 57100, Thailand.

* Corresponding author.

Chemistry & Biodiversity 2024, 21(4): e2024003. https://doi.org/10.1002/cbdv.202400385.

doi.org/10.1002/cbdv.202400385 Research Article CHEMISTRY & BIODIVERSITY

www.cb.wiley.com

Lachnuoic Acids A–F: Ambuic Acid Congeners from a Saprotrophic *Lachnum* Species

Kunthida Phutthacharoen,[a, b] Rita Toshe,[a, c] Syeda J. Khalid,[a, c] Natalia A. Llanos-López,[a, c] Jan-Peer Wennrich,[a, c] Hedda Schrey,[a, c] Sherif S. Ebada,*[a, d] Kevin D. Hyde,[b, e] and Marc Stadler*[a, c]

Chemical prospection of an extract derived from a saprotrophic fungus *Lachnum* sp. IW157 resulted in the isolation and characterization of six unprecedentedly reported ambuic acid analogues named lachnuoic acids A–F (**1**–**6**). Chemical structures of **1**–**6** were determined based on comprehensive 1D and 2D NMR spectroscopic analyses together with HR-ESI-MS spectrometry. The relative configurations of **1**–**3** were defined by ROESY spectroscopic analyses while their absolute configurations were unambiguously determined by Mosher's esters method. All isolated compounds were subjected to cytotoxic, antimicrobial, antibiofilm and nematicidal activity assays where only lachnuoic acid A (**1**) revealed potent antimicrobial activity against *Staphylococcus aureus* and *Bacillus subtilis* at MIC values of 16.6 and 8.3 μg/mL, respectively.

Introduction

The fungal kingdom currently comprises ca, 150,000 described species, which have already yielded numerous unique secondary metabolites with unprecedented chemical scaffolds. Some chemical scaffolds have become the basic structures for various developmental candidates that resulted in marketed drugs or agrochemicals.[1] However, most of the fungal taxa have been neither cultured nor explored for secondary metabolites. In our ongoing study, we are focusing on rare, inoperculate Discomycetes (class Leotiomycetes, order Helotiales) from Germany and have been able to culture the respective species from ascospores for the first time. We have recently reported the isolation and the characterization of two polyketides from the cultures of a *Lachnum* sp. that was derived from apothecia collected off the common reed grass, *Phragmites communis* in Germany.[2] Morphologically, it revealed characteristic features to be closely related to *Lachnum carneolum*. This fungus was selected because of strong activities of its crude extract in a screening of over twenty Leotiomycetes, and because HPLC-DAD/MS profiling revealed that it had an extraordinarily rich secondary metabolite profile. In the current paper, we wish to report the isolation, structure elucidation and biological activities of further metabolites that were produced by the same strain.

[a] *K. Phutthacharoen, R. Toshe, S. J. Khalid, N. A. Llanos-López, J.-P. Wennrich, H. Schrey, S. S. Ebada, M. Stadler*
Department of Microbial Drugs, Helmholtz Centre for Infection Research GmbH (HZI), Inhoffenstraße 7, 38124 Braunschweig, Germany
Tel.: +49-531-6181-4240
Fax +49-531-6181-9499
E-mail: sherif.elsayed@helmholtz-hzi.de
sherif_elsayed@pharma.asu.edu.eg
Marc.Stadler@helmholtz-hzi.de

[b] *K. Phutthacharoen, K. D. Hyde*
Center of Excellence in Fungal Research, Mae Fah Luang University, Chiang Rai 57100, Thailand

[c] *R. Toshe, S. J. Khalid, N. A. Llanos-López, J.-P. Wennrich, H. Schrey, M. Stadler*
Institute of Microbiology, Technische Universität Braunschweig, Spielmannstraße 7, 38106 Braunschweig, Germany

[d] *S. S. Ebada*
Department of Pharmacognosy, Faculty of Pharmacy, Ain Shams University, 11566 Cairo, Egypt

[e] *K. D. Hyde*
School of Science, Mae Fah Luang University, Chiang Rai 57100, Thailand

Supporting information for this article is available on the WWW under https://doi.org/10.1002/cbdv.202400385

Results and Discussions

Characteristics of the Producer Strain

The investigated strain, *Lachnum* sp. IW157 (DSM 116717), was derived from a specimen collected in Germany and tentatively identified as *Lachnum* (cf.) *carneolum*. The characteristics of the apothecia are depicted on the Internet. (https://asco-sonneberg.de/pages/gallery/lachnum-carneolum-220425-iw157-stma22045-nur-lsu-01xsmjj41478.php). A preliminary molecular characterization of the strains was reported in our previous paper[2] where it was also discussed that the clarification of the identity of this discomycete will afford additional work, including type studies, which are outside the scope of the current study.

The secondary metabolites that are described here were obtained from the same extract that yielded the diaporphasines E and F (Figure 1) as described previously.[2]

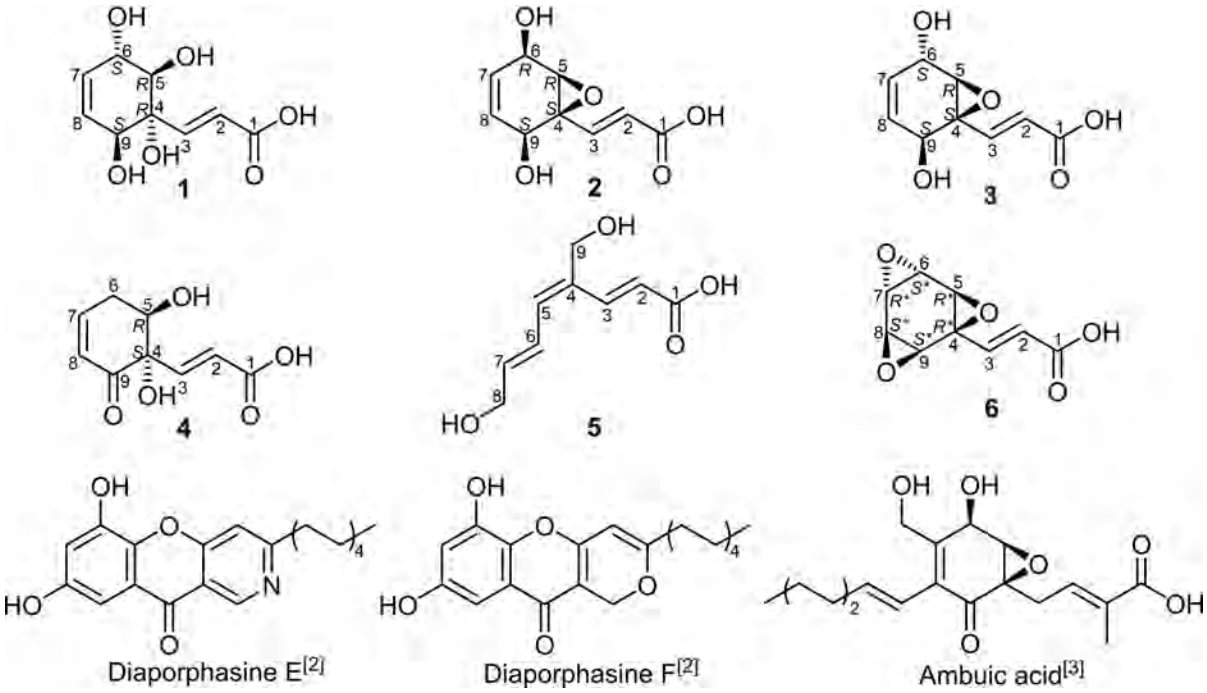

Figure 1. Structures of compounds lachnuoic acids A–F (**1**–**6**), diaporphasines E, F[2] and ambuic acid.[3]

Isolation and Structure Elucidation of Secondary Metabolites 1–6

Compound **1** was isolated as a white amorphous solid. Its molecular formula was determined to be $C_9H_{12}O_6$ based on HR-ESI-MS that revealed a sodium adduct at *m/z* 239.0526 $[M+Na]^+$ (calculated 239.0526) indicating four degrees of unsaturation. The ^{13}C NMR spectral data of **1** (Table 1) revealed the presence of two unprotonated carbon atoms identified as a sp^2 carbonyl carbon at δ_C 167.4 and an oxygenated sp^3 carbon (δ_C 79.4). In addition, the ^{13}C NMR spectrum of **1** also revealed the presence of seven methines distinguished into four sp^2 (δ_C 124.3, 129.5, 130.5, 147.0) and three sp^3 (δ_C 70.9, 74.1, 78.4) carbon atoms. The ^1H NMR and HSQC spectra of **1** revealed the presence of two doublet olefinic protons at δ_H 6.05 and 6.72 ppm with a coupling constant of 15.5 Hz and they were directly correlated to two olefinic carbons at δ_C 124.3 and 147.0, respectively. This notion suggested that compound **1** incorporates in its structure an α,β-unsaturated carbonyl moiety and to be of *trans* configuration. A literature search of **1** revealed that it combines structural features of ambuic acid analogues[3–6] and conduritols.[7,8] Further confirmation to the depicted structure of **1** (Figure 1) was obtained by 2D NMR spectroscopic analyses including ^1H–^1H COSY, HMBC and ROESY (Figure 2). The ^1H–^1H COSY spectrum revealed the first spin system between the two olefinic protons forming the α,β-unsaturated carbonyl moiety while the second spin system extends over three oxygenated methine protons at δ_H 3.39 (d, $J=8.3$ Hz), 3.74 (dd, $J=8.3$, 3.7 Hz) and 4.14 (dt, $J=3.7$, 2.1 Hz) ascribed to H-5, H-6 and H-9 in addition to two olefinic protons at δ_H 5.52 (dt, $J=10.3$,

Table 1. ^1H and ^{13}C NMR data of **1**–**3**.

	1		2		3	
pos.	δ_C[a,c] type	δ_H[b] (multi, *J*[Hz])	δ_C[a,c] type	δ_H[b] (multi, *J*[Hz])	δ_C[a,c] type	δ_H[b] (multi, *J*[Hz])
1	167.4, CO		167.0, CO		167.0, CO	
2	124.3, CH	6.05 (d, 15.5)	122.2, CH	5.95 (d, 15.5)	122.1, CH	5.92 (d, 15.7)
3	147.0, CH	6.72 (d, 15.5)	144.4, CH	7.23 (d, 15.5)	144.5, CH	7.30 (d, 15.7)
4	79.4, C		60.0, C		58.1, C	
5	78.4, CH	3.39 (d, 8.3)	64.2, CH	3.29 (td, 2.3, 1.0)	63.5, CH	3.10 (q, 1.6)
6	70.9, CH	3.74 (dd, 8.3, 3.7)	63.5, CH	4.43 (p, 2.2)	61.8, CH	4.20 (dt, 4.3, 1.7)
7	129.5, CH	5.52 (dt, 10.3, 2.2)	128.1, CH	5.43 (dtd, 10.5, 2.1, 0.8)	125.3, CH	5.58 (ddd, 10.2, 4.3, 1.4)
8	130.5, CH	5.46 (dt, 10.3, 1.8)	126.4, CH	5.60 (ddd, 10.5, 5.0, 2.3)	127.0, CH	5.64 (dd, 10.4, 4.3)
9	74.1, CH	4.14 (dt, 3.7, 2.1)	63.1, CH	4.11 (dd, 4.8, 1.2)	62.8, CH	4.15 (dt, 3.1, 1.5)

Measured in DMSO-d_6 [a] at 125 MHz / [b] at 500 MHz. [c] Assignment confirmed by HMBC and HSQC spectra.

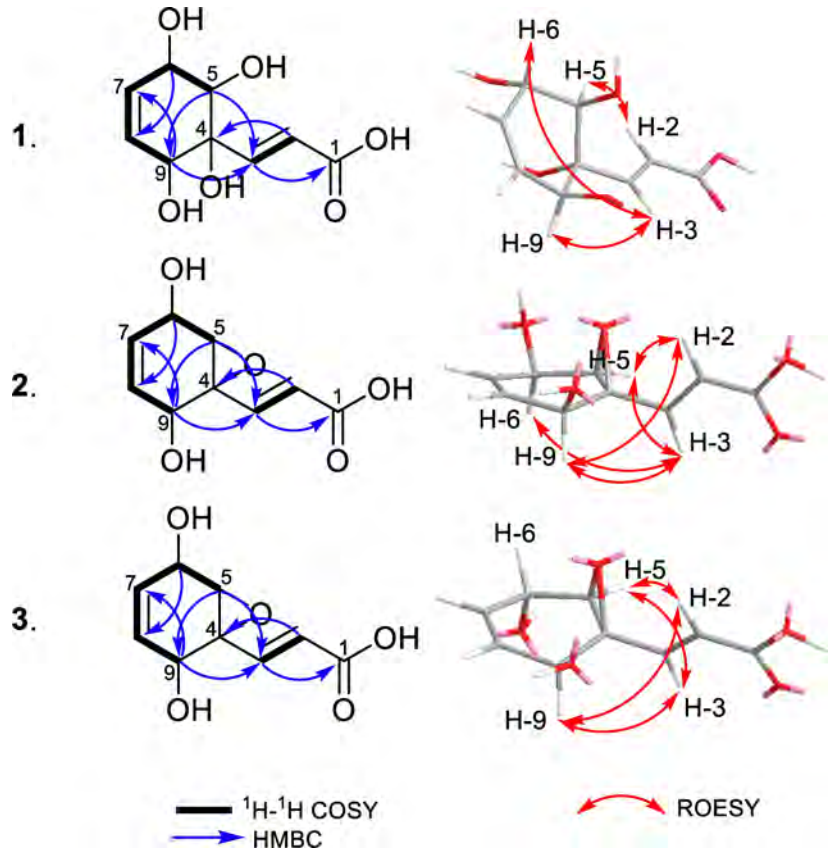

Figure 2. Key ^{1}H-^{1}H COSY, HMBC and ROESY correlations of **1**–**3**.

2.2 Hz) and 5.46 (dt, $J = 10.3$, 1.8 Hz) assigned to H-7 and H-8, respectively.

The HMBC spectrum of **1** (Figure 2) revealed key correlations from H-5 and H-9 to a carbon at δ_C 147.0 (C-3) whose directly connected proton at δ_H 6.72 (d, $J = 15.5$ Hz) revealed key correlation to a carbonyl carbon suggesting its existence as a terminal free carboxylic acid moiety. Further HMBC correlations were noticed from H-5 to C-7 (δ_C 129.5) whereas H-6 and H-9 revealed a key correlation to C-8 (δ_C 130.5). The relative configuration of **1** was deduced by ROESY spectrum that unveiled a key ROE correlation between H-5 and H-9 suggesting to be cofacial while H-6 revealed a key ROE correlation to H-3 and hence suggested to be facing the opposite side of the molecule. The absolute configuration of **1** was determined by analyzing the coupling constant values and performing Mosher's esters method (Figure 3, Table S3) and that revealed $\Delta\delta^{SR}$ values diagnostic for (4*R*,5*R*,6*S*,9*S*) configuration. Based on the obtained results, compound **1** was identified as a previously undescribed natural product that was named lachnuoic acid A.

Compound **2** was obtained as a white amorphous solid. HR-ESI-MS determined its molecular formula to be $C_9H_{10}O_5$ by revealing a sodium adduct at *m/z* 221.0420 $[M+Na]^+$ (calculated 221.0420) indicating the presence of five degrees of unsaturation instead of four degrees in **1**. The ^{1}H and ^{13}C NMR spectra of **1** and **2** (Table 1), revealed an equal number of olefinic and oxygenated methine protons suggesting that the additional degree of unsaturation might be due to an epoxide ring formation. This suggestion was further confirmed by ^{13}C

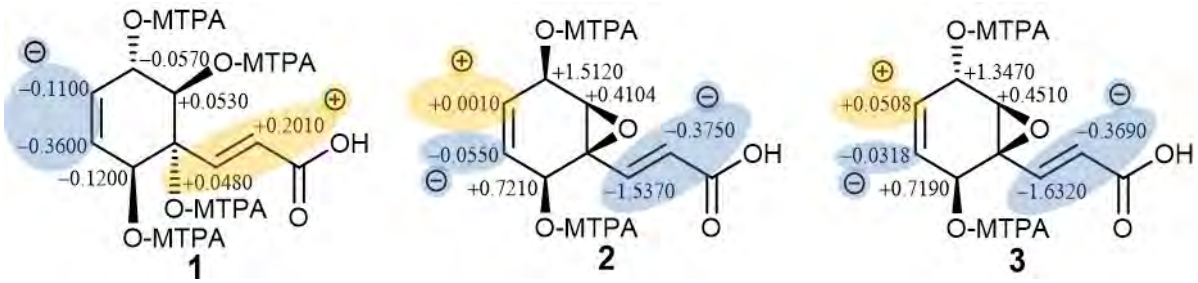

Figure 3. The $\Delta\delta^{SR}$ values of (*S*)/(*R*)-MTPA esters obtained from lachnuoic acid A (**1**) diagnostic for (4*R*,5*R*,6*S*,9*S*); lachnuoic acid B (**2**) diagnostic for (4*S*,5*R*,6*R*,9*S*) and lachnuoic acid C (**3**) diagnostic for (4*S*,5*R*,6*S*,9*S*).

NMR and HSQC spectral data of **2** (Table 1) that revealed relatively shielded carbon resonances at δ_C 60.0, 64.2, 63.5 and 63.1 assigned to C-4, C-5, C-6 and C-9, respectively, compared to their counterparts in **1**. The obtained results and by comparison with those reported of ambuic acid analogues[3–6] and conduritols,[7,8] compound **2** was suggested to have an epoxide ring formed over C-4 and C-5 accounting for the additional degree of unsaturation. Further confirmation of the suggested structure of **2** (Figure 1) was provided by ^{1}H–^{1}H COSY and HMBC spectra (Figure 2). Similar to **1**, the ^{1}H–^{1}H COSY spectrum of **2** revealed a spin system between two doublet olefinic protons at δ_H 5.95 and 7.23 ppm with a coupling constant of 15.5 Hz indicating their presence as an α,β-unsaturated carbonyl moiety in *trans* configuration. The ^{1}H–^{1}H COSY spectrum of **2** exhibited a second spin system extending from three aliphatic methine protons at δ_H 3.29 (dt, J = 2.3, 1.0 Hz, H-5), 4.43 (p, J = 2.2 Hz, H-6) and 4.11 (dd, J = 4.8, 1.2 Hz, H-9) over two olefinic protons at δ_H 5.43 (dtd, J = 10.5, 2.1, 0.8 Hz, H-7) and 5.60 (ddd, J = 10.5, 5.0, 2.3 Hz, H-8). The relative configuration of **2** was determined by ROESY spectrum (Figure 2) that revealed key ROE correlations from H-5, H-6 and H-9 to H-3 indicating that they are all on a cofacial orientation. The absolute configuration of **2** was determined by analyzing the coupling constant values of H-5, H-6 and H-9 in addition to performing Mosher's esters method that revealed $\Delta\delta^{SR}$ values between its (*S*)- and (*R*)-MTPA esters (Figure 3, Table S4) diagnostic for (4*S*,5*R*,6*R*,9*S*) configuration. Based on the aforementioned results, compound **2** was identified as a previously undescribed ambuic acid derivative that was trivially named as lachnuoic acid B.

Similar to **2**, compound **3** was obtained as a white amorphous solid and HR-ESI-MS established its molecular formula to be $C_9H_{10}O_5$ by revealing a sodium adduct at *m/z* 221.0415 $[M+Na]^+$ (calculated 221.0420) indicating five degrees of unsaturation. The ^{1}H and ^{13}C NMR spectral data of **3** (Table 1) revealed close dataset values to those reported for **2** suggesting being of a comparable relative configuration. A major difference was noticed in the chemical shift values assigned to H-5 at δ_H 3.10 (q, J = 1.6 Hz; δ_C 63.5) and H-6 at δ_H 4.20 (dt, J = 4.3, 1.7 Hz; δ_C 61.8) suggesting an opposite configuration at H-6. The relative configuration of **3** was determined by ROESY spectrum (Figure 2) that revealed key ROE correlations from H-5 and H-9 to H-3 and H-2 indicating their cofacial existence while H-6 to be on the opposite side. The absolute configuration of **3** was determined by Mosher's esters method (Figure 3, Table S5) together with analyzing the coupling constant values of H-5, H-6 and H-9 that were diagnostic to (4*S*,5*R*,6*S*,9*S*) configuration. Therefore, compound **3** was identified as a previously undescribed natural product and was given a trivial name lachnuoic acid C.

Compound **4** was isolated as a yellowish-white amorphous solid. Its molecular formula was determined to be $C_9H_{10}O_5$ based on HR-ESI-MS that revealed a sodium adduct at *m/z* 221.0422 $[M+Na]^+$ (calculated 221.0420) indicating five degrees of unsaturation. Despite its identical molecular formula and degrees of unsaturation to those in **2** and **3**, the ^{1}H and ^{13}C NMR spectral data of **4** (Table 2) revealed a second α,β-unsaturated carbonyl moiety appearing as a ketocarbonyl carbon at δ_C 197.7 (C-9) followed by two olefinic sp^2 carbon atoms at δ_C 126.9 (C-8) and 148.6 (C-7). The latter carbons were directly correlated to two proton resonances at δ_H 6.01 (ddd, J = 10.1, 2.6, 1.3 Hz, H-8) and 7.01 (ddd, J = 10.1, 5.1, 2.9 Hz, H-7), respectively, indicating their presence in *cis* configuration. In addition, the ^{1}H spectrum of **4** revealed the presence of one disastereotopic methylene group at δ_H 2.33 (ddt, J = 19.4, 8.4, 2.8 Hz) and 2.69 (dtd, J = 19.4, 5.2, 1.4 Hz) that were directly correlated to a secondary sp^3 carbon at δ_C 32.9 (C-6). The ^{1}H–^{1}H COSY spectrum of **4** (Figure 4) revealed a spin system extending over H-5 at δ_H 3.86 (dd, J = 8.4, 5.2 Hz) to a diasteroptopic methylene group (H_2-6) followed by H-7 and H-8. Based on the obtained results, compound **4** was deduced to incorporate a cyclohexenone moiety in its structure. A literature search of **4**

Table 2. ^{1}H and ^{13}C NMR data of **4**–**6**.

	4		5		6	
pos.	δ_C,[a,e] type	δ_H[b] (multi, *J*[Hz])	δ_C,[c,e] type	δ_H[d] (multi, *J*[Hz])	δ_C,[c,e] type	δ_H[d] (multi, *J*[Hz])
1	167.0, CO		167.9, CO		166.1, CO	12.52 (br s)
2	124.0, CH	5.95 (d, 15.6)	118.7, CH	5.92 (d, 15.8)	125.5, CH	6.19 (d, 16.0)
3	143.8, CH	6.87 (d, 15.6)	137.5, CH	7.65 (d, 15.8)	143.3, CH	6.54 (d, 16.0)
4	80.6, C		134.2, C		54.2, C	
5	72.5, CH	3.86 (dd, 8.4, 5.2)	133.9, CH	6.54 (d, 11.7)	55.3, CH	3.64 (m, overlapped)
6	32.9, CH_2	α 2.33 (ddt, 19.4, 8.4, 2.8) β 2.69 (dtd, 19.4, 5.2, 1.4)	122.9, CH	6.78 (ddt, 15.0, 11.7, 1.8)	46.8, CH	3.47 (m, overlapped)
7	148.6, CH	7.01 (ddd, 10.1, 5.1, 2.9)	139.7, CH	6.08 (dt, 15.0, 4.7)	47.3, CH	3.46 (m, overlapped)
8	126.9, CH	6.01 (ddd, 10.1, 2.6, 1.3)	61.1, CH_2	4.10 (d, 4.7)	50.63,* CH	3.60 (dt, 4.3, 1.5)
9	197.7, CO		61.5, CH_2	4.15 (br s)	50.60,* CH	3.65 (m, overlapped)
4-OH	–	5.40 (br s)				
5-OH	–	5.75 (br s)				

Measured in DMSO-d_6 [a] at 175 MHz / [b] at 700 MHz / [c] at 125 MHz / [d] at 500 MHz. [e] Assignment confirmed by HMBC and HSQC spectra. * Values may switch within the same column.

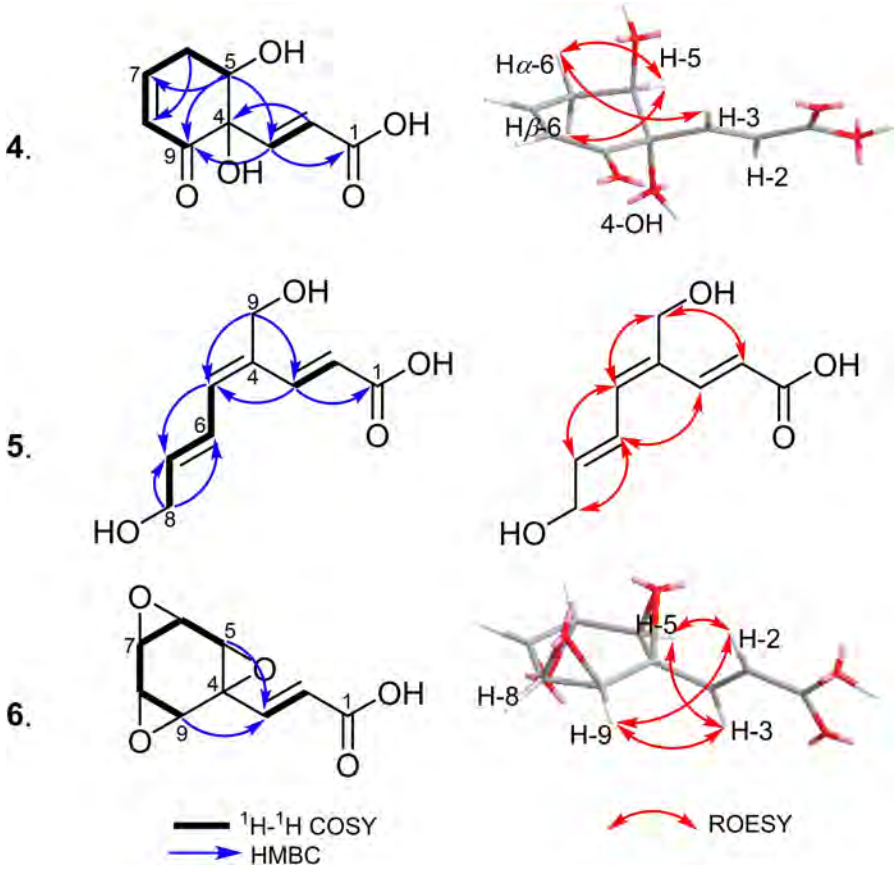

Figure 4. Key ^{1}H-^{1}H COSY, HMBC and ROESY correlations of **4**–**6**.

revealed its structural resemblance to strobiloscyphones[4] and pestallic acids.[5] Further confirmation to the suggested structure of **4** was provided by HMBC spectrum (Figure 4) that revealed key correlations from H-5 to C-3 (δ_C 143.8), C-4 (δ_C 80.6), C-6, C-7 and C-9 whereas H-2 at δ_H 5.95 (d, J = 15.6 Hz) and H-3 at δ_H 6.87 (d, J = 15.6 Hz) exhibited key correlations to a terminal carboxylic acid carbon at δ_C 167.0 (C-1), C-4 and C-9 confirming the binding of the *trans* configured α,β-unsaturated carbonyl moiety at C-4. The relative configuration of **4** was deduced by ROESY spectrum (Figure 4) that revealed a key ROE correlation from H-5 and H-3 suggesting their cofacial projection. The absolute configuration of **4** was determined as (4*S*,5*R*) based on the comparison of coupling constant at H-5 to its peers in **1**–**3** (Table 1) that assigned (*R*) configuration to C-5 and consequently (*S*) configuration to C-4. Based on the obtained results, compound **4** was identified as a previously undescribed cyclohexenone derivative and it was named lachnuoic acid D.

Compound **5** was obtained as a white amorphous solid. HR-ESI-MS revealed a sodium adduct at *m/z* 207.0621 $[M+Na]^+$ (calculated 207.0628) determining its molecular formula as $C_9H_{12}O_4$ thus indicating four degrees of unsaturation. The ^{13}C NMR and HSQC spectra of **5** (Table 2, Figure S41) revealed two unprotonated carbon atoms, a carbonyl carbon at δ_C 167.9 and an olefinic carbon at δ_C 134.2 in addition to five protonated olefinic carbon atoms at δ_C 118.7, 122.9, 133.9, 137.5 and 139.7 that account altogether for four degrees of unsaturation. Thus, compound **5** was deduced to have an acyclic structure. In addition, the ^{13}C NMR spectral data of **5** revealed two oxygenated methylene sp^3 carbon atoms (δ_C 61.1 and 61.5). The ^{1}H NMR and ^{1}H–^{1}H COSY spectra of **5** (Table 2, Figure 4) revealed two distinct spin systems: one between two olefinic *trans* configured protons at δ_H 5.92 (H-2) and 7.65 (H-3) with a characteristic coupling constant of 15.8 Hz while the second spin system originated from an olefinic proton at δ_H 6.54 (d, J = 11.7 Hz, H-5) extending to two olefinic protons at δ_H 6.78 (ddt, J = 15.0, 11.7, 1.8 Hz, H-6) and 6.08 (dt, J = 15.0, 4.7 Hz, H-7) then ending by a doublet hydroxymethylene group at δ_H 4.10 (d, J = 4.7 Hz, H_2-8). These two substructures recognized by the ^{1}H–^{1}H COSY spectrum were correlated by the HMBC spectrum of **5** (Figure 4) that revealed key correlations from a hydroxymethylene group at δ_H 4.15 (br s, H_2-9) to three olefinic carbon atoms at δ_C 137.5 (C-3), 134.2 (C-4) and 133.9 (C-5) indicating that both spin systems and H_2-9 are all connected at C-4 to form the depicted open chain structure of **5** (Figure 1). By analyzing coupling constant values and ROE correlations illustrated by **5** (Figure 4), the two double bonds at C-2/C-3 and C-6/C-7 were determined to be of *trans* configuration while the one at C-4/C-5 was found to be of *cis* configuration. Based on the obtained results, compound **5** was identified as a previously undescribed natural product that was given the trivial name lachnuoic acid E.

Compound **6** was purified as a yellowish-white amorphous solid with its molecular formula established as $C_9H_8O_5$ based on HR-ESI-MS that revealed a sodium adduct at *m/z* 219.0260 $[M+Na]^+$ (calculated 219.0264) and thus indicating six degrees of unsaturation. The ^1H, ^{13}C NMR and HSQC spectra of **6** (Table 2, Figure S49) revealed, similar to **1**–**5**, the presence of an α,β-unsaturated carbonyl moiety in *trans* configuration that account for two degrees of unsaturation. In addition, the ^{13}C NMR spectral data of **6** (Table 2) exhibited the presence of six sp^3 carbon atoms distinguished into five shielded oxygenated methines (δ_C 46.8, 47.3, 50.60, 50.63, 55.3) and one unprotonated oxygenated carbon (δ_C 54.2). Based on the obtained results, compound **6** was deduced to have a cyclohexane ring fused with three epoxide rings over C-4/C-5, C-6/C7 and C-8/C-9. The ^1H NMR spectral data of **6** (Table 2) revealed the presence of five methine protons appearing over three signals. A proton resonance at δ_H 3.60 (dt, $J=4.3$, 1.5 Hz; δ_C 50.63) was assigned to H-8 based on ^1H–^1H COSY spectrum (Figure 4) that revealed key correlations from H-8 to H-9 at δ_H 3.60 (m, overlapped). The latter together with H-5 at δ_H 3.64 (m, overlapped) revealed in the HMBC spectrum (Figure 4) key correlations to an olefinic carbon at δ_C 143.3 assigned to C-3. Only the relative configuration of **6** could be determined by its ROESY spectrum that revealed key ROE correlations from H-5 and H-9 to H-2 at δ_H 6.19 (d, $J=16.0$ Hz) and H-3 at δ_H 6.54 (d, $J=16.0$ Hz) indicating their direction toward the same face of the molecule while H-6 and H-7 directing toward the opposite face. Thus, the relative configuration of **6** was concluded to be (*4R*,5R*,6S*,7R*,8S*,9S**). Based on the aforementioned results, compound **6** was identified as a previously undescribed natural product and was named lachnuoic acid F.

All the isolated compounds were assessed for their cytotoxic, antimicrobial, biofilm inhibitory and nematicidal activities. The results obtained (Tables S1 and S2) revealed that apart from lachnuoic acid A (**1**) featuring significant antimicrobial activities against *Staphylococcus aureus* (MIC = 16.6 μg/mL) and *Bacillus subtilis* (MIC = 8.3 μg/mL), none of the tested compounds unveiled potential activity.

Conclusions

The current study revealed several compounds that bear structural resemblance to a previously reported fungal metabolite ambuic acid (Figure 1), a cyclohexenone-based polyketide first reported from *Pestalotiopsis* and *Monochaetia* associated with rainforest plants and revealed potential activity against several phytopathogens of the genera *Fusarium*, *Diplodia* and *Pythium*.[3] In addition to the suggested phytoprotective role of ambuic acid, several related metabolites were reported such as strobiloscyphones,[4] pestallic acids[5] and pestalotic acids[6] that revealed potential antimicrobial or cytotoxic activities. Interestingly, these compound classes have hitherto only been obtained from members of the Sordariomycetes order Amphisphaeriales to which *Monochaetia* and *Pestalotiopsis* belong[9] and are the first metabolites of this type that were ever isolated from a species of Leotiomycetes. The *Lachnum* strain we studied was thus revealed to have a rather diverse secondary metabolism. None of the metabolites seem to resemble any of the previously reported metabolites from *Lachnum* species.[10–12] However, the fact that the compounds reported here and in the preceding study[2] did not have any prominent antibiotic effects, while the total extract has shown very potent activities, suggests that we may have missed some unstable active principle/s during the isolation procedures. To exploit this will be the subject of future studies.

Experimental Section

General

Optical rotations were obtained on an Anton-Paar MCP 150 polarimeter at 20 °C (Anton-Paar Opto Tec GmbH, Seelze, Germany) and Ultraviolet-Visible (UV/Vis) spectra were recorded using a UV-Vis spectrophotometer UV-2450 (Shimadzu, Kyoto, Japan). Both 1D and 2D NMR spectra were measured using an Avance III 500 spectrometer (Bruker, Billerica, MA, USA, ^1H NMR: 500 MHz, and ^{13}C-NMR: 125 MHz) dissolving compounds in deuterated DMSO-d_6.

High-resolution electrospray ionization mass spectra (HR-ESI-MS) were determined on an Agilent 1200 Infinity Series HPLC-UV system (Agilent Technologies, Santa Clara, CA, USA) equipped with C_{18} Acquity UPLC BEH column (2.1×50 mm, 1.7 μm: Waters, Milford, MA, USA), solvent A: deionized water + 0.1 % formic acid; solvent B: acetonitrile (MeCN) + 0.1 % formic acid, gradient: 5 % B for 0.5 min increasing to 100 % B in 19.5 min, maintaining 100 % B for 5 min, flow rate of 0.6 mL min^{-1}, UV/Vis detection range 190–600 nm) connected to a Time-Of-Flight mass spectrometer (ESI-TOF-MS, Maxis, Bruker, Billerica, MA, USA) (scan range 100–2500 *m/z*, rate 2 Hz, capillary voltage 4500 V, dry temperature 200 °C). Molecular formulas of the detected compounds were calculated using the Smart Formula algorithm of the Compass Data Analysis software (Bruker, version 4.4).

Fungal Material

A sample strain was collected off Sonneberg at location 50° 21′ 39″ N, 11° 7′ 33″ E, direction Meilschnitz, Thüringen (Germany) on an altitude of 359 m above the sea level. If was found saprotrophically growing on the reed grass *Phragmites communis* (Poaceae). The collection date was on 22 April 2022 by Ingo Wagner and a voucher strain was deposited at the German Collection of Microorganisms and Cell Cultures (DSMZ) coded as IW157 (DSM 116717). The sequenced genes were deposited in the GenBank with the accession numbers, OR335757 and OR335766, for ITS and LSU single gene datasets, respectively.

Molecular Study

DNA of the fungus was extracted from the mycelia grown on yeast malt agar (YM agar; malt extract 10 g/L, yeast extract 4 g/L, D-glucose 4 g/L, agar 20 g/L, pH 6.3 before autoclave). Extracted using the fungal gDNA Miniprep Kit EZ-10 Spin Column protocol (NBS Biologicals, Cambridgeshire, UK). The amplification of the ITS and LSU were performed as previously described.[13]

Fermentation, Extraction and Isolation of Metabolites

A pre-culture was initiated by inoculating five well-grown 14-day-old *Lachnum* sp. (DSM 116717) pieces from a YM agar plate into a 500 mL Erlenmeyer flask containing 200 mL of ZM $^1/_2$ medium (5 g/L molasses, 5 g/L oatmeal, 1.5 g/L D-glucose, 4 g/L sucrose, 4 g/mL mannitol, 0.5 g/L edamin, 0.5 g/L ammonium sulfate, 1.5 g/L calcium carbonate, pH = 7.2). The pre-culture underwent a ten-day incubation period at 23 °C with a shaker rotating at 140 rpm. Employing an Ultra-Turrax (T25 easy clean digital, IKA) at 8000 rpm for 10 seconds, the pre-culture was homogenized. Subsequently, a 2-mL aliquot of the homogenized material was added to 200 mL of ZM $^1/_2$ liquid media in a 500-mL Erlenmeyer flask and repeated over 25 flasks to afford 5 L total liquid culture volume. Daily glucose levels were monitored using Medi-Test glucose strips (Macherey-Nagel, Düren, Germany). Three days post-glucose depletion, cultures were extracted. Mycelia and supernatant were separated by vacuum filtration. The supernatant underwent ethyl acetate extraction (2×5 L), discarding the aqueous phase, and filtering the organic phase through anhydrous sodium sulfate. Mycelia were immersed in acetone (2×3 L) and sonicated at 40 °C for 30 minutes. Organic phases were evaporated under vacuum at 40 °C resulting in total mycelial extract of 2.61 g and total broth extract of 1.86 g.

The mycelial total extract (2.61 g) was dissolved in 100 mL of MeCN/deionized water (3 : 7) and subjected to liquid-liquid fractionation against 250 mL of *n*-heptane for defatting. Subsequently, the aqueous phase was separated and evaporated under reduced pressure to afford a solid residue of 170 mg. The obtained solid residue was then purified using preparative HPLC (PLC 2020, Gilson, Middleton, WI, USA) utilizing a Gemini C18 column (250×21.2 mm, 10 μm, Phenomenex, Aschaffenburg, Germany) as the stationary phase, the mobile phase comprised deionized water (Milli-Q, Millipore, Schwalbach, Germany) with 0.1% formic acid (FA) (solvent A) and acetonitrile (MeCN) with 0.1% FA (solvent B). The elution gradient for fractionation encompassed 0–20% of solvent B over 25 min, followed by a 10 min gradient elution from 20–40% of solvent B, continued by a 10 min gradient elution from 40–100% of solvent B with a 10 min hold at 100% solvent B. The flow rate was set at 15 mL/min and UV detection wavelengths of 210, 225, 275, and 330 nm. Six pure compounds were isolated through this purification process: Compounds **1** (3.5 mg; t_R = 6.0 min), **2** (6.0 mg; t_R = 11.0 min), **4** (0.5 mg; t_R = 13.0 min), **3** (4.2 mg; t_R = 15.0 min), **5** (2.9 mg; t_R = 18.0 min), and **6** (6.4 mg; t_R = 21 min).

Lachnuoic acid A (***1***): white amorphous solid; $[\alpha]_D^{20}$ +7.1 (*c* 0.1, MeOH); UV/Vis (MeOH): λ_{max} = 200, 216 nm; NMR data (^{1}H NMR: 500 MHz, ^{13}C NMR: 125 MHz in DMSO-d_6) see Table 1; HR-ESI-MS: *m/z* 239.0526 $[M+Na]^+$ (calcd. 239.0526 for $C_9H_{12}NaO_6^+$).

Lachnuoic acid B (***2***): white amorphous solid; $[\alpha]_D^{20}$ −8.4 (*c* 0.1, MeOH); UV/Vis (MeOH): λ_{max} = 202, 224 nm; NMR data (^{1}H NMR: 500 MHz, ^{13}C NMR: 125 MHz in DMSO-d_6) see Table 1; HR-ESI-MS: *m/z* 221.0420 $[M+Na]^+$ (calcd. 221.0420 for $C_9H_{10}NaO_5^+$).

Lachnuoic acid C (***3***): white amorphous solid; $[\alpha]_D^{20}$-3.2 (*c* 0.1, MeOH); UV/Vis (MeOH): λ_{max} = 198, 214 nm; NMR data (^{1}H NMR: 500 MHz, ^{13}C NMR: 125 MHz in DMSO-d_6) see Table 1; HR-ESI-MS: *m/z* 221.0415 $[M+Na]^+$ (calcd. 221.0420 for $C_9H_{10}NaO_5^+$).

Lachnuoic acid D (***4***): yellowish-white amorphous solid; $[\alpha]_D^{20}$ +19.1 (*c* 0.1, MeOH); UV/Vis (MeOH): λ_{max} = 201, 238 nm; NMR data (^{1}H NMR: 700 MHz, ^{13}C NMR: 175 MHz in DMSO-d_6) see Table 2; HR-ESI-MS: *m/z* 221.0422 $[M+Na]^+$ (calcd. 221.0420 for $C_9H_{10}NaO_5^+$).

Lachnuoic acid E (***5***): white amorphous solid; UV/Vis (MeOH): λ_{max} = 217, 302 nm; NMR data (^{1}H NMR: 500 MHz, ^{13}C NMR: 125 MHz in DMSO-d_6) see Table 2; HR-ESI-MS: *m/z* 207.0621 $[M+Na]^+$ (calcd. 207.0628 for $C_9H_{12}NaO_4^+$).

Lachnuoic acid F (***6***): yellowish-white amorphous soild; $[\alpha]_D^{20}$ +34.0 (*c* 0.1, MeOH); UV/Vis (MeOH): λ_{max} = 200, 222 nm; NMR data (^{1}H NMR: 500 MHz, ^{13}C NMR: 125 MHz in DMSO-d_6) see Table 2; HR-ESI-MS: *m/z* 219.0260 $[M+Na]^+$ (calcd. 219.0264 for $C_9H_8NaO_5^+$).

Preparation of (R)- and (S)-MTPA Ester Derivatives of 1–3

A 0.5-mg aliquot was dissolved in 50 μL of pyridine-d_5 and 10 μL of (*R*)-(−)-methoxy-α-(trifluoromethyl)phenylacetyl (MTPA) chloride were added for the preparation of the (*S*)-MTPA ester. The reaction mixture was incubated at room temperature for 60 minutes and monitored by LC–MS. After the reaction was completed, the mixture was diluted to 200 μL using *pyridine-d*$_5$ for NMR measurements. Similarly, 10 μL of (*S*)-MTPA chloride was added to an equal aliquot (0.5 mg) of the compound to synthesize the (*R*)-MTPA ester. Following these reactions, ^{1}H, ^{1}H–^{1}H COSY and HSQC spectra were obtained. This procedure was done the same way for compounds **2** and **3**.

Antimicrobial Assay

Antifungal and antibacterial activities (Minimum Inhibition Concentration, MIC in μg/mL) of all extracts and isolated compounds were assessed using serial dilution assays against a panel of twelve tested microorganisms including Gram-positive, Gram-negative and fungi (Table S2), following established protocols.[14,15]

Cytotoxicity Assay

In vitro cytotoxicity (IC_{50}) evaluations were conducted for the isolated compounds using the MTT (3-(4,5-dimethylthiayol-2-yl)-2,5-diphenyltetrazolium bromide) test in 96-well plates. The cell lines L929 (mouse fibroblasts) and KB3.1 (human endocervical adenocarcinoma) were employed, following established methodologies.[14,15]

Biofilm Inhibitory Assay

Biofilm inhibitory activity against *Staphylococcus aureus* (DSM 1104) of the isolated compounds were examined following a previously reported protocol.[14,16] In brief, *S. aureus* was pre-cultured, and the biofilm assay involved 24-hour growth with serially diluted compounds (125–1.9 μg/mL). Biofilm inhibition was examined and evaluated by crystal violet staining, washing, and subsequent biomass analysis using a microtiter plate reader (Synergy 2, BioTek). Microporenic acid (MAA)[14] was used as a positive control while methanol served as a solvent control, considered 100% with no inhibition against *S. aureus* biofilms.

Nematicidal Activity

Nematicidal activity was assessed using *Caenorhabditis elegans*. *C. elegans* was kept on a nematode growth media (NGM) that was prepared as previously described.[17] In brief, an aliquot suspension with a concentration of approximately 1,000 nematodes/mL was prepared. Pure compounds were tested against the nematodes at concentrations of 100, 50 and 10 μg/mL. The assay was carried out in a 48-well microtiter plate. The compounds dissolved in MeOH were added to the well plate and subsequently dried under nitrogen. Once the solvent was completely evaporated, 300 μL of the nematode suspension was added to each well. Each treatment was replicated three times. Ivermectin at 1 μg/mL was used as a positive control, and MeOH was used as the negative control. Nematodes were monitored 15 minutes after inoculation. The plates were incubated at 150 rpm and 24 °C for 18 h. After

incubation, both alive and dead nematodes were counted in three replicates under a stereomicroscope, and the mortality rate was calculated. Erect and non-moving nematodes were considered dead. A compound is deemed active if the lethal dose at 100 μg/ml is at least 50%.

Author Contributions

Conceptualization: K.P., S.S.E. and M.S.; fungal isolation and identification: K.P., M.S.; methodology: K.P., R.T. and S.S.E.; formal analysis: K.P., R.T. and S.S.E.; data curation and structure elucidation: S.S.E.; antibiofilm assay: H.S. and S.J.K.; nematicidal activity: N.A.L.-L, J.-P.W.; writing—original draft preparation: K.P., R.T. and S.S.E.; writing—review and editing: S.S.E. and M.S.; project administration: M.S.; funding acquisition, M.S. All authors have read and agreed on the published version of the manuscript.

Acknowledgements

The authors thank Ingo Wagner for collecting, identifying and providing the *Lachnum* specimen. S. Pfütze and Ö. Demir are acknowledged for their expert advisory assistance. Authors thank A. Skiba, S. Reinecke, C. Kakoschke, E. Surges and W. Collisi for their generous technical assistance, acquiring HR-ESI-MS, NMR spectroscopy, antimicrobial and cytotoxicity assays. K.P. is grateful for a Royal Golden Jubilee PhD stipend of the Thailand Research fund (Grant no PHD/002/2560). The Georg-Forster Fellowship for Experienced Researchers stipend (Ref 3.4-1222288-EGY-GF-E) granted to S.S.E. and funded by the Alexander von Humboldt (AvH) foundation is gratefully acknowledged. Financial support by a personal PhD stipend from the German Academic exchange service (DAAD) to S.J.K. (Program ID 91726436) and N.A.L.-L. (Program ID 57552340) is immensely acknowledged. Open Access funding enabled and organized by Projekt DEAL.

Conflict of Interests

The authors declare no conflict of interest.

Data Availability Statement

The data that support the findings of this study are available in the supplementary material of this article.

Keywords: *Lachnum* · cytotoxicity · antimicrobial · biofilm inhibition

[1] G. F. Bills, J. B. Gloer, *Microbiol. Spec.* **2016**, *4(6)*, FUNK-0009-2016.
[2] K. Phutthacharoen, S. J. Khalid, H. Schrey, K. D. Hyde, M. Stadler, S. S. Ebada, *ACS Omega* **2023**, *8(44)*, 41689–41695.
[3] J. Y. Li, J. K. Harper, D. M. Grant, B. O. Tombe, B. Bashyal, W. M. Hess, G. A. Strobel, *Phytochemistry* **2001**, *56*, 463–468.
[4] W. Qu, E. M. K. Wijeratne, B. P. Bashyal, J. Xu, Y.-M. Xu, M. X. Liu, M. C. Inácio, A. E. Arnold, J. M. U'Ren, A. A. L. Gunatikala, *J. Nat. Prod.* **2021**, *84*, 2575–2586.
[5] C.-S. Li, B.-J. Yang, J. Turkson, S. Cao, *Phytochemistry* **2017**, *140*, 77–82.
[6] J. Li, J. Xie, F.-X. Yu, Y.-H. Chen, P.-J. Zhao, *Arch. Pharmacal Res.* **2016**, https://doi.org/10.1007/s12272-016-0837-2.
[7] A. H. Ekanayaka, K. D. Hyde, E. Gentekaki, E. H. C. McKenzie, Q. Zhao, T. S. Bulgakov, E. Camporesi, *Mycosphere* **2019**, *10(1)*, https://doi.org/10.5943/mycosphere/10/1/7.
[8] K. Kadota, M. Takeuschi, T. Taniguchi, K. Ogasawara, *Org. Lett.* **2001**, *3(11)*, 1769–1772.
[9] N. N. Wijayawardene, K. D. Hyde, D. Q. Dai, et al., *Mycosphere* **2022**, *13*, 53–453.
[10] H. Anke, M. Stadler, A. Mayer, O. Sterner, *Can. J. Bot.* **1995**, *73S1*, S932–S939.
[11] M. Zhao, L.-Y. Yuan, D.-L. Guo, Y. Ye, Z.-M. Da–Wa, X.-L. Wang, F.-W. Ma, L. Chen, Y.-C. Gu, L.-S. Ding, Y. Zhou, *Phytochemistry* **2018**, *148*, 97–103.
[12] V. Rukachaisirikul, S. Chantaruk, W. Pongcharoen, M. Isaka, S. Lapanun, *J. Nat. Prod.* **2006**, *69*, 980–982.
[13] R. Vilgalys, M. Hester, *J. Bacteriol.* **1990**, *172(8)*, 4238–4246.
[14] C. Chepkirui, K. T. Yuyama, L. A. Wanga, C. Decock, J. C. Matasyoh, W. R. Abraham, M. Stadler, *J. Nat. Prod.* **2018**, *81(4)*, 778–784.
[15] K. Becker, A. C. Wessel, J. J. Luangsa-ard, M. Stadler, *Biomol. Eng.* **2020**, *10(5)*. https://doi.org/10.3390/biom10050805.
[16] K. J. Soliga, S. I. Bär, N. Oberhuber, H. Zeng, H. Schrey, R. Schobert, *Mar. Drugs* **2021**, *19*, 583.
[17] S. E. Helaly, S. Ashrafi, R. B. Teponno, S. Bernecker, A. A. Dababat, W. Maier, M. Stadler, *J. Nat. Prod.* **2018**, *81*, 2228–2234.

Manuscript received: February 13, 2024
Accepted manuscript online: February 29, 2024
Version of record online: March 15, 2024

Publication VI

Pochoniatoxin, a Cytotoxic Pentacyclic Metabolite from the Nematode-Associated Fungus *Pochonia chlamydosporia*

Jan-Peer Wennrich[1,2], Katharina Schmidt[2,3], Samad Ashrafi[4,5], **Natalia A. Llanos-Lopez[1,2]**, Felix Kaspar[1,#], Jennifer Hermann[6], Theresia E.B. Stradal[2,3], Jana Held[7], Laìs Pessanha de Carvalho[7], Wolfgang Maier[4], Frank Surup[1,2], and Marc Stadler[1,2,*]

[1] Department of Microbial Drugs, Helmholtz Centre for Infection Research (HZI), Inhoffenstrasse 7 & German Center for Infection Research, Partner Site Hannover-Braunschweig, 38124 Braunschweig, Germany.

[2] Institute of Microbiology, Technische Universität Braunschweig, Spielmannstraße 7, 38106 Braunschweig, Germany.

[3] Department of Cell Biology, Helmholtz Centre for Infection Research, Inhoffenstrasse 7, 38124 Braunschweig, Germany.

[4] Institut für Epidemiologie und Pathogendiagnostik, Julius Kühn-Institut, Messeweg 11/12, 38104 Braunschweig, Germany.

[5] Department of Zoology and Entomology, University of the Free State, Bloemfontein 9300, South Africa.

[6] Department Microbial Natural Products, Helmholtz Institute for Pharmaceutical Research Saarland (HIPS), Helmholtz Centre for Infection Research (HZI), Saarbrücken, Germany

[7] Institute of Tropical Medicine, Eberhard Karls University Tübingen & German Center for Infection Research, Partner Site Tübingen, 72074, Tübingen, Germany.

[#] Present address: Dept Organic Chemistry, Saarland University and Helmholtz Institute for Pharmaceutical Research Saarland (HIPS), 66123 Saarbrücken, Germany.

* Corresponding author.

ACS Omega (submitted).

Pochoniatoxin, a cytotoxic pentacyclic metabolite from the nematode-associated fungus *Pochonia chlamydosporia*

Jan-Peer Wennrich[a,b], Katharina Schmidt[b,c] , Samad Ashrafi[d,e], Natalia A. Llanos-Lopez[a,b], Felix Kaspar[a,#], Jennifer Hermann[f], Theresia E.B. Stradal[b,c] , Jana Held[g], Laìs Pessanha de Carvalho[g], Wolfgang Maier[d], Frank Surup[a,b] and Marc Stadler[a,b,*]

a Department of Microbial Drugs, Helmholtz Centre for Infection Research (HZI), Inhoffenstrasse 7 & German Center for Infection Research, Partner Site Hannover-Braunschweig, 38124 Braunschweig, Germany

b Institute of Microbiology, Technische Universität Braunschweig, Spielmannstraße 7, 38106 Braunschweig, Germany

c Department of Cell Biology, Helmholtz Centre for Infection Research, Inhoffenstrasse 7, 38124 Braunschweig, Germany

d Institut für Epidemiologie und Pathogendiagnostik, Julius Kühn-Institut, Messeweg 11/12, 38104 Braunschweig, Germany

e Department of Zoology and Entomology, University of the Free State, Bloemfontein 9300, South Africa

[f] Department Microbial Natural Products, Helmholtz Institute for Pharmaceutical Research Saarland (HIPS), Helmholtz Centre for Infection Research (HZI), Saarbrücken, Germany

[g] Institute of Tropical Medicine, Eberhard Karls University Tübingen & German Center for Infection Research, Partner Site Tübingen, 72074, Tübingen, Germany

[#] Present address: Dept Organic Chemistry, Saarland University and Helmholtz Institute for Pharmaceutical Research Saarland (HIPS), 66123 Saarbrücken, Germany

* Correspondence: Marc.Stadler@helmholtz-hzi.de (M.S.); Tel.: +49-531-6181-424

Abstract

In the course of our attempts to find new fungal biocontrol agents / against plant parasitic nematodes, we found an antagonistic strain from eggs of the cereal-parasitic worm *Heterodera filipjevi* that was identified as *Pochonia chlamydosporia*. We isolated a novel tetramic acid derivative, pochoniatoxin (**1**), from its submerged cultures. Structure elucidation of this compound was achieved via HRESIMS and comprehensive NMR analysis. Since overlapping signals, absence of long-range correlations and signal duplication severely hampered the analysis, NMR data sets had to be obtained in five different solvents. The relative and absolute configurations were assigned through the analysis of coupling constants, ROESY data and by Marfey's method. The scaffold is closely related to that of PF1018, yet distinguished by an epoxide moiety at C–8/C–9 and a hydroxylation at C–10. Pochoniatoxin (**1**) exhibited potent nematicidal activity against *Caenorhabditis elegans* and moderate inhibition of *Plasmodium falciparum,* while being devoid of antibacterial and antifungal effects. The compound also showed strong cytotoxicity against various human cancer cell lines and was thus further characterized on its mode of action. In U-2OS cells, it induced apoptosis and necrosis, suppressed proliferation, and impaired lamellipodial dynamics without affecting microtubule integrity, suggesting interference with actin-driven motility and potential cell cycle regulators. We suggest that *Pochonia* strains should be carefully examined for the presence of the toxin before they are being developed as myconematicides for biocontrol.

Keywords: Hypocreales; biocontrol; tetramic acids; nematicidal, cytotoxic.

1. Introduction

Biological control mechanisms have been studied for decades, in particular for plant pathogenic nematodes that are dwelling in the rhizosphere of the cultivated crop plants, where they cannot be reached by spraying pesticides.[1]

We have recently intensified our search for hitherto untapped nematode-associated fungi and were able to find several new species that could become candidates for development of bionematicides. Some of them constitute new genera of dark septate endophytes.[-4] In order to prioritize these new strains with regard to development as biocontrol agents, it is not only necessary to test the efficacy in greenhouse and field experiments but also exclude the production of toxins, because the registration of a given product on this market is dependent on safety issues.[5]

We have already found many secondary metabolites with potentially beneficial properties from these new nematode antagonists, and some of those showed remarkable cytotoxicity, which precluded the further development of their producer strains as biocontrol agents.[6,7]

The current study deals with another strain that was isolated during the same project, but turned out to belong to a known species, which has been used in biocontrol for many years. We here describe the identification of this fungus and the isolation, structure elucidation and biological characterization of a new secondary metabolite that constitutes one of its major active principles.

2. Materials and Methods

2.1 General experimental procedures

Solutions of crude extracts and isolated compounds were prepared at concentrations of 4.5 mg mL^{-1} and 1 mg mL^{-1}, respectively, utilizing acetone or methanol as solvents. Subsequently, LC-ESI-MS spectra were recorded using an amaZon speed ESI ion trap

mass spectrometer by Bruker Daltonics (Bremen, Germany) coupled with a Dionex UltiMate 3000 UHPLC system from Thermo Scientific Inc. (Waltman, MA, USA) equipped with a C18 Acquity UPLC BEH column (2.1 x 50 mm, 1.7 µm; Waters, MA, USA). This setup utilized a binary mobile phase of water (solvent A) and acetonitrile (solvent B) both supplemented with 0.1% formic acid (FA) at a flow rate of 0.6 mL min^{-1}. The analytical gradient initiated at 5% of phase B for 0.5 min, reaching 100% in 20 minutes and maintained for an additional 5 minutes, with a column temperature of 40 °C. Detection of analytes was facilitated using a UV-Visible detector across the 190–600 nm wavelength range. For the advanced spectrometric profiling, HRESI-MS/MS analyses was executed under similar conditions on an Agilent 1200 series HPLC-UV (Agilent Technologies, Böblingen, Germany) combined with an ESI-TOF-MS system (maXis, Bruker Daltonics), with a capillary voltage set to 4500 V, drying gas temperature of 200 °C, scan range 100-2500 *m/z* and a rate of 2 Hz. The positive ion mode was selected for the ESI-MS of crude extracts and purified metabolites. Optical rotation measurements were conducted using an MCP 150 circular polarimeter (Anton Paar, Seelze, Germany) at a temperature of 20 °C, UV/Visible spectroscopy was carried out with a Shimadzu UV-2450 spectrophotometer, and ECD spectra were recorded with a Jasco J-815 spectropolarimeter (Jasco, Pfungstadt, Germany). The characterization of each metabolite was conducted in methanol. Nuclear magnetic resonance (NMR) spectroscopy was employed to elucidate the structures of isolated compounds using an Avance III 700 with a 5 mm TCI cryoprobe (Bruker ^{1}H: 700 MHz, ^{13}C: 175 MHz, Billerica, MA, USA) and an Avance III 500 (Bruker ^{1}H: 500 MHz, ^{13}C: 125 MHz spectrometer for 1D and 2D NMR spectra. NMR spectra were referenced to the respective solvent peaks (^{1}H 7.27ppm, ^{13}C 77.00ppm for chloroform-*d*; ^{1}H 3.31ppm, ^{13}C 49.15ppm for methanol-d_4; ^{1}H 2.05ppm, ^{13}C 29.32ppm for acetone-d_6; ^{1}H 7.22ppm, ^{13}C 123.87ppm for pyridine-d_5; ^{1}H 7.16ppm, ^{13}C 128.39ppm for benzene-d_6).

2.2 Origin and taxonomy of the producer strain

The fungal strain DSM 119501 was isolated from eggs of the cereal cyst nematode, *Heterodera filipjevi*, which were collected from agricultural fields in Yozgat, Turkey following the methodology outlined in detail by Ashrafi et al.[2,3,4]

Briefly, for morphological and molecular identification the culture was grown on potato dextrose agar (PDA) for 4 weeks. Genomic DNA was isolated from mycelia using a modified cetyle trimethylammonium bromide (CTAB) method. Four DNA loci (ITS, SSU, LSU, rbp2, TEF1) were amplified using the polymerase chain reaction (PCR): The amplicons were sequenced by Eurofins Genomics GmbH, (Ebersberg, Germany). The sequences obtained were assembled, edited and trimmed with Sequencher 5.4.1 (Gene Codes Corporation, Ann Arbor, Michigan, USA) and deposited in GenBank under the following accession numbers: ITS: PV094893; LSU: PV094897; SSU: PV094896; rpb2: PV424434; Tef1: PV155637.

The taxonomic identification of the strain was then performed following our previous paper, using a conventional multi-locus molecular phylogeny and it was established that it belongs to *Pochonia chlamydosporia*.[4] The methodology for the evaluation of the taxonomy of the strain has already been described in a PhD thesis, where, however, the strain itself was not included.[8]

2.3 Fermentation, extraction and isolation of secondary metabolites

The isolate was kept on YM6.3 agar, which included 4 g L^{-1} D-glucose, 10 g L^{-1} malt extract, 4 g L^{-1} yeast extract, and 20 g L^{-1} agar. The pH was adjusted to 6.3 before sterilization and the cultures were stored at room temperature in the dark.[7] In order to prepare a seed culture, 200 mL of Q6/2 medium (D-glucose 2.5 g L^{-1}, glycerol 10 g L^{-1}, cottonseed flour 5 g L^{-1}, pH 7.2) in a 500 mL Erlenmeyer flask was inoculated with three 25 mm^2 pieces of the well-grown

mycelia and cultivated at 140 rpm and 23°C in dark conditions. Glucose content was monitored daily with test stripes (Medi-Test Glucose, Machery-Nagel, Düren, Germany). The cultivation process was terminated once a sufficient biomass had been reached without the consumption of all available free glucose.[7]

Thereafter, the cultures underwent homogenization employing an Ultra-Turrax (T25 easy clean digital, IKA) fitted with an S25 N-25F dispersing element, operating at 10,000 rpm for a duration of 10 seconds. 2 mL of homogenized culture served as the inoculum for the main cultivation of 12 1000 mL flasks containing 400 mL of Q6/2 medium each. Subsequently, the mycelia and supernatant were separated using a Büchner funnel. The extraction protocol follows the methodology described by Wennrich et al..[7] In short, the culture broth was mixed with 2% of AmberLite XAD 16N polymeric absorbent and stirred for 4 h. After eluting the extract from the polymer with acetone, the organic solvent was removed under vacuum. The remaining aqueous phase was then extracted three times with equal parts of ethyl acetate. Finally, the sample was dried and prepared for further analysis. The extraction with XAD yielded a total amount of 132 mg and 295 mg crude extract, respectively to the first and second batch. The first batch was further processed with a Gilson 2250 PLC preparative HPLC utilizing a Nucleodur C18ec column (250 x 21 mm, 10 µm, Machery-Nagel). Mobil Gemini C18 column (250 x 50 mm, 10 µm, Phenomenex CA, USA). Mobile phases consist of water (solvent A) and acetonitrile (solvent B) both supplemented with 0.1% FA starting at a concentration of 30% B, increasing to 85% B in 50 min, raising to 100% B in 5 min and maintaining 100% B for 10 min.

The following yields and retention times were recorded: **1** (16.7 mg, t_R= 35.3 min), monocillin II **2** (1.1 mg $_R$= 21.6 min), monocillin III **3** (1.7 mg, t_R= 11.8 min), monocillin IV **4** (0.8 mg, t_R= 26.3 min), monorden **5** (2.0 mg, t_R= 12.6 min). The second batch was performed with a Gemini C18 column (250 x 50 mm, 10 µm, Phenomenex) with slight modifications to the gradient: starting at a concentration of 20% B for 5 min, increasing to 65% B in 10 min, raising

to 100% B in 25 min and maintaining 100% B for 10 min. This purification resulted in 33 mg of compound **1** (t_R= 35.3 min).

Pochoniatoxin (**1**): $C_{28}H_{36}NO_5$; yellow amorphous solid; $[\alpha]_D^{20}$ +13 (*c* 0.1, MeOH); UV/Vis (MeOH): λ_{max} (log ε) = 319 (4.1), 248 (4.2), 205 (4.3) nm; ECD (c = 2.15 × 10^{-5} M; MeOH) λ [nm], (Δε) 359 (-3.1), 317 (4.5), 279 (0.1), 243 (8.2), 216 (−50.1), 194 (46.5) NMR data (^{1}H NMR: 700 MHz, ^{13}C NMR: 175 MHz) see Table 1; HR-(+)ESI-MS: *m/z* 466.2599 $[M + H]^+$ (calcd. 466.2588 for $C_{28}H_{36}NO_5^+$).

2.4 Determination of the absolute configuration

To ascertain the configuration of the proline-derived moiety, a chemical degradation was carried out first. This was followed by the application of Marfey's method, through which the presence of proline was identified, and its L or D configuration was determined.[9] All procedures were conducted in accordance with a published protocol, with slight modifications, which are described in the following paragraph.

Initially, three mL of NaClO solution (13-15% Cl) were added to 5 mg of compound **1**, which had been dissolved in methanol. The mixture was stirred for 20 minutes at room temperature and then dried. Subsequently, the dried product was dissolved in 5 mL of water and washed twice with 5 mL of fresh $CHCl_3$. The aqueous phase was dried under vacuum using a rotary evaporator, following the modified protocol for Marfey's method.[9] Hydrolysis was performed on the sample using 500 µL of 6 M HCl for 18 hours at 90 °C. After the hydrolysis, the reaction mixture was dried and dissolved in 200 µL of ultrapure water. To this solution, 20 µL of 1 M $NaHCO_3$ and 100 µL of FDAA (1% solution in acetone) were added. An incubation period of 40 minutes was observed, followed by drying and dissolving in 1 mL of methanol for LC-ESI-MS analysis. The procedure was also conducted with authentic standards of proline. Retention times were compared, and the configuration of proline was determined: L-proline at 5.9

minutes, D-proline at 6.3 minutes, and the reaction product of compound **1** at 5.9 minutes. We also tried to apply Mosher's method to solve the absolute configuration (see Supplementary Information) but unfortunately the compound decayed under the standard experimental conditions.

2.5 Biological assays

2.5.1 Standard bioassays

Compound **1** was first subjected to a serial of biological standard assays to assess the antimicrobial effect (Gram-positive, Gram-negative bacteria and fungi and two mammalian cell lines). The results are shown in the Supplementary Information (Tables S1-S3). Later, it was tested for nematicidal effects against *Caenorhabditis elegans*, antiplasmodial activity and cytotoxicity against additional mammalian cell lines (Table S3). Further examination of the cytotoxic effects was conducted on U-2OS cells.

The antibacterial and antifungal efficacy was quantified by determining the minimum inhibitory concentrations (MIC) using a serial dilution assay following established protocols. [6] This assay included the organisms *Bacillus subtilis*, *Staphylococcus aureus*, *Mycobacterium smegmatis*, *Chromobacterium violaceum*, *Acinetobacter baumannii*, *Escherichia coli*, *Pseudomonas aeruginosa*, *Candida albicans*, *Mucor hiemalis*, *Wickerhamomyces anomalus*, *Rhodotorula glutinis* and *Schizosaccharomyces pombe*.

Cytotoxicity was assessed using the MTT (3-(4,5-dimethylthiayol-2-yl)-2,5-diphenyltetrazolium bromide) against several mammalian cell lines, namely L929 (mouse fibroblast), KB3.1 (endocervical adenocarcinoma), A431 (epidermoid carcinoma), A549 (lung carcinoma), PC-3 (prostate adenocarcinoma), SK-OV-3 (ovarian adenocarcinoma) and MCF-7 (breast adenocarcinoma). The cell lines were incubated in a serial dilution with the tested

compound, with epothilone B serving as positive control, and the half-maximal inhibitory concentrations (IC_{50}) were subsequently determined following described protocols.[4,6]

The compounds' effect on *C. elegans* was measured in a 48-well plate setup where methanol solutions of the compounds were applied and allowed to evaporate, followed by the addition of a 0.9% NaCl solution with nematodes. Initial observations were made after 15 minutes, and nematode mortality was assessed after 18 hours of shaking incubation at 23 °C in accordance with a published protocol.[6]

Antiplasmodial activity was evaluated against asexual stages of *Plasmodium falciparum* laboratory strains 3D7 (chloroquine sensitive), and Dd2 (multidrug - resistant), as described previously.[10,11] Serial dilutions of the compound and a comparator drug with known antiplasmodial activity (chloroquine) were pre-dosed on a 96-well plate before the ring stage parasites were added at a defined parasitaemia and haematocrit and incubated for three days. Subsequently, growth inhibition was measured by a histidine rich protein 2 (HRP-2)-based enzyme linked immunosorbent assay (ELISA). The IC_{50} were evaluated by nonlinear regression analysis of log concentration-response curves. All experiments were repeated two times in duplicates.

2.5.2. Effects on U-2OS cells

Cell culture: For the following cell biological experiments, adherent human osteosarcoma cells (U-2OS; ATCC HTB-96) were cultivated and maintained in DMEM (Life Technologies, Carlsbad, CA, USA) containing 10% FBS (Sigma- Aldrich, St. Louis, MO, USA), 1% minimum essential medium nonessential amino acids (MEM NEAA, Life Technologies), 1% L-glutamine, 1% sodium-pyruvate, and 1% penicillin-streptomycin at 37 °C and 7.5% CO_2. Cells were passaged 1:3 – 1:5 every 2–3 days.

Cell proliferation assay: U-2OS cells were seeded into a 24-well plate at a density of 10.000 cells/ well and incubated overnight at 37°C and 7.5% CO_2. Cells were treated with 4.9 µg mL^{-1}, corresponding to previously determined IC_{50} for L929, 100 µg mL^{-1} of **1** as highest possible concentration, and DMSO as vehicle control and recorded immediately for a duration of 72 h using the Incucyte S3 live-cell analysis system (Sartorius, Göttingen, Germany) with a 10× objective at 37 °C and 5 % CO_2. Two images per well and two wells per condition were assessed. Phase contrast images were acquired every 4 h. Phase object counts per well were quantified using the Adherent Cell-by-Cell analysis module of the Live Cell Analysis Software (Sartorius) and normalized to the average, respective initial phase object counts. The normalized values were plotted against the time.

Annexin V apoptosis and necrosis assay: The annexin V apoptosis and necrosis assay was adapted from Kirchenwitz et al.[12] Briefly, U-2OS cells were seeded into a fibronectin-coated (25 µg mL^{-1}) 96-well plate (flat bottom) at a density of 3.000 cells/well and treated with 4.9 µg mL^{-1} and 100 µg mL^{-1} of **1** for 48 h. An equivalent volume of DMSO was used as control. Cells were washed once in Annexin V-binding buffer (10 mM HEPES, 140 mM NaCl, 2.5 mM $CaCl_2$, pH 7.4) and incubated for 15 min at RT in Annexin V-binding buffer (Thermo Fisher Scientific, Waltham, USA) containing Alexa488-conjugated Annexin V, diluted 1:100, and 10 µg mL^{-1} propidium iodide (PI, BioLegend, San Diego, USA) to stain for apoptotic and necrotic cells. Images were acquired and analyzed using the Adherent Cell-by-Cell module of the Live Cell Analysis Software (Sartorius) with a 10x objective. Single cells were categorized by high or low fluorescence in green and red channels and categorized as viable (AnnexinV-/PI-), apoptotic (Annexin V+/PI-), and necrotic (Annexin V+/PI+) based on the fluorescence intensities.

Immunofluorescence: For immunofluorescent analysis of filamentous actin (F-actin) and microtubules, U-2OS cells were seeded (10.000 cells/well) onto fibronectin-coated (25 µg mL^{-1}

[1]) coverslips and cultured over night at 37°C and 7.5% CO_2. The treatment was performed for 48 h with either 4.9 µg mL^{-1} or 100 µg mL^{-1} compound **1**, 76 ng mL^{-1} epothilone B, or an equivalent volume of DMSO under cell culture conditions. Cells were fixed using 4% para-formaldehyde and 0.2 % glutaraldehyde diluted in PBS for 20 min at 37°C and permealized in 0.1 % triton/PBS for 1 min. After three wash steps with PBS, fixed cells were blocked with 5% horse serum diluted in 1% bovine serum albumin (BSA)/PBS for 1h and incubated with monoclonal anti-α-tubulin primary antibody (clone DM1A, 1:300; Sigma) in 1% BSA for an additional hour. Cover-slips were washed thrice in PBS and incubated with AlexaFluor594-linked secondary antibody (1:500; Invitrogen) combined with ATTO488-phalloidin (1:100; Sigma) for actin staining in 1% BSA for 1h. Cells were washed trice in PBS again and mounted in ProLong Diamond Antifade Mountant (Invitrogen) containing DAPI to stain for nuclear DNA. An inverted microscope (Nikon eclipse Ti2, Duesseldorf, Germany) equipped with a 60x Nikon oil immersion objective (Plan Apofluar, 1.4 NA), a pE-4000 (CoolLED, Andover, UK) as a light source, and a pco.edge back- illuminated sCMOS camera (Excelitas Technologies, Mississauga, ON, Canada) were used for cell micrographs. Images were operated by NIS elements (Nikon) and processed by ImageJ/FiJi (https://imagej.net/ij/).

3. Results and Discussion

3.1. Taxonomy of the producer strain and chemotaxonomic studies

By multi-gene genealogy and morphological studies, the strain DSM 119501 was identified unambiguously as *Pochonia chlamydosporia*. This fungus has been recognized as an important nematode antagonist for a long time, even though the taxonomy of the genus has changed over time. We will give a brief overview to clarify this matter since not all the readership of this journal is supposed to be familiar.

The genus *Pochonia* was previously recognized as part of "*Verticilium* sect, *Prostrata*" and comprises hypocrealean ascomycetes that show manifold associations with

invertebrates and other fungi. Zare et al. found that it has affinities to the Clavicipitaceae and erected *Pochonia chlamydosporia*, which they synonymized with other taxa like *Verticillium chlamydosporium* and *Diheterospora chlamydosporia*.[13]

Many *Pochonia* strains produce characteristic secondary metabolites of the pseurotin and, monorden/monocillin (resorcylic acid lactones) type, which was established in a chemotaxonomic study / over 20 years.[14] Monorden and some monocillin derivatives (**2**-**5**, see Fig. 1) were also detected and isolated as major metabolites in the cultures of strain DSM 119501. However, one of the prevalent metabolites (compound **1**) was different from all the previously reported compounds known from *Pochonia* according to a preliminary examination of the crude extracts by HPLC-MS. Its isolation is described in the Experimental and we explain the somewhat complicated structure determination further below.

3.2. Structure elucidation of compound 1

As described in the Experimental section, the fermentation of strain DSM 119501 and fractionation of its extracts by preparative HPLC resulted in the targeted isolation of the main metabolite **1** (Figure 1).

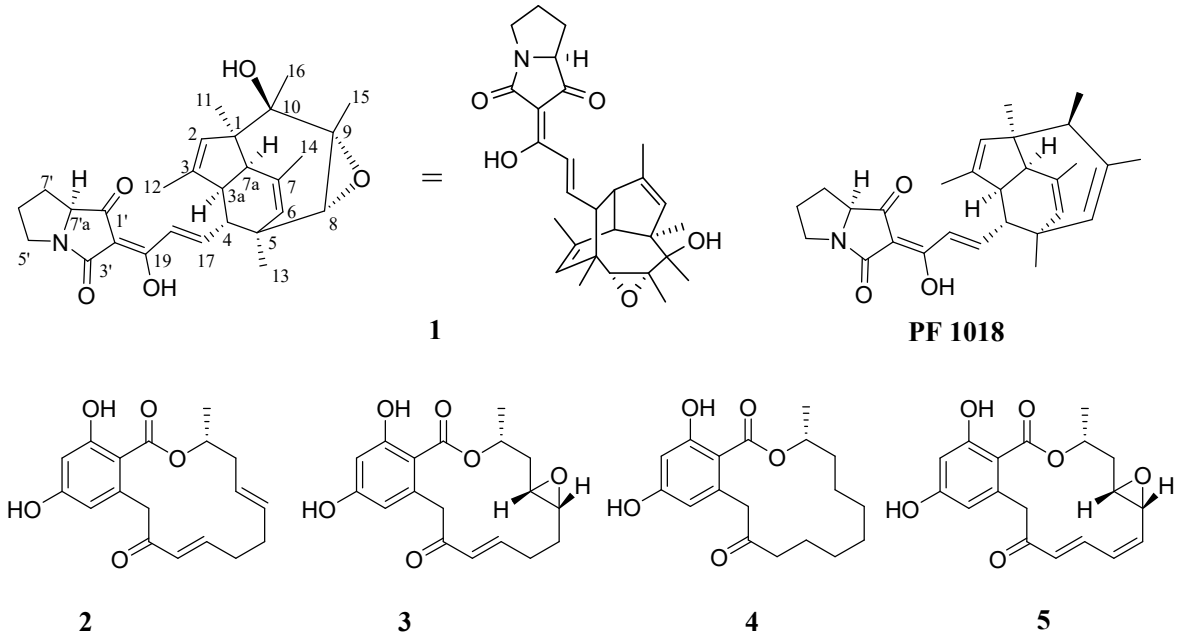

Figure 1. Chemical structures of compound **1**, PF 1018, monocillin II (**2**), monocillin III (**3**), monocillin IV (**4**), and monorden (**5**).

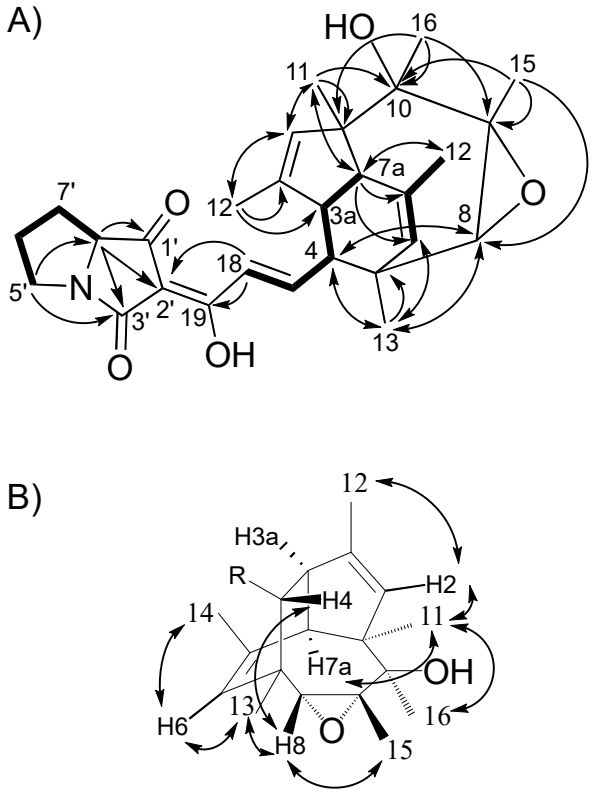

Figure 2. A) Key COSY (bold bonds) and HMBC (arrows) correlations used for the structure elucidation of **1**; **B)** diagnostic ROESY correlations (arrows).

The molecular formula of **1** was established from the HR-ESI-MS spectrum as $C_{25}H_{35}NO_5$, derived from the quasimolecular ion peak cluster at m/z 466.2599 [M +

H]$^+$. For structure elucidation, NMR data (Table 1) had to be obtained consecutively in multiple solvents because of strongly overlapping signals. The ^{1}H and HSQC NMR spectra measured in chloroform–*d* revealed the presence of six methyls, two methylenes as well as two olefinic methines, two oximethines and three further methines. In the ^{13}C NMR spectrum additional five carbons were visible, three of them oxygenated. However, overlaps of two pairs of methines (δ_H 5.12/5.11 and 2.59/2.58) as well as a pronounced doubling of multiple signals in the ^{1}H NMR spectrum, indicating an isomeric equilibrium in this solvent, impeded structure elucidation. Measurement of NMR data in methanol–d_4 resolved both problems of overlapping signals and signal doubling. Based on COSY and HMBC correlations (Figure 2) the complex tricyclic part spanning between C–1 and C–18 was assembled. Especially the HMBC correlations emanating from methyls CH_3–11, CH_3–12, CH_3–13, CH_3–14, CH_3–15, CH_3–16 were helpful in this process.

Further parts of the molecule remained elusive, mainly due to missing signals. With NMR data obtained in acetone–d_6 the five-membered tetrahydro-pyrrol ring structure of the proline residue was finally assigned, with C–7a' and N–4' carrying additional carbonyl carbons. However, missing long-range HMBC correlations prevented the connection of the two substructures. Finally, a full NMR data set was measured in pyridine–d_5, in which a HMBC optimized for small coupling constants showed clear correlations from 7a'–H and 18–H to C–2', connecting both moieties and finalizing the assignment of the planar structure of **1**. A literature search with this planar structure uncovered a close relationship to PF1018, an insecticidal tetramic acid known from a "*Humicola"* sp.[15] It should be mentioned that the producer strain of PF1018 was identified tentatively by microscopy, and that it remains unclear whether it would be referable to the genus *Humicola* (Sordariales) in the current definition based on

molecular phylogenetic data.[16] The strain is unfortunately not available today in the public domain according to our diligent search.

Compared to PF1018, the C–8/C–9 epoxide moiety of **1** replaces the $\Delta^{8,9}$ double bond of PF1018, and C–10 is hydroxylated. The close relatedness eased the configurational assignment for **1**, since an X-Ray structure is available for PF1018. The coupling constants $J_{3a,7a} = 9.8$ Hz and $J_{4,5} << 1$ Hz in combination with a ROESY correlation between 7a–H and 11–H_3 confirmed the common relative configuration of C–1, C–3a, C–4 and C–7a between both compounds. At the same time, the bridged ring junction predetermines the stereochemistry at C–5, as no configurational flexibility is possible at this position. A strong ROESY correlation between 11–H_3 and 16–H_3 accounts for a 10*R* configuration. The ROESY correlations between 8–H and 4–H, 13–CH_3 as well as 15–H_3, which was confirmed by a 1D NOE experiment irradiating 8–H, can only be explained by a 8*R*,9*R* configuration. This 1D NOE NMR experiment was conducted in benzene-d_6, since signal distances were maximized with this solvent. Finally, **1** was degraded with sodium hypochlorite, followed by treatment with HCl for the assignment of absolute configuration; L-proline was detected by Marfey's method as described in the Experimental section.[9] The doubling of NMR signals, most prominent in solvents $CHCl_3$–*d* and benzene–d_6, is attributed to *cis-trans*-isomerism at the Δ(C19,C2') double bond geometry, analogous to that described for PF1018, with the *E* form (major) dominating over the *Z* form (minor).[15]

We did not study the biosynthesis of compound **1** in detail, but hypothesize that the complex of its core scaffold could arise analogously to that of PF1018: The polyunsaturated product of a NRPS-PKS hybrid system undergoes an 8π electrocyclization reaction, immediately followed by a Diels-Alder reaction. These reactions have only recently been reconstructed by total synthesis and transition state calculations in detail.[17,18] However, the biosynthesis of pochoniatoxin (**1**) would

probably require additional P450-catalyzed incorporation of the C-8/C-9 epoxide and a hydroxylation at C-10. Interestingly, another (although structurally less complex), relative of **1** is talarotoxin, known from the eurotialean fungus *Talaromyces bacillosporus*.[19] Otherwise, we did not find any examples in the literature to even remotely similar secondary metabolites.

Some colleagues who are not really familiar with the currently available options in fungal natural products research may even argue that we should have employed ECD calculations or similar computational methods that are based on other computational data. However, such methods will never unambiguously resolve the real absolute configurations of natural molecules and will still deliver only hypothetical results. Aside from the traditional methods like total synthesis and crystallography, we now even have synthetic biotechnology at our disposal that can even lead to total biosynthesis of interesting molecules from Nature. [20]

In any case, we would like to point out that the discovery of compound **1** from a fungal strain that has been deposited preserved permanently in a culture collection from where it can be obtained by others makes it now possible to evaluate the biosynthesis of a very interesting class of fungal PKS-NRPS hybrids. This has not been possible for the producer stain of PF1018, which seems to have been lost according to our diligent search in the inventories of international biodiversity repositories.

371 Table 1: NMR data (^{1}H 700 MHz, ^{13}C 175 MHz) of **1** in methanol-d_5, acetone-d_6, pyridine-d_5 and benzene-d_6.

	chloroform-d [a]		methanol-d_4		acetone-d_6		pyridin-d_5		benzene-d_6 [b]	
#	δ_C (mult)	δ_H (mult)	δ_C (mult)	δ_H (mult)	δ_C (mult)	δ_H (mult)	δ_C (mult)	δ_H (mult)	δ_C (mult)	δ_H (mult)
1	63.7, C		65.0, C		64.5, C		64.2, C		64.1, C	
2	131.7, CH	5.12, m	132.9, CH	5.20, br s	132.7, CH	5.24, br s	132.2, CH	5.08, s	132.3, CH	4.72, s
3	141.2, C		143.0, C		142.1, C		142.0, C		141.5, C	
3a	53.8, CH	2.59, m	55.5, CH	2.62, d (9.8)	54.9, CH	2.62, d (9.9)	54.6, CH	2.64, m	54.3, CH	2.35, d (9.8)
4	49.6, CH	2.67, m	50.8, CH	2.78, d (10.4)	50.0, CH	2.85, d (10.7)	49.9, CH	2.76, d (10.5)	50.2, CH	2.38, d (10.5)
5	40.0, C		41.3, C		43.8, C		40.5, C		40.4, C	
6	123.6, CH	5.12, m	125.2, CH	5.12, s	124.3, CH	5.08, s	124.3, CH	4.97, s	123.8, CH	4.77, s
7	145.6, C		147.3, C		146.5, C		145.8, C		145.8, C	
7a	53.8, CH	2.67, m	55.3, CH	2.75, d (9.8)	54.7, CH	2.73, d (9.9)	54.5, CH	2.64, m	54.4, CH	2.41, d (9.8)
8	77.2, CH [c]	2.59, m	78.5, CH	2.71, s	77.7, CH	2.75, s	77.6, CH	2.69, s	77.4, CH	2.30, s
9	66.5, C		67.9, C		67.1, C		67.0, C		66.7, C	
10	76.1, C		77.8, C		76.8, C		76.8, C		76.5, C	
11	26.0, CH_3	1.40, s	26.5, CH_3	1.39, s	26.4, CH_3	1.38, s	26.5, CH_3	1.41, s	26.6, CH_3	1.34, s
12	14.9, CH_3	1.82, m	15.1, CH_3	1.85, br s	15.1, CH_3	1.85, br s	15.1, CH_3	1.76, br s	15.0, CH_3	1.50, s
13	27.6, CH_3	1.18, s	28.1, CH_3	1.17, s	27.9, CH_3	1.15, s	28.1, CH_3	1.22, s	28.1, CH_3	1.08, s
14	24.7, CH_3	1.98, d (1.3)	25.17, CH_3	1.94, d (1.3)	25.1, CH_3	1.96, d (1.4)	25.1, CH_3	1.91, d (1.0)	25.09, CH_3	1.82, br s

15	24.7, CH_3	1.23, s	25.14, CH_3	1.24, s	25.0, CH_3	1.21, s	25.2, CH_3	1.29, s	25.12, CH_3	1.06, s
16	27.1, CH_3	1.24, s	27.6, CH_3	1.23, s	27.8, CH_3	1.19, s	28.0, CH_3	1.31, s	28.0, CH_3	1.20, s
17	152.6, CH	6.94, dd (15.7,10.4)	153.8, CH	6.96, dd (15.6,10.4)	152.8, CH	6.96, dd (15.3,10.7)	150.6, CH	7.15, dd (15.6,10.4)	153.1, CH	7.10, dd (15.6,10.4)
18	120.9, CH	7.07, d (15.7)	122.4, CH	7.14, d (15.6)	121.7, CH	7.09, d (15.3)	124.2, CH	7.82, d (15.6)	121.6, CH	7.52, d (15.6)
19	173.7, C		175.4, C		173.7, C		176.3, C		174.1, C	
1’	195.1, C		n.o.		195.4, C		197.4, C		195.0, C	
2’	101.7, C		n.o.		102.7, C		103.6, C		102.7, C	
3’	177.2, C		n.o.		178.0, C		177.6, C		177.9, C	
5’	43.1, CH_2	3.76, dt (11.6,7.9) 3.29, m	44.4, CH_2	3.69, dt (11.1,7.7) 3.25, m	43.8, CH_2	3.69, dt (10.9,7.7) 3.23, m	44.2, CH_2	3.84, m 3.14, m	43.3, CH_2	3.39, m 2.61, m
6’	26.8, CH_2	2.18, m 2.10, m	28.0, CH_2	2.14, m	27.44, CH_2	2.12, m	27.4, CH_2	1.85, m 1.79, m	26.8, CH_2	1.21, m 1.09, m
7’	26.8, CH_2	1.57, m	n.o.		27.40, CH_2	2.12, m 1.57, m	27.7, CH_2	2.12, m 1.52, m	27.0, CH_2	1.49, m 0.93, m
7a’	68.8, CH	3.98, dd (10.1, 6.9)	69.6, CH	4.07, br dd (9.4, 6.3)		4.01, m	68.7, m	4.08, br dd (9.6, 7.2)	69.1, m	3.40, m

a Chemical shifts for these signals are different in CHCl3–*d* for minor isomer, ^{13}C: δ_C 203.7 (C, C–1’), 175.1 (C, C–19), 170.5 (C–3’), 153.4 (CH, C–17), 120.5 (CH, C–18), 104.1 (C, C–2’), 66.4, (CH, C–7a’), 49.8 (CH, C–4), 43.3 (CH_2, C–5’); ^1H: δ_H 7.21 (d, J = 15.6 Hz, H–18), 6.98 (dd, J = 15.7, 10.5 Hz, H–17), 4.08 (dd, J = 10.1, 6.9 Hz, H–7a’). b Chemical shifts for these signals are different in benzene–d_6 for minor isomer, ^1H: δ_H 7.71 (d, J = 15.6 Hz, H–18), 7.13 (m, H–17), 3.46 (dd, J = 7.8, H_a–5’), 2.73 (m, H_b–5’). c chemical shift extracted from HSQC data

The nematicidal effect of pochoniatoxin (**1**) was confirmed against *Caenorhabditis elegans.* The results, detailed in Table S4, show that **1** caused high mortality rates even at a lower concentration of 2 µg/mL with 82.1%. Besides, we found a weak inhibition of *Plasmodium falciparum*. IC_{50} values 15 µM for the chloroquine-sensitive 3D7 strain and 8.2 µM for the chloroquine-resistant Dd2 strain. Pochoniatoxin (**1**) showed no activity against Gram-positive as well as Gram-negative bacteria and fungi in our standard panel of test organisms.[21] Notably, it showed high cytotoxicity against the PC-3 cell line with an IC_{50} value of 8 nM, indicating potent activity. Strong cytotoxicity was observed against KB3.1 (107 nM), A431 (112 nM), and SK-OV-3 (97 nM) cell lines. The murine non-malignant L929 cell line was the least sensitive to compound **1** with an IC_{50} value of 10.5 µM (Table S3). This apparent selectivity towards malignant cell lines prompted us to study the mechanism of action of the cytotoxic effects further using an established model in U-2OS cells.[22] Upon treatment of cells with 4.9 µg mL^{-1} and 100 µg mL^{-1} of compound **1** vs. a DMSO control for 72 h, the cell proliferation was analysed using the IncuCyte S3 Adherent Cell-by-Cell module of the Live Cell Analysis Software (Figure S1A). We observed significantly retarded cell growth for 4.9 µg mL^{-1} after an initial lag phase of 44 h and complete suppression for 100 µg mL^{-1} directly after compound addition.

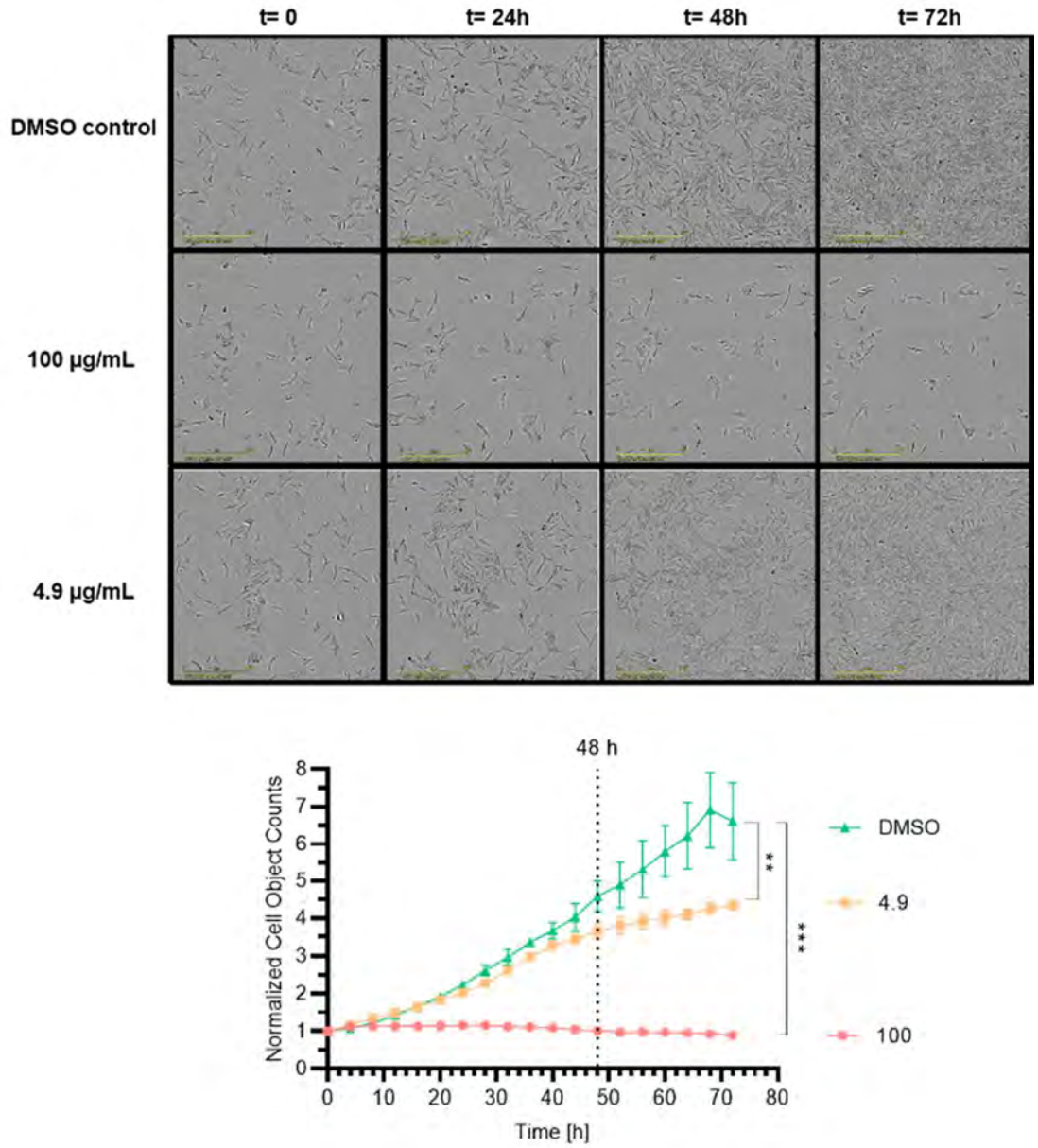

Figure 3. Compound **1** showed inhibited cell proliferation in U-2OS cells in a dose-dependent manner. Cells were treated as indicated, recorded and analyzed by Incucyte S3 live-cell analysis system. Representative phase contrast images of U-2OS cells acquired before and after 24h, 48, and 72 h treatment. Graph showing the normalized mean object counts ± SD from at least two independent experiments with two replicates. ** $p < 0.0029$; *** $p < 0.001$, repeated measures one-way ANOVA.

To better understand the massive reduction in cell proliferation, two further parameters were accessed: First, we quantified the amount of cells lost by either apoptosis or necrosis and thus performed an Annexin V assay combined with propidium iodide (PI) staining. The cytoplasmatic protein Annexin V targets phosphatidylserine (PS) lipids,

which are normally present in the inner plasma membrane but can translocate to the extracellular face during apoptosis.[21] In contrast, PI accumulation occurs exclusively in necrotic cells, ensuring the precise discrimination between apoptotic and necrotic cells. Moreover, cells were treated not only with **1** but also with a microtubule-blocking drug known to halt the cell cycle. Thus, U-2OS cells were treated with 4.9 µg mL^{-1} and 100 µg mL^{-1} of **1** or 76 ng mL^{-1} epothilone B (EpoB)[25], and compared to DMSO as a control for 48 h and stained for apoptotic and necrotic events using Alexa488-Annevin V and PI (Figure 1B). Compared to DMSO, 100 µg mL^{-1} compound significantly reduced the percentage of viable cells (-38%), and elevated the number of apoptotic (+13%), and necrotic (+25%) cells in a similar pronounced way as EpoB. Lower concentrations of **1** caused apoptosis (+2%) and necrosis (+6%) only slightly but not significantly as compared to DMSO. Therefore, the observed growth inhibition upon increased compound concentrations appears to, at least in part, be based on accelerated cell death. However, we wondered, why cell proliferation is completely suppressed at 100 µg mL^{-1} of **1** despite 45% of cells still being viable. Due to the similar efficacy of **1** and EpoB, we hypothesized that possible alterations of the cytoskeleton might impair the cell cycle as e.g. the cytotoxicity of EpoB is caused by blocking microtubule dynamics, leading to cell cycle arrest at the G2-M transition.[24]

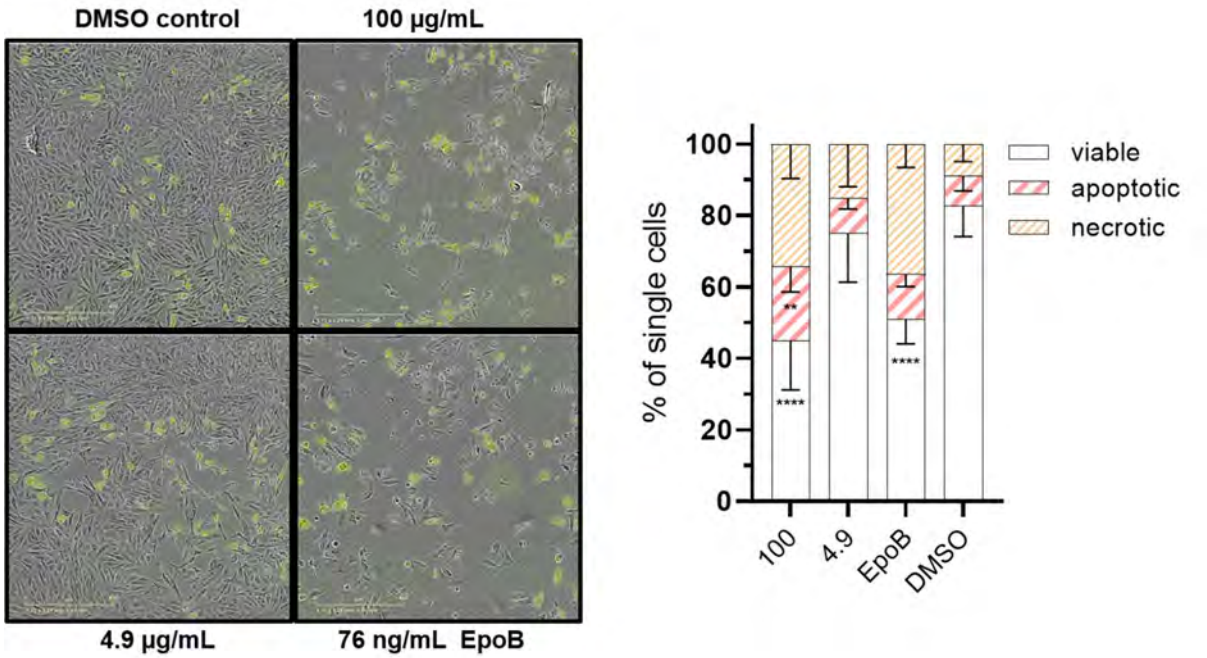

Figure 4: Compound **1** induced apoptosis and necrosis. Representative phase contrast images overlayed with fluorescence channels for Annexin V (green) and PI (red; yellow in merge) of treated U-2OS cells after 48 h. The graph depicts the percentage of single cells ± SD categorized in viable, apoptotic and necrotic cells based on the fluorescence intensities in the green and red channels. Three independent experiments were conducted with at least three replicates. ** $p < 0.0089$, **** $p < 0.0001$, ordinary two-way ANOVA.

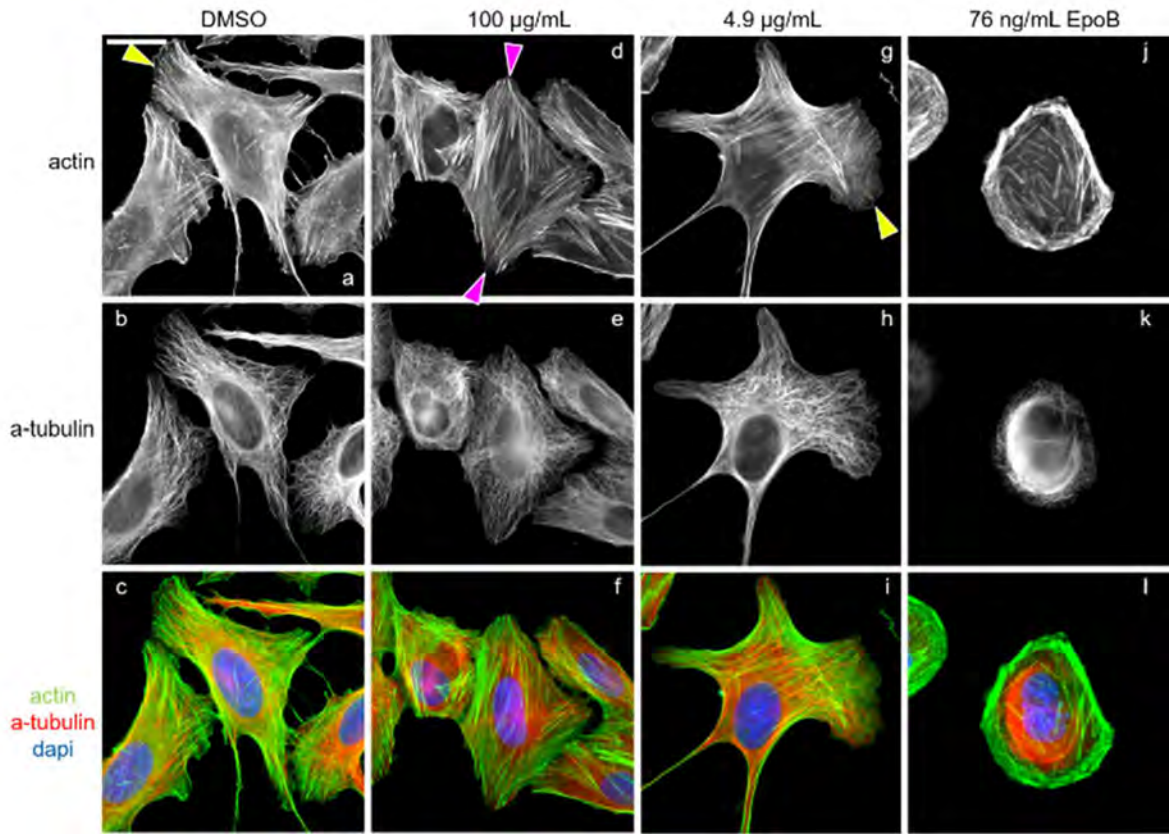

Figure 5. High concentrations of compound **1** diminished lamellipodial cell protrusions and cell motility. U-2OS cells were treated as indicated for 48 h and stained for actin (upper row, green - yellow and magenta arrows highlighting differences in lamellipodial protrusion events), α-tubulin (middle row, red), and nuclear DNA (blue), and visualized by epifluorescence microscopy. A representative scale bar corresponding to 25 µm is shown in a.

To investigate structural alterations of the cytoskeleton, U-2OS cells were treated as indicated and stained for their microtubule and actin network after 48 h of treatment (Figure 4). Compared to EpoB treated cells, exhibiting stabilized microtubules as described in Kirchenwitz et al.[21] (Figure 4; k), the microtubule cytoskeleton of cells treated with **1** remained unchanged (Figure 4; e, h) similar to DMSO treatment (Figure 4; b). Interestingly, the actin network of cells treated with **1** displayed reduced lamellipodial protrusions (compare yellow and magenta arrows), driven by dynamic actin assembly, whereas actin bundles – so called stress fibers – were unaffected, even at 100 µg mL^{-1} of **1** (Figure 2; d) indicating diminished cell motility. Thus, we

hypothesize that pochoniatoxin (**1**) could interfere with the cell cycle or cell cycle regulators. Curiously, these data strongly deviate from the reported ones on PF1018, which was also tested against some cell lines with marginal activities and no details were reported about the applied methodology. The authors of the previous study mainly discussed the insecticidal effect of PF1018 and promised the readership that some follow-up data would be reported, but to the best of our knowledge this has never happened.

In summary, these results indicate that compound **1** could be a promising lead candidate for a novel anticancer agent as it clearly shows similar activities against malignant cells as the precursor of a marketed anticancer agent.

On the other hand, it would certainly not be favourable to develop a strain that is capable of overproducing such a compound as a biocontrol agent. Curiously, the observed lack of antibacterial effects can be explained by the fact that **1** acts on an eukaryotic target, but it remains unclear why fungi, which have a similar cytoskeleton, are not affected by the compound. One reason could be that fungi cannot take it up.

In conclusion, the current study has shown once again that *Pochonia* and its allies are very creative producers of secondary metabolites with various potentially beneficial effects. Other compounds from these fungi including the monorden derivatives[26], and tetrapeptides[27] are certainly more promising to develop antiparasitic or nematicidal agents because they do not show such a pronounced cytotoxic effect. Yet the current study showed that new chemical entities can still be discovered even from relatively well-studied fungi that are involved in ecological interactions with animals.

Supporting Information

The supplementary information can be accessed online. The supplementary information file includes the methodology and results of the phylogenetic identification, all 1D

($^{1}H/^{13}C$) and 2D (^{1}H-^{1}H COSY, HMBC, HSQC and ROESY) spectra of **1** in addition to all HRESIMS of **1**-**5**. It also includes some test data that have been discussed in the manuscript, including the cytotoxicity assays.

Author Contributions

Conceptualization: J.P.W., F.S., M.S. and T.E.B.S; Strain isolation and characterization: S.A., W.M.; Methodology and investigation: J.P.W., L.G. C, K.S. J.H. and N.L ; Data curation and Interpretation: J.P.W., F.S., S.A. W.M. and J.H; Visualization: J.P.W., F.S. K.S..; Writing—original draft preparation: J.P.W.,F.S., K.S; writing—review and editing: All authors read and approved the final manuscript.

Conflicts of interest

The authors declare no conflict of interest.

Acknowledgements

Anke Skiba, Silke Reinecke, Christel Kakoschke, Esther Surges, and Wera Collisi are thanked for their expert technical assistance. *Caenorhabditis elegans* nematodes were provided by the CGC, which is funded by NIH Office of Research Infrastructure Programs (P40 OD010440). We express our sincere gratitude to the late Soleiman Helaly and the Alexander von Humboldt foundation, supporting him by a scholarship. This work was furthermore supported by funds of the Landwirtschaftliche Rentenbank, Germany, who funded the project "Myconem". Natalia Llanos-Lopez is grateful for a PhD stipend grant from the German Academic Exchange Service (DAAD).

References

1) Lopez-Llorca, L. V.; Maciá-Vicente, J. G.; Jansson, H. B. 2008. Mode of action and interactions of nematophagous fungi. In: Ciancio, A., Mukerji, K.G. (eds) Integrated management and biocontrol of vegetable and grain crops nematodes. Integrated management of plant pests and diseases, vol 2. Springer, Dordrecht.

2) Ashrafi, S.; Wennrich, J.P.; Becker, Y; Macia-Vice,nte, J.G.; Brisske-Rode, A.; Daub, M.; Thunen, T.; Dababat, A.A.; Finckh, M.R.; Stadler, M.; Maier, W. *Polydomus karssenii* gen. nov. sp. nov. is a dark septate endophyte with a bifunctional lifestyle parasitising eggs of plant parasitic cyst nematodes (*Heterodera* spp.). *IMA Fungus* **2023**, *14*, 6.

3) Ashrafi, S.; Knapp, D. G.; Blaudez, D.; Chalot, M.; Maciá-Vicente, J. G.; Zagyva, I.; Dababat, A. A.; Maier, W.; Kovács, G. M. Inhabiting plant roots, nematodes, and truffles-*Polyphilus*, a new helotialean genus with two globally distributed species. *Mycologia* **2018**, *110*, 286-299.

4) Ashrafi, S.; Helaly, S.; Schroers, H.-J.; Stadler, M.; Richert-Poeggeler, K. R.; Dababat, A. A.; Maier, W. *Ijuhya vitellina* sp. nov., a novel source for chaetoglobosin A, is a destructive parasite of the cereal cyst nematode *Heterodera filipjevi*. *PLoS ONE* **2017**, *12*, e0180032. https://doi.org/10.1371/journal.pone.0180032.

5) Deising, H.B.; Gase, I.; Kubo, Y. The unpredictable risk imposed by microbial secondary metabolites: how safe is biological control of plant diseases?. *J Plant Dis Prot* **2017**, *124*, 413–419. https://doi.org/10.1007/s41348-017-0109-5

6) Wennrich, J.-P.; Ebada, S. S.; Sepanian, E.; Holzenkamp, C.; Khalid, S. J.; Schrey, H.; Maier, W.; Mándi, A.; Kurtán, T.; Ashrafi, S.; Stadler, M. Omnipolyphilins A and B: chlorinated cyclotetrapeptides and naphtho-α-pyranones from the plant nematode-derived fungus *Polyphilus sieberi*. J. Agric. Food Chem. **2024**, *72*, 6998–7009. https://doi.org/10.1021/acs.jafc.4c00572.

7) Wennrich, J.-P.; Sepanian, E.; Ebada, S. S.; Llanos-Lopez, N. A.; Ashrafi, S.; Maier, W.; Kurtán, T.; Stadler, M. Bioactive naphtho-α-pyranones from two endophytic fungi of the genus *Polyphilus*. *Antibiotics* **2023**, 12 (8), 1273. https://doi.org/10.3390/antibiotics12081273.

8) Ashrafi, S. Isolation and characterisation of novel nematophagous fungi from eggs of the cereal cyst nematode *Heterodera filipjevi* and identifying their secondary metabolites with nematicidal activity. Ph.D. Dissertation, University of Kassel, Germany, 2018. https://www.grafiati.com/en/literature-selections/samad/dissertation/

9) Marfey P. Determination of D-amino acids. II. Use of a bifunctional reagent, 1,5-difluoro-2,4-dinitrobenzene. *Carlsberg Res. Commun*. **1984**, *49*, 591–596. https://doi.org/10.1007/BF02908688

10) de Carvalho L.P.; Sandri, T.L., de Melo, E.J.T; Fendel, R.; Kremsner, P.G.; Mordmüller, B.; Held, J. Ivermectin impairs the development of sexual and asexual stages of *Plasmodium falciparum* in vitro. *Antimicrob. Agents Chemother*. **2019**, *63*, e00085. https://doi.org/10.1128/AAC.00085-19.

11) Hofer, W; Oueis E; Abou Fayad A; Deschner F; Andreas A; Pessanha de Carvalho L; Hüttel S; Bernecker S; Pätzold L; Morgenstern B; Zaburannyi N; Bischoff M; Stadler M; Held J; Herrmann J; Müller R. Regio- and stereoselective epoxidation and acidic epoxide opening of antibacterial and antiplasmodial chlorotonils yield highly potent derivatives. *Angew. Chem. Int. Ed.* **2022**, *61*, e202202816

12) Kirchenwitz, M.; Stahnke, S.; Grunau, K.; Melcher, L.; van Ham, M.; Rottner, K.; Steffen, A.; Stradal, T. E. B. The autophagy inducer SMER28 attenuates microtubule dynamics mediating neuroprotection. *Sci. Rep*. **2022**, *12* (1), 1–14. https://doi.org/10.1038/s41598-022-20563-3

13) Zare, R.; Gams, W.; Evans, H. C. The genus *Pochonia*, with notes on *Rotiferophthora*. *Nova Hedwigia* **2001**, *73*, 51–86. (1)

14) Stadler, M.; Tichy, H.-V.; Katsiou, E.; Hellwig, V. Chemotaxonomy of *Pochonia* and other conidial fungi with *Verticillium*-like anamorphs. *Mycol. Progress* **2003**, 2 (2), 95–122. (2)

15) Gomi, S.; Imamura, K.-I.; Yaguchi, T.; Kodama, Y.; Minowa, N.; Koyama, M. PF1018, a novel insecticidal compound produced by *Humicola* sp. *J. Antibiot*. **1994**, *47*, 571–580.

16) Marin-Felix, Y.; Miller, A.N. Corrections to recent changes in the taxonomy of the Sordariales. *Mycol. Progress* **2022**, *21*, 69. https://doi.org/10.1007/s11557-022-01814-z

17) Niwa, K.; Ohashi, M.; Xie, K.; Chiang, C. Y.; Jamieson, C. S.; Sato, M.; Watanabe, K.; Liu, F.; Houk, K. N.; Tang, Y. Biosynthesis of polycyclic natural products from conjugated polyenes via tandem isomerization and pericyclic reactions. *J. Am. Chem. Soc.* **2023**, *145*, 13520–13525.

18) Quintela-Varela, H.; Jamieson, C. S.; Shao, Q.; Houk, K. N.;Trauner, D. Bioinspired Synthesis of (-)-PF-1018. Angew. Chem. Int. Ed. **2020**, *59*, 5263–5267.

19) Ishii, K.; Itoh, T.; Kobayashi, K.; Horie, Y.; & Ueno, Y. Isolation and characterization of a cytotoxic metabolite of *Talaromyces bacillosporus*. *Appl. Environ. Microbiol.* **1995**, *61*, 941–943.

20) Cox, R.J. Engineered and total biosynthesis of fungal specialized metabolites. *Nat. Rev. Chem*. **2024**, *8*, 61–78.

21) Becker, K.; Pfütze, S.; Kuhnert, E.; Cox, R. J.; Stadler, M.; Surup, F. Hybridorubrins A-D: azaphilone heterodimers from stromata of *Hypoxylon fragiforme* and insights into the biosynthetic machinery for azaphilone diversification. *Chem. Eur. J.* **2021**, *27*, 1438–1450.

571 22) Kirchenwitz, M.; Stahnke, S.; Prettin, S.; Borowiak, M.; Menke, L.; Sieben C,
572 Birchmeier, C.; Rottner, K.; Stradal, T.E.B; Steffen, A. SMER28 attenuates
573 PI3K/MTOR signaling by direct inhibition of PI3K P110 delta. *Cells* **2022**, *11*),
574 1–22. https://doi.org/10.3390/cells11101648. 13)
575 23) Crowley, L. C.; Marfell, B. J.; Scott, A. P.; Waterhouse, N. J. Quantitation of
576 apoptosis and necrosis by annexin V binding, propidium iodide uptake, and flow
577 cytometry. *Cold Spring Harb. Protoc.* **2016**, *2016*, 953–957.
578 https://doi.org/10.1101/pdb.prot087288.
579 24) Reichenbach, H.; Höfle, G. Discovery and development of the epothilones: A
580 novel class of antineoplastic drugs. *Drugs R D* **2008**, *9* (1), 1–10.
581 https://doi.org/10.2165/00126839-200809010-00001.
582 25) Bollag, D. M.; McQueney, P. A.; Zhu, J.; Hensens, O.; Koupal, L.; Liesch, J.;
583 Goetz, M.; Lazarides, E.; Woods, C. M. Epothilones, a new class of microtubule-
584 stabilizing agents with a taxol-like mechanism of action. *Cancer Res.* **1995**, *55*,
585 2325–2333.
586 26) Hellwig, V.; Mayer-Bartschmid, A.; Müller, H.; Greif, G.; Kleymann, G.;
587 Zitzmann, W.; Tichy, H.-V.; Stadler, M. Pochonins A−F, New antiviral and
588 antiparasitic resorcylic acid lactones from *Pochonia chlamydosporia* var.
589 *catenulata*. *J. Nat. Prod.* **2003**, *66*, 829–837.x
590 27) Watanabe, Y.; Hachiya, K.; Ikeda, A.; Nonaka, K.; Higo, M.;et al. Koshidacins A
591 and B, antiplasmodial cyclic tetrapeptides from the Okinawan fungus *Pochonia*
592 *boninensis* FKR-0564. *J. Nat. Prod*. **2022**, *85*, 2641–2649.
593 https://doi.org/10.1021/acs.jnatprod.2c00719.

- This research benefitted from funding by the European Union's Horizon 2020 research and innovation program (RISE) under the Marie Skłodowska-Curie grant agreement No. 101008129, project acronym "Mycobiomics".